BULLETIN OF RUSSIAN STATE MEDICAL UNIVERSITY

BIOMEDICAL JOURNAL OF PIROGOV RUSSIAN NATIONAL RESEARCH MEDICAL UNIVERSITY

Indexed in Scopus. CiteScore 2020: 0.4

Indexed in WoS. JCR 2020: 0.4

Five-year h-index is 6

Scopus®

WEB OF SCIENCE™

Google scholar

Indexed in RSCI. IF 2018: 0,5

Listed in HAC 31.01.2020 (№ 507)

Open access to archive

НАУЧНАЯ ЭЛЕКТРОННАЯ БИБЛИОТЕКА ELIBRARY.RU

ВЫСШАЯ АТТЕСТАЦИОННАЯ КОМИССИЯ (ВАК)

CYBERLENINKA

ВЕСТНИК РОССИЙСКОГО ГОСУДАРСТВЕННОГО МЕДИЦИНСКОГО УНИВЕРСИТЕТА

НАУЧНЫЙ МЕДИЦИНСКИЙ ЖУРНАЛ РНИМУ ИМ. Н. И. ПИРОГОВА

BULLETIN OF RSMU   3, 2021

ВЕСТНИК РГМУ

Contents
Содержание

PERSISTENCE OF SARS-COV-2 IN DECEASED PATIENTS AND SAFE HANDLING OF INFECTED BODIES

Shchegolev AI[1,2] ✉, Tumanova UN[1]

[1] Kulakov National Medical Research Centre of Obstetrics, Gynecology and Perinatology, Moscow, Russia

[2] Pirogov Russian National Research Medical University, Moscow, Russia

This article analyzes the literature on SARS-CoV-2 persistence in the corpses of patients infected with COVID-19, possible routes of viral transmission from the bodies and biosafety measures to prevent the spread of the infection. SARS-CoV-2 persists for quite long in the tissues and bodily fluids of decedents with COVID-19 and on various surfaces. The longest viability of the virus is on stainless steel and plastic surfaces that come in contact with the infected body. Autopsies on decedents with COVID-19 must be performed at specially conditioned facilities. Medical and forensic pathologists and other mortuary workers must adhere to stringent biosafety requirements.

Keywords: COVID-19, SARS-CoV-2, persistence, corpse, autopsy, biosafety

ПЕРСИСТЕНЦИЯ КОРОНАВИРУСА SARS-COV-2 В ТЕЛАХ УМЕРШИХ И МЕРЫ ЗАЩИТЫ ОТ ИНФИЦИРОВАНИЯ

А. И. Щеголев[1,2] ✉, У. Н. Туманова[1]

[1] Национальный медицинский исследовательский центр акушерства, гинекологии и перинатологии имени В. И. Кулакова, Москва, Россия

[2] Российский национальный исследовательский медицинский университет имени Н. И. Пирогова, Москва, Россия

Представлен анализ данных литературы о времени сохранения SARS-CoV-2 в телах умерших, путях заражения от трупов больных с COVID-19 и необходимых способах защиты от такого заражения. Показано, что для SARS-CoV-2 характерен достаточно длительный период персистенции в тканях и жидкостях тел умерших больных с COVID-19, а также на различных поверхностях, при этом наиболее долго вирус сохраняется на стальных и пластиковых изделиях, находившихся в соприкосновении с трупом. Согласно проанализированным данным, вскрытие тел умерших больных с COVID-19 должно проходить только в специально перепрофилированных отделениях с обязательным соблюдением мер, обеспечивающих биологическую безопасность, сотрудники патологоанатомических отделений и бюро судебно-медицинской экспертизы обязаны соблюдать при этом меры индивидуальной и коллективной защиты.

Ключевые слова: COVID-19, SARS-CoV-2, персистенция, труп, аутопсия, меры защиты

The novel coronavirus infection (2019-nCoV, novel coronavirus disease 2019, abbreviated COVID-19) was first officially reported in 2019 in Wuhan, China. By August 2020, the infection had spread to 213 countries [1]. As of January 1 and May 1, 2021, there were a total of 84,092,619 and 152,196,159 diagnosed COVID-19 cases worldwide, respectively [2].

Approximately 20% of individuals infected with SARS-CoV-2 were hospitalized; of them, about 20% needed intensive care [3]. Of those needing intensive care, 50–80% died; this figure corresponds to 2–4% mortality in countries with resourceful healthcare systems. At the same time, death rates from the coronavirus varied across the world from 0.1% to 14% in May 2020 and from 1.5% to 14% in July 2020. [1]. By May 1, 2021 the total death toll from COVID-19 had reached 3,192,763 [2]. Naturally, healthcare workers and the relatives of COVID-19 victims come in contact with the bodies of the decedents.

One of the most serious challenges facing the medical community today is to understand how the virus can be contracted from the bodies of deceased persons with confirmed or suspected COVID-19.

Routes of microbial transmission from corpses

Throughout its history, mankind has suffered from infectious diseases, including life-threatening infections characterized by high mortality rates. The bodies of diseased individuals have always been thought to be a potential source of infection, and their handling required additional biosafety measures [4].

For example, skin and mucosal infections caused primarily by *Streptococcus pyogenes* (a group A pathogen) and methicillin-resistant *Staphylococcus aureus* (MRSA) can be transmitted through direct contact with the infected skin of the decedent or contaminated fomites. There is a risk of contracting noxious microorganisms, like *Salmonella typhi*, which causes typhoid fever, and *Hepatovirus A*, the causative agent of viral hepatitis A, through direct contact with the stools of the infected person or contaminated fomites.

Airborne transmission is typical for *Mycobacterium tuberculosis*; therefore, autopsy suite staff and morgue workers are at high risk for tuberculosis [5]. The increased risk of TB among funeral home workers handling the bodies of TB-afflicted individuals is inferred from their tuberculin skin

test results [6]. Notably, formalin used for tissue fixation is a tuberculocidal agent.

Direct contact with blood or other bodily fluids coming, among other things, from skin wounds can result in contracting hepatitis B, C (*Hepacivirus B* and *C*) and AIDS-causing HIV (Human Immunodeficiency Virus) [4]. Viable HIV was isolated from the bone fragments, spleen, brain, bone marrow and lymph nodes of an AIDS patient during the autopsy performed 6 days postmortem [7]. Moreover, HIV was detected in the pleural and pericardial effusions and blood of human corpses stored at 2 °C for 16.5 days after death [8]. Direct contact with infected bodily fluids like blood, saliva, sweat, or urine can result in the transmission of Ebola virus (*Ebolavirus*), Marburg virus (*Marburgvirus*) and Lassa hemorrhagic fever (*Lassa mammarenavirus*), all of which are endemic to Africa.

The decision to perform an autopsy on a patient who fell victim to an infectious disease was always based on the careful consideration of the causative agent, biosafety and the existing policies on human autopsies.

In the USSR, an autopsy was mandatory in the case of death from a highly infectious disease, and the organs of the decedent were subjected to a histopathological and bacteriological/virological examination [9]. However, autopsies were prohibited if death was caused by anthrax (regardless of its form) bacteriologically confirmed during life. Today, an autopsy is mandatory in the case of death from a suspected or confirmed infectious disease [10].

Autopsy and SARS-CoV-2

SARS-CoV-2 is a representative of group II pathogens, i.e. those that cause highly contagious epidemic diseases in humans. In Russia, autopsies are performed on all deceased individuals with COVID-19.

That said, some foreign authors think that it is unreasonable to perform an autopsy on a patient infected with SARS-CoV-2. For instance, some Polish forensic pathologists hold the opinion that there are no medical indications for autopsy in the case of death from confirmed SARS-CoV-2 [11]. Italian researchers think that autopsy on a COVID-19 patient should be well-justified, but propose no criteria for such justification [12].

Interestingly, medical autopsies are not performed routinely in China. At the outset of the epidemic in China, the bodies of patients with COVID-19 were not autopsied, but later administrative authorization was obtained to perform autopsies on COVID-19 patients, with strict adherence to biosafety guidelines. However, at that time there were not enough autopsy suites in Wuhan meeting the stringent biosafety requirements [13].

In the spring of 2020, there was a surge in COVID-19 cases in Italy. On April 1, 2020 the Ministry of Healthcare of Italy issued a recommendation to avoid autopsies or postmortem diagnostic examinations on corpses infected COVID-19 [14].

At the outset of the epidemic, the Robert Koch Institute, one of the leading research facilities in Germany, advised against performing autopsies on patients with COVID-19; so postmortem examinations were carried out only in some parts of the country [15]. However, in Hamburg, the second largest German city with 1.8 million population, all necessary arrangements were made in the early stage of the epidemic to ensure that full autopsies could be performed on COVID-19 victims [15].

Despite the diversity of opinions and autopsy policies, one of the major arguments in favor of autopsies during the coronavirus pandemic is the need to determine the exact cause of death, be it COVID-19 or a preexisting condition. Besides, the main body of knowledge about morphological changes and organ pathology associated with COVID-19 came from the autopsies and full pathomorphological examinations of COVID-19 patients' organs and tissues.

So far, we know that COVID-19 is caused by SARS-CoV-2, one of 7 human coronaviruses [16]. This enveloped single-stranded RNA β-coronavirus has the largest genome known and a crown-like appearance visible under a microscope.

Similar to other coronaviruses, SARS-CoV-2 has 4 basic structural components: spikes (S), a membrane (M), an envelope (E) and a nucleocapsid (N). It has been established that the S protein helps the virus latch onto and enter the host cell. The C-terminal domain of the S protein binds to a human angiotensin converting enzyme 2 (hACE2) receptor expressed on the cell surface and thus mediates fusion of the virus membrane and the plasma membrane of the host cell, resulting in endocytosis and infection [17].

This mechanism is analogous to that employed by SARS-CoV, but according to electronic microscopy data, the affinity of the SARS-CoV-2 S protein for ACE2 is 10-20 times higher than that of SARS-CoV [18], which presumably determines the high transmissibility of the novel coronavirus.

A study has identified potential routes of entry and target sites for SARS-CoV-2 based on the information about the sites of ACE2 expression [19]. ACE2 is expressed in the alveolar type II cells of the lungs, cardiomyocytes, the epithelial lining of the renal proximal tubule, the esophagus, ileal epithelial cells, the epithelium of the urinary bladder, lymph nodes, the thymus, the bone marrow, the spleen, the liver and the brain [20]. ACE2 receptors also occur on the surface of keratinocytes, fibroblasts, endothelial cells, osteoblasts and osteoclasts.

Consequently, autopsies followed by immunohistological and molecular biological analysis were instrumental in describing changes to the organs and tissues of COVID-19 patients, mapping them against infection sites and the sites of SARS-CoV-2 receptors and determining the time interval during which the viral RNA is present in the tissues of a dead infected patient.

Coronaviruses have been known to persist in the organs and tissues of dead infected patients since 2007 [21]. A comparative postmortem analysis of viral load in the internal organs of 7 patients who had died from severe acute respiratory syndrome (SARS) revealed that the SARS–CoV/GAPDH RNA ratio was the highest (≥ 1) in the lungs and small bowel and was < 1 in the heart, spleen and kidneys. Time from death to tissue sampling for PCR was 90–180 h. Unfortunately, the researchers failed to find out how virulent the viral particles were [21].

Reportedly, SARS-CoV-2 is detected in the organs and tissues of dead patients who tested positive for this virus during life. For example, of all nasopharyngeal swabs collected from 29 patients with COVID-19 2–24 h postmortem, 10 were positive for SARS-CoV-2 2 h and 4 h after death, 9 were positive 6 h after death and 7 were positive 12 h postmortem [22]. Remarkably, the nasopharyngeal swabs obtained from the forensic pathologists performing the autopsies were all negative. Another study compared the results of antemortem and postmortem nasopharyngeal COVID-19 swab testing [23]. Antemortem swabs were collected 2–14 days before death. Comparison of SARS-CoV-2 RNA levels in the obtained specimens demonstrated the high viability of the viral RNA in the bodies within 2.7–482.6 h after death. The authors note that all patients had pronounced immunosuppression and their bodies were refrigerated and kept at 4 °C before being autopsied [23].

Another study detected SARS-CoV-2 RNA in the bodies of 4 patients with SARS-CoV-2 infection confirmed during life: a full autopsy was performed followed by real-time PCR analysis of the obtained tissue specimens. SARS-CoV-2 RNA was detected in the lung tissue of each body [24]. Besides, one of the decedents had SARS-CoV-2 RNA in their brain, another had the virus in the small intestine and the kidney. Notably, time between the autopsy and death varied from 1 to 17 days.

SARS-CoV-2 might persist in the eyes, specifically in the retina and the vitreous body [25]. A study reports that 2 of 10 vitreous body swabs collected from patients with COVID-19 were positive for SARS-CoV-2 RNA. Importantly, the viral RNA persisted in the vitreous body even after the specimens were stored at –20 °C and then thawed.

There is an interesting case of a 60-year-old male hospitalized after a fall at home; the man died in the hospital the next day [26]. The preliminary cause of death was SARS-CoV-2-associated pneumonia; the infection was comorbid with Steinert's disease and ischemic cardiomyopathy. After death, the patient's body was stored at 4 °C awaiting cremation, which was performed 35 days later. Before cremation, a forensic pathologist collected nasal and oropharyngeal swabs from the decedent; real-time PCR performed the same day, i.e. 35 days after death, detected the presence of SARS-CoV-2 RNA in the swabs. The authors of the cited article think that the long persistence of SARS-CoV-2 RNA could be explained by the absence of antiviral therapy and the temperature of the mortuary refrigerator (4 °C) [28].

SARS-CoV-2 was also detected in the decomposing tissues of a human corpse subjected to a postmortem examination 17 days after death [24]. There is a report of SARS-CoV-2 presence in necrotic placental villi collected from a pregnant woman with COVID-19; the virus was detected immunohistochemically in the reaction with anti-SARS-CoV-2 Nucleocapsid antibodies [27].

Coronaviruses can persist on non-biological surfaces like metal, plastic, paper, and glass [28]. The endemic human coronavirus strain HCoV-229E remains infectious on different types of surfaces from 2 h to 9 days. TGEV (*transmissible gastroenteritis virus*) and MHV (*mouse hepatitis virus*) are reported to persist for up to 28 days at 4 °C. At higher temperatures (30 °C or 40 °C), the duration of highly pathogenic MERS-CoV (*Middle East respiratory syndrome coronavirus*), TGEV and MHV is shorter. At room temperature, HCoV-229E persists longer at 50% vs 30% relative humidity.

A comparative study of stability and decay rates of SARS-CoV-2 and SARS-CoV-1 in aerosols and on 4 different surfaces (plastic, stainless steel, copper and cardboard) showed that SARS-CoV-2 remained viable in aerosols for 3 h, but its tissue-culture infectious dose TCID50, which kills 50% of monolayer cells, was decreasing over time from 103.5 to 102.7 per liter of air. For SARS-CoV-1, TCID50 went down from 104.3 to 103.5 per liter of air.

At the same time, viable SARS-CoV-2 was detected on plastic and stainless steel after 72 h and 48 h, respectively, with TCID50 falling from 103.7 to 100.6 per milliliter of medium. The dynamics of SARS-CoV-1 concentrations were the same. On cardboard and copper, no viable SARS-CoV-2 was detected after 24 h and 4 h, respectively; viable SARS-CoV-1 was no longer detected on these surfaces after 8 h [29]. For SARS-CoV-2, the longest viability was on stainless steel and plastic. These are the materials dissection tables, autopsy instruments and body bags are made of. This is an important factor that needs to be accounted for when developing biosafety and disinfection guidelines for autopsy suites.

An example to illustrate this point is an incident with the Diamond Princess cruise ship: SARS-CoV-2 RNA was detected on various surfaces in the cabins 17 days after all symptomatic and asymptomatic patients with COVID-19 had come ashore [30]. Of 3,711 passengers and crew members, 712 (19.2%) tested positive for SARS-CoV-2; of them 331 (46.5%) had no clinical symptoms at the time of testing.

It should be born in mind that viral transmission is determined by the type of the virus and the duration of contact. It is reported that 31.6% of influenza A virus and 1.5% of parainfluenza virus was transferred from the surface contaminated with influenza A and parainfluenza, respectively, to a hand during a 5-second-long contact between the hand and the surface [31]. Interestingly, students touch their faces 23 times an hour on average; skin is the most touched organ (56%), followed by the mouth (16%), nose (14%) and eyes (12%) [28].

Unfortunately, despite a wealth of reports, there is no clarity on how long the novel coronavirus persists in the organs and tissues of deceased patients with COVID-19, and no clear correlations between the results of PCR testing for SARS-CoV-2 RNA and the results of culture tests have been established. Post- and antemortem studies of tissue samples collected from patients with COVID-19 could shed more light on these issues [32].

Considering that organs and tissues of deceased individuals with COVID-19, as well as equipment, instruments and other items used for their transportation, storage and autopsying, may contain or be contaminated with viral particles, they can be the source of infection for autopsy suite staff and funeral home workers. SARS-CoV-2 is transmitted via respiratory droplets, through direct contact, via the fecal-oral and airborne routes.

Although there are few reports of COVID-19 infection among dissection room staff unsupported by strong evidence of SARS-CoV-2 transmission during autopsies [33], deaths of medical and forensic pathologists who performed autopsies on "red zone" patients suggest that such transmission is highly probable.

Biosafety measures against SARS-CoV-2

This leads us to conclude that the respiratory tract specimens of any human corpse must be PCR-tested for SARS-CoV-2 to ensure safety of autopsy suite staff [34]. A positive SARS-CoV-2 test is not a pretext for not performing an autopsy; it is a warning that adequate biosafety measures should be taken to protect the personnel.

All foreign and Russian guidelines on the safe handling of deceased persons with COVID-19 prescribe that personal protective equipment (PPE), i.e. gloves and a disposable gown, should be worn by the involved staff (see Table). Additionally, in some countries, including China [35] and India [36], a water-resistant apron, googles and a face shield must be worn. A body of a patient with COVID-19 must be transported to a morgue as soon as possible. According to Chinese [35] and Indian [36] guidelines, the skin of the deceased person must be disinfected; wounds must be disinfected and dressed with impermeable material. Natural body orifices, including the mouth, nose and anus, must be plugged. In accordance with Russian guidelines, all natural body orifices must be plugged with cotton balls and wounds must be dressed with gauze soaked in a 3,000–5,000 mg/L chlorine-based disinfectant or 0.5% peracetic acid [43].

In most countries, bodies are transported to morgues in leak-proof plastic body bags to prevent contact with the body or bodily fluids. In China [35] and India [36] body bags must be wrapped in a mortuary sheet. According to Indian guidelines, corpses infected with SARS-CoV-2 must be stored separately

Table. Personal protective equipment recommended for staff involved in the handling and autopsying of dead bodies of patients with COVID-19

Source	Standard PPE	Water-resistant apron	Face shield	Googles	Double gloves
No autopsy performed					
China [35]	+	+	+	+	
India [36]	+	+	+	+	
USA [37]	+		+	+	
Netherlands [38]	+		–	–	
UK [39]	+		+	+	
Europe [40]	+				
WHO [41]	+	+	+	+	
During autopsy					
China [35]	+	+	+		+
India [36]	+	+	+	+	+
USA [37]	+	+	+	+	+
UK [39]	+	+	+	+	+
Germany [42]	+	+	+	+	+
Europe [40]	+		+	+	+
WHO [41]	+	+	+	+	+

Note: standard PPE are gloves, a disposable gown and hand hygiene.

from SARS-CoV-2 negative bodies in a room fitted with an autonomous ventilation system [36]. In Germany, the body of a patient with COVID-19 must be wrapped in a double-layer sheet treated with a disinfectant, placed into a double-layer leak-proof bag and then placed into a casket, which must be immediately sealed [42].

A pathologist must follow stringent biosafety guidelines while performing an autopsy on a COVID-19 patient. In our opinion, Russia can boast the most effective biosafety measures for the handling of dead bodies with COVID-19. The Ministry of Healthcare of Russia requires that autopsies on COVID-19 patients should be performed at specially conditioned facilities [44]. In Moscow, some anatomic pathology units have been modernized to ensure compliance with the biosafety guidelines of the Russian Ministry of Healthcare [45].

In Russia, autopsies must be conducted in a negative pressure room with 6 air changes per hour (for existing facilities) or 12 air changes per hour (for newly built or renovated facilities); air must be exhausted directly outside or HEPA-filtered [43]. In UK [39] and India [36] autopsies must be performed in a properly ventilated negative pressure room fitted with a down-draught table. In Germany, autopsies must be performed in a separate building with autonomous sewage and ventilation systems and shower cabins for staff [42].

In Russia, the number of people in the dissection room must be limited to those participating in autopsying and tissue sampling, i.e. a pathologist, a laboratory assistant and a diener. Medical and forensic autopsies of persons with COVID-19 must be performed in the presence of a federal state sanitary and epidemiological surveillance representative [43]. However, this requirement does not apply to the anatomic pathology units of Moscow specially conditioned for autopsying COVID-19 patients and authorized for such procedures by Rospotrebnadzor [45]. The autopsy itself is performed and supervised by the head of the unit or the most experienced pathologist [43]. Paradoxically, some foreign researchers think that experienced autopsy pathology trainees, including pregnant trainees, can be recruited for autopsies on COVID-19 patients [46].

All foreign guidelines require that a pathologist performing an autopsy should wear standard PPE, including gloves and a disposable gown, and practice good hand hygiene (see Table). In Germany [42] and India [36], the standard PPE set is complemented by double gloves. In the USA [37], UK [39] and Germany [42], a protective whole-body gown and vented respirators are recommended.

According to Russian guidelines [43], a pathologist involved in autopsying a person with COVID-19 must wear:
– double surgical gloves with a layer of cut-proof synthetic mesh;
– a disposable water-resistant or impermeable long-sleeved protective garment (a surgical scrub suit, a gown);
– a water-resistant apron;
– a plastic face shield or googles to protect the face and the eyes from splashes of fluid;
– a disposable respirator with the high level of respiratory protection;
– disposable shoe covers, a surgical cap.

Alternatively, a pathologist can wear type I or II biohazard suit and "Quartz" PPE or type II biohazard suit plus double surgical gloves with a layer of cut-proof synthetic mesh, googles, an oilcloth or polyethylene apron, protective sleeve covers and an FFP3 respirator. Quartz-1M protective wear for infectious disease specialists is also recommended [44].

Most guidelines advise against procedures accompanied by inadvertent splashes (from high-pressure water jets or placing a cadaver in the water) and aerosol generation or recommend they should be minimized. Russian guidelines suggest the "dry autopsy" approach [43–45]. Using an oscillating saw is not recommended or the saw should be attached to a vacuum shroud to contain bone dust; biological specimen should be collected using a sterile instrument set.

In India [36], UK [39] and Germany [42] autopsies are performed by dissecting body cavities consecutively. Some researchers suggest that a staged autopsy protocol should be applied [46]: first, a biological specimen is collected for SARS-CoV-2 testing and then a full autopsy is carried out.

Some international authors insist on a minimally invasive autopsy in the case of a COVID-19 patient: tissue and fluid specimens are collected based on antemortem and/or postmortem radiographic data [13, 47]. CT complemented by a histopathological examination is increasingly employed for

postmortem imaging of lung tissue in adult patients [48, 49]. In the case of a neonatal death, a postmortem MRI examination is recommended, since it can effectively and reliably verify congenital pneumonia [50, 51]. Postmortem ultrasonography can be used to accurately collect tissue specimens while minimizing the risk of infection at autopsy [52]. However, in order to prevent artifacts, postmortem ultrasonography should be conducted no sooner than 1–2 h after the body has been retrieved from the mortuary refrigerator and reached room temperature [52].

The final stage of any autopsy involves disinfection of the cadaver's skin, medical instruments and the dissection room itself. For skin disinfection, sodium hypochlorite (1% or 5.25%) is recommended. All surfaces that come in contact with the dead body must be cleared of all visible stains and decontaminated with sodium hypochlorite or 70% ethanol. In Germany, it is prohibited to drain wastewater down the shared drain [42], and air in the dissecting room must be disinfected with an ultraviolet lamp for 1 h and filtered for 2 h [42].

Russian researchers [43–45] advise against embalming; instead, the body should be placed in a plastic body bag, the outer surface of the bag should be disinfected and left in the storage room until the funeral. Before the body is collected by the relatives, it should be placed in the second plastic bag, the outer surface of the bag should be disinfected, and then placed into a casket, which should be then sealed for further burying or cremation. In China [35] and India [36] the embalming of bodies infected with COVID-19 is prohibited. Almost in every country a physical contact with the body is not recommended, except the Netherlands [38], where touching is allowed, providing that good hand hygiene is practiced. In China, the bodies of patients with COVID-19 are subjected to cremation [35]; in Germany, it is allowed to bury the bodies if the grave is at least 2 m deep [42].

CONCLUSION

SARS-CoV-2 persists for quite long in the tissues and bodily fluids of decedents with COVID-19 and on various surfaces that come in contact with the infected deceased person. The longest viability of the virus is on stainless steel and plastic surfaces. Autopsies on decedents with COVID-19 must be performed at specially conditioned facilities ensuring biosafety of the involved personnel. Medical and forensic pathologists and other mortuary workers must adhere to stringent biosafety requirements imposed by the existing guidelines.

References

1. Matta S, Chopra KK, Arora VK. Morbidity and mortality trends of Covid 19 in top 10 countries. Indian J Tuberc. 2020; 67 (4S): S167–S172.
2. Publichnyj dashbord Yandex DataLens. Available from: https://datalens.yandex/7o7is1q6ikh23?tab=0Ze&utm_source=cbmain&state=7e29b15887.
3. Sekhawat V, Green A, Mahadeva U. COVID-19 autopsies: conclusions from international studies. Diagn Histopathol (Oxf). 2021; 27 (3): 103–7.
4. Aubert AC, Lampurlanés XS. Servicios funerarios: exposición laboral a agentes biológicos. Notas Técnicas de Prevenció. 2010; 858: 1–6.
5. Sterling TR, Pope DS, Bishai WR, Harrington S, Gershon RR, Chaisson RE. Transmission of mycobacterium tuberculosis from a cadaver to an embalmer. N Engl J Med. 2000; 342 (4): 246–8.
6. Gershon RR, Vlahov D, Escamilla-Cejudo JA, Badawi M, McDiarmid M, Karkashian C. et al. Tuberculosis risk in funeral home employees. J Occup Environ Med. 1998; 40 (5): 497–503.
7. Nyberg M, Suni J, Haltia M. Isolation of human immunodeficiency virus infection in health care workers. Arch Intern Med. 1990; 153: 1451–8.
8. Douceron H, Deforges L, Gherardi R, Sobel A, Chariot P. Long-lasting postmortem viability of human immunodeficiency virus: A potential risk in forensic medicine practice. Forensic Sci Int. 1993; 60 (1–2): 61–6.
9. Instrukcii o protivojepidemicheskom rezhime raboty s materialom, zarazhennym ili podozritel'nym na zarazhennost' vozbuditeljami chumy, holery, sapa, melioidoza, natural'noj ospy, sibirskoj jazvy, tuljaremii i brucelleza, Ministerstvo zdravoohranenija SSSR. Alma-Ata, 1975.
10. Federal'nyj zakon "Ob osnovah ohrany zdorov'ja grazhdan v Rossijskoj Federacii" ot 21.11.2011 N 323-FZ.
11. Teresiński G, Jurek T. Recommendations of the polish society of forensic medicine and criminology and national consultant for forensic medicine with regard to performing forensic post-mortem examinations in case of confirmed COVID-19 disease and suspected SARS CoV-2 infections. Arch Med Sadowej Kryminol. 2019; 69 (4): 147–57.
12. Sapino A, Facchetti F, Bonoldi E, Gianatti A, Barbareschi M, Società Italiana di Anatomia Patologica e Citologia — SIAPEC. The autopsy debate during the COVID-19 emergency: the Italian experience. Virchows Arch. 2020; 476 (6): 821–3,
13. Tian S, Xiong Y, Liu H, Niu L, Guo J, Liao M, et al. Pathological study of the 2019 novel coronavirus disease (COVID-19) through postmortem core biopsies. Mod Pathol. 2020; 33 (6): 1007–14.
14. Moretti M, Malhotra A, Visonà SD, Finley SJ, Osculati AMM, Javan GT. The roles of medical examiners in the COVID-19 era: a comparison between the United States and Italy. Forensic Sci Med Pathol. 2021; 17 (2): 262–70.
15. Sperhake JP. Autopsies of COVID-19 deceased? Absolutely! Leg Med (Tokyo). 2020; 47: 101769.
16. Zhu N, Zhang D,Wang W, Li X, Yang B, Song J, et al. A novel coronavirus from patients with pneumonia in China, 2019. N Engl J Med. 2020; 382 (8): 727–33.
17. He F, Deng Y, Li W. Coronavirus disease 2019: What we know? J Med Virol. 2020; 92 (7): 719–25.
18. Wrapp D, Wang N, Corbett KS, Goldsmith JA, Hsieh CL, Abiona O, et al. Cryo-EM structure of the 2019-nCoV spike in the prefusion conformation. Science. 2020; 367 (6483): 1260–3.
19. Xu H, Zhong L, Deng J, Peng J, Dan H, Zeng X, et al. High expression of ACE2 receptor of 2019-nCoV on the epithelial cells of oral mucosa. Int J Oral Sci. 2020; 12 (1): 8.
20. Zou X, Chen K, Zou J, Han P, Hao J, Han Z. Single-cell RNA-seq data analysis on the receptor ACE2 expression reveals the potential risk of different human organs vulnerable to 2019-nCoV infection. Front Med. 2020; 14 (2): 185–92.
21. Tang JW, To KF, Lo AW, Sung JJ, Ng HK, Chan PK. Quantitative temporal-spatial distribution of severe acute respiratory syndrome-associated coronavirus (SARSCoV) in post-mortem tissues. J Med Virol. 2007; 79 (9): 1245–53.
22. Aquila I, Ricci P, Bonetta CF, Sacco MA, Longhini F, Torti C, et al. Analysis of the persistence time of the SARS-CoV-2 virus in the cadaver and the risk of passing infection to autopsy staff. Med Leg J. 2021; 89 (1): 40–53.
23. Heinrich F, Meißner K, Langenwalder F, Püschel K, Nörz D, Hoffmann A, et al. Postmortem stability of SARS-CoV-2 in nasopharyngeal mucosa. Emerg Infect Dis. 2021; 27 (1): 329–31.
24. Plenzig S, Bojkova D, Held H, Berger A, Holz F, Cinatl J, et al. Infectivity of deceased COVID-19 patients. Int J Legal Med. 2021 Mar 5; 1–6.
25. Bogdanović M, Skadrić I, Atanasijević T, Stojković O, Popović V, Savić S, et al. Case Report: Post-mortem histopathological and molecular analyses of the very first documented COVID-19-related death in Europe. Front Med. 2021; 8: 612758.

26. Beltempo P, Curti SM, Maserati R, Gherardi M, Castelli M. Persistence of SARS-CoV-2 RNA in post-mortem swab 35 days after death: A case report. Forensic Sci Int. 2021; 319: 110653.

27. Sukhikh G, Petrova U, Prikhodko A, Starodubtseva N, Chingin K, Chen H, et al. Vertical transmission of SARS-CoV-2 in second trimester associated with severe neonatal pathology. Viruses. 2021; 13: 447.

28. Kampf G, Todt D, Pfaender S, Steinmann E. Persistence of coronaviruses on inanimate surfaces and their inactivation with biocidal agents. J Hosp Infect. 2020; 104 (3): 246–51.

29. van Doremalen N, Bushmaker T, Morris DH, Holbrook MG, Gamble A, Williamson BN, et al. Aerosol and surface stability of SARS-CoV-2 as compared with SARS-CoV-1. N Eng J Med. 2020; 382 (16): 1564–7.

30. Leah FM, Plucinski MM, Marston BJ, Kurbatova EV, Knust B, Murray EL, et al. Public health responses to COVID-19 outbreaks on cruise ships — worldwide, February–March 2020. MMWR Morb Mortal Wkly Rep. 2020; 69 (12): 347–52.

31. Ansari SA, Springthorpe VS, Sattar SA, Rivard S, Rahman M. Potential role of hands in the spread of respiratory viral infections: studies with human parainfluenza virus 3 and rhinovirus 14. J Clin Microbiol. 1991; 29 (10): 2115–9.

32. Cevik M, Tate M, Lloyd O, Maraolo AE, Schafers J, Ho A. SARS-CoV-2, SARS-CoV, and MERS-CoV viral load dynamics, duration of viral shedding, and infectiousness: a systematic review and meta-analysis. Lancet Microbe. 2021; 2: e13–22.

33. Davis GG, Williamson AK. Risk of Coronavirus Disease 2019 transmission during autopsy. Arch Pathol Lab Med. 2020; 144 (12): 1445a–1445.

34. Nakamura M, Tojo M, Takaso M, Hitosugi M. A regional approach for infection prevention in death investigations during the COVID-19 era. Leg Med (Tokyo). 2021; 48: 101829.

35. Centre for Health Protection. Precautions for Handling and Disposal of Dead Bodies, Hong Kong, China, 2020. Available from: https://www.chp.gov.hk/files/pdf/grp-guideline-hp-ic-precautions_for_handling_and_disposal_of_dead_bodies_en.pdf.

36. Government of India Ministry of Health & Family Welfare Directorate General of Health Services. COVID-19: Guidelines on dead body management, India, 2020. Available from: https://www.mohfw.gov.in/pdf/1584423700568_COVID19GuidelinesonDeadbodymanagement.pdf.

37. Centers for Disease Control and Prevention. Collection and Submission of Postmortem Specimens from Deceased Persons with Known or Suspected COVID-19 (Postmortem Guidance). Available from: https://www.cdc.gov/coronavirus/2019-ncov/hcp/guidance-postmortem-specimens.html.

38. Rijksinstituut voor Volksgezondheid en Milieu. COVID-19 richtlijn (guideline). Available from: https://lci.rivm.nl/richtlijnen/covid-19.

39. Health and Safety Executive. Managing infection risks when handling the deceased. Guidance for the mortuary, post-mortem room and funeral premises, and during exhumation. Available from: https://www.hse.gov.uk/pUbns/priced/hsg283.pdf.

40. European Centre for Disease Prevention and Control. Considerations related to the safe handling of bodies of deceased persons with suspected or confirmed COVID-19, Europe, 2020. Available from: https://www.ecdc.europa.eu/en/publications-data/considerations-related-safe-handling-bodies-deceased-persons-suspected-or.

41. WHO Guidelines. Infection prevention and control of epidemic- and pandemic-prone acute respiratory infections in health care — WHO Guidelines. Available from: https://apps.who.int/iris/bitstream/handle/10665/112656/9789241507134_eng.pdf?sequence=1.

42. Keten D, Okdemir E, Keten A. Precautions in postmortem examinations in Covid-19 — Related deaths: Recommendations from Germany. J Forensic Leg Med. 2020; 73: 102000.

43. Frank GA, Kovalev AV, Gribunov YuP, Zaslavskij GI, Kildjushov EM, Jagmurov OD, i dr. Issledovanie umershih s podozreniem na koronavirusnuju infekciju (COVID-19). V sbornike: Vremennye metodicheskie rekomendacii. Versija 22 (23.07.2020). M., 2020; 428 s. Russian.

44. Vremennye metodicheskie rekomendacii: profilaktika, diagnostika i lechenie novoj koronavirusnoj infekcii (COVID-19). Versija 10 (08.02.2021). M., 2021; 262 s. Russian.

45. Zajratyanc OV, Kanibolockij AA, Mihaleva LM, Mishnev OD, Savelov NS, Avdalyan AM, i dr. Novaja koronavirusnaja infekcija (COVID-19). Organizacija raboty patologoanatomicheskoj sluzhby. V sbornike: Vremennye metodicheskie rekomendacii. Versija 3 (15.11.2020). M., 2020; 36 s. Russian.

46. Hanley B, Lucas SB, Youd E, Swift B, Osborn M. Autopsy in suspected COVID-19 cases. J Clin Pathol. 2020; 73: 239–42.

47. Monteiro RAA, Duarte-Neto AN, Silva LFFD, Oliveira EP, Filho JT, Santos GABD, et al. Ultrasound-guided minimally invasive autopsies: A protocol for the study of pulmonary and systemic involvement of COVID-19. Clinics (Sao Paulo). 2020; 75: e1972.

48. Roberts IS, Benamore RE, Benbow EW, Lee SH, Harris JN, Jackson A, et al. Post-mortem imaging as an alternative to autopsy in the diagnosis of adult deaths: a validation study. Lancet. 2012; 379 (9811): 136–42.

49. Kniep I, Lutter M, Ron A, Edler C, Püschel K, Ittrich H, et al. Postmortem imaging of the lung in cases of COVID-19 deaths. Radiologe. 2020; 60 (10): 927–33.

50. Tumanova UN, Lyapin VM, Bychenko VG, Shchegolev AI, Sukhikh GT. Posmertnaja MRT dlja diagnostiki vrozhdennoj pnevmonii. Vestnik Rossijskogo gosudarstvennogo medicinskogo universiteta. 2016; 4: 48–55. Russian.

51. Tumanova UN, Shchegolev AI. Vozmozhnosti i ogranichenija virtual'noj autopsii v neonatologii. REJR. 2017; 7 (1): 20–33. Russian.

52. Kanchan T, Shrestha R, Krishan K. Post-mortem ultrasonography: a safer alternative to autopsies in COVID-19 deaths. J Ultrasound. 2020 Oct 31; 1–2.

Литература

1. Matta S, Chopra KK, Arora VK. Morbidity and mortality trends of Covid 19 in top 10 countries. Indian J Tuberc. 2020; 67 (4S): S167–S172.

2. Публичный дашборд Yandex DataLens. Available from: https://datalens.yandex/7o7is1q6ikh23?tab=0Ze&utm_source=cbmain&state=7e29b15887.

3. Sekhawat V, Green A, Mahadeva U. COVID-19 autopsies: conclusions from international studies. Diagn Histopathol (Oxf). 2021; 27 (3): 103–7.

4. Aubert AC, Lampurlanés XS. Servicios funerarios: exposición laboral a agentes biológicos. Notas Técnicas de Prevenció. 2010; 858: 1–6.

5. Sterling TR, Pope DS, Bishai WR, Harrington S, Gershon RR, Chaisson RE. Transmission of mycobacterium tuberculosis from a cadaver to an embalmer. N Engl J Med. 2000; 342 (4): 246–8.

6. Gershon RR, Vlahov D, Escamilla-Cejudo JA, Badawi M, McDiarmid M, Karkashian C. et al. Tuberculosis risk in funeral home employees. J Occup Environ Med. 1998; 40 (5): 497–503.

7. Nyberg M, Suni J, Haltia M. Isolation of human immunodeficiency virus infection in health care workers. Arch Intern Med. 1990; 153: 1451–8.

8. Douceron H, Deforges L, Gherardi R, Sobel A, Chariot P. Long-lasting postmortem viability of human immunodeficiency virus: A potential risk in forensic medicine practice. Forensic Sci Int. 1993; 60 (1–2): 61–6.

9. Инструкции о противоэпидемическом режиме работы с материалом, зараженным или подозрительным на зараженность возбудителями чумы, холеры, сапа, мелиоидоза, натуральной оспы, сибирской язвы, туляремии и бруцеллеза, Министерство здравоохранения СССР. Алма-Ата, 1975.

10. Федеральный закон «Об основах охраны здоровья граждан в Российской Федерации» от 21.11.2011 N 323-ФЗ.

11. Teresiński G, Jurek T. Recommendations of the polish society of forensic medicine and criminology and national consultant for forensic medicine with regard to performing forensic post-mortem examinations in case of confirmed COVID-19 disease and suspected SARS CoV-2 infections. Arch Med Sadowej Kryminol. 2019; 69 (4): 147–57.

12. Sapino A, Facchetti F, Bonoldi E, Gianatti A, Barbareschi M,

Società Italiana di Anatomia Patologica e Citologia — SIAPEC. The autopsy debate during the COVID-19 emergency: the Italian experience. Virchows Arch. 2020; 476 (6): 821–3,

13. Tian S, Xiong Y, Liu H, Niu L, Guo J, Liao M, et al. Pathological study of the 2019 novel coronavirus disease (COVID-19) through postmortem core biopsies. Mod Pathol. 2020; 33 (6): 1007–14.

14. Moretti M, Malhotra A, Visonà SD, Finley SJ, Osculati AMM, Javan GT. The roles of medical examiners in the COVID-19 era: a comparison between the United States and Italy. Forensic Sci Med Pathol. 2021; 17 (2): 262–70.

15. Sperhake JP. Autopsies of COVID-19 deceased? Absolutely! Leg Med (Tokyo). 2020; 47: 101769.

16. Zhu N, Zhang D,Wang W, Li X, Yang B, Song J, et al. A novel coronavirus from patients with pneumonia in China, 2019. N Engl J Med. 2020; 382 (8): 727–33.

17. He F, Deng Y, Li W. Coronavirus disease 2019: What we know? J Med Virol. 2020; 92 (7): 719–25.

18. Wrapp D, Wang N, Corbett KS, Goldsmith JA, Hsieh CL, Abiona O, et al. Cryo-EM structure of the 2019-nCoV spike in the prefusion conformation. Science. 2020; 367 (6483): 1260–3.

19. Xu H, Zhong L, Deng J, Peng J, Dan H, Zeng X, et al. High expression of ACE2 receptor of 2019-nCoV on the epithelial cells of oral mucosa. Int J Oral Sci. 2020; 12 (1): 8.

20. Zou X, Chen K, Zou J, Han P, Hao J, Han Z. Single-cell RNA-seq data analysis on the receptor ACE2 expression reveals the potential risk of different human organs vulnerable to 2019-nCoV infection. Front Med. 2020; 14 (2): 185–92.

21. Tang JW, To KF, Lo AW, Sung JJ, Ng HK, Chan PK. Quantitative temporal-spatial distribution of severe acute respiratory syndrome-associated coronavirus (SARSCoV) in post-mortem tissues. J Med Virol. 2007; 79 (9): 1245–53.

22. Aquila I, Ricci P, Bonetta CF, Sacco MA, Longhini F, Torti C, et al. Analysis of the persistence time of the SARS-CoV-2 virus in the cadaver and the risk of passing infection to autopsy staff. Med Leg J. 2021; 89 (1): 40–53.

23. Heinrich F, Meißner K, Langenwalder F, Püschel K, Nörz D, Hoffmann A, et al. Postmortem stability of SARS-CoV-2 in nasopharyngeal mucosa. Emerg Infect Dis. 2021; 27 (1): 329–31.

24. Plenzig S, Bojkova D, Held H, Berger A, Holz F, Cinatl J, et al. Infectivity of deceased COVID-19 patients. Int J Legal Med. 2021 Mar 5; 1–6.

25. Bogdanović M, Skadrić I, Atanasijević T, Stojković O, Popović V, Savić S, et al. Case Report: Post-mortem histopathological and molecular analyses of the very first documented COVID-19-related death in Europe. Front Med. 2021; 8: 612758.

26. Beltempo P, Curti SM, Maserati R, Gherardi M, Castelli M. Persistence of SARS-CoV-2 RNA in post-mortem swab 35 days after death: A case report. Forensic Sci Int. 2021; 319: 110653.

27. Sukhikh G, Petrova U, Prikhodko A, Starodubtseva N, Chingin K, Chen H, et al. Vertical transmission of SARS-CoV-2 in second trimester associated with severe neonatal pathology. Viruses. 2021; 13: 447.

28. Kampf G, Todt D, Pfaender S, Steinmann E. Persistence of coronaviruses on inanimate surfaces and their inactivation with biocidal agents. J Hosp Infect. 2020; 104 (3): 246–51.

29. van Doremalen N, Bushmaker T, Morris DH, Holbrook MG, Gamble A, Williamson BN, et al. Aerosol and surface stability of SARS-CoV-2 as compared with SARS-CoV-1. N Eng J Med. 2020; 382 (16): 1564–7.

30. Leah FM, Plucinski MM, Marston BJ, Kurbatova EV, Knust B, Murray EL, et al. Public health responses to COVID-19 outbreaks on cruise ships — worldwide, February–March 2020. MMWR Morb Mortal Wkly Rep. 2020; 69 (12): 347–52.

31. Ansari SA, Springthorpe VS, Sattar SA, Rivard S, Rahman M. Potential role of hands in the spread of respiratory viral infections: studies with human parainfluenza virus 3 and rhinovirus 14. J Clin Microbiol. 1991; 29 (10): 2115–9.

32. Cevik M, Tate M, Lloyd O, Maraolo AE, Schafers J, Ho A. SARS-CoV-2, SARS-CoV, and MERS-CoV viral load dynamics, duration of viral shedding, and infectiousness: a systematic review and meta-analysis. Lancet Microbe. 2021; 2: e13–22.

33. Davis GG, Williamson AK. Risk of Coronavirus Disease 2019 transmission during autopsy. Arch Pathol Lab Med. 2020; 144

(12): 1445a–1445.

34. Nakamura M, Tojo M, Takaso M, Hitosugi M. A regional approach for infection prevention in death investigations during the COVID-19 era. Leg Med (Tokyo). 2021; 48: 101829.

35. Centre for Health Protection. Precautions for Handling and Disposal of Dead Bodies, Hong Kong, China, 2020. Available from: https://www.chp.gov.hk/files/pdf/grp-guideline-hp-ic-precautions_for_handling_and_disposal_of_dead_bodies_en.pdf.

36. Government of India Ministry of Health & Family Welfare Directorate General of Health Services. COVID-19: Guidelines on dead body management, India, 2020. Available from: https://www.mohfw.gov.in/pdf/1584423700568_COVID19GuidelinesonDeadbodymanagement.pdf.

37. Centers for Disease Control and Prevention. Collection and Submission of Postmortem Specimens from Deceased Persons with Known or Suspected COVID-19 (Postmortem Guidance). Available from: https://www.cdc.gov/coronavirus/2019-ncov/hcp/guidance-postmortem-specimens.html.

38. Rijksinstituut voor Volksgezondheid en Milieu. COVID-19 richtlijn (guideline). Available from: https://lci.rivm.nl/richtlijnen/covid-19.

39. Health and Safety Executive. Managing infection risks when handling the deceased. Guidance for the mortuary, post-mortem room and funeral premises, and during exhumation. Available from: https://www.hse.gov.uk/pUbns/priced/hsg283.pdf.

40. European Centre for Disease Prevention and Control. Considerations related to the safe handling of bodies of deceased persons with suspected or confirmed COVID-19, Europe, 2020. Available from: https://www.ecdc.europa.eu/en/publications-data/considerations-related-safe-handling-bodies-deceased-persons-suspected-or.

41. WHO Guidelines. Infection prevention and control of epidemic- and pandemic-prone acute respiratory infections in health care — WHO Guidelines. Available from: https://apps.who.int/iris/bitstream/handle/10665/112656/9789241507134_eng.pdf?sequence=1.

42. Keten D, Okdemir E, Keten A. Precautions in postmortem examinations in Covid-19 — Related deaths: Recommendations from Germany. J Forensic Leg Med. 2020; 73: 102000.

43. Франк Г. А., Ковалев А. В., Грибунов Ю. П., Заславский Г. И., Кильдюшов Е. М., Ягмуров О. Д. и др. Исследование умерших с подозрением на коронавирусную инфекцию (COVID-19). В сборнике: Временные методические рекомендации. Версия 22 (23.07.2020). М., 2020; 428 с.

44. Временные методические рекомендации: профилактика, диагностика и лечение новой коронавирусной инфекции (COVID-19). Версия 10 (08.02.2021). М., 2021; 262 с.

45. Зайратьянц О. В., Каниболоцкий А. А., Михалева Л. М., Мишнев О. Д., Савелов Н. С., Авдалян А. М. и др. Новая коронавирусная инфекция (COVID-19). Организация работы патологоанатомической службы. В сборнике: Временные методические рекомендации. Версия 3 (15.11.2020). М., 2020; 36 с.

46. Hanley B, Lucas SB, Youd E, Swift B, Osborn M. Autopsy in suspected COVID-19 cases. J Clin Pathol. 2020; 73: 239–42.

47. Monteiro RAA, Duarte-Neto AN, Silva LFFD, Oliveira EP, Filho JT, Santos GABD, et al. Ultrasound-guided minimally invasive autopsies: A protocol for the study of pulmonary and systemic involvement of COVID-19. Clinics (Sao Paulo). 2020; 75: e1972.

48. Roberts IS, Benamore RE, Benbow EW, Lee SH, Harris JN, Jackson A, et al. Post-mortem imaging as an alternative to autopsy in the diagnosis of adult deaths: a validation study. Lancet. 2012; 379 (9811): 136–42.

49. Kniep I, Lutter M, Ron A, Edler C, Püschel K, Ittrich H, et al. Postmortem imaging of the lung in cases of COVID-19 deaths. Radiologe. 2020; 60 (10): 927–33.

50. Туманова У. Н., Ляпин В. М., Быченко В. Г., Щеголев А. И., Сухих Г. Т. Посмертная МРТ для диагностики врожденной пневмонии. Вестник Российского государственного медицинского университета. 2016; 4: 48–55.

51. Туманова У. Н., Щеголев А. И. Возможности и ограничения виртуальной аутопсии в неонатологии. REJR. 2017; 7 (1): 20–33.

52. Kanchan T, Shrestha R, Krishan K. Post-mortem ultrasonography: a safer alternative to autopsies in COVID-19 deaths. J Ultrasound. 2020 Oct 31; 1–2.

CHANGES IN AMINO ACID PROFILE OF CORD BLOOD PLASMA AND AMNIOTIC FLUID OF MOTHERS WITH COVID-19

Lomova NA ✉, Chagovets VV, Dolgopolova EL, Novoselova AV, Petrova UL, Shmakov RG, Frankevich VE

National Medical Research Center for Obstetrics, Gynecology and Perinatology named after Academician V. I. Kulakov, Moscow, Russia

Neonates born to mothers with COVID-19 are at risk for infection, they may have high risk of complications during the neonatal period, and long-term health consequences. The study was aimed to define the amino acid profile of blood plasma and amniotic fluid in patients with COVID-19 in order to assess the relationship between the COVID-19 infection during the antenatal period, and metabolomic alterations in the "intrauterine" patient. The levels of 31 amino acids in the samples of amniotic fluid and cord blood plasma of pregnant women with COVID-19, obtained during delivery, were assessed by high-performance liquid chromatography-mass spectrometry. The index group included 29 patients with confirmed diagnosis of COVID-19, and the control group included 17 healthy women with uncomplicated pregnancies. There were significant ($p < 0.05$) differences in the concentrations of eight amino acids between the studied groups. Logistic regression models were developed (sensitivity 0.84; specificity 1) making it possible to define, whether the assessed amniotic fluid was obtained from COVID-19 patients. Significant differences in the concentrations of four amino acids were observed in the umbilical cord blood. The models developed made it possible to define whether the studied cord blood plasma belonged to controls or to COVID-19 patients (sensitivity and specificity 1). Three amino acids were detected, and their levels were significantly different in COVID-19 patients simultaneously in two points (amniotic fluid and cord blood plasma), depicting the fetal metabolome in a holistic manner. The impact of the virus on those infected results in pronounced metabolomic alterations in the amniotic fluid and the fetal cord blood plasma, which may lead to impaired programming of protein production, but never show up at birth.

Keywords: amino acid analysis, cord blood plasma, amniotic fluid, COVID-19, markers of neonatal condition

✉ Correspondence should be addressed: Natalia A. Lomova
Oparina, 4, Moscow, 117997; natasha-lomova@yandex.ru

ИЗМЕНЕНИЕ АМИНОКИСЛОТНОГО ПРОФИЛЯ ПЛАЗМЫ ПУПОВИННОЙ КРОВИ И АМНИОТИЧЕСКОЙ ЖИДКОСТИ ОТ МАТЕРЕЙ С COVID-19

Н. А. Ломова ✉, В. В. Чаговец, Е. Л. Долгополова, А. В. Новоселова, У. Л. Петрова, Р. Г. Шмаков, В. Е. Франкевич

Национальный медицинский исследовательский центр акушерства, гинекологии и перинатологии имени В. И. Кулакова, Москва, Россия

Новорожденные от матерей с COVID-19 подвержены риску заражения, могут иметь высокий риск осложнений в раннем неонатальном периоде и отдаленные последствия для здоровья. Цель исследования — определить аминокислотный профиль пуповинной плазмы и амниотической жидкости пациентов с COVID-19 для анализа связи влияния перенесенного антенатально COVID-19 на изменения в метаболоме «внутриутробного пациента». Для оценки уровня 31 аминокислоты в образцах амниотической жидкости и пуповинной плазмы беременных с COVID-19, полученных при родоразрешении, применяли высокоэффективную жидкостную хроматографию с масс-спектрометрической детекцией. Основную группу составили 29 пациенток с подтвержденным диагнозом COVID-19; контрольную — 17 соматически здоровых женщин с беременностью без осложнений. Концентрации восьми аминокислот в амниотической жидкости статистически значимо ($p < 0,05$) различались между исследуемыми группами. Разработаны модели логистической регрессии (чувствительность 0,84; специфичность — 1), позволяющие определять, что анализируемая амниотическая жидкость взята от пациенток, перенесших COVID-19. В плазме пуповинной крови значимые различия обнаружены для четырех аминокислот. Построенные модели позволяют выявлять принадлежность исследуемой пуповинной плазмы пациентам группы контроля или COVID-19 (чувствительность и специфичность — 1). Одновременно в двух точках (амниотическая жидкость и пуповинная плазма), комплексно отображающих метаболом плода, были выявлены и статистически значимо отличались при COVID-19 три аминокислоты. Воздействие вируса на организм приводит к выраженным изменениям в метаболоме амниотической жидкости и пуповинной плазмы плода, что может привести к нарушению программирования производства белковых молекул, но не проявляется при рождении.

Ключевые слова: аминокислотный анализ, плазма пуповинной крови, амниотическая жидкость, COVID-19, маркеры состояния новорожденного

✉ Для корреспонденции: Наталья Анатольевна Ломова
ул. Академика Опарина, д. 4, г. Москва, 117997; natasha-lomova@yandex.ru

The outbreak of severe acute respiratory syndrome, caused by SARS-CoV-2 coronavirus, emerged in Wuhan (China) in 2019, and quickly led to global pandemic, which forced the countries' healthcare systems to provide intensive care to a huge number of patients. The number of cases around the world is increasing every day due to rapid spread of the infection. Currently, only in Russia a total of 4,700,000 confirmed cases of COVID-19 infection have been registered. Pregnant women are a vulnerable population, susceptible to COVID-19 infection due to physiological changes in immunological and blood circulation parameters. Infants, born to mothers infected with COVID-19, are at risk of infection, as well as at high risk of complications during the early neonatal period, and long-term health consequences. Specific consequences of COVID-19 have not yet been studied, however, studies of influenza virus suggest the possibility of such consequences [1, 2]. To date, little is known about perinatal and neonatal COVID-19 infection, and the available information is largely based on the single case reports. One of the earliest and largest studies involved 33 neonates born to mothers with confirmed diagnosis of COVID-19 [3]. Several viral transmission modes were postulated, such as postnatal transmission (horizontal), transplacental transmission, and transmission via amniotic fluid and breast milk [4–12]. The first study describing the clinical features and aimed at investigation of the SARS-CoV-2 vertical transmission possibility in nine pregnant women with laboratory confirmed COVID-19, showed no evidence of vertical transmission [11, 13]. More recently, however, the reports have been published of vertical viral transmission sporadic cases, as well as of severe disease in pregnant women during the antenatal period [14, 15]. Thus, transplacental transmission of the virus has been demonstrated, confirmed by complex virologic testing of placenta, as well as by symptoms and clinical manifestations in newborns [16].

Due to the fundamental reasons, metabolome is a more sensitive and dynamic indicator of cell and body biochemical status, than proteome or transcriptome [17]. Metabolomic analysis of samples obtained from COVID-19 patients enables investigation of biochemical alterations associated with poorly understood pathways, since it demonstrates the effects of the virus on the host instead of just the presence of the infectious agent. Metabolomic research can provide a number of markers, being potentially important for SARS-CoV-2 infection confirmation, as well as for evaluation of the disease severity and possible outcome. Recently it has been shown that plasma levels of 204 metabolites in COVID-19 patients correlate with the disease severity [18]. Amino acids that are part of metabolome are essential for all human life processes. Biological role of about 300 amino acids in the human body is invaluable. The body cannot develop effectively without the sufficient amounts of amino acids. That is why there are optimal levels of amino acids, which ensure the metabolic balance. Inconsistence of amino acid concentrations with reference values can be indicative of certain disorders. Thus, amino acid concentrations change in individuals with sand fly fever virus infection [19], pneumonia, caused by H1N1 influenza virus [20], and chronic obstructive pulmonary disease [21]. A number of neonatal diseases are detected by amino acid assessment in the dried blood spot specimens [22]. In recent years, the assessment of the small-molecule intermediates of metabolic pathways in the biological systems is becoming increasingly important, since it facilitates understanding of human metabolic pathways interaction and regulation. The disease-related alterations in metabolic profiles of human physiological fluids are studied in order to clarify the complex disorders pathophysiology. For example, metabolomic

analysis has shown that alterations in amino acid metabolism correlate with altered oxygen homeostasis in COVID-19 patients [23]. Another study of amino acid profiles in children and adults has revealed alterations, which can be associated with endothelial dysfunction and T-cell dysregulation [24]. Various metabolic pathways can be described by measuring amino acid concentrations [25].

Thus, the study was aimed to determine the effects of COVID-19 on the amino acid composition of amniotic fluid and cord blood plasma in order to develop the diagnostic panel, and to determine the impact of possible amino acid metabolism alteration consequences on the condition of newborns.

METHODS

From March to May 2020 in the National Medical Research Center for Obstetrics, Gynecology and Perinatology named after Academician V. I. Kulakov the "red zone" was established for examination and treatment of patients with COVID-19, pregnant women among them. A total of 190 beds for patients with COVID-19 and 60 beds for obstetric patients were prepared.

A total of 46 pregnant women were enrolled, who were admitted to and gave birth at the National Medical Research Center for Obstetrics, Gynecology and Perinatology named after Academician V. I. Kulakov. The index group included 29 patients with confirmed diagnosis of COVID-19; the control group included 17 healthy women with uncomplicated pregnancies. The diagnosis of COVID-19 was confirmed by PCR test (DNA-Technology; Russia). The patients were included in the group subsequent to their admission. Inclusion criteria for group I: COVID-19 based on the molecular genetic analysis data (PCR); inclusion criteria for group II: no COVID-19 based on the physical examination data and PCR test results. Exclusion criteria: multiple pregnancy; no Rhesus (Rh) or ABO isoimmunization, chromosomal abnormalities, genetic mutations, and congenital malformations in the fetus. Cord blood plasma and amniotic fluid were sampled for analysis.

Biological fluids were sampled in all patients at the 1st Infectious Diseases Department of the National Medical Research Center for Obstetrics, Gynecology and Perinatology named after Academician V. I. Kulakov, the "red zone", followed by sample preparation and storage. Transportation and subsequent analysis were performed within the territory of the National Medical Research Center for Obstetrics, Gynecology and Perinatology named after Academician V. I. Kulakov in the rooms certified for operating hazard class 2 samples. Standard kit and modified protocol were used for sample preparation and subsequent analysis of 31 amino acids in physiological fluids (JASEM; Turkey). The kit contained two different calibration mixtures of lyophilized amino acids, mixture of internal standards, lyophilized mixture for quality control, mobile phases A and B, Reagent 1 (part number JSM-CL-503), used for plasma sample preparations, and the column for high-performance liquid chromatography (HPLC) of amino acids (part number JSM-CL-575).

During preparation for analysis, 50 µL of sample were mixed with 50 µL of the internal standard solution, stirred for 5 s, added 700 µL of Reagent 1, stirred again for 15 s, and centrifuged at 3000 RPM for 3 minutes. After that, supernatant fluid was transferred into chromatography vial. Samples and auxiliary solutions were prepared and stored in accordance with the JASEM manual.

Samples were analyzed by high-performance liquid chromatography-mass spectrometry using the 1260 Infinity II

Table 1. Clinical characteristics of pregnant women with COVID-19

Clinical characteristics	COVID-19 (n = 29, %)
Symptoms	21 (71.41)
Hyperthermia (> 37 °C)	12 (41.38)
Loss of smell	7 (24.14)
Sore throat	3 (10.34)
Shortness of breath	4 (13.79)
Cough	12 (41.38)
Fatigue	4 (13.79)
Mild course	22 (75.86)
Moderate course	6 (20.69)
Severe course	1 (3.45)

HPLC system (Agilent; USA) and the 6460 Triple Quad mass spectrometer system (Agilent; USA).

Transitions from parent ions to daughter fragments for the assayed amino acids, corresponding chromatography retention time values, internal standard concentrations, as well as data on the analysis sensitivity and reproducibility, are presented in the JASEM manual.

Statistical analysis

Statistical data processing was performed using scripts written in R language (R Core Team, Vienna, Austria, and Rstudio; R. RStudio, Inc.; Boston).

Statistical analysis was carried out using the nonparametric Mann–Whitney U test. Quantitative data were described using median (Me) and quartiles Q_1 and Q_3 in the Me format (Q_1; Q_3). The threshold of significance, p-value, was 0.05. When p-value was less than 0.001, it was reported as $p < 0.001$.

The logistic regression models were developed in order to assess whether the patients could be classified into groups based on the studied parameters. All possible combinations of amino acids were treated as dependent variables. The patient's belonging to certain group was considered an independent variable. Four models with maximum area under the ROC curve (AUC) were selected among the developed models. Wald criterion, 95% confidence interval (95% CI), odds ratio (OR) and its confidence interval were defined for each model. The quality of models developed was defined by constructing the ROC curve, calculating the area under the ROC curve, as well as by defining sensitivity and specificity.

RESULTS

A total of 46 women were enrolled: of them 29 patients were admitted to hospital because of confirmed COVID-19, and 17 patients had no viral infection (control group). The average age of the patients was 30.7 ± 4.9 years: 29.9 ± 5.03 years in group 1, and 32.0 ± 5.03 in the control group. There were no significant differences in the body mass index between two groups: it was 27.85 ± 4.52 in the first group, and 26.12 ± 3.16 in the second group.

The major clinical manifestations were as follows: cough (41.38%), loss of smell (24.14%), and hyperthermia (41.38%) (Table 1). Asymptomatic COVID-19 was observed in 8 patients (28.59%). Patients with mild, moderate and severe course of the disease accounted for 22 (75.86%), 6 (20.69%), and 1 (3.45%) case respectively.

Computed tomography (CT) revealed no typical features of viral pneumonia in 25% of cases (CT 0). High probability of viral pneumonia with minimum lung tissue involvement was revealed in 40% of women (CT 1). High probability of viral pneumonia with 25–50% lung tissue involvement (CT 2) was observed in 10% of women. High probability of viral pneumonia with 50–75% lung tissue involvement (CT 3) was revealed in 10% of patients; critical lung tissue involvement (> 75%, CT-4) was observed in 15% of cases.

In the group of patients with confirmed COVID-19, the delivery time of 38 ± 1.52 weeks of pregnancy was significantly different from that of the controls (39.42 ± 1.14 weeks, p = 0.001). Probably this has something to do with four (13.8%) cases of preterm labor in the group with COVID-19; however, the cause of premature birth was not related to COVID-19 infection severity. In one case, preterm labor resulted from ill-preparedness of soft birth canal and the scarred uterus, in the other case it resulted from increasing severity of preeclampsia, and in two more cases it resulted from preterm prelabor rupture of membranes, and labor onset. Cesarean section was performed in 13 patients (44.8%) (RR: 0.9 [0.5; 1.6]), vacuum extraction due to fetal distress was performed in one patient (3.5%); other patients had normal vaginal delivery. In the control

Table 2. Clinical characteristics of pregnant women enrolled

	COVID-19 (n = 29)	Controls (n = 17)	p
Age, years	29.9 (± 5.03)	32.0 (± 5.03)	0.16
Height, cm	166.62 (± 7.37)	165.76 (± 7.34)	0.71
Weight, kg	77.64 (± 11.58)	71.87 (± 9.75)	0.10
BMI	27.85 (± 4.52)	26.12 (± 3.16)	0.18
Delivery time, months	38 (± 1.52)	39.42 (± 1.14)	0.001
Baby's birth weight, g	3332 (± 484)	3585 (± 424)	0.08
Baby's birth length, cm	52.4 (± 2.66)	53.1 (± 2.29)	0.35
Apgar score at one minute of age	8 (8;8)	9 (9;9)	0.69
Apgar score at five minutes of age	8 (8;8)	9 (9;9)	0.83

Table 3. Amino acid concentrations (nmol/mL) in amniotic fluid of controls and COVID-19 patients

Amino acid	Controls	COVID-19	*p*-value
1-methyl-L-histidine	9.52 (5.78; 23.54)	0 (0; 4.98)	< 0.001
3-methyl-L-histidine	1.32 (0.14; 2.56)	1.62 (0.48; 5.35)	0.258
3-aminoisobutyric acid	7.44 (6.38; 9.22)	5.48 (4.4; 6.17)	0.002
DL-5-hydroxylysine	10.31 (9.98; 10.69)	10.28 (9.99; 10.5)	0.591
Ethanolamine	45.69 (38.94; 67.65)	35.24 (24.53; 46.3)	0.096
L-2-aminobutyric acid	1.5 (1.27; 2.34)	1.27 (1; 2.62)	0.367
L-2-aminoadipic acid	7.21 (5.39; 10.59)	6.66 (5.24; 9.46)	0.615
L-alanine	238.74 (179.29; 329.59)	187.36 (136.91; 257.72)	0.302
L-arginine	26.59 (22.42; 48.86)	16.25 (8.97; 23.61)	0.006
L-asparagine	29.36 (24.49; 40.74)	25.56 (19.32; 41.31)	0.391
L-aspartic acid	13.82 (7.9; 29.75)	11.92 (6.64; 62.9)	0.784
L-carnosine	4.58 (4.43; 5.21)	5.5 (4.54; 6.31)	0.107
L-citrulline	8.6 (6.93; 11.43)	7.57 (4.84; 14.52)	0.632
L-cystathionine	0.96 (0.83; 1.16)	0.8 (0.56; 0.96)	0.036
L-cystine	39.69 (30.93; 46.09)	15.92 (5.48; 35.06)	0.005
L-glutamic acid	176.3 (114.37; 215.51)	112.92 (67.26; 176.17)	0.15
L-glutamine	392.48 (267.94; 450.24)	286.57 (177.62; 369.67)	0.044
L-glycine	216.37 (189.39; 359.66)	219.92 (156.65; 260.22)	0.43
L-histidine	65.35 (34.72; 85.64)	7.9 (0; 30.68)	0.008
L-lysine	153.56 (113.59; 169.06)	149.15 (105.52; 187.74)	0.973
L-methionine	16.55 (10.59; 20.68)	11.21 (7.36; 19.59)	0.252
L-ornithine	24.16 (15.39; 34.42)	42.8 (20.11; 69.65)	0.096
L-phenylalanine	39.63 (24.82; 51.44)	32 (21.48; 55.77)	0.515
L-proline	118.37 (103.97; 154.61)	109.16 (72.85; 125.35)	0.137
L-serine	65.52 (37.24; 89.78)	50.74 (32.72; 95.85)	0.681
L-threonine	150.1 (101.89; 211.52)	136.31 (96.46; 172.32)	0.445
L-tryptophan	11.63 (7.7; 13.69)	7.49 (4.36; 14.33)	0.302
L-tyrosine	24.3 (17.75; 38.24)	18.23 (8.22; 47.62)	0.435
L-valine	378.17 (286.06; 544.61)	412.5 (256.16; 570.82)	0.681
Taurine	12.6 (11.48; 14.32)	12.66 (11.54; 16.48)	0.958
Trans-4-hydroxy-L-proline	18.03 (14.18; 20.08)	13.54 (11.05; 15.96)	0.019

group, cesarean section was performed in 9 patients (52.9 %); other patients had normal vaginal delivery. The reasons for cesarean section were as follows: one or more uterine scars, fetal malpresentation, abnormal pelvic anatomy, and reports of other specialists (ophthalmologist, orthopedist, neurologist). In the group with COVID-19 the average birth weight was 3332 ± 484 g, and in the control groups it was 3585 ± 424 g; the average length of the newborns was 52.4 ± 2.66 cm and 53.1 ± 2.29 cm respectively. The newborns were assigned Apgar score 8 (8; 8) at one minute and 9 (9; 9) and five minutes of age in both groups (Table 2).

No cases of COVID-19 in newborns were registered. Newborns were isolated from their mothers immediately after birth. Breastfeeding was allowed after the mothers tested negative twice for SARS-CoV-2. All newborns were tested for SARS-CoV-2 immediately after birth, and then at three and 10 days of age. All newborns tested negative for the virus, which could indicate no vertical transmission of the infection. No perinatal deaths were registered.

During the laboratory phase, the targeted metabolomics approach was applied with the use of the kit for quantification of 31 amino acids by HPLC-MS in the samples of amniotic fluid and cord blood plasma, collected at the National Medical Research Center for Obstetrics, Gynecology and Perinatology named after Academician V. I. Kulakov. The study was performed in order to describe the levels of amino acids in neonates born to mothers, who tested positive for COVID-19.

Amniotic fluid

Concentrations of 31 amino acids were defined during the analysis of amniotic fluid. Statistical analysis of experimental data made it possible to identify eight amino acids, the levels of which were significantly different in patients with COVID 19 (Table 3; Fig. 1): 1-methylhistidine, 3-methylhistidine, arginine, cystathionine, cystine, glutamine, histidine, trans-4-hydroxyproline.

In view of the HPLC-MS results obtained, of particular interest was the feasibility of developing mathematical model, allowing us to distinguish amniotic fluid samples obtained from COVID-19 patients and controls. For that, logistic regression models were constructed based on the amino acids showing
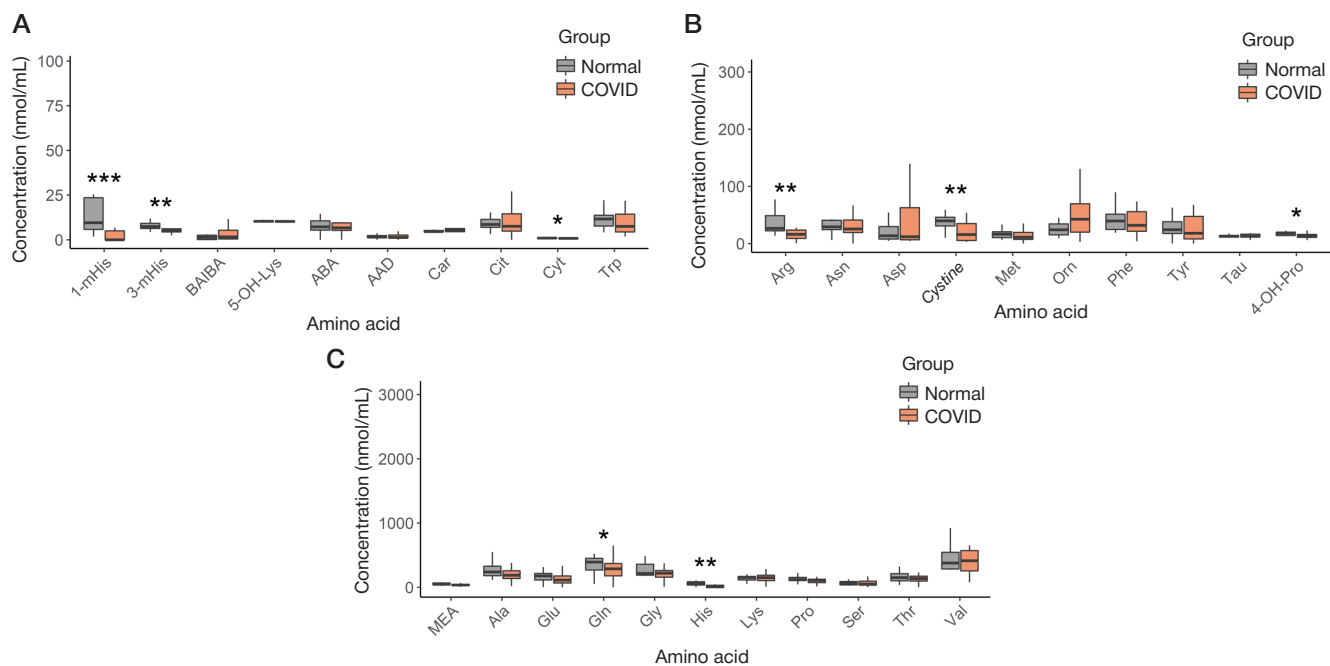
Fig. 1. Amino acid concentrations in amniotic fluid of controls and COVID-19 patients. The first and the third quartiles form the boundaries of the box, the median is shown as a line in the center of the box; the ends of whiskers represent the following: one and a half times interquartile range subtracted from the first quartile, sum of the third quartile and one and a half times interquartile range; * — $p \leq 0.05$; ** — $p \leq 0.01$; *** — $p \leq 0.001$; 1-mHis — 1-methylhistidine; 3-mHis — 3-methylhistidine; BAIBA — 3-aminoisobutyric acid; 5-OH-Lys — 5-hydroxylysine; MEA — ethanolamine; ABA — 2-aminobutyric acid; AAD — 2-aminoadipic acid; Car — carnosine; Cit — citrulline; Cyt — cystathionine; 4-OH-Pro — 4-hydroxyproline

significant differences between the studied groups. All possible combinations of amino acids were used to construct the models. ROC analysis was performed, and four models with maximum area under the ROC curve (AUC) were selected for each model. Parameters of the models constructed are presented in Table 4, and the corresponding ROC curves are presented in Fig. 2. The maximum AUC value of 0.89 was calculated for the model, constructed based on arginine, cystine, histidine, and trans-4-hydroxyproline (Table 5). This model had sensitivity

of 0.84, and specificity of 0.93. Slightly higher sensitivity and specificity (0.84 and 1 respectively) were calculated for the model, constructed based on 1-methylhistidine, cystine, and trans-4-hydroxyproline (Table 5).

Cord blood plasma

The cord blood plasma amino acid profiles were analyzed in two groups during the next phase of the study. Statistical analysis

Table 4. Parameters of logistic regression models allowing one to distinguish patients with COVID-19 from patients with no COVID-19 based on the amino acid concentrations in the amniotic fluid

Model №	Coefficient	Coefficient value	Wald criterion	p-value	CI		OR	OR	
					2.50%	97.50%		2.50%	97.50%
1	Intercept term	5.8782	2.3394	0.019	1.8187	11.8835	357.17	6.1637	144864
	L-arginine	0.0091	0.3735	0.709	−0.042	0.0565	1.0091	0.9588	1.0582
	L-cystine	−0.0842	−2.2358	0.025	−0.1747	−0.0208	0.9192	0.8397	0.9794
	L-histidine	0.0129	1.1644	0.244	−0.0063	0.0386	1.013	0.9937	1.0394
	Trans-4-hydroxy-L-proline	−0.2534	−1.7891	0.074	−0.574	−0.0041	0.7762	0.5633	0.9959
2	Intercept term	2.7692	1.7238	0.085	−0.1116	6.3699	15.9456	0.8944	583.996
	1-methyl-L-histidine	−0.0336	−1.271	0.204	−0.1107	0.0073	0.9669	0.8952	1.0073
	L-cystine	−0.0123	−0.5235	0.601	−0.0621	0.0328	0.9878	0.9398	1.0333
	Trans-4-hydroxy-L-proline	−0.1114	−1.0398	0.298	−0.3392	0.0951	0.8946	0.7123	1.0998
3	Intercept term	2.7231	1.6899	0.091	−0.152	6.3672	15.2278	0.859	582.4
	1-methyl-L-histidine	−0.0339	−1.2824	0.2	−0.1109	0.0071	0.9667	0.895	1.0071
	L-cystine	−0.0156	−0.5326	0.594	−0.0792	0.0395	0.9845	0.9239	1.0402
	L-glutamine	7.00E−04	0.1925	0.847	−0.0066	0.0082	1.0007	0.9934	1.0082
	Trans-4-hydroxy-L-proline	−0.116	−1.0585	0.29	−0.3503	0.0978	0.8905	0.7045	1.1027
4	Intercept term	5.1861	2.146	0.032	1.2261	11.0587	178.765	3.408	63495.7
	1-methyl-L-histidine	−0.0272	−0.8762	0.381	−0.1263	0.0193	0.9731	0.8813	1.0195
	L-cystine	−0.0633	−1.6706	0.095	−0.1559	8.00E−04	0.9387	0.8557	1.0008
	L- histidine	0.0146	2.199	0.028	0.0032	0.0312	1.0147	1.0032	1.0317
	Trans-4-hydroxy-L-proline	−0.2185	−1.5539	0.12	−0.5408	0.0346	0.8038	0.5823	1.0352

Table 5. Characteristics of logistic regression models allowing one to distinguish patients with COVID-19 from patients with no COVID-19 based on the amino acid concentrations in the amniotic fluid

Amino acid	AUC	Threshold	Sensitivity	Specificity	Positive predictive value
L-arginine, L-cystine, L-histidine, *trans*-4- hydroxy-L-proline	0.89	0.46	0.84 (0.58; 1)	0.93 (0.73; 1)	0.94 (0.8; 1)
1-methyl-L-histidine, L-cystine, *trans*-4- hydroxy-L-proline	0.88	0.68	0.84 (0.63; 1)	1 (0.8; 1)	1 (0.86; 1)
1-methyl-L-histidine, L-cystine, L-glutamine, trans-4- hydroxy-L-proline	0.88	0.67	0.82 (0.63; 0.95)	1 (0.87; 1)	1 (0.87; 1)
1-methyl-L-histidine, L-cystine, L- histidine, *trans*-4- hydroxy-L-proline	0.88	0.65	0.79 (0.58; 1)	0.93 (0.67; 1)	0.95 (0.78; 1)

Table 6. Amino acid concentrations (nmol/mL) in cord blood plasma of controls and COVID-19 patients

Amino acid	Controls	COVID-19	*p*-value
1-methyl-L-histidine	0 (0; 1.95)	0 (0; 0)	0.041
3-methyl-L-histidine	3.02 (2.82; 3.46)	3.2 (2.56; 3.68)	0.759
Beta-alanine	1.19 (0.82; 1.61)	2.9 (1.8; 4.35)	0.014
DL-5-hydroxylysine	6.69 (6.48; 6.77)	6.67 (6.56; 6.87)	0.608
Ethanolamine	18.77 (14.52; 21.97)	14.75 (13.43; 16.43)	0.104
L-2-aminobutyric acid	5.97 (1.97; 7.96)	7.04 (3.45; 10.51)	0.255
L-alanine	498.14 (451.48; 554.51)	426.72 (390.15; 530.81)	0.134
L-arginine	55.2 (42.7; 73.97)	69.1 (51.71; 81.33)	0.23
L-asparagine	46.5 (43.4; 51)	51.33 (45.72; 53.85)	0.404
L-aspartic acid	21.69 (12.05; 28.9)	16.66 (11.6; 26.76)	0.753
L-carnosine	2.14 (1.93; 2.3)	2.01 (1.64; 2.33)	0.274
L-citrulline	11.92 (10.83; 13.47)	11.96 (10.46; 15.18)	0.357
L-cystathionine	0.32 (0.17; 0.46)	0.2 (0.16; 0.42)	0.593
L-cystine	28.93 (26.49; 33.43)	2.55 (1.44; 3.81)	< 0.001
L-glutamic acid	138.44 (41.01; 189.32)	92.68 (60.31; 109.28)	0.187
L-glutamine	617.36 (576.47; 725.84)	625.09 (559.72; 689.24)	0.736
L-glycine	277.25 (255.67; 303.25)	259.22 (235.34; 293.13)	0.43
L-histidine	175.97 (138.84; 206.4)	141.92 (103.55; 175.91)	0.04
L-lysine	410.97 (388.38; 448.61)	451.73 (389.8; 488.91)	0.531
L-methionine	33.11 (27.86; 39)	30.61 (25.81; 39.05)	0.753
L-ornithine	119.5 (100.28; 131.19)	100.77 (83.6; 124.42)	0.123
L-phenylalanine	79.88 (76.47; 94.87)	80.5 (75.99; 88.11)	0.982
L-proline	159.61 (153.75; 177.18)	158.5 (143.86; 176.18)	0.417
L-serine	132.49 (125.85; 148.56)	143.03 (128.45; 154.13)	0.558
L-threonine	293.9 (231.79; 339.82)	319.48 (276.25; 352.53)	0.23
L-tryptophan	77.59 (66.69; 84.57)	73.72 (68.93; 78.29)	0.309
L-tyrosine	70.65 (57.22; 78.07)	63.8 (57.51; 77.25)	0.685
Taurine	38.01 (31.1; 49.77)	37.28 (30.51; 46.92)	0.928
Trans-4-hydroxy-L-proline	20.95 (17.68; 26.64)	20.56 (19.28; 23.57)	0.893

of experimental data made it possible to identify four amino acids, the levels of which were significantly different in patients with COVID-19 (Table 6; Fig. 3): 1-methylhistidine, beta-alanine, cystine, histidine.

As in case of amniotic fluid assay, logistic regression models were constructed, allowing us to distinguish cord blood plasma samples obtained from COVID-19 patients and controls. Results of the models' development and analysis are presented in Fig. 4, and Tables 7, 8. All the models constructed included cystine, obviously being the amino acid, which showed the greatest

differences between groups. All the models were characterized by AUC of 1, as well as by sensitivity and specificity of 1 (Table 8).

Of particular interest was the comparison of amino acids in amniotic fluid and cord blood plasma, which showed significant differences between the controls and the COVID-19 patients. Three amino acids were detected, and their levels were significantly different in COVID-19 patients simultaneously in two points (amniotic fluid and cord blood plasma), depicting the fetal metabolome in a holistic manner: 1-methylhistidine, cystine, and histidine (Table 9).
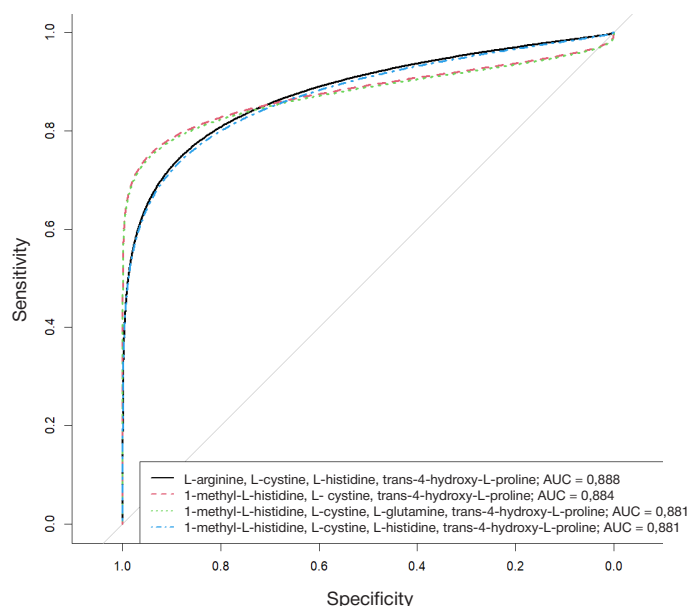
Fig. 2. ROC curves for logistic regression models constructed for classification of controls and COVID-19 patients based on amino acid concentrations in amniotic fluid

DISCUSSION

Viral infections cause characteristic changes in the host cell metabolism in order to ensure the effective replication of the virus [19]. Moreover, the resultant metabolic effects and cellular reprogramming vary between viruses (even within a single family) and host cell types.

The data obtained show significant differences in the concentrations of eight amino acids in amniotic fluid and four amino acids in cord blood plasma between the COVID-19 patients and the controls. Furthermore, concentrations of eight amino acids were reduced in COVID-19 patients. Similar amino acid concentration alterations were observed during assessment of blood plasma in children and adults with COVID-19 [24]. The authors of this study tried to confirm their hypothesis about the possible arginine concentration decrease

in COVID-19 patients. It is known, that endothelial dysfunction contributes to lung damage associated with COVID-19 both in children and adults [27, 28]; low bioavailability of arginine is associated with endothelial dysfunction and T-cell dysregulation [29, 30], it also contributes to pathophysiology of numerous disorders [31]. Indeed, the expected decline in arginine concentration was observed in COVID-19 patients. Furthermore, the significantly reduced concentrations of citrulline, glutamine, alanine, glycine, histidine, proline, and some other amino acids were observed, however, the authors of the article had some difficulty explaining the mechanisms underlying the described effects [24]. The decreased amino acid concentrations were observed in individuals with a number of other disorders [19, 21–24, 32, 33].

In our study, of particular interest was the comparison of amino acid levels in amniotic fluid and cord blood plasma,
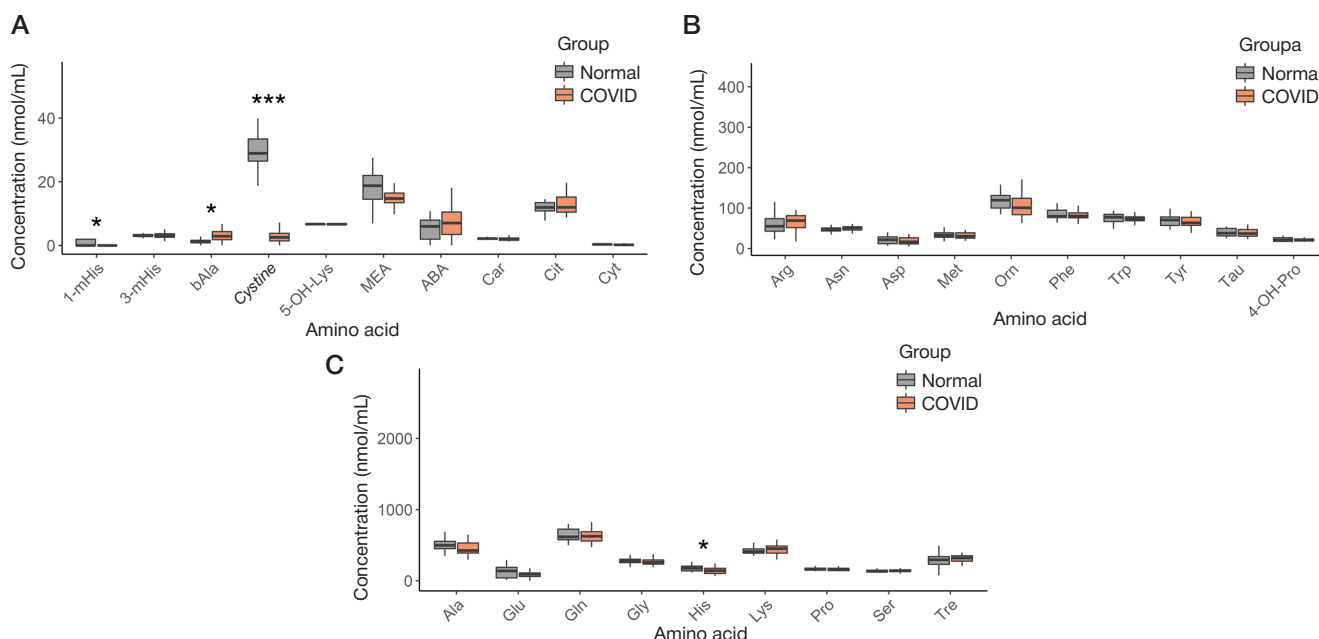
Fig. 3. Amino acid concentrations in cord blood plasma of controls and COVID-19 patients. The first and the third quartiles form the boundaries of the box, the median is shown as a line in the center of the box; the ends of whiskers represent the following: one and a half times interquartile range subtracted from the first quartile, sum of the third quartile and one and a half times interquartile range; * — $p \leq 0.05$; ** — $p \leq 0.01$; *** — $p \leq 0.001$. 1-mHis — 1-methylhistidine; 3-mHis – 3-methylhistidine; bAla — beta-alanine; BAIBA — 3-aminoisobutyric acid; 5-OH-Lys – 5-hydroxylysine; MEA – ethanolamine; ABA — 2-aminobutyric acid; AAD —2-aminoadipic acid; Car — carnosine; Cit — citrulline; Cyt — cystathionine; 4-OH-Pro — 4-hydroxyproline
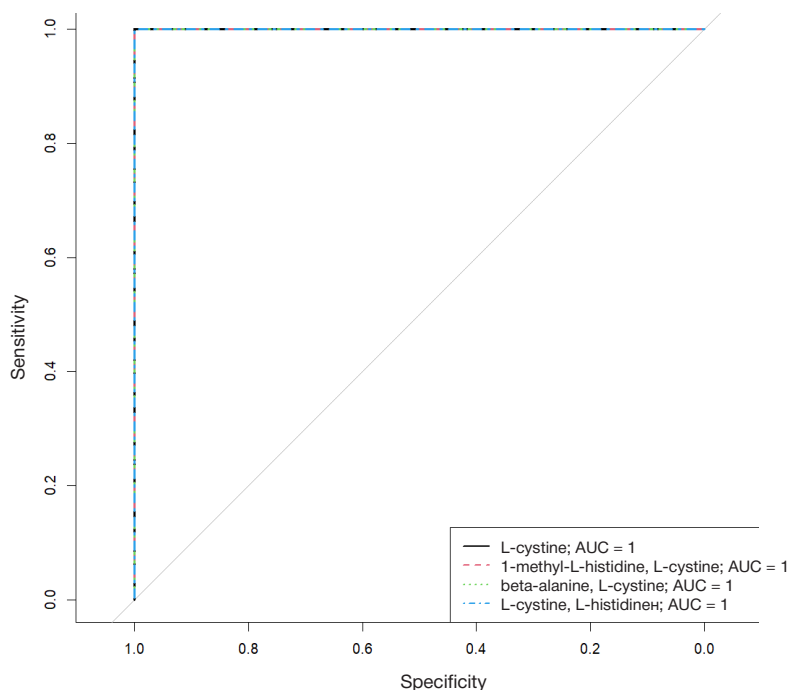
Fig. 4. ROC curves for logistic regression models constructed for classification of controls and COVID-19 patients based on amino acid concentrations in cord blood plasma

which showed significant differences between the controls and the COVID-19 patients. Three amino acids were detected, and their levels were significantly different in COVID-19 patients simultaneously in two points (amniotic fluid and cord blood plasma), depicting the fetal metabolome in a holistic manner: 1-methylhistidine, cystine, and histidine.

L-cystine was one of the three amino acids detected in two fetal matrices at once (amniotic fluid and cord blood plasma),

having a high differentiating significance. L-cystine is a non-coded amino acid, being a derivative, obtained from oxidative dimerization of cysteine. During the post-translational modification of proteins, this amino acid plays a vital part in protein and peptide tertiary structure formation and maintaining, and, consequently, in their biological activity. Thus, such hormones as vasopressin, oxytocin, insulin, and somatostatin, acquire biological activity after the formation of intramolecular disulphide bonds.

Table 7. Parameters of logistic regression models allowing one to distinguish patients with COVID-19 from patients with no COVID-19 based on the amino acid concentrations in the cord blood plasma

Model №	Coefficient	Coefficient value	Wald criterion	*p*-value
1	Intercept term	79.204	0.001	0.9992
	L-cystine	−5.3827	−0.001	0.9992
2	Intercept term	79.4804	0.001	0.9992
	1-methyl-L-histidine	3.1115	3.00E–04	0.9998
	L-cystine	−5.4032	−0.001	0.9992
3	Intercept term	77.8123	9.00E–04	0.9992
	Beta-alanine	−1.4597	−2.00E–04	0.9998
	L-cystine	−5.099	−0.001	0.9992
4	Intercept term	78.9156	9.00E–04	0.9993
	L-cystine	−5.3946	−0.001	0.9992
	L-histidine	0.0027	0	1

Table 8. Characteristics of logistic regression models allowing one to distinguish patients with COVID-19 from patients with no COVID-19 based on the amino acid concentrations in the blood cord plasma

Amino acid	AUC	Threshold	Sensitivity	Specificity	Specificity
L-cystine	1	0.5	1 (1; 1)	1 (1; 1)	1 (1; 1)
1-methyl-L-histidine, L-cystine	1	0.5	1 (1; 1)	1 (1; 1)	1 (1; 1)
Бета-аланин, L-cystine	1	0.5	1 (1; 1)	1 (1; 1)	1 (1; 1)
L-cystine, L- histidine	1	0.5	1 (1; 1)	1 (1; 1)	1 (1; 1)

Table 9. Amino acid concentrations (nmol/mL) in amniotic fluid and cord blood plasma showing significant differences between controls and COVID-19 patients

Sample	Amino acid	Controls	COVID-19	*p*-value
Amniotic fluid	1-methyl-L-histidine	9.52 (5.78; 23.54)	0 (0; 4.98)	< 0.001
	3-methyl-L-histidine	7.44 (6.38; 9.22)	5.48 (4.4; 6.17)	0.002
	L-arginine	26.59 (22.42; 48.86)	16.25 (8.97; 23.61)	0.006
	L-cystathionine	0.96 (0.83; 1.16)	0.8 (0.56; 0.96)	0.036
	L-cystine	39.69 (30.93; 46.09)	15.92 (5.48; 35.06)	0.005
	L-glutamine	392.48 (267.94; 450.24)	286.57 (177.62; 369.67)	0.044
	L-histidine	65.35 (34.72; 85.64)	7.9 (0; 30.68)	0.008
	Trans-4-hydroxy-L-proline	18.03 (14.18; 20.08)	13.54 (11.05; 15.96)	0.019
Cord blood plasma	1-methyl-L-histidine	0 (0; 1.95)	0 (0; 0)	0.041
	Beta-alanine	1.19 (0.82; 1.61)	2.9 (1.8; 4.35)	0.014
	L-cystine	28.93 (26.49; 33.43)	2.55 (1.44; 3.81)	< 0.001
	L- histidine	175.97 (138.84; 206.4)	141.92 (103.55; 175.91)	0.04

There were two amino acids showing significant differences in the amniotic fluid and cord blood plasma levels in neonates born to mothers with COVID-19: L-histidine and its derivative, 1-methylhistidine.

L-histidine is a heterocyclic alpha-amino acid, one of 20 proteinogenic amino acids, and one of two conditionally essential amino acids (along with arginine). It was originally thought to be essential only for children. Histidine residue is a part of active sites of numerous enzymes. Histidine is a precursor of histamine. Histamine plays an important role in inflammation and a number of allergic reactions. Histidine is one of the essential amino acids; it promotes tissue growth and regeneration, and contributes to red blood cell and white blood cell production, as well as to formation of the nerve cell myelin sheaths. Histidine deficiency may result in hearing loss, as well as in degenerative disorders, such as Parkinson's disease and Alzheimer's disease.

Our results demonstrate that the virus can cause major changes in metabolome of amniotic fluid and cord blood plasma, which risks the impaired programming of protein production. However, COVID-19 is often dormant at birth. Metabolic pathway alterations, resulting from violation of required amino acid ratio in the territory of the fetus, could be associated with replication of the virus, host inflammatory response, and altered energy metabolism. Probably, such metabolomic alterations may show up at the time of delivery, however, these have not been observed during our study due to the index group inclusion criteria. All puerperant women had COVID-19 at the time of delivery. May be that was the fact that prevented the virus to realize its entire harmful potential in the territory of the fetus.

CONCLUSION

During the study we used the targeted metabolomics approach for detection of altered amino acid concentrations in pregnant women with COVID-19 infection upon admission to hospital. No such alterations were revealed. It was found that there were significant differences in concentrations of eight amino acids in amniotic fluid (1-methylhistidine, 3-methylhistidine, arginine, cystathionine, cystine, glutamine, histidine, trans-4-hydroxyproline), and four amino acids in cord blood plasma (1-methylhistidine, beta-alanine, cystine, histidine) between the COVID-19 patients and the control group. Our aim was not only to find the markers of the disease, but also to understand the effect of COVID-19 infection of the fetal metabolome. It turns out, that the impaired metabolism of the amino acids detected shows up in individuals with a number of severe disorders, such as acute respiratory distress syndrome with severe sepsis, H1N1-associated pneumonia, bacterial pneumonia, sickle cell anemia, thalassemia, malaria, acute asthma, cystic fibrosis, pulmonary hypertension, cardiovascular disorders, certain cancer types, etc. These results may be used for selection of the areas for further investigation of possible health consequences in neonates born to mothers with COVID-19, as well as to define the requirements for treatment and medical care of pregnant women and newborns after COVID-19 diagnosis, since the long-term health consequences in this cohort of newborns may include endocrine, nervous system and allergic disorders, resulting from metabolomic impairments of protein production programming during the antenatal period.

References

1. Mendez-Figueroa H, Raker C, Anderson BL. Neonatal characteristics and outcomes of pregnancies complicated by influenza infection during the 2009 pandemic. American Journal of Obstetrics and Gynecology. 2011; 204 (6 SUPPL.): 58.
2. Song JY, Park KV, Han SW, Choi MJ, Noh JY, Cheong HJ, et al. Paradoxical long-term impact of maternal influenza infection on neonates and infants. BMC Infect Dis. 2020; 20 (1): 1–8.
3. Zeng L, Xia S, Yuan W, Yan K, Xiao F, Shao J, et al. Neonatal Early-Onset Infection with SARS-CoV-2 in 33 Neonates Born to Mothers with COVID-19 in Wuhan, China. JAMA Pediatr. 2020; 174 (7): 722–5.
4. Yu N, Li W, Kang Q, Zeng W, Feng L, Wu J. No SARS-CoV-2 detected in amniotic fluid in mid-pregnancy. Lancet Infect Dis. 2020. DOI: 10.1016/S1473-3099(20)30320-0.
5. Chen H, Guo J, Wang C, Luo F, Yu X, Zhang W, et al. Clinical characteristics and intrauterine vertical transmission potential of COVID-19 infection in nine pregnant women: a retrospective review of medical records. Lancet. 2020; 395 (10226): 809–15.
6. Zamaniyan M, Ebadi A, Aghajanpoor S, Rahmani Z, Haghshenas M, Azizi S. Preterm delivery, maternal death, and vertical transmission in a pregnant woman with COVID-19 infection. Prenat Diagn. 2020; 40 (13): 1759–61.
7. Sisman J, Jaleel MA, Moreno W, Rajaram V, Collins RRJ, Savani RC, et al. Intrauterine Transmission of SARS-COV-2 Infection in a Preterm Infant. Pediatr Infect Dis J. 2020; 265–7.
8. Costa S, Posteraro B, Marchetti S, Tamburrini E, Carducci B, Lanzone A, et al. Excretion of SARS-CoV-2 in human breast milk. Clin Microbiol Infect. 2020; 26 (10): 1430–2.

9. Buonsenso D, Costa S, Sanguinetti M, Cattani P, Posteraro B, Marchetti S, et al. Neonatal Late Onset Infection with Severe Acute Respiratory Syndrome Coronavirus 2. Am J Perinatol. 2020; 37 (8): 869–72.

10. Qiancheng X, Jian S, Lingling P, Lei H, Xiaogan J, Weihua L, et al. Coronavirus disease 2019 in pregnancy. Int J Infect Dis. 2020; 95: 376–83.

11. Dong L, Tian J, He S, Zhu C, Wang J, Liu C, et al. Possible Vertical Transmission of SARS-CoV-2 from an Infected Mother to Her Newborn. JAMA. 2020; 323 (18): 1846–8.

12. Zhu H, Wang L, Fang C, Peng S, Zhang L, Chang G, et al. Clinical analysis of 10 neonates born to mothers with 2019-nCoV pneumonia. Transl Pediatr. 2020; 9 (1): 51–60.

13. Zeng H, Xu C, Fan J, Tang Y, Deng Q, Zhang W, et al. Antibodies in Infants Born to Mothers with COVID-19 Pneumonia. JAMA. 2020; 323 (18):1848–9.

14. Sukhikh G, Petrova U, Prikhodko A, Starodubtseva N, Chingin K, Chen H, et al. Vertical Transmission of SARS-CoV-2 in Second Trimester Associated with Severe Neonatal Pathology. Viruses. 2021; 13 (3). DOI: 10.3390/v13030447.

15. Ellington S, Strid P, Tong VT, Woodworth K, Galang RR, Zambrano LD, et al. Characteristics of women of reproductive age with laboratory-confirmed SARS-COV-2 infection by pregnancy status — United States, January 22-June 7, 2020. Morb Mortal Wkly Rep. 2020; 69 (25): 769–75.

16. Vivanti AJ, Vauloup-Fellous C, Prevot S, Zupan V, Suffee C, Do Cao J, et al. Transplacental transmission of SARS-CoV-2 infection. Nat Commun. 2020; 11 (1). DOI: 10.1038/s41467-020-17436-6.

17. Kell DB, Oliver SG. The metabolome 18 years on: a concept comes of age. Metabolomics. 2016; 12 (10). DOI: 10.1007/s11306-016-1108-4.

18. Shen B, Yi X, Sun Y, Bi X, Du J, Zhang C, et al. Proteomic and Metabolomic Characterization of COVID-19 Patient Sera. Cell. 2020; 182 (1): 59-72.e15.

19. Wannemacher RW, Pekarek RS, Bartelloni PJ, Vollmer RT, Beisel WR. Changes in individual plasma amino acids following experimentally induced sand fly fever virus infection. Metabolism. 1972; 21 (1): 67–76.

20. Banoei MM, Vogel HJ, Weljie AM, Kumar A, Yende S, Angus DC, et al. Plasma metabolomics for the diagnosis and prognosis of H1N1 influenza pneumonia. 2017; 1–15. DOI: 10.1186/s13054-017-1672-7

21. Inoue S, Ikeda H. Differences in plasma amino acid levels in patients with and without bacterial infection during the early stage of acute exacerbation of COPD. Int J COPD. 2019; 14: 575–83.

22. Moat SJ, George RS, Carling RS. Use of Dried Blood Spot Specimens to Monitor Patients with Inherited Metabolic Disorders. Int J Neonatal Screen. 2020; 6 (2): 1–17.

23. Páez-Franco JC, Torres-Ruiz J, Sosa-Hernández VA, Cervantes-Díaz R, Romero-Ramírez S, Pérez-Fragoso A, et al. Metabolomics analysis reveals a modified amino acid metabolism that correlates with altered oxygen homeostasis in COVID-19 patients. Sci Rep. 2021; 11 (1). DOI: 10.1038/s41598-021-85788-0.

24. Rees CA, Rostad CA, Mantus G, Anderson EJ, Chahroudi A, Jaggi P. Altered amino acid profile in patients with SARS-CoV-2 infection. 2021; 118 (25): 4–6.

25. Hirschel J, Vogel M, Baber R, Garten A, Beuchel C, Dietz Y, et al. Relation of whole blood amino acid and acylcarnitine metabolome to age, sex, BMI, puberty, and metabolic markers in children and adolescents. Metabolites. 2020; 10 (4). DOI: 10.3390/metabo10040149.

26. Thaker SK, Chng J, Christofk HR. Viral hijacking of cellular metabolism. BMC Biol. 2019; 17 (1): 59.

27. Diorio C, McNerney KO, Lambert M, Paessler M, Anderson EM, Henrickson SE, et al. Evidence of thrombotic microangiopathy in children with SARS-CoV-2 across the spectrum of clinical presentations. Blood Adv. 2020; 4 (23): 6051–63.

28. Tay MZ, Poh CM, Rénia L, MacAry PA, Ng LFP. The trinity of COVID-19: immunity, inflammation and intervention. Nature Reviews Immunology. 2020; 20 (6): 363–74.

29. Gambardella J, Khondkar W, Morelli MB, Wang X, Santulli G, Trimarco V. Arginine and endothelial function. Biomedicines. 2020; 8 (8): 277.

30. Rodríguez PC, Ochoa AC. Arginine regulation by myeloid derived suppressor cells and tolerance in cancer: Mechanisms and therapeutic perspectives. Immunological Reviews. 2008; 222 (1): 180–91.

31. Morris CR, Hamilton-Reeves J, Martindale RG, Sarav M, Ochoa Gautier JB. Acquired Amino Acid Deficiencies: A Focus on Arginine and Glutamine. In: Nutrition in Clinical Practice. SAGE Publications Inc.: 2017; 30S–47S.

32. IKEDA H. Plasma amino acid levels in individuals with bacterial pneumonia and healthy controls. 2020; 1–17. DOI: 10.21203/rs.3.rs-18796/v1.

33. Ware LB, Magarik JA, Wickersham N, Cunningham G, Rice TW, Christman BW, et al. Low plasma citrulline levels are associated with acute respiratory distress syndrome in patients with severe sepsis. Crit Care. 2013; 17 (1): 1–8.

Литература

1. Mendez-Figueroa H, Raker C, Anderson BL. Neonatal characteristics and outcomes of pregnancies complicated by influenza infection during the 2009 pandemic. American Journal of Obstetrics and Gynecology. 2011; 204 (6 SUPPL.): 58.

2. Song JY, Park KV, Han SW, Choi MJ, Noh JY, Cheong HJ, et al. Paradoxical long-term impact of maternal influenza infection on neonates and infants. BMC Infect Dis. 2020; 20 (1): 1–8.

3. Zeng L, Xia S, Yuan W, Yan K, Xiao F, Shao J, et al. Neonatal Early-Onset Infection with SARS-CoV-2 in 33 Neonates Born to Mothers with COVID-19 in Wuhan, China. JAMA Pediatr. 2020; 174 (7): 722–5.

4. Yu N, Li W, Kang Q, Zeng W, Feng L, Wu J. No SARS-CoV-2 detected in amniotic fluid in mid-pregnancy. Lancet Infect Dis. 2020. DOI: 10.1016/S1473-3099(20)30320-0.

5. Chen H, Guo J, Wang C, Luo F, Yu X, Zhang W, et al. Clinical characteristics and intrauterine vertical transmission potential of COVID-19 infection in nine pregnant women: a retrospective review of medical records. Lancet. 2020; 395 (10226): 809–15.

6. Zamaniyan M, Ebadi A, Aghajanpoor S, Rahmani Z, Haghshenas M, Azizi S. Preterm delivery, maternal death, and vertical transmission in a pregnant woman with COVID-19 infection. Prenat Diagn. 2020; 40 (13): 1759–61.

7. Sisman J, Jaleel MA, Moreno W, Rajaram V, Collins RRJ, Savani RC, et al. Intrauterine Transmission of SARS-COV-2 Infection in a Preterm Infant. Pediatr Infect Dis J. 2020; 265–7.

8. Costa S, Posteraro B, Marchetti S, Tamburrini E, Carducci B, Lanzone A, et al. Excretion of SARS-CoV-2 in human breast milk. Clin Microbiol Infect. 2020; 26 (10): 1430–2.

9. Buonsenso D, Costa S, Sanguinetti M, Cattani P, Posteraro B, Marchetti S, et al. Neonatal Late Onset Infection with Severe Acute Respiratory Syndrome Coronavirus 2. Am J Perinatol. 2020; 37 (8): 869–72.

10. Qiancheng X, Jian S, Lingling P, Lei H, Xiaogan J, Weihua L, et al. Coronavirus disease 2019 in pregnancy. Int J Infect Dis. 2020; 95: 376–83.

11. Dong L, Tian J, He S, Zhu C, Wang J, Liu C, et al. Possible Vertical Transmission of SARS-CoV-2 from an Infected Mother to Her Newborn. JAMA. 2020; 323 (18): 1846–8.

12. Zhu H, Wang L, Fang C, Peng S, Zhang L, Chang G, et al. Clinical analysis of 10 neonates born to mothers with 2019-nCoV pneumonia. Transl Pediatr. 2020; 9 (1): 51–60.

13. Zeng H, Xu C, Fan J, Tang Y, Deng Q, Zhang W, et al. Antibodies in Infants Born to Mothers with COVID-19 Pneumonia. JAMA. 2020; 323 (18):1848–9.

14. Sukhikh G, Petrova U, Prikhodko A, Starodubtseva N, Chingin K, Chen H, et al. Vertical Transmission of SARS-CoV-2 in Second Trimester Associated with Severe Neonatal Pathology. Viruses. 2021; 13 (3). DOI: 10.3390/v13030447.

15. Ellington S, Strid P, Tong VT, Woodworth K, Galang RR, Zambrano LD, et al. Characteristics of women of reproductive age with

laboratory-confirmed SARS-COV-2 infection by pregnancy status — United States, January 22-June 7, 2020. Morb Mortal Wkly Rep. 2020; 69 (25): 769–75.

16. Vivanti AJ, Vauloup-Fellous C, Prevot S, Zupan V, Suffee C, Do Cao J, et al. Transplacental transmission of SARS-CoV-2 infection. Nat Commun. 2020; 11 (1). DOI: 10.1038/s41467-020-17436-6.

17. Kell DB, Oliver SG. The metabolome 18 years on: a concept comes of age. Metabolomics. 2016; 12 (10). DOI: 10.1007/s11306-016-1108-4.

18. Shen B, Yi X, Sun Y, Bi X, Du J, Zhang C, et al. Proteomic and Metabolomic Characterization of COVID-19 Patient Sera. Cell. 2020; 182 (1): 59-72.e15.

19. Wannemacher RW, Pekarek RS, Bartelloni PJ, Vollmer RT, Beisel WR. Changes in individual plasma amino acids following experimentally induced sand fly fever virus infection. Metabolism. 1972; 21 (1): 67–76.

20. Banoei MM, Vogel HJ, Weljie AM, Kumar A, Yende S, Angus DC, et al. Plasma metabolomics for the diagnosis and prognosis of H1N1 influenza pneumonia. 2017; 1–15. DOI: 10.1186/s13054-017-1672-7

21. Inoue S, Ikeda H. Differences in plasma amino acid levels in patients with and without bacterial infection during the early stage of acute exacerbation of COPD. Int J COPD. 2019; 14: 575–83.

22. Moat SJ, George RS, Carling RS. Use of Dried Blood Spot Specimens to Monitor Patients with Inherited Metabolic Disorders. Int J Neonatal Screen. 2020; 6 (2): 1–17.

23. Páez-Franco JC, Torres-Ruiz J, Sosa-Hernández VA, Cervantes-Díaz R, Romero-Ramírez S, Pérez-Fragoso A, et al. Metabolomics analysis reveals a modified amino acid metabolism that correlates with altered oxygen homeostasis in COVID-19 patients. Sci Rep. 2021; 11 (1). DOI: 10.1038/s41598-021-85788-0.

24. Rees CA, Rostad CA, Mantus G, Anderson EJ, Chahroudi A, Jaggi P. Altered amino acid profile in patients with SARS-CoV-2 infection. 2021; 118 (25): 4–6.

25. Hirschel J, Vogel M, Baber R, Garten A, Beuchel C, Dietz Y, et al. Relation of whole blood amino acid and acylcarnitine metabolome to age, sex, BMI, puberty, and metabolic markers in children and adolescents. Metabolites. 2020; 10 (4). DOI: 10.3390/metabo10040149.

26. Thaker SK, Chng J, Christofk HR. Viral hijacking of cellular metabolism. BMC Biol. 2019; 17 (1): 59.

27. Diorio C, McNerney KO, Lambert M, Paessler M, Anderson EM, Henrickson SE, et al. Evidence of thrombotic microangiopathy in children with SARS-CoV-2 across the spectrum of clinical presentations. Blood Adv. 2020; 4 (23): 6051–63.

28. Tay MZ, Poh CM, Rénia L, MacAry PA, Ng LFP. The trinity of COVID-19: immunity, inflammation and intervention. Nature Reviews Immunology. 2020; 20 (6): 363–74.

29. Gambardella J, Khondkar W, Morelli MB, Wang X, Santulli G, Trimarco V. Arginine and endothelial function. Biomedicines. 2020; 8 (8): 277.

30. Rodríguez PC, Ochoa AC. Arginine regulation by myeloid derived suppressor cells and tolerance in cancer: Mechanisms and therapeutic perspectives. Immunological Reviews. 2008; 222 (1): 180–91.

31. Morris CR, Hamilton-Reeves J, Martindale RG, Sarav M, Ochoa Gautier JB. Acquired Amino Acid Deficiencies: A Focus on Arginine and Glutamine. In: Nutrition in Clinical Practice. SAGE Publications Inc.: 2017; 30S–47S.

32. IKEDA H. Plasma amino acid levels in individuals with bacterial pneumonia and healthy controls. 2020; 1–17. DOI: 10.21203/rs.3.rs-18796/v1.

33. Ware LB, Magarik JA, Wickersham N, Cunningham G, Rice TW, Christman BW, et al. Low plasma citrulline levels are associated with acute respiratory distress syndrome in patients with severe sepsis. Crit Care. 2013; 17 (1): 1–8.

CHANGES IN BLOOD LEVELS OF IL1 FAMILY CYTOKINES IN PATIENTS WITH ESSENTIAL HYPERTENSION AFTER HAVING COVID-19

Radaeva OA[1]✉, Simbirtsev AS[2], Kostina YuA[1], Iskandyarova MS[1], Mashnina SV[1], Bessheynov DD[1], Negodnova EV[1], Kulyapkin VV[1]

[1] National Research Mordovia State University, Saransk, Russia

[2] State Research Institute of Highly Pure Biopreparations of the Federal Medical Biological Agency, St. Petersburg, Russia

Pathogenetic progression mechanisms in the SARS-CoV-2–essential hypertension (EAH) system are more complex than interaction at the level of angiotensin-converting enzyme 2 (ACE2). The study was aimed to assess the dynamic changes of the IL1 members (IL1β, IL1α, IL1ra, IL18, IL18BP, IL37) blood levels in patients with EAH 10, 30, and 180 days after having COVID-19 in order to define cytokine-mediated mechanisms of EAH progression during the period following infection. The study involved four groups of patients: with a history of EAH and COVID-19 (pneumonia/no pneumonia), with a history of COVID-19 (pneumonia/no pneumonia) and no EAH. Cytokine levels were determined by enzyme immunoassay. The study results demonstrate the prolonged proinflammatory immune response during the period following infection in patients with EAH (retaining higher levels of IL1β, IL1α, and IL18 on days 10, 30, and 180 after recovery ($p < 0.001$) compared to levels measured prior to SARS-CoV-2 infection). In the group with no EAH, the balance of assayed cytokines was restored on day 30 of follow-up. The two-fold increase of blood IL18 levels in patients, having a history of EAH and COVID-19 and showing no increase in the IL18BP levels after 30 days of follow up compared to the values measured prior to infection, is associated with cardiovascular complications occurring during the first six months of follow-up. This makes it possible to hypothesize the importance of these immunoregulatory peptides for the pathogenesis of complications and enhances the relevance of further scientific research.

Keywords: COVID-19, arterial hypertension, IL1β, IL1α, IL18, cardiovascular complications

ИЗМЕНЕНИЕ СОДЕРЖАНИЯ ЦИТОКИНОВ СЕМЕЙСТВА IL1 В КРОВИ БОЛЬНЫХ ЭССЕНЦИАЛЬНОЙ ГИПЕРТЕНЗИЕЙ ПОСЛЕ COVID-19

О. А. Радаева[1]✉, А. С. Симбирцев[2], Ю. А. Костина[1], М. С. Искандярова[1], С. В. Машнина[1], Д. Д. Бесшейнов[1], Е. В. Негоднова[1], В. В. Куляпкин[1]

[1] Мордовский государственный университет имени Н. П. Огарева, Саранск, Россия

[2] Государственный научно-исследовательский институт особо чистых биопрепаратов Федерального медико-биологического агентства, Санкт-Петербург, Россия

Механизм патогенетического утяжеления в системе SARS-CoV-2–эссенциальной гипертензии (ЭАГ) носит более сложный характер, чем взаимодействие на уровне ангиотензинпревращающего фермента 2 (ACE2). Целью исследования было проанализировать динамику содержания представителей семейства IL1 (IL1β, IL1α, IL1ra, IL18, IL18BP, IL37) в крови больных ЭАГ через 10, 30 и 180 дней после COVID-19 для определения цитокинопосредованных звеньев прогрессирования ЭАГ в постинфекционном периоде. В исследовании участвовали четыре группы пациентов: с ЭАГ и COVID-19 в анамнезе (с пневмонией/без пневмонии), с COVID-19 в анамнезе (с пневмонией/без пневмонии) без ЭАГ. Содержание цитокинов определяли иммуноферментным методом. Полученные результаты демонстрируют пролонгированный характер провоспалительного иммунного ответа в постинфекционном периоде у больных с ЭАГ (сохранение более высоких уровней IL1β, IL1α, IL18 на 10-й, 30-й и 180-й дни после выздоровления ($p < 0.001$) при сопоставлении с периодом до инфицирования SARS-CoV-2). В группе без ЭАГ выявлено восстановление баланса анализируемых цитокинов к 30-му дню наблюдения. Двукратное увеличение содержания IL18 в крови пациентов с ЭАГ и COVID-19 в анамнезе на фоне отсутствия роста IL18BP через 30 дней наблюдения при сравнении с доинфекционным периодом ассоциируется с развитием сердечно-сосудистых осложнений в период с первого по шестой месяц наблюдения, что позволяет выдвинуть гипотезу о значимости данных иммунорегуляторных пептидов в патогенезе осложнений и актуализирует дальнейший научный поиск.

Ключевые слова: COVID-19, артериальная гипертензия, IL1β, IL1α, IL18, сердечно-сосудистые осложнения

During the pandemic the efforts of healthcare workers and researchers are more broadly focused on combating the infection with SARS-CoV-2 and the acute mortality reduction. However, there have been increasing reports on the importance of the "long COVID-19" investigation [1]. It is important to consider the delayed effects of SARS-CoV-2 realized through imbalance of cytokine-mediated vectors, underlying the progression of a number of cardiovascular disorders during the period following infection, and the increased risk of complications [2, 3]. The data are discussed, showing links between various types of ARVI and a higher rate of subsequent cardiovascular complications [4, 5]: up to four times higher during the first 30 days, and 1.5 times higher over the years, especially in people with arterial hypertension (AH) [6]. The long-term monitoring of patients with SARS-CoV-2 demonstrates the development of cardiovascular complications and metabiomic alterations during the period following infection, however, these data are scarce and require revision in terms of SARS-CoV-2. In addition to the conclusion that individuals with AH may be more susceptible to COVID-19 and are characterized by more severe course of the disease [7, 8], the literature also reports that the SARS-CoV-2 infection may trigger both the progression of pre-existing pathological process, and the initiation of different pathological process [3].

Understanding of the relationship between COVID-19 and chronic disorders is important for management of patients with comorbidities during the period following infection. The pathogenetic progression mechanisms in the SARS-CoV-2–essential hypertension (EAH) system are more complex than interaction at the level of ACE2. Considering the significance if cytokine-mediated vectors in the EAH pathogenesis, there is a decent chance for alteration of the immune regulation principles associated with hypertension progression after having COVID-19. Immune system is a target for SARS-CoV-2 along with the respiratory system [9], however, currently there is little information on the dynamic changes in the immunoregulatory peptides during the period following the COVID-19 infection. COVID-19 is a novel infectious disease, which explains the scientific community declaration of the importance of acquiring more information about delayed complications in patients with chronic neurological and cardiovascular disorders after SARS-CoV-2 infection, as well as about the role of immunoregulatory peptides in the pathogenesis of such complications [10]. The IL1 family members (IL1β, IL1α, IL1ra, IL18, IL18BP, and IL37) involved in COVID-19 [2, 11–12] are considered significant factors of endothelial dysfunction progression and vascular remodeling, both due to alteration of the balance within the vasopressor and vasodilator system, and due to reprogramming of matrix metalloproteinases synthesis [13–15].

The study was aimed to assess the dynamic changes of the IL1 member (IL1β, IL1α, IL1ra, IL18, IL18BP, IL37) levels in peripheral blood serum of patients with EAH 10, 30, and 180 days after having COVID-19 in order to define the cytokine-mediated mechanisms of potential EAH progression during the period following infection.

METHODS

The assessed data were obtained during phase 3 of the open non-randomized prospective study "Cytokines in Pathogenesis and Diagnosis of EAH" launched in 2008. In the course of the study the four groups of patients were formed, the patients were taken from the database of people with stage 2 EAH (402 people) followed up for 10 (7.5–12.3) years (complex functional, clinical and biochemical examination, which included assessment of levels of 32 cytokines, was performed in 2008,

2013, and in January–February 2020): group 1 — patients with stage 2 EAH having a history of COVID-19 without pneumonia; group 2 — patients with stage 2 EAH having a history of SARS CoV-2-associated pneumonia; group 3 — individuals without EAH having a history of COVID-19 without pneumonia; group 4 — individuals without EAH having a history of SARS-CoV-2-associated pneumonia (groups 3 and 4 included generally healthy individuals (no hypertension), who were followed up for a long time (154 people) within the framework of the study and were comparable both by age and major clinical and biochemical characteristics). Inclusion criteria: stage 2 EAH; relatively similar antihypertensive therapy prior to SARS-CoV-2 infection (ACE inhibitors and/or thiazide diuretics); age 60–65; relatively similar levels of total cholesterol, lipoproteins, triglycerides, glucose prior to SARS-CoV-2 infection; waist circumference less than 102 cm in men and less than 88 cm in women, BMI < 25 kg/m². Exclusion criteria: history of associated clinical conditions at the start of phase 3 of the study (acute cerebrovascular event, myocardial infarction (MI), angina pectoris, coronary revascularization), kidney failure, type 1 or type 2 diabetes mellitus, autoimmune disorders, allergic diseases, symptomatic arterial hypertension, alcohol or drug addiction, smoking, patient's refusal to participate in the study on a long term basis. The comparison group included generally healthy individuals with systolic blood pressure (SBP) of 100–130 mm Hg and diastolic blood pressure (DBP) of 70–89 mm Hg.

An essential aspect of the reported study design is the availability of data on the surveyed patients' cytokine status prior to SARS-CoV-2 infection (January–February 2020).

The diagnosis of COVID-19 was established in accordance with the up-to-date interim guidelines for prevention, diagnosis and treatment of the novel coronavirus infection COVID-19 based on the PCR test results (hereinafter PCR test for detection of SARS CoV 2 RNA), as well as the detection of IgM and IgG anti-SARS CoV 2 immunoglobulin level dynamic changes. Two clinical variants were reported in patients: ARVI or pneumonia with no respiratory failure (mild or moderate course). The patients received relatively similar therapy in accordance with the guidelines valid at the time of the therapy (May–October 2020). The fasting blood sanpling was performed at 8 a. m. 10, 60, and 180 days after two negative PCR tests. Blood underwent centrifugation; the separated serum was stored in the labeled tubes at a temperature of –30° C for a period not exceeding 45 days. The levels of IL1β, IL1α, IL1ra, IL18, IL18 BP, and IL37 were assessed using enzyme immunoassay in the laboratory of the Department of Immunology, Microbiology, and Virology (Laboratory of Microbiology and Immunology, unlimited license № 13.01.04.0001.Л.000005.06.11) by certified specialists, who used the Personal Lab TM platform for microELISA testing (Adaltis; Italy). The test systems had adequate sensitivity and specificity: IL1β (eBioscience (Bender MedSystems), measurement range — 0.3–250 pg/mL; IL1α (eBioscience (Bender MedSystems), measurement range — 1.06–100.0 pg/mL; IL1ra (eBioscience (Bender MedSystems), measurement range — 30–7,000 pg/mL; IL18 (eBioscience (Bender MedSystems), range — 9–5,000 pg/mL; IL18BP (R&D Systems, USCN Life Science), range — 0.51–100 ng/mL); IL37 (Fine Biotech), range — 31.2–2,000 pg/mL.

Telephone interviews were conducted monthly in order to detect cardiovascular complications with subsequent verification of information in the medical institution responsible for management of the patient.

Statistical processing of the data was carried out using the Statistica 13.5 software (StatSoft; USA). The data were presented as median (Me) and percentiles ($Q_{0.25}$–$Q_{0.75}$). Data

Table 1. Comparison of serum cytokine levels (pg/mL) in patients with stage 2 EAH prior to COVID-19 and 10, 30, and 180 days after recovery (Me [Q_{25}–Q_{75}])

	Patients with stage 2 EAH and COVID-19							
	no pneumonia (*n* = 53 people)				pneumonia (*n* = 41 people)			
	before COVID-19	10 days after	30 days after	180 days after	before COVID-19	10 days after	30 days after	180 days after
	1	2	3	4	5	6	7	8
IL1β	18.7 [13.2–22.1]	23.9 [20.1–26.4]*¹	19.6*² [13.9–20.8]	25.7 [14.8–31]*¹,³	19.3 [14–21.3]	37.8*2.4 [34.3–39.1]	30.2*3.5^6 [26.7–38.4]	42.3 [33.4–47.2]*4,5,6,7
IL1α	13.2 [10.6–15.5]	16.9 [12.6–19.1]*¹	14.4 [11–16.6]*¹,²	18.3 [13–23.4]*¹,²,³	20.7 [13.1–22.7]*¹	26.7 [18.1–31.8]*2.5	31.1 [25.7–33.4]*3.5,6	35.6 [29.3-38.1]*4,5,6,7
IL1ra	698 [602–754]	750 [665–812]^¹	690 [508–787]*²	984 [733–1187]*¹,²,³	612 [524–690]'¹	645 [572–735]*²	602 [518–720]*³	621 [503–668]*⁴
IL18	301 [243–352]	399 [243–420]^¹	411 [270-452]*¹	412 [264–436] *¹	394 [321–658]^¹	460 [345–732]*2.5	479 [345–532]*3.5	474 [387–609]*1 ^4.5
IL18 BP	5980 [5311–6720]	7900*¹ [7132–8640]	8190*1[7243–8930]	7870*1 [5311–6720]	5110*¹[4963–6265]	4960*² [4872–6120]	5230*³ [4850–6334]	4890*⁴ [4730–5970]
IL37	65.7 [54.7–68.9]	68.3[51.2–72.4]	64.9 [57.2–75.1]	88.3 [76.4–94.4]*¹,²,³	52.7 [48.1–60.3]*¹	51.3 [44.2–55.1]*²	52.1 [46.3–56.7]*³	49.7 [45.4–55.3]*⁴

Note: * — significance level *p* < 0.001, ^ — *p* < 0.01, ' — *p* < 0.05 (the Wilcoxon test was used for related samples, and the Mann–Whitney *U*-Test was used for independent samples).

distribution was different from the Gauss–Laplace distribution, therefore, the Wilcoxon test was used for comparison of dependent samples, and the Mann–Whitney *U*-Test was used for comparison of independent samples.

RESULTS

Prior to SARS-CoV-2 infection, the patients with stage 2 EAH were characterized by higher IL1β, IL1α, IL18, IL18BP, and IL37 levels in peripheral blood serum compared to generally healthy individuals (*p* < 0.001) (Tables 1 and 2). After having COVID-19, the different quantitative and qualitative indicators, reflecting dynamic changes of blood IL1β, IL1α, IL1ra, IL18, IL18BP, and IL37 levels, were measured in patients with stage 2 EAH compared to patients who had been infected with SARS-CoV-2 but had no EAH. Thus, in individuals with stage 2 EAH, regardless of the COVID-19 form (pneumonia/no pneumonia), higher levels of proinflammatory IL1 family members (IL1β, IL1α) were observed 10 days after the second negative PCR test compared to the period prior to infection (*p* < 0.001; see Table 1). Among patients with no hypertension, this pattern was limited to individuals with SARS-CoV-2-associated pneumonia. Furthermore, blood levels of IL1β, IL1α in this category of patients were back to normal (the levels measured prior to infection were achieved) on day 30 after recovery and remained the same after 6 months (see Table 2). Among patients with EAH, the decrease in IL1β and IL1α levels compared to data obtained on day 10 after recovery was also observed, however, the levels measured prior to infection were not achieved in the group of patients having a history of EAH and SARS-CoV-2-associated pneumonia. It is important to note the repeated increase in blood levels of IL1β and IL1α in patients with EAH (regardless of the history of pneumonia) 180 days after negative PCR test compared to levels measured prior to infection and on

day 30 after laboratory-confirmed recovery (negative PCR test; see Table 1). When assessing the individual indicators, it was discovered that the trend of IL1α level increase by the end of month 6 resulted primarily from the level increase in the group of female patients with EAH (in women the level increased by 79% (75% CI [61–87]) compared to data obtained after a month, and in male patients it increased by 32% (75% CI [12–44]) respectively; *p* < 0.001). No sex-related dynamic changes in IL1β levels were observed. Meanwhile, the increase in the IL1β and IL1α levels during the period following infection in the group of patients with EAH and COVID-19 without pneumonia came against the backdrop of elevated anti-inflammatory IL1ra level, which matched trends observed in the group of patients with no hypertension. Patients with EAH and COVID-19 with pneumonia were characterized by the increase in levels of IL1β and IL1α and no increase in blood levels of the natural antagonist IL1ra (see Table 1).

Analysis of dynamic changes in the levels of IL18 and IL18 BP showed that the patients with stage 2 EAH, regardless of COVID-19 disease form (pneumonia/no pneumonia), had elevated serum IL18 levels 10 days after negative PCR test compared to levels measured prior to infection (*p* < 0.001); this pattern remained the same 30 and 180 days after (see Table 1). It is important to note that in the group of patients with EAH and no history of pneumonia, the increase in the levels of IL18 was accompanied by an increase in the levels of IL18 BP (*p* < 0.001), which remained the same both 30 and 180 days after the laboratory-confirmed recovery; no compensatory increase in the levels of IL18 BP during the period following infection was observed in the group of patients having a history of EAH and pneumonia (*p* < 0.05). It was also determined that individuals with stage 2 EAH and the history of COVID-19 without pneumonia had significantly higher levels of IL37 180 days after the negative PCR test compared both to the levels

Table 2. Comparison of serum cytokine levels (pg/mL) in patients with no stage 2 EAH prior to COVID-19 and 10, 30, and 180 days after recovery (Me [Q_{25}–Q_{75}])

	COVID-19 patients with no EAH							
	no pneumonia (*n* = 41 people)				pneumonia (*n* = 44 people)			
	before COVID-19	10 days after	30 days after	180 days after	before COVID-19	10 days after	30 days after	180 days after
	1	2	3	4	5	6	7	8
IL1β	5.12 [4.83–5.32]	5.33 [4.12–5.2]	5.29 [8.89–5.41]	4.97 [3.65–5.44]	5.38 [4.97–5.44]	17.2 [14.1–20.1]*²,⁴	5.72 [3.3–4.15]*⁶	5.42 [4.53–5.65]*4,6
IL1α	3.22 [3.04–3.41]	3.39 [3.16–3.56]	2.99 [2.56–3.45]	3.18 [2.93–3.39]	3.14 [2.97–3.24]	4.72 [3.11–5.82]*2.5	3.25*⁶ [2.61–2.49]	3.18 [2.67–4.14]*⁶
IL1ra	697 [584–791]	830 [690–914]*1	667 [458–733]*¹,²	728 [602–816]*²	657 [504–731]	843 [693–913]*²	609 [515–769]*⁶	642 [526–712]^4*6
IL18	162 [145–197]	157 [137–172]	166 [151–183]	147 [139–203]	234 [177–267]^¹	298 [235–367]*2.5	247 [224–274]*3.6	228 [207–259]*1,4,6
IL18 BP	4880 [3510–5670]	5070 [3670–5830]	4834 [3220–5470]	4993 [3440–5580]	4768 [3640–5721]	5930*2.5 [4930–8216]	6200*³ [4850–7334]	6180*4.5 [4603–7100]
IL37	80 [68.7–93.3]	76 [62.3–89.4]	78.9 [67.4–86.6]	82.3 [61.2–94.6]	77.1 [63.3–95.7]	74.4 [66.2–83.7]	75.3 [65.7–82.3]	79.5 [55.7–85.3]

Note: * — significance level *p* < 0.001, ^ — *p* < 0.01, ' — *p* < 0.05 (the Wilcoxon test was used for related samples, and the Mann–Whitney *U*-Test was used for independent samples)

measured during the period prior to infection ($p < 0.001$) and the indicators measured in patients with stage 2 EAH and a history of COVID-19 with pneumonia ($p < 0.001$). When comparing periods prior to infection and following infection, no changes in the levels of IL18, IL18 BP, and IL37 were detected in patients with EAH, who had had COVID-19 not involving lungs ($p < 0.05$). In the group of patients with SARS-CoV-2-associated pneumonia having no pneumonia, the levels of IL18 and IL18 BP increased compared to levels measured prior to SARS-CoV-2 infection ($p < 0.001$). However, the levels of those were back to the values measured prior to infection 30 days later (see Table 2). No dynamic changes in the IL37 levels were detected in patients having no EAH during the period following infection ($p < 0.05$).

Comparison of cytokine levels measured prior to infection in patients with SARS-CoV-2-associated pneumonia and stage 2 EAH, and patients with EAH and no pneumonia showed that the patients with EAH and pneumonia demonstrated greater increase in the peripheral blood serum levels of IL1α and IL18 ($p < 0.001$) together with lower concentrations of IL1ra, IL18 BP, and IL37 ($p < 0.001$) compared with the patients with EAH and COVID-19 without pneumonia. No such pattern was observed in the group with no EAH.

It is important to mention, that comparison with classical scales for calculation of cardiovascular complication risk in patients with AH showed the following: the patients were comparable both prior to COVID-19 and after COVID-19, however, acute coronary syndrome, acute stroke and transient ischemic attack occurred in eight patients (males) with EAH and COVID-19 (pneumonia) during 1–6 months of follow-up. Considering the limited number of individuals with complications during the period following infection, their data were assessed separately: the patients were characterized by two-fold increase in peripheral blood serum levels of IL18 after 30 days of follow-up compared to levels measured prior to infection, as well as the increase by 50% compared to values measured on day 10 (prior to infection — 410 [397–426] pg/mL; day 10 — 562 [544–681] pg/mL; day 30 — 824 [807–903] pg/mL). In the group of patients with EAH and a history of SARS-CoV-2-associated pneumonia having no cardiovascular complications in the next months (days 30–180 of follow-up), there were no dynamic changes in the IL18 levels on day 30 compared to day 10 of follow-up. The IL18 level increase in cases of subsequent complications was associated with individual low blood levels of IL18BP (prior to infection — 4,805 [4,793–4,826] pg/mL; day 10 — 4,786 [4,741–4,798] pg/mL; day 30 — 4,630 [4,665–4,662] pg/mL); and IL37 (prior to infection — 46.9 [46.7–47.3] pg/mL; day 10 — 44.5 [44.1–44.9] pg/mL; day 30 — 45.1 [44.6–45.5] pg/mL). This corresponded to the first quartile when analyzing the patients' distribution taking into account the levels of IL18BP and IL37 measured both prior to infection and later. Comparison with patients having no complications during the first six months revealed no differences in the levels of other IL1 family members. Two men in the group with a history of EAH and COVID-19 (no pneumonia) also had acute stroke after the laboratory-confirmed recovery (during 1–6 months of follow-up) and had similar features of the IL1 system, as well as individual qualitative and quantitative characteristics, different from that of individuals having a history of EAH and COVID-19 (no pneumonia).

DISCUSSION

The evidence of dynamic changes in the levels of proinflammatory IL1 family members (IL1β, IL1α, and IL18) and

their natural antagonists (IL1ra, IL18BP) in patients, who had had COVID-19, was obtained during the study. These data confirmed the prolonged proinflammatory immune response during the period following infection in patients with EAH (changes from the levels measured prior to infection persisted for 6 months after laboratory-confirmed recovery) compared to generally healthy individuals (cytokine levels reached the values measured prior to infection 30 days after the laboratory-confirmed recovery in individuals with SARS-CoV-2-associated pneumonia, and 10 days after recovery in patients with no pneumonia). Other researchers also noted the significance of changes in the levels of a number of immunoregulatory peptides (IL6, MCP1, IP10, etc.) in COVID-19 patients [16], specifying the proinflammatory activity and the relationship with potential progression of concomitant diseases in the future. These data are scarce due to the novelty of the virus; there is no information about the patterns considering the cytokine levels in COVID-19 patients measured prior to infection. This increases the relevance of the reported study aimed at assessment of the changes in blood levels of IL1β, IL1α, IL1ra, IL18, IL18 BP, IL37 taking into account the period prior to SARS-CoV-2 infection. A long-lasting retention of the elevated proinflammatory IL1β, IL1α and IL18 concentrations in the blood of post-COVID patients is essential for "enhancement" of the hypertension progression pathogenetic aspects. The evidence of the IL1β stimulatory effect on the ADMA levels (mediated vasopressor due to protein arginine methyltransferase (PRMT) activation and inhibition of dimethylarginine dimethylaminohydrolase (DDAH) has been pubished [17, 18]. Moreover, the IL1α-NF-κB-CCL2 signaling pathway has been described, promoting the immune cell migration and consolidation of vascular remodeling [19], which has been also confirmed by our data [13] supporting greater significance in women with EAH. It should be noted that in patients with a history of EAH and SARS-CoV-2-associated pneumonia, the increase in the levels of IL1β and IL1α, IL18 is not accompanied by the compensatory increase in the levels of natural antagonists (IL1ra and IL18BP, IL3). According to the data published so far, the IL37 and IL18BP functional complex formation is due to common receptor subunits of IL37 and IL18ra, it is directed both at leveling of the IL18 vasopressor effect, and at direct blocking of the SDMA synthesis [20, 21]. No increase in their levels in patients with EAH after SARS-CoV-2 infection together with the elevated IL18 levels increase the likelihood of vasopressor and remodeling effects realization in the IL18–IL18BP–IL37 system with a potentially higher risk of target organ (myocardium, brain, etc.) damage in patients with EAH. This hypothesis is partially confirmed by analysis of individual curves for cytokine level changes in the peripheral blood serum of patients with acute coronary syndrome, acute stroke and transient ischemic attack, characterized by two-fold increase in blood IL18 levels without any compensatory increase in the levels of IL18BP and IL37 during the first month of follow-up. The significantly increased IL18 levels in patients with EAH during the period following the COVID infection can be a key element of the pathogenetic chain, which mediates vascular remodeling promoted by AT II [22], with secondary left ventricular dysfunction progression and increased intima–media thickness of the common carotid artery, which is a consequence of AH and a marker of future cardiovascular risk in patients [23]. The increased IL18 synthesis during the period following the COVID infection may be also due to activation of CD147, the potential receptor for SARS-CoV-2 adhesion [24], which induces the IL18 mRNA via stimulation of binding sites in the NF-κB and AP1 (activator protein 1) for the IL18 gene promoter through Rac1-mediated PI3K/Akt/

IKK (phosphatidylinositol 3-kinase/Akt/IκB kinase)-dependent degradation of IκB-α (inhibitory-κB kinase α) and MKK7/JNK (mitogen-activated proteinkinase kinase 7/c-Jun N-terminal kinase)-coupled AP1 activation [25], which is of greater pathophysiological significance in people with high IL18 levels/ low IL18BP–IL37 levels prior to COVID infection and has been revealed during our study.

It is important to mention that patients with SARS-CoV2-associated pneumonia had higher levels of IL1α and IL18 in peripheral blood serum prior to infection amidst lower levels of antagonists (IL1ra, IL18BP and IL37) compared to patients with EAH and COVID-19 without pneumonia. This suggests the importance of the reported cytokine concentrations and ratio (cytokine status of the patient prior to infection) upon SARS-CoV-2 entry for initiation of pathological process in the lung tissue. However, no differences related to presence of pneumonia were revealed in patients with no EAH and low levels of IL1α and IL18 prior to infection. Therefore, one could speak of potential IL1α- and IL18-mediated elements of pneumonia pathogenesis in patients with COVID-19 and EAH, as well as of dose-dependent effects of the reported cytokines in this category of patients.

CONCLUSION

The study results confirm the scientific importance of studying the dynamic changes in blood levels of IL1 family members in patients having a history of EAH and SARS-CoV-2 infection for construction of individual immunopathogenetic schemes of hypertension progression. The data obtained increase the relevance of the further monitoring used to confirm the hypothesis on the IL18–IL18BP role in the immunopathogenesis of delayed cardiovascular complications in patients having a history of EAH and COVID-19. It is necessary to perform the further comparison of quantitative characteristics of a wide range of cytokines, vasoactive substances, and functional indicators, as well as to carry out multivariate correlation analysis and selection of potential independent criteria with high sensitivity and specificity for the risk of cardiovascular complications in order to confirm the hypothesis that cytokines may be considered the predictive markers in this clinical situation. Understanding of the delayed cardiovascular complication cytokine-mediated mechanisms may change therapeutic approach (therapeutic strategy) to management of patients during both the acute COVID-19 period and the period following infection.

References

1. Mitrani RD, Dabas N, Goldberger JJ. COVID-19 cardiac injury: Implications for long-term surveillance and outcomes in survivors. Heart Rhythm. 2020; 17 (11): 1984–90.
2. Huang C, Wang Y, Li X, Ren L, Zhao J, Hu Y, et al. Clinical features of patients infected with 2019 novel coronavirus in Wuhan, China. Lancet. 2020; 395 (10223): 497–506.
3. Alyammahi SK, Abdin SM, Alhamad DW, Elgendy SM, Altell AT, Omar HA. The dynamic association between COVID-19 and chronic disorders: An updated insight into prevalence, mechanisms and therapeutic modalities. Infect Genet Evol. [Internet] 2021 [cited 2021 Mach 8]; 87: [about 1 p.]. Available from: https://www.sciencedirect.com/science/article/pii/S1567134820304780?via%3Dihub.
4. Nguyen JL, Yang W, Ito K, Matte TD, Shaman J, Kinney PL. Seasonal influenza infections and cardiovascular disease mortality. JAMA Cardiol. 2016; 1 (3): 274–81.
5. Brack MC, Lienau J, Kuebler WM, Witzenrath M. Cardiovascular sequelae of pneumonia. Curr Opin Pulm Med. 2019; 25 (3): 257–62.
6. Corrales-Medina VF, Alvarez KN, Weissfeld LA, Angus DC, Chirinos JA, Chang CC, et al. Association between hospitalization for pneumonia and subsequent risk of cardiovascular disease. JAMA. 2015; 313 (3): 264–74.
7. Richardson S, Hirsch JS, Narasimhan M. Presenting characteristics, comorbidities, and outcomes among 5700 patients hospitalized with COVID-19 in the New York City area. JAMA. 2020; 323 (20): 2052–9.
8. Korostovceva LS, Rotar OP, Konradi AO. Covid-19: kakovy riski pacientov s arterial'noj gipertenziej? AG. 2020; 26 (2): 124–32. Russian.
9. Liu Y, Zhang HG. Vigilance on New-Onset Atherosclerosis Following SARS-CoV-2 Infection. Front Med (Lausanne). [Internet] 2021 Jan [cited 2021 Apr 24] 20; 7: [about 1 p.]. Available from: https://jamanetwork.com/journals/jama/fullarticle/2091304.
10. Carod-Artal FJ. Neurological complications of coronavirus and COVID-19. Complicaciones neurológicas por coronavirus y COVID-19. Rev Neurol. 2020; 70 (9): 311–22.
11. Van de Veerdonk FL, Netea MG. Blocking IL1 to prevent respiratory failure in COVID-19. Crit Care. [Internet] 2020 Jul 18 [cited 2021 Apr 24]; 24 (1): [about 1 p.]. Available from: https://ccforum.biomedcentral.com/articles/10.1186/s13054-020-03166-0.
12. Rowaiye AB, Okpalefe OA, Onuh Adejoke O, Ogidigo JO, Hannah Oladipo O, Ogu AC. Attenuating the Effects of Novel COVID-19

13. (SARS-CoV-2) Infection-Induced Cytokine Storm and the Implications. J Inflamm Res. 2021; 14: 1487–510.
13. Radaeva OA. Citokiny v patogeneze i diagnostike jessencial'noj arterial'noj gipertenzii [dissertacija]. M., 2019. Russian.
14. Krishnan SM, Ling YH, Huuskes BM, Ferens DM, Saini N, Chan CT. Pharmacological inhibition of the NLRP3 inflammasome reduces blood pressure, renal damage, and dysfunction in salt-sensitive hypertension. Cardiovasc Res. 2019; 115 (4): 776–87.
15. Savoia C, Volpe M, Kreutz R. Hypertension, a Moving Target in COVID-19: Current Views and Perspectives. Circ Res. 2021; 128 (7): 1062–79.
16. Siripanthong B, Nazarian S, Muser D. Recognizing COVID-19-related myocarditis: The possible pathophysiology and proposed guideline for diagnosis and management. Heart Rhythm. 2020; 17 (9): 1463–71.
17. McMaster WG, Kirabo A, Madhur MS, Harrison DG. Inflammation, immunity, and hypertensive end-organ damage. Circ Res. 2015; 116 (6): 1022–33.
18. Tain Y-L, Hsu C-N. Toxic Dimethylarginines: Asymmetric Dimethylarginine (ADMA) and Symmetric Dimethylarginine (SDMA). Toxins. 2017; 9 (3): 92–97.
19. Paish HL, Kalson NS, Smith GR, et al. Fibroblasts Promote Inflammation and Pain via IL1α Induction of the Monocyte Chemoattractant Chemokine (C-C Motif) Ligand 2. Am J Pathol. 2018; 188 (3): 696–714.
20. Conti P, Lessiani G, Kritas SK, Ronconi G, Caraffa A, Theoharides TC. Mast cells emerge as mediators of atherosclerosis: Special emphasis on IL37 inhibition. Tissue & Cell. 2017; 49 (3): 393–400.
21. Radaeva OA, Simbircev AS. Analiz patogeneticheskih svjazej IL18, IL18BP, IL37 i vazoaktivnyh veshhestv (AT II, ET-1, NO, ADMA, SDMA, ENOS, INOS, NT-PROCNP i NT-PROBNP) pri jessencial'noj arterial'noj gipertenzii. Medicinskij vestnik Severnogo Kavkaza. 2019; 14 (1–2): 235–8.
22. Valente AJ, Yoshida T, Murthy SN, Sakamuri SS, Katsuyama M, Clark RA, et al. Angiotensin II enhances AT1-Nox1 binding and stimulates arterial smooth muscle cell migration and proliferation through AT1, Nox1, and interleukin-18. Am J Physiol Heart Circ Physiol. 2012; 303 (3): 282–96.
23. OZzbiçer S, Ulucam ZM. Association between Interleukin-18 Level and Left Ventricular Mass Index in Hypertensive Patients. Korean Circulation Journal. 2017; 47 (2): 238–44.
24. Wang K, Chen W, Zhang Z, Deng Y, Lian JQ, Du P, et al. CD147-

spike protein is a novel route for SARS-CoV-2 infection to host cells. Signal Transduct Target Ther. [Internet] 2020 Dec 4 [cited 2021 Apr 24]; 5 (1): [about 1 p.]. Available from: https://www.nature.com/articles/s41392-020-00426-x.

25. Venkatesan B, Valente AJ, Prabhu SD, Shanmugam P, Delafontaine P, Chandrasekar B. EMMPRIN activates multiple transcription factors in cardiomyocytes, and induces interleukin-18 expression via Rac1-dependent PI3K/Akt/IKK/NF-κB and MKK7/JNK/AP-1 signaling. Journal of Molecular and Cellular Cardiology. 2010; 49 (4): 655–63.

Литература

1. Mitrani RD, Dabas N, Goldberger JJ. COVID-19 cardiac injury: Implications for long-term surveillance and outcomes in survivors. Heart Rhythm. 2020; 17 (11): 1984–90.

2. Huang C, Wang Y, Li X, Ren L, Zhao J, Hu Y, et al. Clinical features of patients infected with 2019 novel coronavirus in Wuhan, China. Lancet. 2020; 395 (10223): 497–506.

3. Alyammahi SK, Abdin SM, Alhamad DW, Elgendy SM, Altell AT, Omar HA. The dynamic association between COVID-19 and chronic disorders: An updated insight into prevalence, mechanisms and therapeutic modalities. Infect Genet Evol. [Internet] 2021 [cited 2021 Mach 8]; 87: [about 1 p.]. Available from: https://www.sciencedirect.com/science/article/pii/S1567134820304780?via%3Dihub.

4. Nguyen JL, Yang W, Ito K, Matte TD, Shaman J, Kinney PL. Seasonal influenza infections and cardiovascular disease mortality. JAMA Cardiol. 2016; 1 (3): 274–81.

5. Brack MC, Lienau J, Kuebler WM, Witzenrath M. Cardiovascular sequelae of pneumonia. Curr Opin Pulm Med. 2019; 25 (3): 257–62.

6. Corrales-Medina VF, Alvarez KN, Weissfeld LA, Angus DC, Chirinos JA, Chang CC, et al. Association between hospitalization for pneumonia and subsequent risk of cardiovascular disease. JAMA. 2015; 313 (3): 264–74.

7. Richardson S, Hirsch JS, Narasimhan M. Presenting characteristics, comorbidities, and outcomes among 5700 patients hospitalized with COVID-19 in the New York City area. JAMA. 2020; 323 (20): 2052–9.

8. Коростовцева Л. С., Ротарь О. П., Конради А. О. Covid-19: каковы риски пациентов с артериальной гипертензией? АГ. 2020; 26 (2): 124–32.

9. Liu Y, Zhang HG. Vigilance on New-Onset Atherosclerosis Following SARS-CoV-2 Infection. Front Med (Lausanne). [Internet] 2021 Jan [cited 2021 Apr 24] 20; 7: [about 1 p.]. Available from: https://jamanetwork.com/journals/jama/fullarticle/2091304.

10. Carod-Artal FJ. Neurological complications of coronavirus and COVID-19. Complicaciones neurológicas por coronavirus y COVID-19. Rev Neurol. 2020; 70 (9): 311–22.

11. Van de Veerdonk FL, Netea MG. Blocking IL1 to prevent respiratory failure in COVID-19. Crit Care. [Internet] 2020 Jul 18 [cited 2021 Apr 24]; 24 (1): [about 1 p.]. Available from: https://ccforum.biomedcentral.com/articles/10.1186/s13054-020-03166-0.

12. Rowaiye AB, Okpalefe OA, Onuh Adejoke O, Ogidigo JO, Hannah Oladipo O, Ogu AC. Attenuating the Effects of Novel COVID-19 (SARS-CoV-2) Infection-Induced Cytokine Storm and the Implications. J Inflamm Res. 2021; 14: 1487–510.

13. Радаева О. А. Цитокины в патогенезе и диагностике эссенциальной артериальной гипертензии [диссертация]. М., 2019.

14. Krishnan SM, Ling YH, Huuskes BM, Ferens DM, Saini N, Chan CT. Pharmacological inhibition of the NLRP3 inflammasome reduces blood pressure, renal damage, and dysfunction in salt-sensitive hypertension. Cardiovasc Res. 2019; 115 (4): 776–87.

15. Savoia C, Volpe M, Kreutz R. Hypertension, a Moving Target in COVID-19: Current Views and Perspectives. Circ Res. 2021; 128 (7): 1062–79.

16. Siripanthong B, Nazarian S, Muser D. Recognizing COVID-19-related myocarditis: The possible pathophysiology and proposed guideline for diagnosis and management. Heart Rhythm. 2020; 17 (9): 1463–71.

17. McMaster WG, Kirabo A, Madhur MS, Harrison DG. Inflammation, immunity, and hypertensive end-organ damage. Circ Res. 2015; 116 (6): 1022–33.

18. Tain Y-L, Hsu C-N. Toxic Dimethylarginines: Asymmetric Dimethylarginine (ADMA) and Symmetric Dimethylarginine (SDMA). Toxins. 2017; 9 (3): 92–97.

19. Paish HL, Kalson NS, Smith GR, et al. Fibroblasts Promote Inflammation and Pain via IL1α Induction of the Monocyte Chemoattractant Chemokine (C-C Motif) Ligand 2. Am J Pathol. 2018; 188 (3): 696–714.

20. Conti P, Lessiani G, Kritas SK, Ronconi G, Caraffa A, Theoharides TC. Mast cells emerge as mediators of atherosclerosis: Special emphasis on IL37 inhibition. Tissue & Cell. 2017; 49 (3): 393–400.

21. Радаева О. А., Симбирцев А. С. Анализ патогенетических связей IL18, IL18BP, IL37 и вазоактивных веществ (AT II, ET-1, NO, ADMA, SDMA, ENOS, INOS, NT-PROCNP и NT-PROBNP) при эссенциальной артериальной гипертензии. Медицинский вестник Северного Кавказа. 2019; 14 (1–2): 235–8.

22. Valente AJ, Yoshida T, Murthy SN, Sakamuri SS, Katsuyama M, Clark RA, et al. Angiotensin II enhances AT1-Nox1 binding and stimulates arterial smooth muscle cell migration and proliferation through AT1, Nox1, and interleukin-18. Am J Physiol Heart Circ Physiol. 2012; 303 (3): 282–96.

23. OZzbiçer S, Ulucam ZM. Association between Interleukin-18 Level and Left Ventricular Mass Index in Hypertensive Patients. Korean Circulation Journal. 2017; 47 (2): 238–44.

24. Wang K, Chen W, Zhang Z, Deng Y, Lian JQ, Du P, et al. CD147-spike protein is a novel route for SARS-CoV-2 infection to host cells. Signal Transduct Target Ther. [Internet] 2020 Dec 4 [cited 2021 Apr 24]; 5 (1): [about 1 p.]. Available from: https://www.nature.com/articles/s41392-020-00426-x.

25. Venkatesan B, Valente AJ, Prabhu SD, Shanmugam P, Delafontaine P, Chandrasekar B. EMMPRIN activates multiple transcription factors in cardiomyocytes, and induces interleukin-18 expression via Rac1-dependent PI3K/Akt/IKK/NF-κB and MKK7/JNK/AP-1 signaling. Journal of Molecular and Cellular Cardiology. 2010; 49 (4): 655–63.

EMERGENCY SURGICAL CARE FOR PATIENTS WITH COVID-19 AND TUBERCULOSIS COINFECTION AT MULTISPECIALTY HOSPITAL

Reshetnikov MN ✉, Plotkin DV, Zuban ON, Bogorodskaya EM

Moscow Research and Clinical Center for TB Control, Moscow, Russia

The double burden of the novel coronavirus infection and tuberculosis (TB) is a global challenge. The aspects of emergency surgical care for patients with COVID-19 and TB coinfection remain understudied. The aim of this study was to assess treatment outcomes in acute surgical patients with COVID-19 and preexisting TB coinfection. In 2020, our Center delivered surgical care to 465 patients with COVID-19 and preexisting TB; a total of 64 emergency surgeries were performed on 36 (5.6%) patients, of whom 16 had HIV. Thirteen patients (36.1%) were diagnosed with pulmonary TB; 23 patients (63.9%) had disseminated TB. Chest CT scans showed >25% lung involvement in 61.9% of the patients with COVID-19 pneumonia, 25–50% lung involvement in 30.6% of the patients, and 50–75% lung involvement in 5.6% of the patients. By performing abdominal CT, we were able to detect abdominal TB complications, including perforated tuberculous ulcers of the intestine, intestinal obstruction and tuberculous peritonitis, as well as tuberculous spondylitis complicated by psoas abscess. Of all surgical interventions, 28.2% were abdominal, 23.2% were thoracic, 15.6% were surgeries for soft tissue infection, and 32.8% were other types of surgery. Postoperative mortality was 22.2%. We conclude that COVID-19 did not contribute significantly to postoperative mortality among acute surgical patients with TB.

Keywords: COVID-19, tuberculosis, HIV, emergency surgery

✉ Correspondence should be addressed: Mikhail N. Reshetnikov
Barbolina, 3, Moscow, 107014; taxol@bk.ru

ЭКСТРЕННАЯ ХИРУРГИЧЕСКАЯ ПОМОЩЬ БОЛЬНЫМ НОВОЙ КОРОНАВИРУСНОЙ ИНФЕКЦИЕЙ COVID-19 И ТУБЕРКУЛЕЗОМ В МНОГОПРОФИЛЬНОЙ КЛИНИКЕ

М. Н. Решетников ✉, Д. В. Плоткин, О. Н. Зубань, Е. М. Богородская

Московский городской научно-практический центр борьбы с туберкулезом, Москва, Россия

Двойное бремя новой коронавирусной инфекции COVID-19 и туберкулеза является одной из глобальных проблем сегодняшнего дня. Мало изучены особенности оказания экстренной хирургической помощи этому контингенту пациентов. Целью исследования было оценить результаты лечения острой хирургической патологии у пациентов с новой коронавирусной инфекцией COVID-19 в сочетании с туберкулезом. За 2020 г. пролечено 465 пациентов с сочетанной инфекцией COVID-19/туберкулез, при этом экстренная хирургическая помощь потребовалась в 36 (5,6%) случаях, в том числе 16 пациентам с ВИЧ-инфекцией, которым выполнено 64 экстренных оперативных вмешательства. Туберкулез органов дыхания выявлен у 13 (36,1%) больных, генерализованный — у 23 (63,9%). По данным компьютерной томографии (КТ) органов грудной клетки объем вовлечения легочной ткани при вирусной пневмонии COVID-19 менее 25% зарегистрирован у 61,9% больных, 25–50% — у 30,6%, 50–75% — у 5,6%. КТ органов брюшной полости позволила выявить осложнения адбоминального туберкулеза (перфорации туберкулезных язв кишечника, острую кишечную непроходимость, туберкулезный перитонит), туберкулезный спондилит, осложненный псоас-абсцессом. Распределение оперативных вмешательств было следующим: 28,2% — абдоминальных, 23,2% — торакальных, 15,6% — при гнойных заболеваниях мягких тканей, 32,8% — прочих. В послеоперационном периоде летальность составила 22,2%. По результатам исследования можно сделать вывод, что новая коронавирусная инфекция COVID-19 у пациентов с туберкулезом, подвергнутых экстренным оперативным вмешательсвам, не внесла существенного вклада в увеличение послеоперационной летальности.

Ключевые слова: COVID-19, туберкулез, ВИЧ-инфекция, экстренная хирургия

✉ Для корреспонденции: Михаил Николаевич Решетников
ул. Барболина, д. 3, г. Москва, 107014; taxol@bk.ru

The COVID-19 pandemic put tremendous strain on public health services, overwhelmed hospital capacities and dramatically increased the workload for healthcare workers. Elective surgeries were postponed due to the implementation of containment measures and hospital repurposing for patients with COVID-19. At the same time, hospitals for infectious diseases were admitting COVID-19 patients with acute surgical conditions, a urologic or gynecologic emergency or trauma [1–4]. During the pandemic, protecting healthcare workers against occupational exposure to the virus became a top priority. SARS-CoV-2 actively replicates in the respiratory and gastrointestinal tracts; this increases the risk of infection through aerosol transmission during gastrointestinal or respiratory tract surgery [5, 6]. The diagnosis and treatment of the novel coronavirus infection are complicated by misleading symptoms and difficulty implementing international guidelines on operating room practices during the COVID-19 pandemic [7–10].

Significant challenges arise when delivering surgical care to patients with COVID-19 and comorbidities, such as tuberculosis [11–14].

The aim of this study was to assess treatment outcomes among acute surgical patients with the novel coronavirus infection and preexisting tuberculosis.

METHODS

A center for COVID-19 opened at Moscow Research and Clinical Center for Tuberculosis Control of Moscow Healthcare Department on April 16, 2020. The Center has a pulmonary care unit № 4 for COVID-19 patients with TB, as well as radiology, endoscopy, surgical and intensive care units with anesthesiology and critical care experts. In 2020, the Center delivered medical care to 465 patients with TB and COVID-19 coinfection. Of them 36 (5.6%) patients underwent emergency surgery.

Those 36 patients were included in the study. The following inclusion criterion was applied: patients with COVID-19. TB was confined to the lungs in 13 (36.1%) patients, of whom 8 (61.5%) had extensive pulmonary TB, 2 (15.4%) had infiltrative pulmonary TB, 2 (15.4%) had fibrocavernous TB, and 1 (7.7%) had caseous pneumonia. Three patients in this subgroup (23.1%) had HIV coinfection. Disseminated TB involving the lungs and other organs was diagnosed in 23 of 36 patients (63.9%). In this subgroup, 4 (17.4%) patients had abdominal TB, 3 (13.0%) had genitourinary TB; peripheral lymph nodes were involved in 2 (8.7%) cases, 2 more patients (8.7%) had bone and joint TB. Multi-organ involvement (> 2) was observed in 12 (52.2%) patients. In the disseminated TB subgroup, HIV coinfection was detected in 13 (56.5%) patients.

Therapeutic interventions for COVID-19 were conducted following the COVID-19 Treatment Protocol for patients undergoing treatment at healthcare facilities of Moscow Healthcare Department (Moscow, 2020). TB treatment protocols complied with the Federal Clinical Guidelines on treating TB in adults (Moscow, 2020).

Twenty-three (63.9%) patients were referred to the Center by specialized TB hospitals of Moscow City. Thirteen patients (36.1%) were transferred by emergency medical services (EMS) from other medical facilities. Of them, 7 came from non-TB facilities due to suspicion of TB, 6 were taken by EMS either from a computed tomography facility or from their homes. Nineteen (52.8%) patients were Moscow City residents, 9 (25.0%) resided outside Moscow region, 5 (13.9%) were non-Russian residents, and 3 (8.3%) were homeless.

The study included 31 (86.1%) male and 5 (13.9%) female patients aged 26 to 83 years (mean age was 41.9 ± 15.3 years). All of them had TB; 16 (44.4%) had HIV coinfection. On admission, all patients underwent a computed tomography (CT) scan of the chest; in addition, patients with acute abdominal pathology underwent an abdominal CT and/or abdominal ultrasound examination. The clinical diagnosis of COVID-19 was based on PCR tests for SARS-CoV-2 detection in nasopharyngeal swabs and chest CT findings. TB diagnosis was based on radiography findings, urine, sputum and stool tests, and biopsies. The collected specimens were studied for the pathomorphological features of TB and/or the presence of tuberculosis mycobacteria (MTB) using luminescence microscopy, liquid/solid culture-based methods and molecular-genetic analysis.

The significance of differences between quantitative variables was assessed using Student's t-test. For quantitative variables, the chi-square test was used.

RESULTS

The average duration of TB from its onset to the time of hospital admission was 6.7 months. Sputum tests came back negative for most patients (23 patients, or 63.9%). Thirteen patients (36.1%) tested positive for MTB; of them 4 (30.8%) were infected with MDR strains and 1 (7.7%) had XDR-TB.

In all cases, chest CT scans were suggestive of viral pneumonia. SARS-CoV-2 RNA was detected in the nasopharyngeal swabs of 28 (77.8%) patients; 8 (22.2%) tested negative for SARS-CoV-2, so the diagnosis of COVID-19 in these patients was based on the clinical and radiographic findings (Table 1).

Abdominal CT was performed on 11 (30.6%) patients. Two patients had free gas in the peritoneal cavity due to a perforated tuberculous ulcer of the ileum. In another patient, the accumulation of free gas was localized to the right ileal region and was due to the sealed perforation of the cecum. One patient had retroperitoneal abscess due to the retroperitoneal perforation of a tuberculous ulcer in the cecum. One patient had dilated bowel loops resulting from acute intestinal obstruction. Abdominal lymphadenopathy and encysted tuberculous peritonitis were observed in 2 patients. One patient had tense ascites and another one had tuberculous spondylitis complicated by psoas abscess. Two patients with strangulated hernia had no abdominal pathology.

A total of 64 emergency surgeries were performed on 36 patients; 12 patients required repeat surgery (Table 2).

Abdominal surgery was the most common surgical intervention: a total of 18 (28.2%) abdominal surgeries were performed on 8 patients. Five patients underwent surgery for abdominal TB complications: 4 of them had a perforated tuberculous intestinal ulcer due to intestinal TB, one had acute intestinal obstruction due to a stenosing ulcer. It should be noted that abdominal surgical pathology is often characterized by a protracted clinical course and vague symptoms, and the patient starts seeking medical advice after the condition has progressed to advanced stages and requires a series of surgical interventions. Four patients with a perforated tuberculous ulcer of the intestine had to undergo repeat surgery. The patient with acute intestinal obstruction was treated with only one surgery.

Two patients with pulmonary TB and COVID-19 coinfection were admitted to the Center for suspected acute appendicitis. Diagnostic laparoscopy revealed that one of them had

Table 1. Distribution of patients with TB by the severity of viral pneumonia and the presence of SARS-CoV-2 RNA

Severity of viral pneumonia on chest CT (lung involvement score)	Number of patients		SARS-CoV-2 RNA detected	
	Abs.	%	Abs.	%
1 (< 25%)	23	61.9	19	52.8
2 (25–50%)	11	30.6	8	22.2
3 (50–75%)	2	5.6	1	2.8
Total	36	100	28	77.8

Table 2. Number and type of performed surgical interventions

Intervention	Number		Deaths (*n* = 36)	
	Abs.	%	Abs.	%
Abdominal				
Relaparotomy for peritonitis	12	18.8		
Right hemicolectomy	3	4.7		
Diagnostic laparoscopy	2	3.1		
Abdominal paracentesis	1	1.6		
Total:	18	28.2	4	11.1
Thoracic				
Pleural drainage	11	17.2		
Bronchoscopy, bronchial blocker placement	4	6.2		
Total:	15	23.4		
Surgery for soft tissue infection				
Necrectomy	5	7.8		
VAC procedure	3	4.7		
Incision and drainage surgery for phlegmon	2	3.1		
Total:	10	15.6		
Other				
Tracheostomy	7	10.9		
Secondary suture	4	6.2		
Primary wound debridement	3	4.7		
Suprapubic cystostomy	3	4.7		
Herniotomy for strangulated hernia	2	3.1		
Psoas abscess drainage	1	1.6		
Lower limb amputation	1	1.6		
Total:	21	32.8	4	11.1
Total:	64	100	8	22.2

tuberculosis of abdominal lymph nodes and another had tuberculous peritonitis resulting from the spread of the disease from the lungs to other organs. Intraoperatively, multiple miliary lesions of the peritoneum, bowel loops, liver and spleen, abdominal lymphadenopathy, and peritoneal effusion were observed. In both cases, abdominal tuberculosis was confirmed by the histopathologic examination of the biopsied abdominal lymph nodes and peritoneal specimens.

Thoracic surgery was performed on 10 patients with COVID-19 and preexisting TB; of them 5 had to undergo repeat surgery. All thoracic patients received pleural drains (6 patients required drains due to pneumothorax, the rest 4 had pleuritis or pleural empyema; see Figure).

Bronchial blocker placement during rigid bronchoscopy and mechanical ventilation was performed on 4 patients. Of them, 2 had fibrocavernous TB and developed pulmonary hemorrhage. Two other patients had a bronchopleural fistula, a collapsed lung and were unresponsive to pleural drainage. Tracheostomy was performed on 7 patients in intensive care requiring long-term mechanical ventilation.

There were 8 (22.2%) postoperative deaths. Of them, 4 patients with COVID-19/TB and respiratory failure were put on a ventilator and so underwent only one surgical intervention (tracheostomy). In their case, the immediate cause of death was COVID-19 and TB coinfection. Of those 4 patients, 2 had extensive pulmonary TB and COVID-19 coinfection (lung involvement score: 3); the other 2 patients had disseminated TB and COVID-19 coinfection (lung involvement score: 1 and 3, respectively).

Two patients died after multiple surgical interventions for abdominal TB complications, perforated tuberculous ulcers of the intestine accompanied by peritonitis. One patient, who underwent diagnostic laparoscopy for TB peritonitis, died of disseminated TB. Another death was due to decompensated liver cirrhosis and disseminated TB; this patient had tight ascites and had to undergo abdominal paracentesis. Four (50%) of the deceased patients had triple infection: COVID-19/HIV/TB; of them 2 also had hepatitis C.

DISCUSSION

There are a few important aspects to diagnosing and treating acute surgical patients with COVID-19 and TB coinfection. Before the COVID-19 pandemic, an abdominal ultrasound examination was the preferred diagnostic modality for patients with acute abdomen [15]. Now, considering the spread of the novel coronavirus infection, it is essential to assess the extent of lung damage caused not only by TB but also by rapidly progressing COVID-19 pneumonia [16]. We think that performing both chest and abdomen CT in patients with coinfection helps to clarify the underlying cause of abdominal pathology and detect an abdominal catastrophe if presenting symptoms are unobvious. Our opinion is consistent with the opinion of other researchers [17, 18].

However, some authors report that abdominal CT examinations are being decreasingly performed on patients with acute abdomen because CT facilities are overwhelmed during the pandemic; such reports promote laparoscopy as a
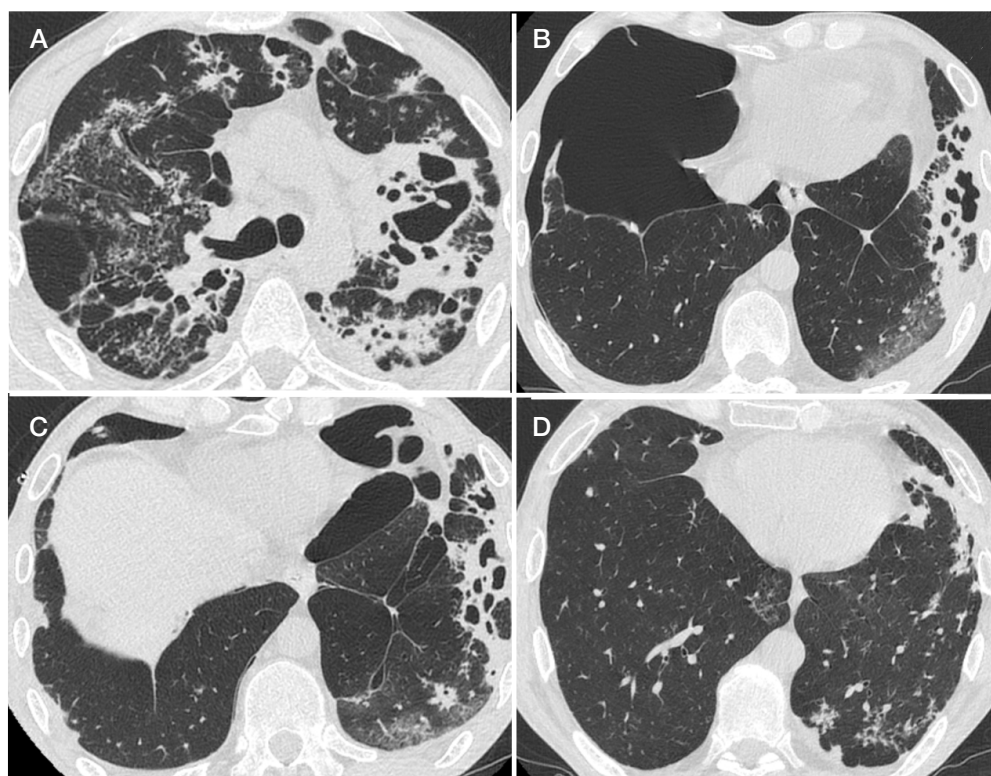
Fig. Chest CT scans. Pneumothorax dynamics. **A**. Date of exam: 18.11.2020. Focal infiltrates and various-sized cavities in both lungs. **B**. Date of exam: 20.11.2020. Right-sided pneumothorax. Ground glass opacities in left S10 (> 25% lung involvement). **C**. Date of exam: 22.11.2020. Scan performed after right pleural drainage; the lung is almost completely expanded. Left-sided pneumothorax; partially resolved ground glass opacities in left S10. **D**. Date of exam: 11.12.2020. Complete resolution of pneumothorax; partially resolved infiltrates

diagnostic modality for patients with acute abdomen [19, 20]. However, patients mentioned in these publications do not have TB. It is well known that abdominal CT can clarify the need for laparoscopy as it is capable of detecting free gas in the peritoneum and fluid accumulation in bowel loops. In other words, abdominal CT can noninvasively detect complications of abdominal TB, including perforated tuberculous ulcers and acute intestinal obstruction. Therefore, we think it reasonable to perform an abdominal CT scan on patients with suspected acute surgical pathology and COVID-19/TB coinfection. In our study, only 2 patients, whose CT scans were inconclusive, were subjected to diagnostic laparoscopy. But the overarching surgical treatment strategy for our patients with abdominal TB complications was unchanged [21, 22].

Pulmonary TB is a common cause of spontaneous pneumothorax. The rate of this complication varies between 0.6% and 1.4% [23]. In patients with TB, spontaneous pneumothorax develops due to ruptured pleural blebs or bullae compromising visceral pleura integrity. However, spontaneous pneumothorax is not always associated with TB in TB patients. For example, it can be linked to bullous emphysema which developed independently of TB. Recent publications report spontaneous pneumothorax in patients with COVID-19 who did not have TB and/or any other preexisting lung disease. Almost all of them were on mechanical ventilation, i.e. they might have sustained injury to the trachea during intubation. Their mortality rate was very high (72.7%) [24–26]. In our study, 6 of 7 patients with pneumothorax underwent pleural drainage. All of them had active pulmonary TB. One of them died: he had a past history of multiple surgeries for abdominal TB complications and pneumothorax.

The analysis of surgical interventions performed in April through December 2019 vs. the same period in 2020 reveals a rise in the total share of tracheostomies from 5.1% (12 of 234

emergency surgeries) in 2019 to 10.9% in 2020, which can be explained by the need for long-term mechanical ventilation in patients with COVID-19.

The analysis of postoperative mortality shows that abdominal TB complications (perforated tuberculous ulcer leading to peritonitis in patients with disseminated TB) was the primary cause of death in 50% of patients in 2019 and 2020. A multicenter cohort study reports an increase in postoperative mortality to 15.9% among COVID-19 patients requiring emergency surgical care, in comparison with patients without the novel coronavirus infection [27].

In our study, there was no reliable increase in postoperative mortality: 16.5% in 2019 vs. 22.2% in 2020 (χ^2 = 0.46; p = 0.49). Therefore, we conclude that COVID-19 did contribute significantly to postoperative mortality in acute surgical patients with TB. According to the literature, hospital mortality from COVID-19 varies from 6% to 25% [28]. Previously, we reported that overall hospital mortality among patients with COVID-19 and TB coinfection was 10.2%, whereas postoperative mortality in this cohort of patients was more than twice as high (22.2%) [14].

One of the limitations of this study is its small sample size due to the specific character of our patient cohort (triple COVID-19/HIV/TB infection). Another limitation is the short follow-up period, which did not allow us to analyze the long-term outcomes of the performed surgical interventions.

CONCLUSION

At our specialized TB hospital providing a wide range of health services to TB patients, emergency surgery was most commonly performed on patients with disseminated TB and COVID-19 coinfection (63.9%); patients with pulmonary TB required emergency surgical care less often (36.1%). Almost half of our

patients admitted during the pandemic for surgical emergency (44.4%) had triple infection (COVID-19/HIV/TB). Abdominal surgery (28.2%) was the most commonly performed procedure among patients with COVID-19/TB, followed by thoracic surgery (23.4%) and surgery for soft tissue infection (15.6%).

The highest postoperative mortality (50%) was observed in the small group of 8 patients operated for abdominal conditions. Of all the patients who died in the postoperative period, 2 (50%) had COVID-19 and TB, and another 2 (50%) had quadruple infection with COVID-19, HIV, TB and hepatitis C.

References

1. Patriti A, Baiocchi GL, Catena F, Marini P, Catarci M; FACS on behalf of the Associazione Chirurghi Ospedalieri Italiani (ACOI). Emergency general surgery in Italy during the COVID-19 outbreak: first survey from the real life. World J Emerg Surg. 2020; 15 (1): 36. PubMed PMID: 32448333. DOI: 10.1186/s13017-020-00314-3.

2. De Simone B, Chouillard E, Di Saverio S, Pagani L, Sartelli M, Biffl WL et al. Emergency surgery during the COVID-19 pandemic: what you need to know for practice. Ann R Coll Surg Engl. 2020; 102 (5): 323–332. PubMed PMID: 32352836. DOI: 10.1308/rcsann.2020.0097.

3. Colosimo C, Kelly J, Coker J, Bhuller S, Ballman E, Baker-Sparret C, et al. Unscreened: Urgent and Emergent Surgical Outcomes in the Early COVID-19 Pandemic. Cureus. 2020; 12 (12): e11878. PubMed PMID: 33415031. DOI: 10.7759/cureus.11878.

4. Krutsri C, Singhatas P, Sumpritpradit P, Thampongsa T, Phuwapraisirisan S, Gesprasert C, et al. Impact of the COVID-19 pandemic on the outcome, morbidity, and mortality of acute care surgery patients: A retrospective cohort study. International Journal of Surgery Open. 2021; (28): 50–55. DOI: 10.1016/j.ijso.2020.11.021.

5. Gupta A, Madhavan MV, Sehgal K, Nair N, Mahajan S, Sehrawat TS, et al. Extrapulmonary manifestations of COVID-19. Nat Med. 2020; 26 (7): 1017–32. PubMed PMID: 32651579. DOI: 10.1038/s41591-020-0968-3.

6. Maev IV, Shpektor AV, Vasilyeva EY, Manchurov VN, Andreev DN Novel coronavirus infection COVID-19: extrapulmonary manifestations. Ter Arkh. 2020; 92 (8): 4–11. PubMed PMID: 33346454. DOI: 10.26442/00403660.2020.08.000767. Russian.

7. Ti LK, Ang LS, Foong TW, Ng BSW. What we do when a COVID-19 patient needs an operation: operating room preparation and guidance. Can J Anaesth. 2020; 67 (6): 756–58. PubMed PMID: 32144591. DOI: 10.1007/s12630-020-01617-4.

8. COVIDSurg Collaborative. Global guidance for surgical care during the COVID-19 pandemic. Br J Surg. 2020; 107 (9): 1097–03. PubMed PMID: 32293715. DOI: 10.1002/bjs.11646.

9. Welsh Surgical Research Initiative (WSRI) Collaborative. Recommended operating room practice during the COVID-19 pandemic: systematic review. BJS Open. 2020; 4 (5): 748–56. PubMed PMID: 32395909. DOI: 10.1002/bjs5.50304.

10. Gote SV, Revishvili ASh, Pushkar DYu, Adamyan LV, Krylov VV, Shelygin YuA, i dr. Metodicheskie rekomendacii "Jekstrennaja hirurgicheskaja pomoshh' v uslovijah COVID-19". M., 2020. Availabe from: https://главный-хирург.рф/docs/metodrec/covid-19-recommendation.pdf [Accessed Apr 10, 2021]. Russian.

11. Tadolini M, Codecasa LR, García-García JM, Blanc FX, Borisov S, Alffenaar JW, et al. Active tuberculosis, sequelae and COVID-19 co-infection: first cohort of 49 cases. Eur Respir J. 2020; 56 (1): 2001398. PubMed PMID: 32457198. DOI: 10.1183/13993003.01398-2020.

12. Elkin AV, Savina TA, Levina LR, Kovaleva RG, Kondakova MN. Mnogoprofil'nyj tuberkuleznyj stacionar goroda Sankt-Peterburga v period pandemii COVID-19. Tuberkulez i social'no znachimye zabolevanija. 2020; (4): 10–15. Russian.

13. Gao Y, Liu M, Chen Y, Shi S, Geng J, Tian J. Association between tuberculosis and COVID-19 severity and mortality: A rapid systematic review and meta-analysis. J Med Virol. 2020; 10.1002/jmv.26311. PubMed PMID: 32687228. DOI: 10.1002/jmv.26311.

14. Zuban ON, Reshetnikov MN, Ustinov AV. COVID-19 u bol'nyh tuberkulezom: odnocentrovoe issledovanie. Tuberkulez i social'no znachimye zabolevanija. 2020; (4): 58–63. Russian.

15. Plotkin DV, Loshkareva EO, Kirillova OV, Reshetnikov MH, Sinicyn MV, Chauzov AYu. Jeho-sonograficheskaja semiotika abdominal'nogo tuberkuleza. Tuberkulez i bolezni legkih. 2020; 98 (8): 32–38. DOI: 10.21292/2075-1230-2020-98-8-32-38. Russian.

16. Petrikov SS, Popugaev KA, Barmina TG, Zabavskaja OA, Sharifullin FA, Kokov LS. Sopostavlenie klinicheskih dannyh i komp'juterno-tomograficheskoj semiotiki legkih pri COVID-19. Tuberkulez i bolezni legkih. 2020; 98 (7): 14–25. DOI: 10.21292/2075-1230-2020-98-7-14-25. Russian.

17. Borofsky S, Taffel M, Khati N, Zeman R, Hill M. The emergency room diagnosis of gastrointestinal tract perforation: the role of CT. Emerg Radiol. 2015; 22 (3): 315–27. PubMed PMID: 25417073. DOI: 10.1007/s10140-014-1283-4.

18. Deshpande SS, Joshi AR, Deshpande SS, Phajlani SA. Computed tomographic features of abdominal tuberculosis: unmask the impersonator! Abdom Radiol (NY). 2019; 44 (1): 11–21. PubMed PMID: 30027495. DOI: 10.1007/s00261-018-1700-3.

19. Korolkov AYu, Teplov VM, Zajcev DA, Cebrovskaja EA, Nikitina TO. Okazanie jekstrennoj hirurgicheskoj pomoshhi v uslovijah mnogoprofil'nogo stacionara, pereprofilirovannogo pod lechenie pacientov s novoj koronavirusnoj infekciej (COVID-19). Vestnik hirurgii imeni I. I. Grekova. 2020; 179 (5): 11–15. DOI: 10.24884/0042-4625-2020-179-5-11-15. Russian.

20. Vechorko VI, Anosov VD, Silaev BV. Diagnosis and treatment of acute surgical diseases in patients with COVID-19. Bulletin of RSMU. 2020; (3): 65–69. DOI: 10.24075/brsmu.2020.038.

21. Reshetnikov MN, Skopin MS, Sinicyn MV, Plotkin DV, Zuban ON. Vybor hirurgicheskoj taktiki pri perforativnyh tuberkuleznyh jazvah kishechnika u bol'nyh VICh-infekciej. Tuberkulez i bolezni legkih. 2017; 95 (9): 19–24. DOI: 10.21292/2075-1230-2017-95-9-19-24. Russian.

22. Gerstein S, Khatri A, Roth N, Wallach F. Coronavirus disease 2019 and extra-pulmonary tuberculosis co-infection — A case report and review of literature. J Clin Tuberc Other Mycobact Dis. 2021; 22: 100213. PubMed PMID: 33521333. DOI: 10.1016/j.jctube.2021.100213.

23. Freixinet JL, Caminero JA, Marchena J, Rodríguez PM, Casimiro JA, Hussein M. Spontaneous pneumothorax and tuberculosis: long-term follow-up. Eur Respir J. 2011; 38 (1): 126–31. PubMed PMID: 20947681. DOI: 10.1183/09031936.00128910.

24. Miheev AB, Aftaeva EV, Kazakova SS, Zinoveva ZV, Gavrikova NV. Spontannyj pnevmotoraks kak oslozhnenie porazhenija legkih pri COVID-19. Tuberkulez i bolezni legkih. 2021; 99 (3): 18–22. DOI: 10.21292/2075-1230-2021-99-3-18-22. Russian.

25. Xu Y, Li S, Liu H. Clinical outcomes of pleural drainage on pneumothorax and hydrothorax in critically ill patients with COVID-19: A case series with literature review. Heart & Lung. 2020; 50 (2): 213–19. PubMed PMID: 33310504. DOI: 10.1016/j.hrtlng.2020.12.007.

26. Martinelli AW, Ingle T, Newman J, Nadeem I, Jackson K, Lane ND, et al. COVID-19 and pneumothorax: a multicentre retrospective case series. Eur Respir J. 2020; 56 (5): 2002697. PubMed PMID: 32907891. DOI: 10.1183/13993003.02697-2020.

27. Carrier FM, Amzallag É, Lecluyse V, Côté G, Couture ÉJ, D'Aragon F, et al. Postoperative outcomes in surgical COVID-19 patients: a multicenter cohort study. BMC Anesthesiol. 2021; 21 (1): 15. PubMed PMID: 33435887. DOI: 10.1186/s12871-021-01233-9.

28. Li J, Huang DQ, Zou B, Yang H, Hui WZ, Rui F, et al. Epidemiology of COVID-19: A systematic review and meta-analysis of clinical characteristics, risk factors, and outcomes. J Med Virol. 2021; 93 (3): 1449–58. PubMed PMID: 32790106. DOI: 10.1002/jmv.26424.

Литература

1. Patriti A, Baiocchi GL, Catena F, Marini P, Catarci M; FACS on behalf of the Associazione Chirurghi Ospedalieri Italiani (ACOI). Emergency general surgery in Italy during the COVID-19 outbreak: first survey from the real life. World J Emerg Surg. 2020; 15 (1): 36. PubMed PMID: 32448333. DOI: 10.1186/s13017-020-00314-3.

2. De Simone B, Chouillard E, Di Saverio S, Pagani L, Sartelli M, Biffl WL et al. Emergency surgery during the COVID-19 pandemic: what you need to know for practice. Ann R Coll Surg Engl. 2020; 102 (5): 323–332. PubMed PMID: 32352836. DOI: 10.1308/rcsann.2020.0097.

3. Colosimo C, Kelly J, Coker J, Bhuller S, Ballman E, Baker-Sparret C, et al. Unscreened: Urgent and Emergent Surgical Outcomes in the Early COVID-19 Pandemic. Cureus. 2020; 12 (12): e11878. PubMed PMID: 33415031. DOI: 10.7759/cureus.11878.

4. Krutsri C, Singhatas P, Sumpritpradit P, Thampongsa T, Phuwapraisirisan S, Gesprasert C, et al. Impact of the COVID-19 pandemic on the outcome, morbidity, and mortality of acute care surgery patients: A retrospective cohort study. International Journal of Surgery Open. 2021; (28): 50–55. DOI: 10.1016/j.ijso.2020.11.021.

5. Gupta A, Madhavan MV, Sehgal K, Nair N, Mahajan S, Sehrawat TS, et al. Extrapulmonary manifestations of COVID-19. Nat Med. 2020; 26 (7): 1017–32. PubMed PMID: 32651579. DOI: 10.1038/s41591-020-0968-3.

6. Маев И. В., Шпектор А. В., Васильева Е. Ю., Манчуров В. Н., Андреев Д. Н. Новая коронавирусная инфекция COVID-19: экстрапульмональные проявления. Терапевтический архив. 2020; 92 (8): 4–11. DOI: 10.26442/00403660.2020.08.000767.

7. Ti LK, Ang LS, Foong TW, Ng BSW. What we do when a COVID-19 patient needs an operation: operating room preparation and guidance. Can J Anaesth. 2020; 67 (6): 756–58. PubMed PMID: 32144591. DOI: 10.1007/s12630-020-01617-4.

8. COVIDSurg Collaborative. Global guidance for surgical care during the COVID-19 pandemic. Br J Surg. 2020; 107 (9): 1097–03. PubMed PMID: 32293715. DOI: 10.1002/bjs.11646.

9. Welsh Surgical Research Initiative (WSRI) Collaborative. Recommended operating room practice during the COVID-19 pandemic: systematic review. BJS Open. 2020; 4 (5): 748–56. PubMed PMID: 32395909. DOI: 10.1002/bjs5.50304.

10. Готье С. В., Ревишвили А. Ш., Пушкарь Д. Ю., Адамян Л. В., Крылов В. В., Шелыгин Ю. А. и др. Методические рекомендации «Экстренная хирургическая помощь в условиях COVID-19». М., 2020; 14 с. Доступно по ссылке: https://главный-хирург.рф/docs/metodrec/covid-19-recommendation.pdf [Дата обращения 10 апреля 2021 г.]

11. Tadolini M, Codecasa LR, García-García JM, Blanc FX, Borisov S, Alffenaar JW, et al. Active tuberculosis, sequelae and COVID-19 co-infection: first cohort of 49 cases. Eur Respir J. 2020; 56 (1): 2001398. PubMed PMID: 32457198. DOI: 10.1183/13993003.01398-2020.

12. Елькин А. В., Савина Т. А., Левина Л. Р., Ковалева Р. Г., Кондакова М. Н. Многопрофильный туберкулезный стационар города Санкт-Петербурга в период пандемии COVID-19. Туберкулез и социально значимые заболевания. 2020; (4): 10–15.

13. Gao Y, Liu M, Chen Y, Shi S, Geng J, Tian J. Association between tuberculosis and COVID-19 severity and mortality: A rapid systematic review and meta-analysis. J Med Virol. 2020; 10.1002/jmv.26311. PubMed PMID: 32687228. DOI: 10.1002/jmv.26311.

14. Зубань О. Н., Решетников М. Н., Устинов А. В. COVID-19 у больных туберкулезом: одноцентровое исследование. Туберкулез и социально значимые заболевания. 2020; (4): 58–63.

15. Плоткин Д. В., Лошкарева Е. О., Кириллова О. В., Решетников М. Н., Синицын М. В., Чаузов А. Ю. Эхо-сонографическая семиотика абдоминального туберкулеза. Туберкулез и болезни легких. 2020; 98 (8): 32–38. DOI: 10.21292/2075-1230-2020-98-8-32-38.

16. Петриков С. С., Попугаев К. А., Бармина Т. Г., Забавская О. А., Шарифуллин Ф. А., Коков Л. С. Сопоставление клинических данных и компьютерно-томографической семиотики легких при COVID-19. Туберкулез и болезни легких. 2020; 98 (7): 14–25. DOI: 10.21292/2075-1230-2020-98-7-14-25.

17. Borofsky S, Taffel M, Khati N, Zeman R, Hill M. The emergency room diagnosis of gastrointestinal tract perforation: the role of CT. Emerg Radiol. 2015; 22 (3): 315–27. PubMed PMID: 25417073. DOI: 10.1007/s10140-014-1283-4.

18. Deshpande SS, Joshi AR, Deshpande SS, Phajlani SA. Computed tomographic features of abdominal tuberculosis: unmask the impersonator! Abdom Radiol (NY). 2019; 44 (1): 11–21. PubMed PMID: 30027495. DOI: 10.1007/s00261-018-1700-3.

19. Корольков А. Ю., Теплов В. М., Зайцев Д. А., Цебровская Е. А., Никитина Т. О. Оказание экстренной хирургической помощи в условиях многопрофильного стационара, перепрофилированного под лечение пациентов с новой коронавирусной инфекцией (COVID-19). Вестник хирургии имени И. И. Грекова. 2020; 179 (5): 11–15. DOI: 10.24884/0042-4625-2020-179-5-11-15.

20. Вечорко В. И., Аносов В. Д., Силаев Б. В. Диагностика и лечение острых хирургических заболеваний у пациентов с COVID-19. Вестник РГМУ. 2020; (3): 71–76. DOI: 10.24075/vrgmu.2020.038.

21. Решетников М. Н., Скопин М. С., Синицын М. В., Плоткин Д. В., Зубань О. Н. Выбор хирургической тактики при перфоративных туберкулезных язвах кишечника у больных ВИЧ-инфекцией. Туберкулез и болезни легких. 2017; 95 (9): 19–24. DOI: 10.21292/2075-1230-2017-95-9-19-24.

22. Gerstein S, Khatri A, Roth N, Wallach F. Coronavirus disease 2019 and extra-pulmonary tuberculosis co-infection — A case report and review of literature. J Clin Tuberc Other Mycobact Dis. 2021; 22: 100213. PubMed PMID: 33521333. DOI: 10.1016/j.jctube.2021.100213.

23. Freixinet JL, Caminero JA, Marchena J, Rodríguez PM, Casimiro JA, Hussein M. Spontaneous pneumothorax and tuberculosis: long-term follow-up. Eur Respir J. 2011; 38 (1): 126–31. PubMed PMID: 20947681. DOI: 10.1183/09031936.00128910.

24. Михеев А. В., Афтаева Е. В., Казакова С. С., Зиновьева З. В., Гаврикова Н. В. Спонтанный пневмоторакс как осложнение поражения легких при COVID-19. Туберкулез и болезни легких. 2021; 99 (3): 18–22. DOI: 10.21292/2075-1230-2021-99-3-18-22.

25. Xu Y, Li S, Liu H. Clinical outcomes of pleural drainage on pneumothorax and hydrothorax in critically ill patients with COVID-19: A case series with literature review. Heart & Lung. 2020; 50 (2): 213–19. PubMed PMID: 33310504. DOI: 10.1016/j.hrtlng.2020.12.007.

26. Martinelli AW, Ingle T, Newman J, Nadeem I, Jackson K, Lane ND, et al. COVID-19 and pneumothorax: a multicentre retrospective case series. Eur Respir J. 2020; 56 (5): 2002697. PubMed PMID: 32907891. DOI: 10.1183/13993003.02697-2020.

27. Carrier FM, Amzallag É, Lecluyse V, Côté G, Couture ÉJ, D'Aragon F, et al. Postoperative outcomes in surgical COVID-19 patients: a multicenter cohort study. BMC Anesthesiol. 2021; 21 (1): 15. PubMed PMID: 33435887. DOI: 10.1186/s12871-021-01233-9.

28. Li J, Huang DQ, Zou B, Yang H, Hui WZ, Rui F, et al. Epidemiology of COVID-19: A systematic review and meta-analysis of clinical characteristics, risk factors, and outcomes. J Med Virol. 2021; 93 (3): 1449–58. PubMed PMID: 32790106. DOI: 10.1002/jmv.26424.

CHANGES IN PLASMA SPHINGOLIPID LEVELS AGAINST THE BACKGROUND OF LIPID-LOWERING THERAPY IN PATIENTS WITH PREMATURE ATHEROSCLEROSIS

Rogozhina AA[1,2], Alessenko AV[3], Kurochkin IN[3], Minushkina LO[1] ✉, Gutner UA[3], Shupik MA[3], Maloshitskaya OA[4], Lebedev AT[4], Zateyshchikov DA[1,2]

[1] Central State Medical Academy of Department of Presidential Affairs, Moscow, Russia

[2] City Clinical Hospital № 51, Moscow, Russia

[3] Institute of Biochemical Physics named after N. M. Emanuel, Moscow, Russia

[4] Lomonosov Moscow State University, Moscow, Russia

Lipid-lowering drugs affect standard lipoproteins. However, we have no knowledge of changes in other plasma lipids upon treatment. The study was aimed to assess the dynamic changes in cholesterol, high- and low-density lipoproteins (HDL and LDL), triglycerides, and sphingolipids against the background of lipid-lowering therapy in patients with premature coronary artery disease, atherosclerosis and hypercholesterolemia. A total of 18 patients were enrolled (the average age was 53 ± 6.7 years): in group 1, six patients received starting statin doses; group 2 included six patients, who failed to achieve LDL target levels against the background of treatment with starting statin doses, and received escalated statin doses; seven patients in group 3 failed to achieve LDL target levels against the background of treatment with maximum tolerated doses of statins and ezetimibe, and received alirocumab. Sphingolipid levels were assessed by mass spectrometry. In group 1, the decreased levels of ceramide Cer 14:1 ($p = 0.046$) and sphingomyelins SM 22:1, SM 22:0, SM 24:0 ($p = 0.028$) were observed. There were no significant changes in the levels of total cholesterol, LDL-C, HDL-C, and triglycerides. In group 2, the significantly decreased levels of total cholesterol ($p = 0.028$), LDL ($p = 0.043$), sphingomyelins SM 18:1, SM 24:1 and SM 26:1, and ceramide Cer 16:1 ($p = 0.028$) were observed. The level of Cer 22:1 significantly increased ($p = 0.028$). In group 3, total cholesterol decreased by 36.2%, and LDL-C ($p = 0.018$) decreased by 60.1% compared to baseline (ΔLDL-C = -2.67 ± 3.12); the elevated levels of ceramide Cer 22:1 ($p = 0.028$) were observed. It has been shown, that decreased sphingomyelin levels are associated with statin therapy and correlate with decreased levels of LDL-C. No significant dynamic changes in ceramides and ceramide risk against the background of statin therapy were observed, however, PCSK9 inhibitor added to therapy reduced the Cer 16:0/24:0 ratio.

Keywords: atherosclerosis, sphingomyelins, sphingosine, ceramides, lipid-lowering therapy

ИЗМЕНЕНИЕ КОНЦЕНТРАЦИИ СФИНГОЛИПИДОВ В ПЛАЗМЕ КРОВИ НА ФОНЕ ГИПОЛИПИДЕМИЧЕСКОЙ ТЕРАПИИ У ПАЦИЕНТОВ С РАННИМ АТЕРОСКЛЕРОЗОМ

А. А. Рогожина[1,2], А. В. Алесенко[3], И. Н. Курочкин[3], Л. О. Минушкина[1] ✉, У. А. Гутнер[3], М. А. Шупик[3], О. А. Малошицкая[4], А. Т. Лебедев[4], Д. А. Затейщиков[1,2]

[1] Центральная государственная медицинская академия управления делами президента РФ, Москва, Россия

[2] Городская клиническая больница № 51, Москва, Россия

[3] Институт биохимической физики имени Н. М. Эмануэля, Москва, Россия

[4] Московский государственный университет имени М. В. Ломоносова, Москва, Россия

Гиполипидемические препараты влияют на стандартные липопротеины, но как изменяются при лечении другие липиды плазмы — не известно. Целью работы было оценить динамику холестерина (ХС), липопротеинов высокой и низкой плотности (ЛВП и ЛНП), триглицеридов (ТГ) и сфинголипидов у пациентов с преждевременно развившейся ишемической болезнью сердца, атеросклерозом и гиперхолистеринемией на фоне гиполипидемической терапии. В исследование включено 18 больных (средний возраст 53 ± 6,7 года): в 1-й группе 6 пациентов получили стартовые дозы статинов; во 2-ю группу вошли 6 пациентов, не достигших на фоне стартовой терапии статинами целевых уровней ЛНП и принимавших увеличенные дозы статинов; 7 пациентов 3-й группы не достигли целевых уровней ЛНП на фоне терапии максимально переносимыми дозами статинов и эзетимиба и получали алирокумаб. Исследование уровня сфинголипидов проводили методом масс-спектрометрии. В 1-й группе отмечено снижение уровня церамида Cer 14:1 ($p = 0,046$) и сфингомиелинов SM 22:1, SM 22:0, SM 24:0 ($p = 0,028$). Уровни общего ХС (ОХС), ХС ЛНП, ХС ЛВП и ТГ существенно не изменились. Во 2-й группе отмечено достоверное снижение уровня ОХС ($p = 0,028$), ЛНП ($p = 0,043$), сфингомиелинов SM 18:1, SM 24:1 и SM 26:1, церамида Cer 16:1 ($p = 0,028$). Cer 22:1 достоверно увеличился ($p = 0,028$). В 3-й группе ОХС снизился на 36,2%, ХС ЛНП ($p = 0,018$) — на 60,1% от исходных значений (ΔХС ЛНП = $-2,67$ ± 3,12), выявлено повышение уровня церамида Cer 22:1 ($p = 0,028$). Показано, что снижение содержания сфингомиелинов происходит на фоне терапии статинами и коррелирует со снижением уровня ХС ЛНП. Значимой динамики церамидов и церамидного риска на фоне терапии статинами не зарегистрировано, однако при добавлении к терапии ингибитора PCSK9 произошло уменьшение соотношения Cer 16:0/24:0.

Ключевые слова: атеросклероз, сфингомиелины, сфингозин, церамиды, гиполипидемическая терапия

In connection with increasing disability and mortality due to coronary artery disease (CAD) among young people [1], as well as with emergence of novel diagnostic methods, the in-depth investigation of risk factors, prevention methods, and complications of premature CAD (i. e. with the onset before the age of 55 years in men, and before the age of 60 years in women) [2], becomes more and more urgent.

The most significant risk factor for atherosclerosis is dyslipidemia, in particular, the elevated levels of low-density lipoproteins (LDL-C). These are directly associated with increased risk of cardiovascular disease [3]; hypercholesterolemia exceeding 4.9 mmol/L increases the risk of CAD by six times [4].

Due to developing mass spectrometry methods, the new laboratory parameters have been increasingly determined as additional markers of cardiovascular risk in patients with CAD, among them sphingolipids.

Sphingolipids contain the molecules of organic aliphatic amino alcohol sphingosine. It has been found, that sphingolipid catabolism is associated with cholesterol catabolism [5]. Cholesterol content of the membranes strongly correlates with the sphingolipid content (ceramides, sphingosines, and sphingosine-1-phosphate). Sphingomyelins form the myelin sheath cell membranes, and are detected in the atherosclerotic plagues [6]; ceramides contribute to cell proliferation, apoptosis and inflammation associated with atherosclerosis [7]. Currently, there is some evidence that ceramide levels, especially the levels of Cer16:0, correlate with the risk of atherosclerosis complications. These data served as the basis for calculation of the specific ceramide risk score (CRS) [8].

All the patients at high and extremely high risk for atherosclerosis have indications for high-intensity lipid-lowering therapy aimed to correct dyslipidemia and to reduce the risk of atherosclerosis progression.

The study was aimed to assess the dynamic changes in standard lipid indicators and sphingolipids against the background of lipid-lowering therapy in patients with premature CAD, atherosclerosis and hypercholesterolemia.

METHODS

The study was carried out in 2019–2020 at Moscow City Clinical Hospital № 51. A total of 18 patients (4 women and 14 men) aged 53 ± 6.7 (35–65 years) eligible for intensive lipid-lowering therapy were enrolled. Inclusion criteria: clinical manifestations of CAD or peripheral artery disease in men aged under 55, and women aged under 60, or hyperlipidemia (LDL-C levels exceeding 4.9 mmol/L). Exclusion criteria: no submitted informed consent. Fifteen patients had a history of acute myocardial infarction and coronary artery stent placement: two of them had multivessel disease and underwent coronary artery bypass grafting (CABG), others had peripheral artery disease or dyslipidemia. Among patients, 16 individuals (36.4%) had hypertension, three individuals (6.8%) had diabetes mellitus, 11 individuals (25%) reported smoking at the time of enrollment, and four individuals (9.1%) reported the history of smoking.

All patients were divided into three groups based on the fact of receiving lipid-lowering therapy at the time of enrollment (see Fig.). Dynamic changes in blood lipid levels were assessed prior to therapy and 4–8 weeks after starting treatment. The efficiency of initial statin therapy was analyzed in group 1 (n = 6). All patients in this group have had received no lipid-lowering medications prior to enrollment: at least three months prior to enrollment because of their own decision to discontinue treatment.

All patients in group 2 (n = 6) had a history of myocardial infarction in young age (the average age was 54.5 ± 1.87

years). At the time of enrollment, the patients received lipid-lowering drugs prescribed by attending physicians outside the scope of the study, however, LDL-C target levels (<1.4 mmol/L) had not been achieved. Five people received 20–40 mg doses of atorvastatin, and one person received 10 doses of rosuvastatin. Lipid-lowering therapy was adjusted, and the dose was escalated in all patients.

All patients receiving statins were analyzed separately (groups 1 and 2) (n =12).

Group 3 (n = 7) included five men and two women (the average age was 52.29 ± 9.1 years) (one patient moved to group 3 after having completed the assessment in group 2 in accordance with the protocol). Five patients had a history of myocardial infarction. All of them received lipid-lowering drugs (atorvastatin 40–80 mg once daily, rosuvastatin 40 mg once daily in combination with ezetimibe 10 mg once daily or, in case of statin intolerance or contraindications, only ezetimibe 10 mg once daily). Against the background of such therapy, all patients had LDL-C levels exceeding 1.7 mmol/L at the time of enrollment. All patients were prescribed alirocumab 150 mg once daily for two weeks in accordance with the study protocol. Group 3 also included two patients with provisional or established diagnosis of familial hypercholesterolemia made in accordance with the Dutch Lipid Clinical Network Score. One of these patients could not take statins due to concomitant diseases of the hepatobiliary tree (chronic pancreatitis, hepatitis C) and elevated levels of transaminases. The second patient with stable CAD failed to achieve LDL-C target levels when receiving maximum tolerated statin doses.

Blood sampling for biochemical tests and mass spectrometry was performed on the day of enrollment (in the morning after 12-hour fasting) and after 4–8 weeks of therapy. Blood was collected from cubital vein into sterile Vacutainer tubes. Serum was obtained by blood centrifugation at 3000 rpm for 15 min. CLIMA MC-15 biochemistry analyzer (RAL; Spain) was used to determine the parameters of serum. The following reference values were used: total cholesterol 2.0–5.2 mmol/L; LDL-C up to 3.3 mmol/L; HDL-C 0.91–1.56 mmol/L; serum triglycerides 0.50–1.70 mmol/L.

Measuring plasma sphingolipid levels

Sphingolipids were determined in blood plasma of the described above patients. During sample preparation blood was centrifuged at 3000 rpm for 10 min, 1.5 ml of supernatant were collected. Then 1.5 ml of supernatant were centrifuged at 15,000 rpm for 10 min in order to ensure complete sedimentation of cells. Lipids for mass spectrometry were extracted from blood plasma by the Bligh and Dyer method [9].

Mass spectrometric detection of various molecular species of sphingomyelins, ceramides and sphingoid bases (sphingosine and sphinganine) was performed with the TSQ Endura Triple Quadrupole Mass Spectrometer (Thermo Fisher Scientific; Germany) using the multiple reaction monitoring (MRM) technique, the pressure in the collision cell was 2.0 mTorr. Resolution of Q1 and Q3 was 1.2 Da. For ceramides, fragmentation of protonated and dehydrated parent molecules was performed at the energy of 20 eV down to ion with m/z 264.2 Da, the dwell time was 35 ms. For sphingomyelins, fragmentation of protonated parent molecules was performed at the energy of 20 eV down to ion with m/z 184.1 Da, the dwell time was 35 ms. For sphingosine and sphingosine deuterated standard (d7, Avanti; USA), fragmentation of protonated parent molecules was performed at the energy of 12.5 eV down to ions with m/z 259.3 and 252.3 Da respectively, the dwell time was 35 ms. For

sphinganine, fragmentation of protonated parent molecule was performed at the energy of 12.5 eV down to ion with m/z 266.3 Da, the dwell time was 35 ms. The following parameters of the ionization source were used: heater temperature set to 300 °C, capillary temperature 340 °C, sheath gas flow rate 45 arb (arbitrary units), auxiliary gas flow rate 13 arb, sweep gas flow rate 1 arb. Sphingosine d7, sphinganine, sphingomyelin d18:1/16:0, sphingomyelin d18:1/18:0, ceramide d18:1/16:0, ceramide d18:1/18:1, ceramide d18:1/18:0, ceramide d18:1/24:1, ceramide d18:1/24:0 (Avanti; USA) were used as standards. Chromatographic separation was carried out using the Ultimate 3000 system (Thermo Fisher Scientific; Germany) and the Eclipse Plus C8 column 3.0 × 150 mm (Agilent; USA), the particle size was 3.5 µm. Temperature was set to 50 °C, and flow rate was set to 400 µL/min. When determining sphingosine, ceramides and sphingomyelin, the following mobile phases were used: phase A, 0.1% formic acid (v/v) in water, phase B, 0.1% formic acid (v/v) in methanol (55% of phase B at 0.7 min, 100% of phase B at 7 min, 100% of phase B at 12 min, 55% of phase B from13 to 17 min, 55% of phase B at 13 min). When determining sphinganine, the following mobile phases were used: phase A, 0.1% formic acid (v/v) in water, phase B, 50% methanol + 50% acetonitrile + 0.1% formic acid (v/v) (20% of phase B at 1.5 min, 100% of phase B at 2 min, 100% of phase B at 7 min, 20% of phase B at 7 min, 20 of phase B at 10 min). The relative ceramide value was assessed using external calibration (method of standard addition). The Ceramide Porcine Brain 860052P ceramide mixture (Avanti; USA) containing 50% of d18:1/18:0 50% and 20% of d18:1/24:1 was used as a standard. Calculations were performed based on the peak areas for MRM transitions MH+·→ m/z 264.4 Da and (M+H-H2O)+·→ m/z 264.4 Da. The content of sphingosine d18:1 was determined by internal calibration (internal standard method, the standard was D-erythro-sphingosine d7, Sigma; USA) based on the sum of peak areas for MRM transitions (m/z 300+·→ m/z 252.3 Da for non-deuterated and m/z 307+·→ m/z 259.3 for deuterated sphingosine). The content of sphingosine d18:0 was defined using external calibration (the standard was DL-erythro-dihidrosphingosine, Sigma; USA) based on the peak areas for MRM transitions m/z 302+·→ m/z 266.3 Da.

CRS, described as a predictor for coronary artery disease mortality, was assessed using the previously reported scale involving the use of certain ceramide molecular species [8]. In order to access the ceramide risk, the following ratios were calculated: Cer16:0/Cer24:0, Cer18:0/Cer24:0, Cer24:1/Cer24:0. The levels of Cer16:0, Cer18:0, Cer24:1, and the values of these ceramides' ratios with Cer24:0, were divided into quartiles. The patients falling within the third quartile were assigned score 1 for each of six parameters, and the patients falling within the fourth quartile were assigned score 2. The total score was considered the ceramide risk score.

Statistical analysis

Statistical processing of the results was performed using the SPSS ver. 21.0 software package (IBM; USA). Quantitative variables were presented as mean and standard deviation ($M \pm SD$). All quantitative variables were tested for normality using the Shapiro–Wilk test. Distribution of all the quantitative variables was other than normal. The Wilcoxon signed-rank test was used to compare related samples. Significance of differences between two independent samples was determined using the Mann–Whitney test. Significance of correlations was assessed using the Spearman's rank correlation coefficient. The differences were considered significant when $p < 0.05$ in all types of analysis.

RESULTS

Changes in cholesterol and sphingolipid levels were assessed by groups of patients at the time of lipid-lowering therapy initiation and adjustment (statins or alirocumab) (Table 1).

In group 1, a significant decrease in the levels of short-chain ceramides Cer 14:1 was observed ($p = 0.046$). Long-chain sphingomyelins SM 22:1, SM 22:0, SM 24:0 significantly decreased against the background of lipid-lowering therapy initiation in all patients of this group ($p = 0.028$).

In group 2, the levels of total cholesterol ($p = 0.028$), LDL-C ($p = 0.043$), long-chain sphingomyelins SM18:1, SM 24:1 and SM 26:1, ceramide Cer 16:1 ($p = 0.028$), and SM 22:1 ($p = 0.046$) significantly decreased against the background
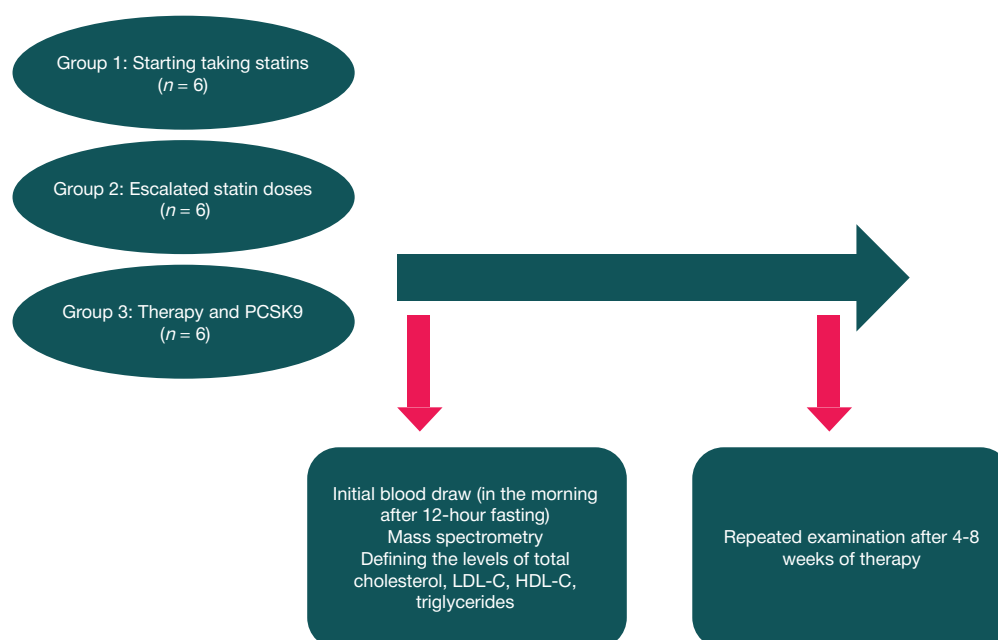
Figure. Study protocol

Table 1. Dynamic changes in lipid levels in the studied groups

Indicators		Group 1 (n = 6)		Group 2 (n = 6)		All patients receiving statins (groups 1 and 2) (n = 12)		Group 3 (n = 7)	
		M ± SD	p	M ± SD	p	M ± SD	p	M ± SD	p
Standard lipid indicators (mmol/L)									
TC	before	7.42 ± 2.39	0.249	4.75 ± 1.46	0.028*	6.09 ± 2.35	0.028*	7.51 ± 5.36	0.063
	after	5.83 ± 1.38		4.31 ± 1.36		5.07±1.53		4.79 ± 1.49	
LDL-C	before	4.98 ± 2.45	0.116	3.07 ± 1.29	0.043*	4.03 ± 2.12	0.021*	4.44 ± 2.87	0.018*
	after	3.42 ± 0.83		2.57 ± 1.22		2.99 ± 1.09		1.77 ± 1.46	
HDL-C	before	1.09 ± 0.16	0.528	1.01 ± 0.32	0.686	1.05 ± 0.25	0.755	1.12 ± 0.39	0.176
	after	1.18 ± 0.33		0.98± 0.23		1.08 ± 0.29		1.51 ± 1.08	
TG	before	2.93 ± 1.77	0.463	1.5± 0.34	0.463	2.22 ± 1.43	0.814	3.4 ± 4.34	0.753
	after	2.69 ± 2.20		1.65±0.59		2.17 ± 1.63		4.85 ± 8.2	
CERAMIDES (ng/mL)									
Cer 14:1	before	0.96 ± 0.16	0.046*	0.71 ± 0.09	0.463	0.83 ± 0.18	0.158	0.39 ± 0.42	0.612
	after	0.7 ± 0.11		0.76 ± 0.09		0.73 ± 0.1		0.49 ± 0.4	
Cer 14:0	before	38.52 ± 18.73	0.463	22.93 ± 8.55	0.345	30.72 ± 16.09	1	20.29 ± 12.3	0.866
	after	33.61 ± 9.85		23.81 ± 6.93		28.71 ± 9.6		22.3 ± 5.42	
Cer 16:1	before	9.10 ± 2.26	0.173	11.32 ± 1.90	0.028*	10.21 ± 2.31	0.937	7.17 ± 3.35	0.612
	after	13.26 ± 6.34		9.62 ± 2.18		11.44 ± 4.91		7.09 ± 2.96	
Cer 16:0	before	470.34 ± 221.52	0.6	222.07 ± 23.74	0.753	346.2 ± 198.42	0.583	370.49 ± 353.84	0.612
	after	438.73 ± 145.74		222.27 ± 55.34		330.5 ± 154.36		338.64 ± 240.77	
Cer 18:1	before	2.01 ± 0.98	0.6	2.48 ± 0.46	0.6	2.24 ± 0.77	0.48	1.7 ± 0.74	0.176
	after	2.37 ± 0.49		2.60 ± 0.71		2.48 ± 0.6		2.01 ± 0.64	
Cer 18:0	before	45.10 ± 31.72	0.463	40.67 ± 7.68	0.463	42.89 ± 22.13	0.754	34.78 ± 11.13	1
	after	46.63 ± 18.84		38.31 ± 7.83		42.47 ± 14.43		33.36 ± 9.92	
Cer 20:1	before	0.66 ± 0.12	0.345	0.64 ± 0.12	0.463	0.65 ± 0.11	0.388	0.46 ± 0.5	0.499
	after	0.7 ± 0.8		0.71 ± 0.16		0.71 ± 0.12		0.59 ± 0.2	
Cer 20:0	before	71.84 ± 36.27	0.917	81.88 ± 23.78	0.917	76.86 ± 29.71	1	61.72 ± 31.72	0.237
	after	72.3 ± 18.41		78.59 ± 17.31		75.45 ± 17.35		81.18 ± 50.40	
Cer 22:1	before	5.44 ± 3.96	0.753	4.08 ± 1.10	0.028*	4.76 ± 2.86	0.182	3.47 ± 2.34	0.028*
	after	4.73 ± 1.04		5.62 ± 0.81		5.18 ± 1		6.20 ± 5.03	
Cer 22:0	before	1948.4 ± 1113.75	0.753	1254.62 ± 181.13	0.345	1601.51 ± 842.63	0.695	979.11 ± 715.92	0.499
	after	1821.5 ± 765.99		1358.95 ± 299.06		1590.22 ± 604.74		1336.47 ± 743.56	
Cer 24:1	before	578.1 ± 147.68	0.249	537.41 ± 77.21	0.753	557.76 ± 114.34	0.308	585.77 ± 362.55	0.612
	after	632.9 ± 179.15		541.90 ± 122.05		587.4 ± 153.68		538.53 ± 299.16	
Cer 24:0	before	2083.59 ± 1180.12	0.345	1451.87 ± 143.86	0.917	1767.73 ± 866.77	0.48	1205.09 ± 719.65	0.176
	after	1896.72 ± 833.38		1490.96 ± 245.89		1693.84 ± 622.96		1777.98 ± 1078.81	
Cer 26:1	before	12.50 ± 8.24	0.116	13.10 ± 8.14	0.6	12.80 ± 7.82	0.388	11.36 ± 7.62	0.398
	after	16.35 ± 8.14		11.30 ± 4.55		13.83 ± 6.82		15.19 ± 11.41	
Cer 26:0	before	49.67 ± 7.68	0.917	45.48 ± 3.33	0.917	47.57 ± 6.05	1	28.75 ± 14.25	0.31
	after	50.28 ± 5.59		45.40 ± 5.72		47.84 ± 5.96		37.56 ± 6.61	
Cer 16:0/24:0	before	0.24 ± 0.12	0.753	0.15 ± 0.02	0.6	0.2 ± 0.1	0.875	0.29 ± 0.09	0.043*
	after	0.24 ± 0.86		0.15 ± 0.03		0.2 ± 0.08		0.19 ± 0.04	
Cer 18:0/24:0	before	0.028 ± 0.027	0.345	0.03 ± 0.01	0.6	0.03 ± 0.02	0.814	0.04 ± 0.02	0.128
	after	0.03 ± 0.01		0.03 ± 0.01		0.03 ± 0.02		0.02 ± 0.01	
Cer 24:1/24:0	before	0.33 ± 0.16	0.249	0.37 ± 0.03	0.917	0.35 ± 0.11	0.347	0.58 ± 0.28	0.063
	after	0.37 ± 0.17		0.37 ± 0.08		0.37 ± 0.13		0.33 ± 0.11	
Ceramide risk score	before	4.83 ± 3.71	0.336	2.67 ± 2.07	0.593	3.75 ± 3.08	0.231	5.57 ± 2.44	0.233
	after	5.83 ± 4.17		3.33 ± 2.73		4.58 ± 3.60		4.0 ± 2.58	
SPHINGOMYELINS (ng/mL)									
SM 14:1	before	1243.79 ± 579.25	0.345	1076.05 ± 456.93	0.345	1159.92±505.07	0.158	578.70 ± 721.70	0.866
	after	1107.35 ± 539.53		969.59 ± 329.81		1038.47 ± 432.36		655.45 ± 463.86	
SM 14:0	before	15560.92 ± 7789.49	0.249	10218.99 ± 4643.12	0.753	12889.95 ± 6720.27	0.308	5379.57 ± 6666.57	0.866
	after	13293.42 ± 4925.96		9803.30 ± 3771.31		11548.36 ± 4562.52		6516.82 ± 4797.92	
SM 16:1	before	27147.34 ±9245.24	0.345	14994.30 ± 4552.79	0.463	21070.82 ± 9410.35	0.209	9288.60 ± 11795.93	0.866
	after	24289.12 ± 8455.16		14567.22 ± 4838.38		19428.17 ± 8301.39		12154.21 ± 9026.99	

Table 1 (continuation).

SM 16:0	before	68884.57 ± 29300.16	0.6	43109.35 ± 5476.51	0.249	55996.96 ± 24187.79	0.53	29457.23 ± 26795.25	0.612
	after	58719.28 ± 18464.01		41511.66 ± 8959.72		50115.47 ± 16498.73		42283.32 ± 25753.31	
SM 18:1	before	4998.28 ± 2970.69	0.917	4138.09 ± 957.21	0.028*	4568.18 ± 2151.66	0.182	3513.39 ± 2645.09	0.612
	after	4254.22 ± 2140.22		3786.43 ± 1074.09		4020.32 ± 1632.83		3483.78 ± 1193.06	
SM 18:0	before	18597.76 ± 10587.79	0.345	14163.76 ± 1608.14	0.116	16380.76 ± 7582.39	0.071	8957.79 ± 7701.24	0.612
	after	15006.64 ± 5504.22		12963.34 ± 2468.85		13984.99 ± 4204.79		10214.96 ± 5423.62	
SM 20:1	before	19571.11 ± 9063.27	0.463	34801.84 ± 6713.68	0.249	27186.47 ± 11004.16	0.182	19003.09 ± 7981.50	0.499
	after	15399.44 ± 4090.53		33308.30 ± 7232.94		24353.87 ± 10902.14		21255.95 ± 11508.78	
SM 20:0	before	122191.42 ± 61041.05	0.463	107398.59 ± 12787.35	0.463	114795.00 ± 42750.99	0.239	83678.97 ± 38585.26	0.31
	after	95985.48 ± 23943.68		104156.92 ± 15085.34		100071.20 ± 19550.99		108695.09 ± 50687.07	
SM 22:1	before	32751.55 ± 7675.39	0.028*	37536.42 ± 11536.91	0.046*	35143.98 ± 9670.69	0.004*	14233.44 ± 15712.63	0.866
	after	27480.53 ± 7931.12		33221.35 ± 10422.30		30350.94 ± 9324.97		18164.23 ± 11614.33	
SM 22:0	before	49975.11 ± 7453.47	0.028*	50443.83 ± 11076.52	0.753	50209.47 ± 9004.42	0.071	17147.95 ± 18892.94	1
	after	39664.55 ± 10888.20		49134.09 ± 16770.24		44399.32 ± 14358.99		25262.43 ± 16913.88	
SM 24:1	before	86437.81 ± 20948.28	0.173	87494.43 ± 21994.99	0.028*	86966.12 ± 20485.92	0.012*	31116.71 ± 31595.14	1
	after	80493.43 ± 14190.94		76736.87 ± 22166.55		78615.15 ± 17853.01		43885.51 ± 28272.08	
SM 24:0	before	44680.38 ± 11292.01	0.028*	41334.09 ± 7361.87	0.463	43007.24 ± 9254.61	0.028*	11042.64 ± 12530.05	0.735
	after	33338.06 ± 6060.00		38593.57 ± 12040.46		35965.82 ± 9493.26		15850.33 ± 10223.83	
SM 26:1	before	992.02 ± 541.84	0.116	944.03 ± 417.87	0.028*	968.02 ± 462.01	0.010*	248.38 ± 269.04	0.499
	after	769.60 ± 301.79		752.44 ± 269.19		761.02 ± 272.79		398.84±285.35	
SPHINGOID BASES (ng/mL)									
SPN	before	5.26 ± 6.71	0.345	3.18 ± 1.59	0.753	4.22 ± 4.77	0.433	2.30 ± 1.21	0.735
	after	3.20 ± 0.92		3.28 ± 1.14		3.24 ± 0.99		2.47 ± 1.50	
SPH	before	13.32 ± 17.58	0.463	9.39 ± 4.25	0.753	11.35 ± 12.36	0.388	7.00 ± 2.98	0.237
	after	10.85 ± 5.28		9.85 ± 4.61		10.35 ± 4.75		8.27 ± 4.78	
S1P	before	17.28 ± 5.13	0.753	19.32 ± 2.88	0.116	18.30 ± 4.11	0.433	14.57 ± 2.75	0.31
	after	16.84 ± 2.01		17.54 ± 1.50		17.19 ± 1.73		16.18 ± 3.61	

Note: SPN — sphingosine, SPH — sphingonine, S1P — sphingosine-1-phosphate.

of the escalated statin doses. Cer 22:1 levels significantly increased ($p = 0.028$).

After the lipid-lowering therapy adjustment, the levels of cholesterol decreased by 9.5% (Δ cholesterol = −0.45 ± 0.40), and the levels of LDL-C decreased by 16.2% (ΔLDL-C = −0.50 ± 0.44) in all patients. LDL-C target levels were achieved in only one patient, in other patients, advice was provided on lifestyle correction, the lipid-lowering drug dose was escalated, or the second drug was prescribed (ezetimibe 10 mg once daily). One female patient maintained LDL-C levels ≥ 2.6 mmol/L against the background of dual lipid-lowering therapy (maximum tolerated doses of statins: atorvastatin 80 mg, ezetimibe 10 mg). She was prescribed alirocumab.

Analysis of data obtained in all patients receiving statins revealed significantly decreased levels of cholesterol ($p = 0.028$), LDL-C ($p = 0.021$), and long-chain sphingomyelins SM 24:1 ($p = 0.012$), SM 24:0 ($p = 0.028$), SM 26:1 ($p = 0.010$), SM 22:1 ($p = 0.004$).

In group 3, the levels of total cholesterol decreased by 36.2% (ΔTC = −2.72 ± 4.48), and the levels of LDL-C ($p = 0.018$) decreased by 60.1% compared to baseline (ΔLDL-C = −2.67 ± 3.12) against the background of alirocumab therapy.

Of all the defined ceramide ratios (Cer 16:0/24:0, 18:0/24:0, 24:1/24:0), only the Cer 16:0/24:0 ratio significantly decreased in the group receiving alirocumab ($p = 0.043$). No significant changes in ceramide risk score were observed in any of the groups.

Comparison of dynamic changes in sphingolipid levels was performed in patients, who had started therapy for the first time, and against the background of escalated statin doses

(groups 1 and 2), as well as in each group of patients receiving alirocumab (group 3) (Table 2).

When comparing dynamic changes in sphingolipid levels in each group, it was observed that in group 1 the level of ceramide Cer 16:1 increased slightly (Δ Cer 16:1 = 4.1 ± 7.17), and in group 2 it decreased (Δ Cer 16:1 = −1.70 ± 1.32). The differences were considered significant ($p = 0.015$).

Against the background of alirocumab therapy, the increase in the levels of Cer 14:1 (Δ Cer 14:1 = 0.10 ± 0.35) was observed ($p = 0.022$), however, the levels of this ceramide decreased (Δ Cer 14:1 = −0.26 ± 0.259) in patients, who had started taking statins. When comparing dynamic changes in groups 1 and 3, the significant differences were observed in the levels of SM 22:0 (Δ SM 22:0 = −10310.6 vs 8114.48) ($p = 0.035$) and SM 24:0 (Δ SM 24:0 = −11342.31 vs 4807.69) ($p = 0.022$). In patients receiving statins and patients receiving alirocumab the dynamic changes of SM 22:1 (Δ SM 22:1 = −4793.04 vs 3930.79) ($p = 0.045$) and SM 26:1 (ΔSM 26:1 = −207.00 vs 150.46) ($p = 0.005$) were different in groups 2 and 3 (ΔSM 26:1= −191.58 vs 150.46).

When conducting correlation analysis in group 1, a significant strong positive correlation was observed between the dynamic changes of Cer 14:1 and the changes in the levels of LDL-C (ρ = 0.829; $p = 0.042$); there was a significant strong negative correlation with baseline LDL-C level (ρ = −0.829; $p = 0.042$) (Table 3). In the same group, a positive correlation was observed between the dynamic changes of long-chain sphingomyelins, and the changes in the levels of LDL — Δ SM 24:1 with Δ LDL (ρ = 0.943; $p = 0.005$), Δ SM 26:1 with Δ LDL (ρ = 0.829; $p = 0.042$), together with negative correlation

Table 2. Dynamic changes of the lipidome in the studied groups

	Group 1 ($n = 6$)	Group 2 ($n = 6$)	All patients receiving statins (groups 1 and 2) ($n = 12$)	Group 3 ($n = 7$)	p			
	M ± SD	M ± SD	M ± SD	M ± SD	1 vs 2	1 vs 3	2 vs 3	1+2 vs 3
ΔTotal cholesterol, mmol/L	−1.59 ± 2.26	−0.45 ± 0.40	−1.02 ± 1.66	−2.72 ± 4.48	1	1	0.366	0.592
ΔLDL-C, mmol/L	−1.57 ± 2.05	−0.50 ± 0.44	−1.03 ± 1.52	−2.67 ± 3.12	0.589	0.445	0.101	0.142
CERAMIDES (ng/mL)								
Δ Cer 14:1	−0.26± 0.259	0.05 ± 0.10	−0.10±0.25	0.10 ± 0.35	0.065	0.022*	0.731	0.299
Δ Cer 14:0	−4.9 ± 16.8	0.87 ± 6.07	−2.01 ± 12.41	2.01 ± 14.44	0.699	0.445	0.534	0.967
Δ Cer 16:1	4.1 ± 7.17	−1.70 ± 1.32	1.23 ± 5.79	−0.08 ± 5.64	0.015*	0.181	0.945	0.482
Δ Cer 16:0	−31.61 ± 128.6	0.20 ± 39.22	−15.70 ± 92.17	−31.85 ± 186.90	0.485	0.731	0.295	0.384
Δ Cer 18:1	0.36 ± 1.44	0.12 ± 1.10	0.24 ± 1.23	0.31 ± 0.87	0.699	1	0.731	0.837
Δ Cer 18:0	1.53 ± 22.4	−2.36 ± 8.61	−0.41 ± 16.33	−1.42 ± 14.20	0.24	0.534	0.945	0.773
Δ Cer 20:1	0.04 ± 0.96	0.07 ± 0.22	0.05 ± 0.16	0.13 ± 0.49	0.937	0.534	0.836	0.592
Δ Cer 20:0	0.46 ± 31.2	−3.30 ± 23.91	−1.42 ± 26.57	19.45 ± 33.98	1	0.366	0.366	0.261
Δ Cer 22:1	−0.71 ± 3.12	1.55 ± 0.86	0.42 ± 2.48	2.73 ± 3.13	0.24	0.073	0.731	0.196
Δ Cer 22:0	−126.9 ± 455.6	104.33 ± 253.10	−11.29 ± 371.56	357.35 ± 684.10	0.699	0.366	0.628	0.837
Δ Cer 24:1	54.8 ± 80.02	4.48 ± 76.78	29.64 ± 79.25	−47.24 ± 276.47	0.24	0.366	0.836	0.482
Δ Cer 24:0	−186.9 ± 377	39.09 ± 303.56	−73.89 ± 347.01	572.89 ± 946.70	0.394	0.366	0.731	0.432
Δ Cer 26:1	3.85 ± 5.3	−1.80 ± 8.47	1.03 ± 7.35	3.83 ± 8.54	0.31	0.731	0.445	0.837
Δ Cer 26:0	0.60 ± 9.61	−0.09 ± 3.01	0.26 ± 6.80	8.82 ± 16.90	0.818	0.534	0.731	0.536
SPHINGOMYELINS, (ng/mL)								
Δ SM 14:1	−136.44 ± 264.64	−106.46 ± 222.84	−121.45 ± 233.78	76.75 ± 597.50	1	0.945	0.628	0.711
Δ SM 14:0	−2267.50 ± 4319.4	−415.69 ± 2599.93	−1341.60 ± 3533.89	1137.25 ± 7185.34	0.394	0.534	0.731	0.536
Δ SM 16:1	−2858.22 ± 5090.2	−427.07 ± 2668.56	−1642.65 ± 4077.53	2865.61 ± 12002.14	0.589	1	0.945	0.967
Δ SM 16:0	−10165.3 ± 42892.64	−1597.70 ± 4740.43	−5881.49 ± 29436.31	12826.09 ± 39663.43	1	0.445	0.945	0.592
Δ SM 18:1	−744.05 ± 3065.24	−351.66 ± 255.92	−547.86 ± 2083.88	−29.60 ± 2322.63	0.394	0.366	0.234	0.196
Δ SM 18:0	−3591.13 ± 9189.7	−1200.41 ± 1637.43	−2395.77 ± 6415.91	1257.17 ± 7871.83	0.699	0.366	0.445	0.299
Δ SM 20:1	−4171.7 ± 10715.9	−1493.53 ± 3174.60	−2832.60 ± 7663.77	2252.86 ± 10836.10	0.699	0.295	0.366	0.227
Δ SM 20:0	−26205.9 ± 68374.9	−3241.66 ± 9337.83	−14723.80 ± 48047.04	25016.12 ± 54734.68	0.699	0.234	0.234	0.142
Δ SM 22:1	−5271.02 ± 2725.40	−4315.07 ± 3580.24	−4793.04 ± 3074.40	3930.79 ± 13493.31	0.485	0.101	0.101	0.045*
Δ SM 22:0	−10310.6 ± 7398.5	−1309.75 ± 15485.82	−5810.15 ± 12489.23	8114.48 ± 20690.12	0.24	0.035*	0.534	0.1
Δ SM 24:1	−5944.38 ± 9369.28	−10757.56 ± 7584.82	−8350.97 ± 8507.03	12768.79 ± 34445.18	0.485	0.445	0.138	0.167
Δ SM 24:0	−11342.31 ± 7409.98	−2740.53 ± 7497.64	−7041.42 ± 8407.70	4807.69 ± 13661.89	0.132	0.022*	0.445	0.068
Δ SM 26:1	−222.42 ± 267.17	−191.58 ± 204.63	−207.00 ± 227.46	150.46 ± 270.72	1	0.073	0.005*	0.005*

with baseline LDL-C level — with Δ SM 24:1 ($\rho = -0.943$; $p = 0.005$), with Δ SM 26:1 ($\rho = -0.829$; $p = 0.042$). In group 2, only changes in SM 18:0 positively correlated with baseline LDL-C level ($\rho = 0.812$; $p = 0.05$).

In group 1, there was a significant strong correlation between the dynamic changes in Δ SM 26:1 and the baseline HDL-C level ($\rho = -0.829$; $p = 0.042$); no significant correlations were observed in patients of group 2. Significant correlations with baseline HDL-C level in all patients receiving statins were observed for Δ SM 14:1 ($\rho = -0.602$; p = 0.038), Δ SM 14:0 ($\rho = -0.676$; $p = 0.016$), Δ SM 16:1 ($\rho = -0.630$; $p = 0.028$), Δ SM 24:0 ($\rho = -0.581$; p = 0.047, Δ SM 26:1($\rho = -0.595$; $p = 0.041$). In group 3, there was a significant strong negative correlation between changes in SM 20:1 ($\rho = -0.929$; $p = 0.003$) and SM 20:0 ($\rho = -0.929$; $p = 0.003$) and baseline HDL-C level.

DISCUSSION

Currently, the major classes of lipid-lowering drugs are inhibitors of HMG-CoA reductase (statins) inhibiting hepatic cholesterol biosynthesis, cholesterol absorption inhibitors (ezetimibe), and proprotein convertase subtilisin/kexin type 9 (PCSK9) inhibitors

acting through inhibiting of PCSK9, binding to LDL receptor, and the increase in the number of such receptors on the surface of hepatocytes. When applying lipid-lowering therapy, the main clinical reference is the decrease in the LDL-C levels to target levels [2]. The differences in the mechanism of action may also contribute to differences in effect on the levels of other lipid fractions, such as sphingomyelins and ceramides. It is known, that ceramide levels may be considered as an additional risk factor for complications of atherosclerosis (myocardial infarction and stroke). This has been shown in the cohort study Rochester Epidemiology Project (REP) when observing 1131 healthy individuals aged over 45. The ratios Cer 16:0/Cer 24:0, Cer 18:0/Cer 24:0, Cer 24:1/Cer 24:0, and the ceramide risk score were the main predictors of adverse outcomes [10]. The same ceramides and their ratios were found to be independent predictors of cardiovascular death in the cohort of 1704 patients with CAD [11]. In the course of our study, we also assessed the dynamic changes of these ratios and the ceramide risk score against the background of lipid-lowering therapy.

Elevated sphingomyelin levels can be also considered as an independent predictor of adverse outcomes. This has been shown in analysis of cohorts of patients with familial lipid

Table 3. Correlation analysis of dynamic changes with baseline levels of LDL-C, HDL-C, and dynamic changes of LDL-C

	Baseline LDL-C	Δ LDL-C	Baseline HDL-C
Group 1 (n = 6)			
Δ Cer 14:1	ρ = −0.829; p = 0.042	ρ = 0.829; p = 0.042	ρ = −0.6; p = 0.208
Δ SM 24:1	ρ = −0.943; p = 0.005	ρ = 0.943; p = 0.005	ρ = −0.657; p = 0.156
Δ SM 26:1	ρ = −0.829; p = 0.042	ρ = 0.829; p = 0.042	ρ = −0.829; p = 0.042
Group 2 (n = 6)			
Δ SM 18:0	ρ = 0.812; p = 0.05	ρ = −0.200; p = 0.704	ρ = 0.029; p = 0.957
All patients receiving statins (groups 1 and 2) (n = 12)			
Δ SM 14:1	ρ = −0.329 p = 0.296	ρ = 0.606; p = 0.037	ρ = −0.602; p = 0.038
Δ SM 14:0	ρ = −0.417; p = 0.178	ρ = 0.504 p = 0.094	ρ = −0.676; p = 0.016
Δ SM 16:1	ρ = −0.109; p = 0.737	ρ = 0.245; p = 0.442	ρ = −0.630; p = 0.028
Δ SM 24:0	ρ = −0.235; p = 0.463	ρ = 0.343; p = 0.275	ρ = −0.581; p = 0.047
Δ SM 26:1	ρ = −0.452; p = 0.140	ρ = 0.480; p = 0.114	ρ = −0.595; p = 0.041
Group 3 (n = 7)			
Δ SM 20:1	ρ = −0.143; p = 0.760	ρ = −0.036; p = 0.939	ρ = −0.929; p = 0.003
Δ SM 20:0	ρ = −0.179; p = 0.702	ρ = 0.107; p = 0.819	ρ = −0.929; p = 0.003

disorders using the methods of big data analysis and machine learning [12]. Prognostic value of certain sphingomyelins has been also shown for cerebrovascular disease [13].

There is little literature data on the effect of therapy with statins, PCSK9 inhibitors, and ezetimibe on the sphingolipid levels. The randomized trial showed that the combination of atorvastatin and fibrates ensured reduced levels of acylglycerols and the majority of ceramides, as well as the elevated levels of sphingomyelins. Atorvastatin dose escalation modestly decreased the levels of lysophosphatidylcholine [14]. The randomized trial aimed to compare the effect of 80 mg simvastatin and 10 mg simvastatin/ezetimibe combination showed the differences in the effects of these regimens on the levels of lipid and sphingolipid fractions. High-dose statin therapy resulted in more prominent changes in sphingolipid levels. Meanwhile, the dynamic changes in the cholesterol and LDL-C levels were comparable. The high-dose statin reduced the levels of sphingomyelins and ceramides much more; it also affected the levels of phosphotidylcholine, which could partially explain the pleiotropic effect of statins [15].

In the course of randomized trial involving the use of different rosuvastatin doses (10 and 40 mg) in patients with metablic syndrome, both low and high statin doses significantly decreased the levels of ceramides and sphingolipids. The significant dose-dependent differences were shown for dynamic changes of phosphatidylcholine, lysophosphatidylcholine, alkylphosphatidylcholine, alkenylphosphatidylcholine (plasmalogen), and phosphatidylinositol. The dose-dependent effect was also shown for sphingolipids after being normalized to phosphatidylcholine level [16].

During treatment with rosuvastatin, the dynamic changes in blood ceramide levels negatively correlated with the dynamic changes in the levels of ApoB100 very low-density lipoproteins (VLDL). No association between the dynamic changes in the levels of ceramides and sphingomyelins, and the dynamic changes in the levels of total cholesterol, LDL-C, triglycerides, and ApoA1 LDL was observed. The discovered association between the dynamic changes in ApoB VLDL and the dynamic changes in ceramides against the background of rosuvastatin therapy demonstrates the potential features of the mechanism of action for this statin [17].

In our study, the initial treatment with statins resulted in significantly decreased levels of Cer 14:1 and reduced levels

of sphingomyelins SM 22:1, SM 22:0, and SM 24:0. Reduced levels of Cer 14:1 and long-chain sphingomyelins correlated with baseline levels of LDL-C and dynamic changes in LDL. With the lipid-lowering treatment intensification (escalation of statin dose and addition of ezetimibe in some patients), the overall dynamic changes in sphingomyelins were more prominent, which correlated with the results of the studies cited. No significant impact on the levels of ceramides and ceramide risk was observed.

Association between PCSK9 level and blood ceramide and sphingolopid levels was investigated in the course of the study, involoving 31 patients with liver diseases of different etiology. In patients with high PCSK9 level, LDL-C levels were higher than expected. However, the levels of total cholesterol, sphingolopids, and ceramides showed no correlation with PCSK9 level. After the patients were divided into groups with high and low PCSK9 levels, it turned out that the patients with plasma PCSK9 levels above the median had significantly lower levels of certain sphingolipids and ceramides: CE 16:0, CE 20:5, CE 20:4, CE 22:6, CE 22:4, SM 18:0, SM 20:1, SM 24:2, SM 24:1. To date, the mechanism, underlying such association, is unclear [18].

The EQUATOR trial, involving the use of monoclonal antibody against PCSK9 RG7652, showed the predominant decline in the levels of ceramides CE 24:1, CE 24:0, and CE 26:0, contained mainly in LDL [19]. The other study, involving PCSK9 inhibitor prescription against the background of treatment at the maximum tolerated statin dose, also showed both reduced ceramide levels and reduced ceramide risk score, the integral parameter, which correlated with the risk of adverse outcome in patients with dyslipidemia [20]. Earlier, the Ludwigshafen Risk and Cardiovascular Health (LURIC) trial showed that homozygous state for the rare mutant allele R46L (PCSK9), characterized by low enzyme activity, was associated with 30% decrease in the ceramide risk score compared to other allelic variants [21]. This trial also demonstrated 13% decrease in the ceramide risk score against the background of simvastatin therapy, and lack of ceramide dynamic changes against the background of taking ezetimibe.

During our study, alirocumab added to therapy resulted in significantly decreased LDL-C, however, no significant changes in the levels of sphingomyelins and ceramides were observed. Only significant increase in Cer 22:1 and decreased ratio Cer

16:0/24:0, being the marker of ceramide risk, were observed. In the course of our study, alirocumab was added to therapy in patients, who had previously received maximum tolerated statin doses in accordance with indications registered for appropriate drug [2, 22]. However, the baseline sphingolipid levels were relatively low; these were significantly lower compared to groups 1 and 2 against the background of four-week statin therapy. Against the background of low baseline sphingomyelin levels, PCSK9 inhibitor had no significant effect of the levels of sphingomyelins and ceramides. It was probably due to the drug mechanism of action, different from the statin mechanism of action.

This study had the following limitations: the sample of patients was small, the study was conducted with the use of background therapy with various statins.

CONCLUSION

Sphingomyelin levels decrease against the background of statin therapy; when applying starting doses of statins, these correlate with reduced levels of LDL-C. When escalating lipid-lowering therapy, the correlation between dynamic changes in sphingomyelins and LDL becomes less prominent. Treatment with PCSK9 inhibitors results in significantly reduced LDL-C levels, however, it does not affect the levels of sphingomyelins. No significant dynamic changes in ceramides and ceramide risk are observed against the background of statin therapy. However, PCSK9 inhibitor added to therapy reduces the Cer 16:0/24:0 ratio, which can be considered a marker of decreased cardiovascular risk.

References

1. Bossard M, Latifi Y, Fabbri M, Kurmann R, Brinkert M, Wolfrum M, et al. Increasing Mortality From Premature Coronary Artery Disease in Women in the Rural United States. J Am Heart Assoc. 2020; 9 (9): e015334. DOI: 10.1161/JAHA.119.015334.

2. Mach F, Baigent C, Catapano AL, Koskinas KC, Casula M, Badimon L, et al; ESC Scientific Document Group. 2019 ESC/EAS Guidelines for the management of dyslipidaemias: lipid modification to reduce cardiovascular risk. Eur Heart J. 2020; 41 (1): 111–88. DOI: 10.1093/eurheartj/ehz455.

3. Ference BA, Ginsberg HN, Graham I, Ray KK, Packard CJ, Bruckert E, et al. Low-density lipoproteins cause atherosclerotic cardiovascular disease. 1. Evidence from genetic, epidemiologic, and clinical studies. A consensus statement from the European Atherosclerosis Society Consensus Panel. Eur Heart J. 2017; 38 (32): 2459–72. DOI: 10.1093/eurheartj/ehx144.

4. Khera AV, Won HH, Peloso GM, Lawson KS, Bartz TM, Deng X, et al. Diagnostic Yield and Clinical Utility of Sequencing Familial Hypercholesterolemia Genes in Patients With Severe Hypercholesterolemia. J Am Coll Cardiol. 2016; 67 (22): 2578–89. DOI: 10.1016/j.jacc.2016.03.520.

5. Barenholz Y. Sphingomyelin and cholesterol: from membrane biophysics and rafts to potential medical applications. Subcell Biochem. 2004; 37: 167–215. DOI: 10.1007/978-1-4757-5806-1_5.

6. Manicke NE, Nefliu M, Wu C, Woods JW, Reiser V, Hendrickson RC, et al. Imaging of lipids in atheroma by desorption electrospray ionization mass spectrometry. Anal Chem. 2009; 81 (21): 8702–7. DOI: 10.1021/ac901739s.

7. Brunkhorst R, Friedlaender F, Ferreirós N, Schwalm S, Koch A, Grammatikos G, et al. Alterations of the Ceramide Metabolism in the Peri-Infarct Cortex Are Independent of the Sphingomyelinase Pathway and Not Influenced by the Acid Sphingomyelinase Inhibitor Fluoxetine. Neural Plast. 2015; 2015: 503079. DOI: 10.1155/2015/503079.

8. Laaksonen R, Ekroos K, Sysi-Aho M, Hilvo M, Vihervaara T, Kauhanen D, et al. Plasma ceramides predict cardiovascular death in patients with stable coronary artery disease and acute coronary syndromes beyond LDL-cholesterol. Eur Heart J. 2016; 37 (25): 1967–76. DOI: 10.1093/eurheartj/ehw148.

9. Bligh EG, Dyer WJ. A rapid method of total lipid extraction and purification. Can J Biochem Physiol. 1959; 37 (8): 911–7.

10. Vasile VC, Meeusen JW, Medina Inojosa JR, Donato LJ, Scott CG, Hyun MS, et al. Ceramide Scores Predict Cardiovascular Risk in the Community. Arterioscler Thromb Vasc Biol. 2021; 41 (4): 1558–69. DOI: 10.1161/ATVBAHA.120.315530.

11. Li Q, Wang X, Pang J, Zhang Y, Zhang H, Xu Z, et al. Associations between plasma ceramides and mortality in patients with coronary artery disease. Atherosclerosis. 2020; 314: 77–83. DOI: 10.1016/j.atherosclerosis.2020.09.004.

12. Poss AM, Maschek JA, Cox JE, Hauner BJ, Hopkins PN, Hunt SC, et al. Machine learning reveals serum sphingolipids as cholesterol-independent biomarkers of coronary artery disease. J Clin Invest. 2020; 130 (3): 1363–76. DOI: 10.1172/JCI131838.

13. You Q, Peng Q, Yu Z, Jin H, Zhang J, Sun W, et al. Plasma lipidomic analysis of sphingolipids in patients with large artery atherosclerosis cerebrovascular disease and cerebral small vessel disease. Biosci Rep. 2020; 40 (9): BSR20201519. DOI: 10.1042/BSR20201519.

14. Han JS, Kim K, Jung Y, Lee JH, Namgung J, Lee HY, et al. Metabolic Alterations Associated with Atorvastatin/Fenofibric Acid Combination in Patients with Atherogenic Dyslipidaemia: A Randomized Trial for Comparison with Escalated-Dose Atorvastatin. Sci Rep. 2018; 8 (1): 14642. DOI: 10.1038/s41598-018-33058-x.

15. Snowden SG, Grapov D, Settergren M, D'Alexandri FL, Haeggström JZ, Fiehn O, et al. High-dose simvastatin exhibits enhanced lipid-lowering effects relative to simvastatin/ezetimibe combination therapy. Circ Cardiovasc Genet. 2014; 7 (6): 955–64. DOI: 10.1161/CIRCGENETICS.114.000606.

16. Ng TW, Ooi EM, Watts GF, Chan DC, Weir JM, Meikle PJ, et al. Dose-dependent effects of rosuvastatin on the plasma sphingolipidome and phospholipidome in the metabolic syndrome. J Clin Endocrinol Metab. 2014; 99 (11): E2335–40. DOI: 10.1210/jc.2014-1665.

17. Ng TW, Ooi EM, Watts GF, Chan DC, Meikle PJ, Barrett PH. Association of Plasma Ceramides and Sphingomyelin With VLDL apoB-100 Fractional Catabolic Rate Before and After Rosuvastatin Treatment. J Clin Endocrinol Metab. 2015; 100 (6): 2497–501. DOI: 10.1210/jc.2014-4348.

18. Feder S, Wiest R, Weiss TS, Aslanidis C, Schacherer D, Krautbauer S, et al. Proprotein convertase subtilisin/kexin type 9 (PCSK9) levels are not associated with severity of liver disease and are inversely related to cholesterol in a cohort of thirty eight patients with liver cirrhosis. Lipids Health Dis. 2021; 20 (1): 6. DOI: 10.1186/s12944-021-01431-x.

19. Hilvo M, Simolin H, Metso J, Ruuth M, Öörni K, Jauhiainen M, et al. PCSK9 inhibition alters the lipidome of plasma and lipoprotein fractions. Atherosclerosis. 2018; 269: 159–65. DOI: 10.1016/j.atherosclerosis.2018.01.004.

20. Ye Q, Svatikova A, Meeusen JW, Kludtke EL, Kopecky SL. Effect of Proprotein Convertase Subtilisin/Kexin Type 9 Inhibitors on Plasma Ceramide Levels. Am J Cardiol. 2020; 128: 163–7. DOI: 10.1016/j.amjcard.2020.04.052.

21. Tarasov K, Ekroos K, Suoniemi M, Kauhanen D, Sylvänne T, Hurme R, et al. Molecular lipids identify cardiovascular risk and are efficiently lowered by simvastatin and PCSK9 deficiency. J Clin Endocrinol Metab. 2014; 99 (1): E45–52. DOI: 10.1210/jc.2013–2559.

22. Instrukcija k preparatu Pralujent. Dostupno po ssylke: http://grls.rosminzdrav.ru/Grls_View_v2.aspx?routingGuid=e7885c43-2824-42ee-8673-f6221d7f2f5a&t=. Russian.

Литература

1. Bossard M, Latifi Y, Fabbri M, Kurmann R, Brinkert M, Wolfrum M, et al. Increasing Mortality From Premature Coronary Artery Disease in Women in the Rural United States. J Am Heart Assoc. 2020; 9 (9): e015334. DOI: 10.1161/JAHA.119.015334.

2. Mach F, Baigent C, Catapano AL, Koskinas KC, Casula M, Badimon L, et al; ESC Scientific Document Group. 2019 ESC/EAS Guidelines for the management of dyslipidaemias: lipid modification to reduce cardiovascular risk. Eur Heart J. 2020; 41 (1): 111–88. DOI: 10.1093/eurheartj/ehz455.

3. Ference BA, Ginsberg HN, Graham I, Ray KK, Packard CJ, Bruckert E, et al. Low-density lipoproteins cause atherosclerotic cardiovascular disease. 1. Evidence from genetic, epidemiologic, and clinical studies. A consensus statement from the European Atherosclerosis Society Consensus Panel. Eur Heart J. 2017; 38 (32): 2459–72. DOI: 10.1093/eurheartj/ehx144.

4. Khera AV, Won HH, Peloso GM, Lawson KS, Bartz TM, Deng X, et al. Diagnostic Yield and Clinical Utility of Sequencing Familial Hypercholesterolemia Genes in Patients With Severe Hypercholesterolemia. J Am Coll Cardiol. 2016; 67 (22): 2578–89. DOI: 10.1016/j.jacc.2016.03.520.

5. Barenholz Y. Sphingomyelin and cholesterol: from membrane biophysics and rafts to potential medical applications. Subcell Biochem. 2004; 37: 167–215. DOI: 10.1007/978-1-4757-5806-1_5.

6. Manicke NE, Nefliu M, Wu C, Woods JW, Reiser V, Hendrickson RC, et al. Imaging of lipids in atheroma by desorption electrospray ionization mass spectrometry. Anal Chem. 2009; 81 (21): 8702–7. DOI: 10.1021/ac901739s.

7. Brunkhorst R, Friedlaender F, Ferreirós N, Schwalm S, Koch A, Grammatikos G, et al. Alterations of the Ceramide Metabolism in the Peri-Infarct Cortex Are Independent of the Sphingomyelinase Pathway and Not Influenced by the Acid Sphingomyelinase Inhibitor Fluoxetine. Neural Plast. 2015; 2015: 503079. DOI: 10.1155/2015/503079.

8. Laaksonen R, Ekroos K, Sysi-Aho M, Hilvo M, Vihervaara T, Kauhanen D, et al. Plasma ceramides predict cardiovascular death in patients with stable coronary artery disease and acute coronary syndromes beyond LDL-cholesterol. Eur Heart J. 2016; 37 (25): 1967–76. DOI: 10.1093/eurheartj/ehw148.

9. Bligh EG, Dyer WJ. A rapid method of total lipid extraction and purification. Can J Biochem Physiol. 1959; 37 (8): 911–7.

10. Vasile VC, Meeusen JW, Medina Inojosa JR, Donato LJ, Scott CG, Hyun MS, et al. Ceramide Scores Predict Cardiovascular Risk in the Community. Arterioscler Thromb Vasc Biol. 2021; 41 (4): 1558–69. DOI: 10.1161/ATVBAHA.120.315530.

11. Li Q, Wang X, Pang J, Zhang Y, Zhang H, Xu Z, et al. Associations between plasma ceramides and mortality in patients with coronary artery disease. Atherosclerosis. 2020; 314: 77–83. DOI: 10.1016/j.atherosclerosis.2020.09.004.

12. Poss AM, Maschek JA, Cox JE, Hauner BJ, Hopkins PN, Hunt SC, et al. Machine learning reveals serum sphingolipids as cholesterol-independent biomarkers of coronary artery disease. J Clin Invest. 2020; 130 (3): 1363–76. DOI: 10.1172/JCI131838.

13. You Q, Peng Q, Yu Z, Jin H, Zhang J, Sun W, et al. Plasma lipidomic analysis of sphingolipids in patients with large artery atherosclerosis cerebrovascular disease and cerebral small vessel disease. Biosci Rep. 2020; 40 (9): BSR20201519. DOI: 10.1042/BSR20201519.

14. Han JS, Kim K, Jung Y, Lee JH, Namgung J, Lee HY, et al. Metabolic Alterations Associated with Atorvastatin/Fenofibric Acid Combination in Patients with Atherogenic Dyslipidaemia: A Randomized Trial for Comparison with Escalated-Dose Atorvastatin. Sci Rep. 2018; 8 (1): 14642. DOI: 10.1038/s41598-018-33058-x.

15. Snowden SG, Grapov D, Settergren M, D'Alexandri FL, Haeggström JZ, Fiehn O, et al. High-dose simvastatin exhibits enhanced lipid-lowering effects relative to simvastatin/ezetimibe combination therapy. Circ Cardiovasc Genet. 2014; 7 (6): 955–64. DOI: 10.1161/CIRCGENETICS.114.000606.

16. Ng TW, Ooi EM, Watts GF, Chan DC, Weir JM, Meikle PJ, et al. Dose-dependent effects of rosuvastatin on the plasma sphingolipidome and phospholipidome in the metabolic syndrome. J Clin Endocrinol Metab. 2014; 99 (11): E2335–40. DOI: 10.1210/jc.2014-1665.

17. Ng TW, Ooi EM, Watts GF, Chan DC, Meikle PJ, Barrett PH. Association of Plasma Ceramides and Sphingomyelin With VLDL apoB-100 Fractional Catabolic Rate Before and After Rosuvastatin Treatment. J Clin Endocrinol Metab. 2015; 100 (6): 2497–501. DOI: 10.1210/jc.2014-4348.

18. Feder S, Wiest R, Weiss TS, Aslanidis C, Schacherer D, Krautbauer S, et al. Proprotein convertase subtilisin/kexin type 9 (PCSK9) levels are not associated with severity of liver disease and are inversely related to cholesterol in a cohort of thirty eight patients with liver cirrhosis. Lipids Health Dis. 2021; 20 (1): 6. DOI: 10.1186/s12944-021-01431-x.

19. Hilvo M, Simolin H, Metso J, Ruuth M, Öörni K, Jauhiainen M, et al. PCSK9 inhibition alters the lipidome of plasma and lipoprotein fractions. Atherosclerosis. 2018; 269: 159–65. DOI: 10.1016/j.atherosclerosis.2018.01.004.

20. Ye Q, Svatikova A, Meeusen JW, Kludtke EL, Kopecky SL. Effect of Proprotein Convertase Subtilisin/Kexin Type 9 Inhibitors on Plasma Ceramide Levels. Am J Cardiol. 2020; 128: 163–7. DOI: 10.1016/j.amjcard.2020.04.052.

21. Tarasov K, Ekroos K, Suoniemi M, Kauhanen D, Sylvänne T, Hurme R, et al. Molecular lipids identify cardiovascular risk and are efficiently lowered by simvastatin and PCSK9 deficiency. J Clin Endocrinol Metab. 2014; 99 (1): E45–52. DOI: 10.1210/jc.2013–2559.

22. Инструкция к препарату Пралуэнт. Доступно по ссылке: http://grls.rosminzdrav.ru/Grls_View_v2.aspx?routingGuid=e7885c43-2824-42ee-8673-f6221d7f2f5a&t=

BENZIMIDAZOLE DERIVATIVE AS ANTITUMOR DRUG AGAINST EXPERIMENTALLY INDUCED LUNG CARCINOMA

Komarova EF[1,2], Zhukovskaya ON[3], Lukbanova EA[1] ✉, Yengibaryan MA[1], Vashenko LN[1], Kharagezov DA[1], Pozdnyakova VV[1], Ushakova ND[1], Shatova YuS[1], Przhedetsky YuV[1]

[1] National Medical Research Center for Oncology, Rostov-on-Don, Russia

[2] Rostov State Medical University, Rostov-on-Don, Russia

[3] Research Institute for Physical and Organic Chemistry of Southern Federal University, Rostov-on-Don, Russia

Most cancer drugs used in a clinical setting are insufficiently effective and insufficiently safe. This prompts the search for novel substances to fight cancer. The aim of this study was to explore the effects of dihydrobromide 2-(3,4-dihydroxyphenyl)-9-diethylaminoethylimidazo[1,2-a] benzimidazole (RU-185) on the growth and metastasis of experimentally induced Lewis lung carcinoma (LLC). Fifty-five C57/Bl6 male mice (weight 18–20 g) were subcutaneously inoculated with LLC cells. The tested substance (0.5 ml) was administered intragastrically at 50, 220, and 500 mg/kg (groups 1, 2 and 3, respectively) once a day for 10 days starting at 48 h after inoculation. The control group received normal saline. Intragastric administration of the tested substance resulted in significantly longer survival in group 2 only (162.3%) and in the significant reduction of tumor size on day 1 after treatment in all groups. After the end of treatment, tumor sizes in groups 2 and 3 were 3.4 and 1.3 times smaller, respectively, on day 7 and 2.2. and 1.3 times smaller, respectively, on day 14 than in the control group ($p < 0.05$). The growth delay rate was sustained in group 2 by day 14 after the end of treatment; tumor regression was observed in 20% of the animals. The number of metastases in the lungs was lower in groups 1 and 2 than in the control group (2.6 and 3.1-fold, respectively), and the metastasis inhibition was 68.1% and 80%, respectively. The tested substance RU-185 has an anticancer effect in mice: it results in longer survival, slower growth of the primary tumor and fewer lung metastases of Lewis lung carcinoma.

Keywords: Lewis lung carcinoma, dihydrobromide 2-(3,4-dihydroxyphenyl)-9-diethylaminoethylimidazo[1,2-a] benzimidazole, antitumor activity, antimetastatic activity, intragastric administration.

ПРОИЗВОДНОЕ БЕНЗИМИДАЗОЛА КАК ПРОТИВООПУХОЛЕВОЕ СРЕДСТВО В ОТНОШЕНИИ ЭКСПЕРИМЕНТАЛЬНОЙ ЗЛОКАЧЕСТВЕННОЙ ОПУХОЛИ ЛЕГКОГО

Е. Ф. Комарова[1,2], О. Н. Жуковская[3], Е. А. Лукбанова[1] ✉, М. А. Енгибарян[1], Л. Н. Ващенко[1], Д. А. Харагезов[1], В. В. Позднякова[1], Н. Д. Ушакова[1], Ю. С. Шатова[1], Ю. В. Пржедецкий[1]

[1] Национальный медицинский исследовательский центр онкологии, Ростов-на-Дону, Россия

[2] Ростовский государственный медицинский университет, Ростов-на-Дону, Россия

[3] Научно-исследовательский институт физической и органической химии Южного федерального университета, Ростов-на-Дону, Россия

Значительное число применяемых в клинике противоопухолевых средств недостаточно эффективно и безопасно, что обусловливает поиск новых лекарственных субстанций. Цель работы — изучить влияние дигидробромида 2-(3,4-дигидроксифенил)-9-диэтиламиноэтилимидазо[1,2-а]бензимидазола (РУ-185) на рост и метастазирование перевиваемой экспериментальной опухоли легкого Льюис (LLC). LLC прививали 55 мышам-самкам С57/Bl6 массой 18–20 г подкожно. Внутрижелудочное (0,5 мл в сут.) введение препарата начинали через 48 ч после перевивки опухоли 1 раз в сутки 10 дней в разовых дозах 50, 220, 500 мг/кг (группы 1, 2 и 3 соответственно). Мышам контрольной группы вводили физиологический раствор. При внутрижелудочном введении субстанции происходило достоверное увеличение продолжительности жизни животных только в группе 2 (162,3%), а также значимое уменьшение объемов опухоли уже на 1-е сутки после окончания лечения. На 7-е и 14-е сутки от момента окончания лечения размеры опухоли в группах 2 и 3 были снижены по сравнению с контрольной группой в 3,4 и 1,3 раза (на 7-е сутки) и в 2,2 и 1,3 раза (на 14-е сутки) соответственно ($p < 0.05$). Индекс торможения роста опухоли сохранился в группе 2 к 14-м суткам после окончания лечения и у 20% животных отмечен регресс опухоли. Число метастазов в легких в группах 1 и 2 было снижено относительно контроля в 2,6 и 3,1 раза соответственно, а индекс ингибирования метастазирования составил 68,1 и 80% соответственно. Исследованный РУ-185 оказывает противоопухолевое действие, что выражено в увеличении продолжительности жизни животных, снижении скорости роста первичной опухоли, а также частоты развития и количества легочных метастазов экспериментальной эпидермоидной карциномы легкого Льюис мышей.

Ключевые слова: эпидермоидная карцинома легких Льюис, дигидробромид 2-(3,4-дигидроксифенил)-9-диэтиламиноэтилимидазо[1,2-а]бензимидазо-ла, противоопухолевая активность, антиметастатическая активность, внутрижелудочное введение

Numerous studies of mechanisms underlying tumor growth and progression are laying the groundwork for the discovery of new therapeutic targets [1–3]. Development of novel antineoplastic and antimetastatic targeted therapies is in progress. Still, a lot of anticancer medications used in the clinical setting cannot boast sufficient efficacy or safety. This makes the search for novel anticancer drugs a priority field of experimental medicine.

DNA is the main target of many antineoplastic and antimetastatic drugs from various classes and chemical groups with different mechanisms of action. Studies have shown that 3H-triazolo[1,5-a]benzimidazole, the parent compound for tricyclic benzimidazole-based systems, effectively binds to the ADP site of checkpoint kinase 2 and inhibits this enzyme. Since checkpoint kinase 2 plays the definitive role in the activation of signal transduction pathways participating in cellular response to DNA damage, its inhibition in tumor cells is expected to block DNA repair and trigger apoptosis [4]. In addition, the anticancer activity of benzimidazole derivatives is associated with their effects on other cellular targets involved in DNA repair. For example, they are capable of inhibiting poly(ADP-ribose) polymerase (PARP-1 and -2), the key enzyme of the DNA repair system, and potentiating the cytotoxicity of DNA damaging agents [5]. Simpler monocyclic imidazole-based compounds can block effective DNA replication through electrostatic interactions, intercalation and groove binding [6].

Another important target for anticancer drugs is tubulin; by binding to this protein, anticancer drugs prevent its participation in some processes critical for cell division, including tubulin polymerization and depolymerization. For example, tubulin can be inhibited by benzimidazole derivatives that disrupt microtubule assembly [7]. Some benzimidazole derivatives are characterized by good pharmacokinetics and can overcome multidrug resistance in many cell lines. For instance, benzimidazole-2-urea derivatives are potent β-tubulin inhibitors: according to the literature, they exert a cytotoxic effect on human NCI-H460, Colo205, K562, A431, HepG2, Hela, and MDA-MB-435S cells [8].

The cytotoxic effect of benzimidazole derivatives on A549 (human lung adenocarcinoma) cells in hypoxic conditions is linked to the activation of their caspase-dependent apoptosis [9]. It is reported that one of structurally complex benzimidazole derivatives inhibits oncogenic kinases MEK1 and PI3K [10].

The aim of this study was to investigate the effect of 2-(3,4-dihydroxyphenyl)-9-diethylaminoethylimidazo[1,2-a] benzimidazole dihydrobromide (RU-185) on the growth and metastasis of LLC cells.

METHODS

The experiment was conducted on 55 male C57Bl/6 mice weighing 18–20 g. The animals were purchased from Andreevka breeding facility (Moscow region).

Cancer was modelled using transplantable Lewis lung carcinoma cells characterized by 100% spontaneous spread to the lungs. The cells were obtained from the tumor bank of the Laboratory for Combination Therapy of Tumors (Research Institute of Experimental Diagnostics and Therapy of Tumors of Blokhin National Medical Research Center of Oncology). The cells were maintained and subcutaneously transplanted following standard protocols.

The tested compound RU-185 was synthesized at the Research Institute of Physical and Organic Chemistry, Southern Federal University, from 1-diathylaminethyl-2-aminobenzimidazole by quaternization with 3,4-dimethoxyphenacylbromide followed by cyclization of the produced quaternary salt in the presence of 48% boiling hydrobromic acid, which was accompanied by O-demethylation [11].

The compound was dissolved in normal saline. The animals were divided into 3 groups. The tested compound was administered to the animals intragastrically via a nasogastric tube, at 50 mg/kg (group 1), 220 mg/kg (group 2) and 500 mg/kg (group 3), which equals to 1/40, 1/8 and 1/4 of LD_{50}, once a day for 10 days. Treatment was initiated 48 after inoculation with LLC cells (Table 1). The control group consisted of mice with transplantable LLC and received normal saline (placebo) intragastrically in the same volumes following the same regimen.

On day 26 after inoculation, the mice were sacrificed in a CO_2 chamber and subsequently necropsied. The antineoplastic and antimetastatic activities of the compound were studied according to the guidelines from [12]. The antineoplastic and antimetastatic activities were estimated using standard parameters, such as tumor volume, survival time (T/C%) calculated as the ratio of mean survival time in the treatment group to that in the control group, and the number of metastases. Based on the obtained estimates, tumor growth inhibition index (TGI%) and metastasis inhibition index (MII%) were calculated [12].

Prior to the experiment, LD_{50} for intragastrically administered RU-185 was calculated. The obtained value (1,980,4 mg/kg) corresponded to Category 4 of GHS criteria for acute toxicity. According to criteria described in [13], the compound can be classified as moderately hazardous (Class 3).

Statistical analysis was conducted in STATISTICA 12.0 (StatSoft Inc.; USA). Normality of distribution was tested using the Shapiro-Wilk and Kolmogorov-Smirnov tests. For mean values, the significance of differences between independent samples was determined using Student's t-test. Differences were considered significant at $p \leq 0.05$.

RESULTS

The antitumor effects of intragastrically administered RU-185 are analyzed in Table 2. At the studied doses, RU-185 had different effects on survival times in the groups. A significant

Table 1. The design of the experiment

Basic parameters	Groups			
	Experimental			Control
	1	2	3	
Number of animals in group	18	18	19	10
Treatment	2-(3,4-dihydroxyphenyl)-9-diethylaminoethylimidazo[1,2-a]benzimidazole dihydrobromide			Normal saline
Dose, mg/kg	50	220	500	
Treatment duration	10 days			
Volume administered	0.5 ml a day			
Route of administration	Intragastric via a nasogastric tube			

Table 2. Effects of intragastrically administered 2-(3,4-dihydroxyphenyl)-9-diethylaminoethylimidazo[1,2-a]benzimidazole dihydrobromide on LLC growth

Dose, mg/kg	T/C, %	Tumor volume (cm³), M ± m (TPO, %)		
		Day after end of treatment		
50	94.3	2.34 ± 0.42	8.63 ± 1.3[1,2]	10.4 ± 0.52
220	162.3	0.41 ± 0.3[1,2]	2.04 ± 0.5[1,2]	4.5 ± 0.1[1,2] (55.0) – 80% of animals 0 (100) – 20% of animals
500	112.9	1.08 ± 0.45[1,2] (30.1)	5.21 ± 1.21.2 (22.1)	7.4 ± 0.3[1,2] (28.6)
Control	0	1.56 ± 1.4	6.7 ± 0.4	9.8 ± 0.7

Note: 1 — differences are significant relative to the control group ($p < 0.05$); 2 — differences are significant relative to the subgroups of the experimental group ($p < 0.05$).

increase in survival time was observed only in group 2 (T/C = 162.3%). In group 3, survival time was longer than in the control group, but T/C did not differ significantly between these two groups. By contrast, survival time was shorter in group 1 than in the control group.

The dynamics of primary tumor growth was assessed based on tumor volume on days 1, 7 and 14 after the end of treatment. The volume of the primary tumor differed between the groups as early as day 1 after inoculation. Moderate and high doses of RU-185 (groups 2 and 3, respectively) resulted in the reduction of tumor volume relative to the control group indicated by the TGI index. However, significant changes in tumor volume at this time was observed only in group 2. In group 1, the tumor was progressing and its size exceeded 1.5 times the tumor size in the control group ($p < 0.05$).

Measurements of tumor volumes on days 7 and 14 after the end of treatment revealed the dynamics of tumor growth relative to the first days of therapy in all groups. For example, tumor volume in group 1 was larger than in the control group, whereas tumor volume in groups 2 and 3 was 3.4 and 1.3 times smaller (day 7) and 2.2 and 1.3 times smaller (day 14) than in the control group, respectively ($p < 0.05$). The value of the TGI index suggested the significant efficacy of the tested compounds at 220 mg/kg; tumor growth inhibition was observed on day 14 after the end of treatment. Importantly, tumor regression confirmed by necropsy was noted among 20% of the animals in this group (Table 2).

Interestingly, the intragastric administration of the tested compound had an antimetastatic effect against LLC (Table 3).

This effect manifested as the pronouncedly reduced rate of metastasis and fewer lung metastases in groups 1 and 2: the number of lung metastases in these groups was 2.6 and 3.1 times lower, respectively, in comparison with that in the control group, and MII was 68.1% and 80%, respectively. In group 3, administration of high doses of the tested compound resulted in the inhibition of metastasis.

Thus, we conclude that intragastrically administered RU-185 exhibited antitumor activity against experimentally induced Lewis lung carcinoma, inhibiting its growth and metastasis. At 220 mg/kg, RU-185 increased mean survival time and caused

tumor regression in 20% of the animals by day 14 after the beginning of treatment. The most pronounced antitumor and antimetastatic effect of the studied benzimidazole derivative was observed at 220 mg/kg. Reduction in the number of lung metastases and the metastatic rate (the metastasis inhibition index) was observed at all tested doses, indicating the pronounced antimetastatic effect of RU-185 against the spread of LLC to the lungs.

DISCUSSION

Earlier studies investigating the effects of intragastrically administered RU-185 on the growth of transplantable subcutaneous B16 melanoma showed that the compound had a greater inhibiting effect on metastasis to the lungs than on the growth of the primary tumor [14, 15]. However, our study has demonstrated a pronounced antitumor effect on both primary LLC and its metastases. Perhaps, the antitumor effect of the studied compound against the primary tumor can be explained by differences in the phenotypic characteristics of melanoma and lung carcinoma [16, 17]. Pronounced inhibition of metastatic spread to the lungs suggests that there are common factors that determine the adaptation of cancer cells to the metastatic niche and the growth of metastases in a given metabolic environment, predicating the mechanism of action of the tested compound [18]. The metastatic proteome and transcriptome of the tumor are dynamically modulated by the metabolome. Metabolome-induced signal cascades can modulate tumor aggression and metastatic spread via different pathways involved at each stage of the metastatic cascade [19]. However, further research is needed to support the hypothesis about the possible mechanism underlying the antitumor effect of the tested compound.

CONCLUSION

RU-185 administered intragastrically at 220 mg/kg once a day exerts antitumor activity reflected in the significant increase in survival time, slower primary tumor growth, the reduced rate of metastasis and the reduced number of metastases of

Table 3. Effects of intragastrically administered 2-(3,4-dihydroxyphenyl)-9-diethylaminoethylimidazo[1,2-a]benzimidazole dihydrobromide on LLC spread

Dose, mg/kg	Number of mts per mouse	MII, %
50	12.3 ± 1.0[1,2]	68.1 ± 2.1[1,2]
220	10.3 ± 0.6[1,2]	80.0 ± 3.1[1,2]
500	27.5 ± 0.92	13.9 ± 1.1
Control	32.2 ± 1.2	–

Note: 1 — differences are significant relative to the control group ($p < 0.05$); 2 — differences are significant relative to the subgroups of the experimental group ($p < 0.05$).

experimentally induced epidermal LLC in a mouse model. The antimetastatic effect of the compound against transplantable LLC is observed at 50 and 500 mg/kg. Identification of metabolic mechanisms underlying the antitumorigenic and antimetastatic effects of RU-185 will help to detect its therapeutic targets and make it a candidate drug against lung cancer.

References

1. Kit OI, Shaposhnikov AV, Zlatnik EYu, Nikipelova EA, Novikova IA. Mestnyj kletochnyj immunitet pri adenokarcinome i polipah tolstoj kishki. Sibirskoe medicinskoe obozrenie. 2012; 4 (76): 11–16. Russian.
2. Kit OI, Franciyanc EM, Nikipelova EA, Komarova EF, Kozlova LS, Tavarjan IS, i dr. Izmenenija markerov proliferacii, neoangiogeneza i sistemy aktivacii plazminogena v tkani raka prjamoj kishki. Jeksperimental'naja i klinicheskaja gastrojenterologija. 2015; 2 (114): 40–45. Russian.
3. Bashraheel SS, Domling A, Goda SK. Update on targeted cancer therapies, single or in combination, and their fine tuning for precision medicine. Biomed Pharmacother. 2020; 125: 110009.
4. Silva-Santisteban MC, Westwood IM, Boxall K. Fragment-based screening maps inhibitor interactions in the ATP-binding site of checkpoint kinase 2. PLoS One. 2013; 8 (6): e65689.
5. Penning TD, Zhu G-D, Gandhi VB, Gong J, Liu X, Shi Y, at al. Discovery of the Poly(ADP-ribose) Polymerase (PARP) Inhibitor 2-[(R)-2-Methylpyrrolidin-2-yl]-1H-benzimidazole-4-carboxamide (ABT-888) for the Treatment of Cancer. J Med Chem. 2009; 52: 514.
6. Ali I, Lone MN, Aboul-Enein H.Y. Imidazoles as potential anticancer agents. Medchemcomm. 2017; 8 (9): 1742–73.
7. Torres FC, Garcia-Rubino ME, Lozano-Lopez C, Kawano DF, Eifler-Lima VL, von Poser GL. Imidazoles and benzimidazoles as tubulin-modulators for anti-cancer therapy. Curr Med Chem. 2015; 14: 306–18.
8. Khattab M. Theoretical study of the geometric and electronic characterization of carbendazim-based drug (Nocodazole). Heliyon. 2020; 6 (6): e04055.
9. Blaszczak-Swiatkiewicz K, Olszewska P, Mikiciuk-Olasik E. Biological approach of anticancer activity of new benzimidazole derivatives. Pharmacological Reports. 2014; 66 (1): 100–6.
10. Marcian E, Dort V, Hong H, Wang H, Nino CA, Lombardi RL. Discovery of Bifunctional Oncogenic Target Inhibitors against Allosteric Mitogen-Activated Protein Kinase (MEK1) and Phosphatidylinositol 3-Kinase (PI3K). Journal of Medicinal Chemistry. 2016; 59 (6): 2512–22.
11. Anisimova VA, Kosolapov VA, Minkin VI, i dr., patentoobladatel'. Digidrobromid 9-(3,4-digidroksifenil)-9-dijetilamiino- jetilimidazo[1,2-a]benzimidazola i farmacevticheskaja kompozicija na ego osnove. Patent RF # 2391979/ 12.05.2008.
12. Mezhgosudarstvennyj standart. Sistema standartov bezopasnosti truda. Vrednye veshhestva. Klassifikacija i obshhie trebovanija bezopasnosti. GOST 12.1.007-76. Dostupno po ssylke: https://docs.cntd.ru/document/5200233.
13. Mironova AN, redaktor. Rukovodstvo po provedeniju doklinicheskih issledovanij lekarstvennyh sredstv. Chast 1, M.: Grif i K, 2013; 944 s.
14. Kit OI, Komarova EF, Spasov AA, Morkovnik AS, Zhukovskaya ON, Korobejnikova EP, Vanzha LV, Shihljarova AI, Bragina MI, Barteneva TA, Lukbanova EA, Shirnina EA, Zlatnik EJu, Novikova IA, Pozdnjakova VV, Maksimov AJu, Anisimova VA, avtory; FGBU «Nacional'nyj medicinskij issledovatel'skij centr onkologii», patentoobladatel'. Sredstvo dlja ingibirovanija metastazirovanija v legkih. Patent RF # 2632703. 12.12.2016. Russian.
15. Komarova EF, Shihljarova AI, Bragina MI, Shirnina EA, Barteneva TA, Korobejnikova EP, i dr. Ocenka protivoopuholevoj aktivnosti antioksidanta jenoksifol na modeli melanomy V16 v jeksperimente. Izvestija Vuzov. Severo-Kavkazskij region. Estestvennye nauki. 2017; 3–2: 67–73. Russian.
16. Aminzadeh–Gohari S, Weber DD, Catalano L, Feichtinger RG, Kofler B, Lang R. Targeting Mitochondria in Melanoma. Biomolecules. 2020; 10 (10): 1395.
17. Wu M. Multiparameter metabolic analysis reveals a close link between attenuated mitochondrial bioenergetic function and enhanced glycolysis dependency in human tumor cells. Am J Physiol Cell Physiol. 2007; 292: 125–36.
18. Ohshima K, Morii E. Metabolic Reprogramming of Cancer Cells during Tumor Progression and Metastasis. Metabolites. 2021; 11 (1): 28.
19. Wei Q, Qian Y, Yu J, Wong CC. Metabolic rewiring in the promotion of cancer metastasis: mechanisms and therapeutic implications. Oncogene. 2020; 39 (39): 6139–56.

Литература

1. Кит О. И., Шапошников А. В., Златник Е. Ю., Никипелова Е. А., Новикова И. А. Местный клеточный иммунитет при аденокарциноме и полипах толстой кишки. Сибирское медицинское обозрение. 2012; 4 (76): 11–16.
2. Кит О. И., Франциянц Е. М., Никипелова Е. А., Комарова Е. Ф., Козлова Л. С., Таварян И.С., и др. Изменения маркеров пролиферации, неоангиогенеза и системы активации плазминогена в ткани рака прямой кишки. Экспериментальная и клиническая гастроэнтерология. 2015; 2 (114): 40–45.
3. Bashraheel SS, Domling A, Goda SK. Update on targeted cancer therapies, single or in combination, and their fine tuning for precision medicine. Biomed Pharmacother. 2020; 125: 110009.
4. Silva-Santisteban MC, Westwood IM, Boxall K. Fragment-based screening maps inhibitor interactions in the ATP-binding site of checkpoint kinase 2. PLoS One. 2013; 8 (6): e65689.
5. Penning TD, Zhu G-D, Gandhi VB, Gong J, Liu X, Shi Y, at al. Discovery of the Poly(ADP-ribose) Polymerase (PARP) Inhibitor 2-[(R)-2-Methylpyrrolidin-2-yl]-1H-benzimidazole-4-carboxamide (ABT-888) for the Treatment of Cancer. J Med Chem. 2009; 52: 514.
6. Ali I, Lone MN, Aboul-Enein H.Y. Imidazoles as potential anticancer agents. Medchemcomm. 2017; 8 (9): 1742–73.
7. Torres FC, Garcia-Rubino ME, Lozano-Lopez C, Kawano DF, Eifler-Lima VL, von Poser GL. Imidazoles and benzimidazoles as tubulin-modulators for anti-cancer therapy. Curr Med Chem. 2015; 14: 306–18.
8. Khattab M. Theoretical study of the geometric and electronic characterization of carbendazim-based drug (Nocodazole). Heliyon. 2020; 6 (6): e04055.
9. Blaszczak-Swiatkiewicz K, Olszewska P, Mikiciuk-Olasik E. Biological approach of anticancer activity of new benzimidazole derivatives. Pharmacological Reports. 2014; 66 (1): 100–6.
10. Marcian E, Dort V, Hong H, Wang H, Nino CA, Lombardi RL. Discovery of Bifunctional Oncogenic Target Inhibitors against Allosteric Mitogen-Activated Protein Kinase (MEK1) and Phosphatidylinositol 3-Kinase (PI3K). Journal of Medicinal Chemistry. 2016; 59 (6): 2512–22.
11. Анисимова В. А., Косолапов В. А., Минкин В. И., и др., патентообладатель. Дигидробромид 9-(3,4-дигидроксифенил)-9-диэтиламиино- этилимидазо[1,2-a]бензимидазола и фармацевтическая композиция на его основе. Патент РФ № 2391979/ 12.05.2008.
12. Межгосударственный стандарт. Система стандартов безопасности труда. Вредные вещества. Классификация и общие требования безопасности. ГОСТ 12.1.007-76. Доступно по ссылке: https://docs.cntd.ru/document/5200233.
13. Миронова А. Н., редактор. Руководство по проведению доклинических исследований лекарственных средств. Часть 1, М.: Гриф и К, 2013; 944 с.

14. Кит О. И., Комарова Е. Ф., Спасов А. А., Морковник А. С., Жуковская О. Н., Коробейникова Е. П., Ванжа Л. В., Шихлярова А. И., Брагина М. И., Бартенева Т. А., Лукбанова Е. А., Ширнина Е. А., Златник Е. Ю., Новикова И. А., Позднякова В. В., Максимов А. Ю., Анисимова В. А., авторы; ФГБУ «Национальный медицинский исследовательский центр онкологии», патентообладатель. Средство для ингибирования метастазирования в легких. Патент РФ № 2632703. 12.12.2016.

15. Комарова Е. Ф., Шихлярова А. И., Брагина М. И., Ширнина Е. А., Бартенева Т. А., Коробейникова Е. П. и др. Оценка противоопухолевой активности антиоксиданта эноксифол на модели меланомы B16 в эксперименте. Известия Вузов.

Северо-Кавказский регион. Естественные науки. 2017; 3–2: 67–73.

16. Aminzadeh–Gohari S, Weber DD, Catalano L, Feichtinger RG, Kofler B, Lang R. Targeting Mitochondria in Melanoma. Biomolecules. 2020; 10 (10): 1395.

17. Wu M. Multiparameter metabolic analysis reveals a close link between attenuated mitochondrial bioenergetic function and enhanced glycolysis dependency in human tumor cells. Am J Physiol Cell Physiol. 2007; 292: 125–36.

18. Ohshima K, Morii E. Metabolic Reprogramming of Cancer Cells during Tumor Progression and Metastasis. Metabolites. 2021; 11 (1): 28.

19. Wei Q, Qian Y, Yu J, Wong CC. Metabolic rewiring in the promotion of cancer metastasis: mechanisms and therapeutic implications. Oncogene. 2020; 39 (39): 6139–56.

STRUCTURAL AND FUNCTIONAL BIOMARKERS OF EFFICACY OF NAVIGATED REPETITIVE TRANSCRANIAL MAGNETIC STIMULATION IN THERAPY FOR TRIGEMINAL NEURALGIA

Poydasheva AG ✉, Sinitsyn DO, Bakulin IS, Suponeva NA, Piradov MA

Research Center of Neurology, Moscow, Russia

Repetitive transcranial magnetic stimulation (rTMS) is an alternative treatment option for patients with drug-resistant trigeminal neuralgia (TN). However, the effect of rTMS is variable. The aim of this study was to find neuroimaging biomarkers of clinical efficacy of navigated rTMS. Seventeen patients with TN (14 women and 3 men, median age 56 years) received 10 sessions of high-frequency rTMS of the motor cortex contralateral to pain side. The data were analyzed for correlations between functional connectivity (FC), the grey matter (GM) volume and the reduction in pain intensity. Positive correlations were established between the reduction in average pain intensity and GM volume in caudate nuclei in both hemispheres (p(unc) = 0.03), both cerebellar hemispheres (p(unc) = 0.002) and the postcentral gyrus contralateral to pain side (p(unc) = 0.005); between the reduction in peak pain intensity and GM volume in the caudate nucleus contralateral to pain side (p(unc) = 0.04) and the cerebellar hemisphere ipsilateral to pain (p(unc) = 0.03). Significant positive correlations were discovered between the reduction in average pain intensity and FC between the thalamus contralateral to pain side, the postcentral gyrus and the insular operculum (both ipsilateral to pain side; p(FWE) = 0.018), as well as between the cingulate cortex and the anterior cingulate cortex ipsilateral to pain (p(FWE) = 0.017), between the contralateral subcallosal gyrus and the cerebellar hemisphere ipsilateral to pain (p(FWE) = 0.018). A negative correlation was established for FC between the contralateral putamen and the occipital lobes in both hemispheres (p(FWE) = 0.001). Our findings may spur the development of individual predictors of rTMS efficacy in patients with chronic pain.

Keywords: neuralgia, trigeminal nerve, voxel-based morphometry, functional connectivity, biomarker, transcranial magnetic stimulation

СТРУКТУРНО-ФУНКЦИОНАЛЬНЫЕ БИОМАРКЕРЫ ЭФФЕКТИВНОСТИ НАВИГАЦИОННОЙ РИТМИЧЕСКОЙ ТРАНСКРАНИАЛЬНОЙ МАГНИТНОЙ СТИМУЛЯЦИИ В ЛЕЧЕНИИ НЕВРАЛГИИ ТРОЙНИЧНОГО НЕРВА

А. Г. Пойдашева ✉, Д. О. Синицын, И. С. Бакулин, Н. А. Супонева, М. А. Пирадов

Научный центр неврологии, Москва, Россия

У пациентов с невралгией тройничного нерва (НТН), не отвечающих на фармакотерапию, в качестве альтернативы можно применять ритмическую транскраниальную магнитную стимуляцию (рТМС). Однако эффект рТМС вариабелен. Целью исследования был поиск нейровизуализационных биомаркеров клинической эффективности навигационной рТМС. Семнадцати пациентам с НТН (14 женщин; медиана возраста — 56 лет) проведено 10 сессий высокочастотной рТМС моторной коры полушария, контрлатерального локализации боли. Проводили анализ корреляций функциональной коннективности (ФК) и объема серого вещества головного мозга (СВГМ) со снижением интенсивности боли. Показана положительная корреляция между снижением средней интенсивности боли и объемом СВГМ в области хвостатых ядер (p(unc) = 0,03), мозжечка билатерально (p(unc) = 0,002) и контрлатеральной постцентральной извилине (p(unc) = 0,005); между снижением максимальной интенсивности боли и объемом СВГМ в области хвостатого ядра контрлатерально боли (p(unc) = 0,04) и мозжечка ипсилатерально (p(unc) = 0,03). Продемонстрирована положительная связь снижения средней интенсивности боли с ФК между таламусом (контрлатерально локализации боли) и ипсилатеральной постцентральной извилиной и покрышкой островка (p(FWE) = 0,018), между поясной корой и передними отделами поясной коры ипсилатерально боли (p(FWE) = 0,017), между контрлатеральной паратерминальной извилиной и мозжечком ипсилатерально (p(FWE) = 0,018); отрицательная корреляция для ФК между контрлатеральной скорлупой и затылочными долями обоих полушарий (p(FWE) = 0,001). Полученные результаты могут стать предпосылкой к разработке индивидуальных предикторов эффективности рТМС у пациентов с хроническими болевыми синдромами.

Ключевые слова: невралгия, тройничный нерв, воксель-ориентированная морфометрия, функциональная коннективность, биомаркеры, транскраниальная магнитная стимуляция

Trigeminal neuralgia (TN) is characterized by short-lived paroxysms of acute severe facial pain in the cutaneous trigeminal distribution. The prevalence of TN in the general population is estimated at 0.03–0.3% [1]. Although therapy with sodium channel blockers is highly effective against TN, as many as half of the affected patients develop resistance to it over time [2].

Invasive procedures (e.g. microvascular decompression) and transcranial magnetic stimulation (TMS) offer an alternative to conventional pharmacotherapy for TN [3–5].

TMS is a non-invasive technique for brain stimulation that uses a high-density alternating magnetic field to modulate the excitability of a target (stimulated) brain area. During

repetitive (rhythmic) transcranial magnetic stimulation (rTMS), multiple magnetic pulses (usually over 1,000) are applied in succession; the directionality of their effect on the target depends on stimulation frequency. It is widely hypothesized that the underlying mechanisms of rTMS share similarity with long-term potentiation (LTP) and long-term depression (LTD) or may affect neurotransmitter synthesis and the genetic apparatus of the cell [6]. Regarding the analgesic effect of rTMS, studies show that rTMS can modulate endogenous opioid neurotransmission in the antinociceptive structures of the brain, restore cortical excitability and impaired intracortical interactions [7]. The panel of European experts has concluded that rTMS has the highest level of evidence-based efficacy for chronic neuropathic pain (level A, or "definitely effective") [4]. According to the systematic review of 11 studies investigating the efficacy of rTMS against chronic neuropathic orofacial pain, including trigeminal neuralgia, rTMS is an effective and safe modality [8]. At the same time, in another study the protocol recommended for chronic pain relief (high-frequency stimulation of the primary motor cortex contralateral to pain side) had no significant analgesic effect in patients with TN and atypical facial pain [9]. The reason for such inconsistency and one of the factors impeding wide use of rTMS in clinical practice is the variability in the rTMS-induced effect [10]. Conducting a search for predictors of response to rTMS may hold promise for finding the right solution [11]. Here, one of the approaches is to identify brain regions in which structural or functional changes are correlated with rTMS efficacy. This approach was best elaborated for depressive disorders. For example, 4 biotypes were identified from patient resting-state fMRI data based on patient response to rTMS [12]. Other studies demonstrated that functional connectivity (FC) between various brain regions can serve as a predictor of response to rTMS, but the results of those studies were very heterogenous and no clear concept was proposed for identifying patients with a potentially good response to stimulation from specific connections [11, 13]. It is reported that structural data can be used to predict response to rTMS among patients with depressive disorders, tinnitus and schizophrenia [14, 15]. But no similar studies have been conducted in patients with trigeminal neuralgia so far.

The aim of this study was to find neuroimaging markers of clinical efficacy of navigated rTMS in patients with trigeminal neuralgia.

METHODS

Methodology of the study

The study included patients aged 18-80 years with classical TN according to the International Classification of Headache Disorders 3rd edition, 2013 (ICHD-3). The following inclusion criteria were applied: primary trigeminal neuralgia; mean pain intensity ≥ 4 points on the Pain Numeric Rating Scale (NRS); insufficient efficacy or intolerance of standard medication therapy for TN. Exclusion criteria: contraindications for MRI or rTMS; refusal to participate in the study; severe adverse effects; pregnancy. Prior to the study, all the participants underwent at least a one-month long fixed-dose therapy with sodium channel blockers. The patients did not receive other drugs that could have affected their central nervous system.

Neuroimaging

Every patient underwent a neuroimaging examination, which was conducted using a Siemens 3T Magnetom Verio scanner (Erlangen, Siemens; Germany).

Anatomical T1-weighted scans were acquired at isotropic resolution for further multiplanar reconstruction (MPR) (TR 1900 ms, TE 2.47 ms, slice thickness 1 mm, number of slices 176, scan time 4 min 18 s). The obtained structural data were analyzed by means of voxel-based morphometry (VBM) and used for neuronavigation and coil orienting during rTMS. Before the VBM analysis, the obtained structural MR images of the brain were preprocessed in SPM 12 using the Dartel method for VBM [16]. Briefly, the images were segmented into different tissue types; then, a common (TN-group specific) template was created and nonlinear transformations were computed to normalize the images to this template using the Dartel algorithm. After that, the data were normalized to MNI space using the option of preserving the amount of tissue and smoothed with a Gaussian kernel (FWHM = 10 mm). Statistical analysis of the resulting images was done in SPM 12. Specifically, the relative volumes of the grey matter (GM) were analyzed; for that, the images were normalized by the brain volume for each study participant.

Resting-state fMRI images for the subsequent FC analysis were acquired in the multiplanar gradient echo mode (ep2d_bold_moco: TR 2400 ms, TE 30 ms; flip angle 90°, matrix 64 × 64; FoV 192 × 192 mm^2, 36 slices in the axial plane). The obtained functional images were preprocessed in the CONN functional connectivity toolbox, ver. 17f (Alfonso Nieto-Castanon; USA) and SPM12 (The Wellcome Centre for Human Neuroimaging; UK). Preprocessing included realignment (head motion correction), slice-timing correction, structural/functional co-registration, segmentation of structural images, normalization to a standard MNI (Montreal Neurological Institute) space, identification and rejection of outlier scans using the ART tool, and spatial smoothing with an 8 mm Gaussian kernel. For each patient, the total number of outlier scans had to be less than a half. To denoise the images, a 0.008–0.09 Hz band-pass filter was applied.

Navigated rTMS

Navigated rTMS was performed using a Magstim Rapid2 stimulator (The Magstim Company Ltd; US) calibrated for NBS (Navigated Brain System) Eximia Nexstim (Nexstim Plc.; Finland). Each patient received a total of 10 rTMS session (5 daily sessions a week, except weekends) of high-frequency rTMS of the primary motor cortex contralateral to pain localization (stimulation frequency 10 Hz, intensity 90% of the resting motor threshold, train duration 4 s, intertrain interval 26 s, a total of 1,600 pulses per session). The hotspot of the abductor pollicis brevis muscle on the body side ipsilateral to pain side was used as a target. The resting motor threshold was determined once, before the beginning of the first rTMS session, by means of the Rossini–Rothwell method. The stability of coil position was monitored during each session using the neuronavigation system. The analgesic effect of rTMS was measured on NRS. Peak and average pain intensity was assessed before and immediately after 10 rTMS sessions. Statistical analysis was carried out in MATLAB R2017a (Mathworks, Inc.; USA) using the Wilcoxon signed rank test. Differences were considered significant at $p = 0.05$.

Study of clinical and neuroimaging correlations

To identify neuroimaging biomarkers of clinical efficacy of rTMS, we analyzed how changes in average and peak (for VBM analysis only) pain intensity measured on NRS were correlated

Table 1. Areas of interest (Henssen et al., 2019) selected for the analysis of clinical and neuroimaging correlations between the strength of response evoked by rTMS and structural/functional features of the brain

Cluster	Gyrus/region	Brodmann areas	R/L	Cluster volume, mm^3	Cluster coordinates (MNI) x, y, z, mm		
1	Pulvinar		L	880	−11.1	−27.2	7.1
2	Superior Temporal Gyrus	22	L	736	−49.8	−17.8	4.7
3	Subcallosal Gyrus	47	L	592	−13.7	22.2	−10
4	Insula	13	R	552	29.3	−21.9	16.2
5	Thalamus		R	520	5.2	−8.7	5.4
6	Cingulate Gyrus	31	R	520	4.9	−42.7	28.3
7	Middle Temporal Gyrus	21	R	496	39	−6.8	−12.8
8	Caudate Head		R	360	7.6	8.2	−5.1
9	Putamen		L	296	−23.3	−7.8	7.7
10	Transverse Temporal Gyrus	41	R	216	35.8	−32.3	11
11	Caudate Head		L	136	−8.5	7.8	1.9
12	Precentral Gyrus	6	L	136	−55.9	0.7	27.5
13	Anterior Cingulate Cortex	24	L	128	−1.7	33.7	8
14	Putamen		L	120	−20.6	7.7	3.7
15	Anterior Cerebellar Lobe		L	112	−3.6	−43.9	−7.3
16	Medial Frontal Gyrus	10	R	112	17.8	60.6	2.1
17	Middle Frontal Gyrus	9	R	112	48.7	12	33.3
18	Postcentral Gyrus	1	L	112	−53.5	−18.7	45.8
19	Insula	13	R	104	34.3	12.7	−8.3
20	Culmen		R	104	6.3	−48	−5.4
21	Precuneus	31	R	104	9.7	−62.3	27.2
22	Medial Frontal Gyrus	9	R	104	10	27.4	32.3

Note: R — right hemisphere; L — left hemisphere.

with FC and GM volume (measured before rTMS) in those brain regions that, according to [17], are characterized by a significantly lower amount of grey matter in patients with TN than in healthy volunteers (Table 1).

The neuroimaging data of patients who had pain on the left side ($n = 4$) were intentionally flipped so that pain was localized to the right side for all study participants. For the analysis of functional biomarkers, the average signal in each area of interest was correlated with the signals from all voxels in the brain (seed-based analysis). The significance of rTMS effects was assessed from the resultant statistical parametric maps using Gaussian random field theory. The voxel-wise significance threshold was assumed to be 0.001 (uncorrected); significant clusters were selected, using a two-sided test with FWER control at 0.05. The results were not corrected for the number of areas of interest. For the analysis of structural biomarkers, we also employed the regression analysis of associations between GM volume in the areas of interest and changes in average and peak pain intensity. The analysis was carried out in MarsBaR

(Matthew Brett; UK) for SPM, with a significance threshold of 0.05, without correction for multiple comparisons.

RESULTS

Voluntary informed consent to participate in the study was given by 20 patients. Two patients decided to drop out after sessions 4 and 7, respectively, due to commuting problems; one more patient was excluded from the analysis due to the presence of strong motion artifacts on his MRI scans. Thus, the final dataset subjected to the analysis included data of 17 patients (median age: 56 years [38; 65]).

While analyzing the effects of navigated rTMS, we discovered a statistically significant reduction in peak ($p = 0.01$) and average ($p < 0.01$) pain intensity on NRS. For half of the patients, the analgesic effect was significant: peak pain intensity had dropped by more than 30% relative to its initial level.

The analysis of correlations between the reduction in peak and average pain intensity on the numeric rating scale and

Table 2. Correlations between grey matter volume and rTMS effect

Clinical parameter	Areas in which grey matter volume positively correlates with rTMS effect	ROI (coordinates), x, y, z (Henssen et al., 2019)	p (unc)
Reduction of average pain intensity	Caudate Head (I)	7.6 8.2 −5.1	0.033
	Caudate Head (C)	−8.5 7.8 1.9	0.034
	Anterior Cerebellar Lobe (C)	−3.6 −43.9 −7.3	0.002
	Postcentral Gyrus (C)	−53.5 −18.7 45.8	0.005
	Culmen (I)	6.3 −48 −5.4	0.003
Reduction of peak pain intensity	Caudate Head (C)	−8.5 7.8 1.9	0.04
	Culmen (I)	6.3 −48 −5.4	0.033

Note: C — the area of interest is localized to the hemisphere contralateral to pain side; I — the area of interest is localized to the hemisphere ipsilateral to pain side.

Fig. 1. Brain areas in which grey matter volume is positively correlated with the reduction in peak or average pain intensity (*p*(unc) < 0.05)

GM volume in the areas of interest identified in [17] showed that the reduction in average pain intensity was positively correlated with GM volume in the caudate head (bilaterally), in the postcentral gyrus contralateral to pain side and in both cerebellar hemispheres (Table 2).

In turn, the reduction in peak pain intensity was positively correlated with GM volume in the caudate head contralateral to pain and in the cerebellar region ipsilateral to pain (Table 2; Fig. 1).

The analysis of correlations between the clinical effect of rTMS and functional connectivity in the areas of interest identified in [17] revealed a positive correlation between the reduction in average pain intensity on NRS and the functional connectivity between the thalamus (contralateral to pain), the postcentral gyrus ipsilateral to pain side and the insular operculum ipsilateral to pain side (Table 3).

In addition, a positive correlation was established between the reduction in average pain intensity and FC between 1) the cingulate cortex ipsilateral to pain side and the anterior cingulate cortex ipsilateral to pain side, and 2) the subcallosal gyrus contralateral to pain localization and the cerebellar hemisphere and peduncle contralateral to pain. A negative correlation was established between the reduction in average pain intensity and FC between the putamen contralateral to pain side and the occipital lobes in both hemispheres (Fig. 2).

DISCUSSION

After a series of navigated repetitive transcranial magnetic stimulation sessions, a significant reduction in peak and average pain intensity was observed among patients with TN. The response to magnetic stimulation was correlated with some anatomical and functional changes in central nervous system structures detected prior to the beginning of rTMS therapy. Specifically, we found correlations between the effect of rTMS and the functional connectivity of brain areas involved in the primary processing of pain inputs (the thalamus and

Table 3. Correlations between the functional connectivity of brain regions and rTMS effect on average pain intensity. The table features cluster-wise FWE-corrected *p* values for the areas of interest on each connectivity map, uncorrected for the number of such zones (clusters with *p*(FWE) < 0.05)

Areas of interest	Anatomical regions	Cluster coordinates (MNI) *x, y, z*, mm	Cluster volume, mm³	*p* (FWE)	Direction of correlation
Thalamus (C)	Postcentral Gyrus (I) Insular Operculum (I)	+60 −16 +18	133	0,018	+
Subcallosal Gyrus (C)	Cerebellar Hemisphere and Cerebellar Peduncle (I)	+32 −62 −38	126	0,018	+
Cingulate Cortex (I)	Anterior Cingulate Cortex (I)	+26 +34 +06	151	0,017	+
Putamen (C)	Occipital Pole (I) Fusiform Gyrus (I)	+20 −100 +00	211	0,001	−
	Occipital Pole (C) Lateral Occipital Cortex (C)	−18 −100 −08	195	0,002	−

Note: C — the area of interest is localized to the hemisphere contralateral to pain side; I — the area of interest is localized to the hemisphere ipsilateral to pain side.
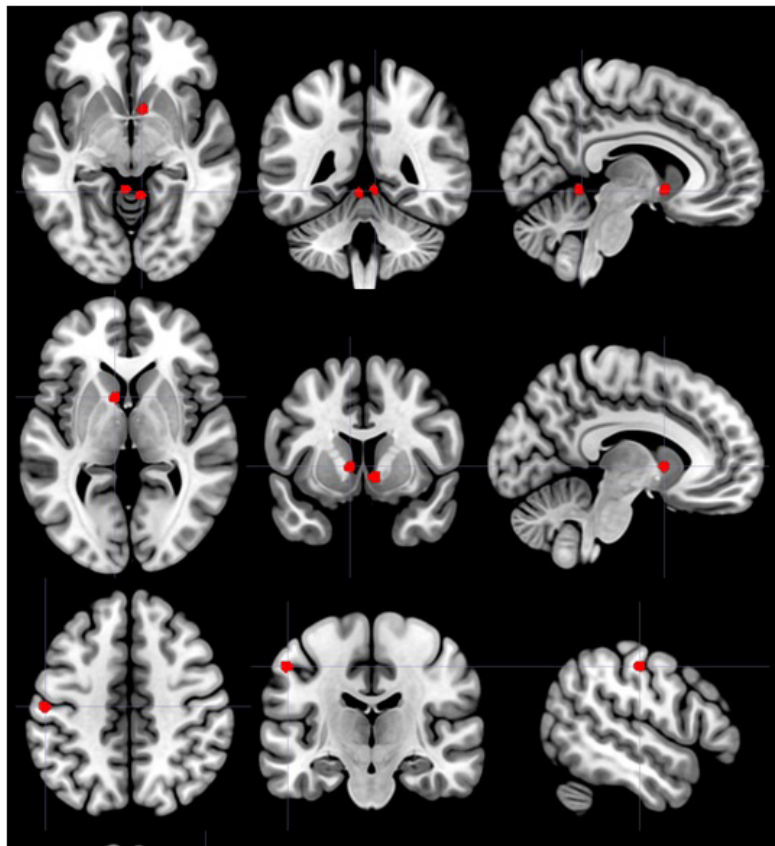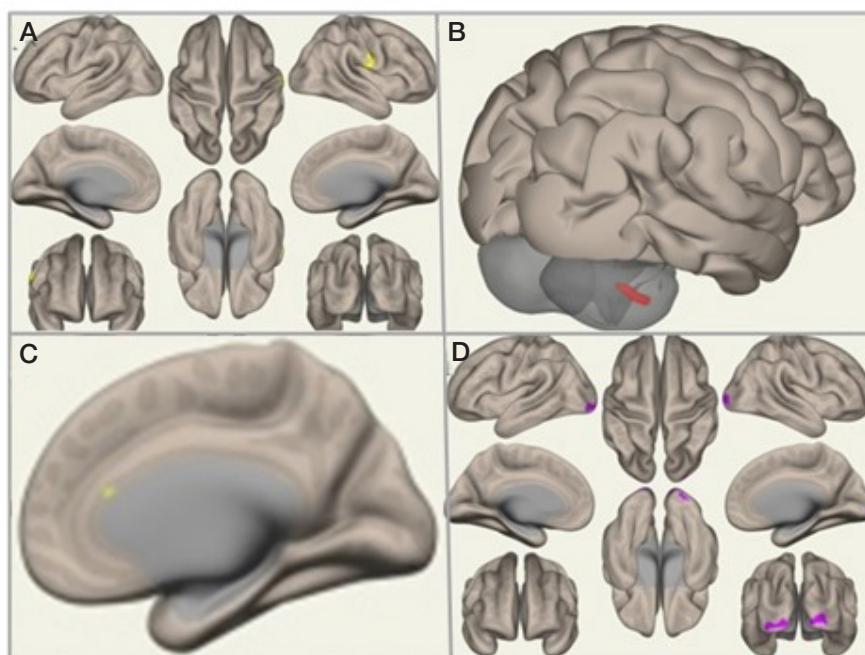
Fig. 2. Brain areas for which FC is correlated with the reduction in average pain intensity (p(FWE) < 0.05). **A**. Thalamus contralateral to pain side. **B**. Subcallosal gyrus contralateral to pain side. **C**. Cingulate gyrus ipsilateral to pain side. **D**. Putamen ipsilateral to pain side

the postcentral gyrus), the affective component of pain and behavioral response to it (the insula and the cingulate cortex). While investigating the structural biomarkers of response to rTMS, we found that the strength of the rTMS effect was positively correlated with GM volume in the caudate nuclei, the postcentral gyrus and the cerebellum.

Before embarking on a more detailed discussion of specific zones, their role and function in the development of TN, we would like to highlight the use of intentional dataset flipping as part of the methodology employed for this study: patient data was flipped left to right for group analysis so that the left hemisphere was contralateral to pain side for all study participants. Our intention was to obtain more homogeneous data in the areas associated with pain transmission and primary processing (the thalamus, primary somatosensory regions, the insula of the contralateral hemisphere, etc.). At the same time, this manipulation resulted in the increase in the heterogeneity of the signal from structures which had been previously shown to have structural and functional left-right asymmetries. For example, large-sample VBM-based studies reported an asymmetry in the frontal, temporal, occipital poles, Heschl gyrus, hippocampus, regions involved in speech and language, etc. [18]. Similar findings were reported in a study of functional connectivity; the greatest asymmetry was observed in the associative areas of the frontal, temporal and occipital lobes and language-related regions [19]. In a study [20], GM volumes were compared between patients with TN and healthy volunteers; the same areas were identified using flipped and non-flipped datasets, but the strength of the effect was less for the non-flipped data. So, having analyzed the literature, we decided to flip our dataset. However, this may have been the reason why no expected correlations for the rTMS effect were observed in the dorsolateral prefrontal cortex and the superior and middle temporal gyri, which were structurally and functionally changed in patients with TN in comparison with healthy volunteers.

The thalamus in the hemisphere contralateral to pain side stands out among the areas whose functional connectivity was correlated with the effect of rTMS in our study. The nuclei of the thalamus are the central relay that forwards nociceptive pulses

from the sensory nuclei of the trigeminal nerve to the primary somatosensory cortex; i.e., the thalamus is the key player involved in the processing of pain signals. Destruction of the specific complex of thalamic nuclei by means of gamma knife surgery in patients with drug-resistant TN effectively reduces pain intensity without causing a sensory deficit [21]. Importantly, the thalamus might be immediately involved in producing the analgesic effect in response to rTMS. In the experiment on rats, the neuronal activity of some thalamic nuclei was inhibited by invasive direct current stimulation of the motor cortex [22]. Thus, the established correlations between FC of the thalamus and the response to rTMS may be associated with the diverse roles of thalamic nuclei in the processing of pain inputs, the development of chronic pain and the response to the stimulation of the motor cortex.

Our study established a correlation between the rTMS-induced effect and the functional connectivity of the anterior cingulate cortex. It is traditionally held that the anterior cingulate cortex plays an essential role in the development and maintenance of neuropathic pain; specifically, it participates in the modulation and processing of pain affect [23]. Moreover, the inhibition of the cingulate cortex in rats with optogenetically induced trigeminal neuropathy attenuates pain-associated behaviors and inhibits the pathologic activity of thalamic sensory neurons [24]. However, experiments involving deafferentation pain models demonstrate that the analgesic effect of direct current stimulation of the motor cortex is associated with the activation of the anterior cingulate cortex [25]. Despite controversial data on the possible association between the activity of the anterior cingulate cortex and pain, it is clear that modulation of this brain region may be associated with a change in the intensity of pain, primarily due to its involvement in the affective processing of pain inputs.

Another correlation discovered in this study is between GM volume and the functional connectivity of striatum structures, including the putamen and the caudate nucleus, and the rTMS effect. This finding is supported by the results of other experimental works, including a PET-based study in macaques in which rTMS of the primary motor cortex led to an increase in extracellular dopamine concentrations in the ventral striatum

and a decline in dopamine levels in the putamen [26]. In turn, the effect of rTMS on dopaminergic neurotransmission is hypothesized to underly the analgesic effect of this modality [7].

Interestingly, we established an association between GM volume in cerebellar structures and the response to rTMS. A PET-based experimental study revealed reduced functional connectivity between the cerebellum and some prefrontal brain regions in animals with neuropathic pain [27]. The role of the cerebellum in the processing of pain inputs and development of chronic pain was confirmed by a number of studies. Specifically, it was reported that signals from primary nociceptive afferent nociceptors are transmitted to cerebellar structures [28], cerebellar structures were activated following modeling of acute and chronic pain [29], and the current stimulation of the cerebellum modulated the processing of pain inputs [30]. Besides, GM volume was reduced in the cerebellar structures of patients with TN [17, 20].

Brain areas identified in our study coincide with brain areas where changes had been previously associated not only with TN, but also with other types of chronic pain [31]. This may indicate that imaging biomarkers of rTMS response bear connection to perception, integration and processing of pain inputs, as well as mechanisms implicated in the development of chronic pain, but are not associate with a particular disease, which is confirmed by the efficacy of rTMS against a variety of chronic pains [32].

The optimization of treatment choice for expediting recovery, minimizing adverse effects and reducing therapy-associated costs is one of priority tasks facing the research community. Methods of patient selection based on neuroimaging data are being intensively developed in psychiatry: there are ongoing studies of biomarkers of response to pharmacotherapy, psychotherapy, rTMS [12; 33]. This approach holds promise for other nosologies. Our findings may create a premise for developing neuroimaging predictors of response to rTMS in patients with chronic pain and confirm the feasibility of this approach in the context of noninvasive brain stimulation.

Study limitations

The first limitation is the absence of multiple comparisons correction for the number of areas of interest. Because of that, the established correlations indicate the areas of the brain with the highest probability of finding the effects and require verification in further studies. Second, our sample size was quite small and thus was a constraint for the generalization of the obtained results. Finally, we had no control group and therefore cannot assert that the identified biomarkers are absolutely specific for active, non-placebo rTMS. However, previous controlled studies provided compelling evidence on the advantage of active rTMS effects over placebo in patients with TN [8], and the proportion of responsive individuals in our study was consistent with previously reported data [4].

CONCLUSIONS

Our study was the first to identify structural and functional biomarkers that are the most likely predictors of the analgesic effect of navigated transcranial magnetic stimulation therapy in patients with TN. We have established a few positive and negative correlations between the response to rTMS and the functional connectivity of the thalamus, the postcentral gyrus, the insular operculum, the anterior cingulate cortex and other regions, as well as between the response to rTMS and GM volume in caudate nuclei, the postcentral gyrus and the cerebellum. Our findings may create a premise for developing individual predictors of rTMS effect and tailoring noninvasive brain stimulation methods to individual patients with chronic pain.

References

1. De Toledo IP, Conti Réus J, Fernandes M, Porporatti AL, Peres MA, Takaschima A, et al. Prevalence of trigeminal neuralgia: A systematic review. J Am Dent Assoc. 2016; 147 (7): 570–6.e2.

2. Bendtsen L, Zakrzewska JM, Abbott J, Braschinsky M, Di Stefano G, Donnet A, et al. European Academy of Neurology guideline on trigeminal neuralgia. Eur J Neurol. 2019; 26 (6): 831–49.

3. Tomasello F, Esposito F, Abbritti RV, Angileri FF, Conti A, Cardali SM, et al. Microvascular Decompression for Trigeminal Neuralgia: Technical Refinement for Complication Avoidance. World Neurosurg. 2016; 94: 26–31.

4. Lefaucheur JP, Aleman A, Baeken C, Benninger DH, Brunelin J, Di Lazzaro V, et al. Evidence-based guidelines on the therapeutic use of repetitive transcranial magnetic stimulation (rTMS): An update (2014–2018). Clin Neurophysiol. 2020; 131 (2): 474–528.

5. Khokhlova TYu, Stepanchenko AV, Mamedov TR, Grigoreva SE, Zhikhoreva EA. ranskranial`naya magnitnaya stimulyaciya — sovremenny`j metod lecheniya obostreniya nevralgii trojnichnogo nerva. Nejrodiagnostika i vy`sokie biomedicinskie texnologii. 2007; (3): 32–38. Russian.

6. Terranova C, Rizzo V, Cacciola A, Chillemi G, Calamuneri A, Milardi D, et al. Is There a Future for Non-invasive Brain Stimulation as a Therapeutic Tool? Front Neurol. 2019; 9: 1146.

7. DosSantos MF, Oliveira AT, Ferreira NR, Carvalho ACP, Rosado de Castro PH. The Contribution of Endogenous Modulatory Systems to TMS- and tDCS-Induced Analgesia: Evidence from PET Studies. Pain Res Manag. 2018; 2018: 2368386.

8. Herrero Babiloni A, Guay S, Nixdorf DR, de Beaumont L, Lavigne G. Non-invasive brain stimulation in chronic orofacial pain: a systematic review. J Pain Res. 2018; 11: 1445–57.

9. Ayache SS, Ahdab R, Chalah MA, Farhat WH, Mylius V, Goujon C, et al. Analgesic effects of navigated motor cortex rTMS in patients with chronic neuropathic pain. Eur J Pain. 2016; 20 (9): 1413–22.

10. Guerra A, López-Alonso V, Cheeran B, Suppa A. Variability in non-invasive brain stimulation studies: Reasons and results. Neurosci Lett. 2020; 719: 133330.

11. Kar SK. Predictors of Response to Repetitive Transcranial Magnetic Stimulation in Depression: A Review of Recent Updates. Clin Psychopharmacol Neurosci. 2019; 17 (1): 25–33.

12. Drysdale AT, Grosenick L, Downar J, Dunlop K, Mansouri F, Meng Y, et al. Resting-state connectivity biomarkers define neurophysiological subtypes of depression. Nat Med. 2017; 23 (1): 28–38.

13. Ge R, Downar J, Blumberger DM, Daskalakis ZJ, Vila-Rodriguez F. Functional connectivity of the anterior cingulate cortex predicts treatment outcome for rTMS in treatment-resistant depression at 3-month follow-up. Brain Stimul. 2020; 13 (1): 206–14.

14. Furtado CP, Hoy KE, Maller JJ, Savage G, Daskalakis ZJ, Fitzgerald PB. An investigation of medial temporal lobe changes and cognition following antidepressant response: a prospective rTMS study. Brain Stimul. 2013; 6 (3): 346–54.

15. Poeppl TB, Langguth B, Lehner A, Frodl T, Rupprecht R, Kreuzer PM, et al. Brain stimulation-induced neuroplasticity underlying therapeutic response in phantom sounds. Hum Brain Mapp. 2018 Jan; 39 (1): 554–62.

16. Ashburner J. A fast diffeomorphic image registration algorithm. NeuroImage. 2007; 38(1): 95–113.

17. Henssen D, Dijk J, Knepflé R, Sieffers M, Winter A, Vissers K. Alterations in grey matter density and functional connectivity in trigeminal neuropathic pain and trigeminal neuralgia: A systematic review and meta-analysis. Neuroimage Clin. 2019; 24: 102039.

18. Ocklenburg S, Friedrich P, Güntürkün O, Genç E. Voxel-wise grey matter asymmetry analysis in left- and right-handers. Neurosci Lett. 2016; 633: 210–4.

19. Liang X, Zhao C, Jin X, Jiang Y, Yang L, Chen Y, et al. Sex-related human brain asymmetry in hemispheric functional gradients. Neuroimage. 2021; 229: 117761.

20. Obermann M, Rodriguez-Raecke R, Naegel S, Holle D, Mueller D, Yoon MS, et al. Gray matter volume reduction reflects chronic pain in trigeminal neuralgia. Neuroimage. 2013; 74: 352–8.

21. Lovo EE, Torres B, Campos F, Caceros V, Reyes WA, Barahona KC, et al. Stereotactic Gamma Ray Radiosurgery to the Centromedian and Parafascicular Complex of the Thalamus for Trigeminal Neuralgia and Other Complex Pain Syndromes. Cureus. 2019; 11 (12): e6421.

22. Henssen D, Giesen E, van der Heiden M, Kerperien M, Lange S, van Cappellen van Walsum AM, et al. A systematic review of the proposed mechanisms underpinning pain relief by primary motor cortex stimulation in animals. Neurosci Lett. 2020; 719: 134489.

23. Xiao X, Zhang YQ. A new perspective on the anterior cingulate cortex and affective pain. Neurosci Biobehav Rev. 2018; 90: 200–11.

24. Moon HC, Heo WI, Kim YJ, Lee D, Won SY, Kim HR, et al. Optical inactivation of the anterior cingulate cortex modulate descending pain pathway in a rat model of trigeminal neuropathic pain created via chronic constriction injury of the infraorbital nerve. J Pain Res. 2017; 10: 2355–64.

25. Kudo K, Takahashi T, Suzuki S. The changes of c-Fos expression by motor cortex stimulation in the deafferentation pain model. Neurol Med Chir (Tokyo). 2014; 54 (7): 537–44.

26. Ohnishi T, Hayashi T, Okabe S, Nonaka I, Matsuda H, Iida H, et al. Endogenous dopamine release induced by repetitive transcranial magnetic stimulation over the primary motor cortex: an [11C] raclopride positron emission tomography study in anesthetized macaque monkeys. Biol Psychiatry. 2004; 55 (5): 484–9.

27. Kim CE, Kim YK, Chung G, Jeong JM, Lee DS, Kim J, et al. Large-scale plastic changes of the brain network in an animal model of neuropathic pain. Neuroimage. 2014; 98: 203–15.

28. Cerminara NL, Koutsikou S, Lumb BM, Apps R. The periaqueductal grey modulates sensory input to the cerebellum: a role in coping behaviour? Eur J Neurosci. 2009; 29: 2197–206.

29. Helmchen C, Mohr C, Erdmann C, Petersen D, Nitschke MF. Differential cerebellar activation related to perceived pain intensity during noxious thermal stimulation in humans: a functional magnetic resonance imaging study. Neurosci Lett. 2003; 335: 202–6.

30. Moulton EA, Schmahmann JD, Becerra L, Borsook D. The cerebellum and pain: passive integrator or active participator? Brain Res Rev. 2010 Oct 5; 65 (1): 14–27.

31. Yang S, Chang MC. Chronic Pain: Structural and Functional Changes in Brain Structures and Associated Negative Affective States. Int J Mol Sci. 2019; 20 (13): 3130.

32. Hamid P, Malik BH, Hussain ML. Noninvasive Transcranial Magnetic Stimulation (TMS) in Chronic Refractory Pain: A Systematic Review. Cureus. 2019; 11 (10): e6019.

33. Fonseka TM, MacQueen GM, Kennedy SH. Neuroimaging biomarkers as predictors of treatment outcome in Major Depressive Disorder. J Affect Disord. 2018; 233: 21–35.

Литература

1. De Toledo IP, Conti Réus J, Fernandes M, Porporatti AL, Peres MA, Takaschima A, et al. Prevalence of trigeminal neuralgia: A systematic review. J Am Dent Assoc. 2016; 147 (7): 570–6.e2.

2. Bendtsen L, Zakrzewska JM, Abbott J, Braschinsky M, Di Stefano G, Donnet A, et al. European Academy of Neurology guideline on trigeminal neuralgia. Eur J Neurol. 2019; 26 (6): 831–49.

3. Tomasello F, Esposito F, Abbritti RV, Angileri FF, Conti A, Cardali SM, et al. Microvascular Decompression for Trigeminal Neuralgia: Technical Refinement for Complication Avoidance. World Neurosurg. 2016; 94: 26–31.

4. Lefaucheur JP, Aleman A, Baeken C, Benninger DH, Brunelin J, Di Lazzaro V, et al. Evidence-based guidelines on the therapeutic use of repetitive transcranial magnetic stimulation (rTMS): An update (2014–2018). Clin Neurophysiol. 2020; 131 (2): 474–528.

5. Хохлова Т. Ю., Степанченко А. В., Мамедов Т. Р., Григорьева С. Е., Жихорева Е. А. Транскраниальная магнитная стимуляция — современный метод лечения обострения невралгии тройничного нерва. Нейродиагностика и высокие биомедицинские технологии. 2007; (3): 32–38.

6. Terranova C, Rizzo V, Cacciola A, Chillemi G, Calamuneri A, Milardi D, et al. Is There a Future for Non-invasive Brain Stimulation as a Therapeutic Tool? Front Neurol. 2019; 9: 1146.

7. DosSantos MF, Oliveira AT, Ferreira NR, Carvalho ACP, Rosado de Castro PH. The Contribution of Endogenous Modulatory Systems to TMS- and tDCS-Induced Analgesia: Evidence from PET Studies. Pain Res Manag. 2018; 2018: 2368386.

8. Herrero Babiloni A, Guay S, Nixdorf DR, de Beaumont L, Lavigne G. Non-invasive brain stimulation in chronic orofacial pain: a systematic review. J Pain Res. 2018; 11: 1445–57.

9. Ayache SS, Ahdab R, Chalah MA, Farhat WH, Mylius V, Goujon C, et al. Analgesic effects of navigated motor cortex rTMS in patients with chronic neuropathic pain. Eur J Pain. 2016; 20 (9): 1413–22.

10. Guerra A, López-Alonso V, Cheeran B, Suppa A. Variability in non-invasive brain stimulation studies: Reasons and results. Neurosci Lett. 2020; 719: 133330.

11. Kar SK. Predictors of Response to Repetitive Transcranial Magnetic Stimulation in Depression: A Review of Recent Updates. Clin Psychopharmacol Neurosci. 2019; 17 (1): 25–33.

12. Drysdale AT, Grosenick L, Downar J, Dunlop K, Mansouri F, Meng Y, et al. Resting-state connectivity biomarkers define neurophysiological subtypes of depression. Nat Med. 2017; 23 (1): 28–38.

13. Ge R, Downar J, Blumberger DM, Daskalakis ZJ, Vila-Rodriguez F. Functional connectivity of the anterior cingulate cortex predicts treatment outcome for rTMS in treatment-resistant depression at 3-month follow-up. Brain Stimul. 2020; 13 (1): 206–14.

14. Furtado CP, Hoy KE, Maller JJ, Savage G, Daskalakis ZJ, Fitzgerald PB. An investigation of medial temporal lobe changes and cognition following antidepressant response: a prospective rTMS study. Brain Stimul. 2013; 6 (3): 346–54.

15. Poeppl TB, Langguth B, Lehner A, Frodl T, Rupprecht R, Kreuzer PM, et al. Brain stimulation-induced neuroplasticity underlying therapeutic response in phantom sounds. Hum Brain Mapp. 2018 Jan; 39 (1): 554–62.

16. Ashburner J. A fast diffeomorphic image registration algorithm. NeuroImage. 2007; 38(1): 95–113.

17. Henssen D, Dijk J, Knepflé R, Sieffers M, Winter A, Vissers K. Alterations in grey matter density and functional connectivity in trigeminal neuropathic pain and trigeminal neuralgia: A systematic review and meta-analysis. Neuroimage Clin. 2019; 24: 102039.

18. Ocklenburg S, Friedrich P, Güntürkün O, Genç E. Voxel-wise grey matter asymmetry analysis in left- and right-handers. Neurosci Lett. 2016; 633: 210–4.

19. Liang X, Zhao C, Jin X, Jiang Y, Yang L, Chen Y, et al. Sex-related human brain asymmetry in hemispheric functional gradients. Neuroimage. 2021; 229: 117761.

20. Obermann M, Rodriguez-Raecke R, Naegel S, Holle D, Mueller D, Yoon MS, et al. Gray matter volume reduction reflects chronic pain in trigeminal neuralgia. Neuroimage. 2013; 74: 352–8.

21. Lovo EE, Torres B, Campos F, Caceros V, Reyes WA, Barahona KC, et al. Stereotactic Gamma Ray Radiosurgery to the Centromedian and Parafascicular Complex of the Thalamus for Trigeminal Neuralgia and Other Complex Pain Syndromes. Cureus. 2019; 11 (12): e6421.

22. Henssen D, Giesen E, van der Heiden M, Kerperien M, Lange S, van Cappellen van Walsum AM, et al. A systematic review of the

proposed mechanisms underpinning pain relief by primary motor cortex stimulation in animals. Neurosci Lett. 2020; 719: 134489.

23. Xiao X, Zhang YQ. A new perspective on the anterior cingulate cortex and affective pain. Neurosci Biobehav Rev. 2018; 90: 200–11.

24. Moon HC, Heo WI, Kim YJ, Lee D, Won SY, Kim HR, et al. Optical inactivation of the anterior cingulate cortex modulate descending pain pathway in a rat model of trigeminal neuropathic pain created via chronic constriction injury of the infraorbital nerve. J Pain Res. 2017; 10: 2355–64.

25. Kudo K, Takahashi T, Suzuki S. The changes of c-Fos expression by motor cortex stimulation in the deafferentation pain model. Neurol Med Chir (Tokyo). 2014; 54 (7): 537–44.

26. Ohnishi T, Hayashi T, Okabe S, Nonaka I, Matsuda H, Iida H, et al. Endogenous dopamine release induced by repetitive transcranial magnetic stimulation over the primary motor cortex: an [11C] raclopride positron emission tomography study in anesthetized macaque monkeys. Biol Psychiatry. 2004; 55 (5): 484–9.

27. Kim CE, Kim YK, Chung G, Jeong JM, Lee DS, Kim J, et al. Large-scale plastic changes of the brain network in an animal model of neuropathic pain. Neuroimage. 2014; 98: 203–15.

28. Cerminara NL, Koutsikou S, Lumb BM, Apps R. The periaqueductal grey modulates sensory input to the cerebellum: a role in coping behaviour? Eur J Neurosci. 2009; 29: 2197–206.

29. Helmchen C, Mohr C, Erdmann C, Petersen D, Nitschke MF. Differential cerebellar activation related to perceived pain intensity during noxious thermal stimulation in humans: a functional magnetic resonance imaging study. Neurosci Lett. 2003; 335: 202–6.

30. Moulton EA, Schmahmann JD, Becerra L, Borsook D. The cerebellum and pain: passive integrator or active participator? Brain Res Rev. 2010 Oct 5; 65 (1): 14–27.

31. Yang S, Chang MC. Chronic Pain: Structural and Functional Changes in Brain Structures and Associated Negative Affective States. Int J Mol Sci. 2019; 20 (13): 3130.

32. Hamid P, Malik BH, Hussain ML. Noninvasive Transcranial Magnetic Stimulation (TMS) in Chronic Refractory Pain: A Systematic Review. Cureus. 2019; 11 (10): e6019.

33. Fonseka TM, MacQueen GM, Kennedy SH. Neuroimaging biomarkers as predictors of treatment outcome in Major Depressive Disorder. J Affect Disord. 2018; 233: 21–35.

CDKN2B-AS1 GENE POLYMORPHISM IS ASSOCIATED WITH PRIMARY OPEN-ANGLE GLAUCOMA IN WOMEN OF THE CENTRAL BLACK EARTH REGION, RUSSIA

Eliseeva NV, Ponomarenko IV, Churnosov MI ✉

Belgorod State University, Belgorod, Russia

Primary open-angle glaucoma (POAG) is a complex disorder. Genetic factors play a vital part in POAG. The prevalence of POAG is gender-specific: the disorder is more often diagnosed in women. Results of the genome-wide association studies (GWAS) strongly support the association of *CDKN2B-AS1* gene polymorphism with POAG. The aim was to perform the replicative study of *CDKN2B-AS1* gene polymorphic loci association with POAG in women of the Central Black Earth Region, Russia. Five *CDKN2B-AS1* gene single nucleotide polymorphisms (SNP), rs1063192, rs7865618, rs2157719, rs944800, and rs4977756, were genotyped in 290 female patients with POAG and 220 female controls. The differences in the haplotype block structure between the POAG patients (no haplotype blocks) and the controls (haplotype block consisting of three SNPs, rs1063192, rs7865618 and rs2157719, was detected) for the set of studied *CDKN2B-AS1* SNPs were revealed using the Solid Spine algorithm ($D' > 0.8$). *CDKN2B-AS1* gene haplotype GGG rs1063192–rs7865618–rs2157719 is associated with POAG in women. This haplotype is considered a protective factor of the disorder (OR = 0.66; $p = 0.006$, $p_{perm} = 0.037$).

Keywords: primary open-angle glaucoma, *CDKN2B-AS1*, polymorphism, associations, women

✉ **Correspondence should be addressed:** Mikhail I. Churnosov
Pobedy St., 85, Belgorod, 308015; churnosov@bsu.edu.ru

ПОЛИМОРФИЗМ ГЕНА *CDKN2B-AS1* АССОЦИИРОВАН С ПЕРВИЧНОЙ ОТКРЫТОУГОЛЬНОЙ ГЛАУКОМОЙ У ЖЕНЩИН ЦЕНТРАЛЬНОГО ЧЕРНОЗЕМЬЯ РОССИИ

Н. В. Елисеева, И. В. Пономаренко, М. И. Чурносов ✉

Белгородский государственный национальный исследовательский университет, Белгород, Россия

Первичная открытоугольная глаукома (ПОУГ) — это многофакторное заболевание, в развитии которого значимую роль играют наследственные факторы. Распространенность ПОУГ имеет гендерные особенности — заболевание чаще выявляют у женщин. Результаты полногеномных исследований (GWAS) свидетельствуют в пользу ассоциации полиморфизма гена *CDKN2B-AS1* с ПОУГ. Целью исследования было репликативное изучение ассоциаций полиморфных локусов гена *CDKN2B-AS1* с ПОУГ у женщин Центрального Черноземья России. У 290 пациенток с ПОУГ и 220 женщин контрольной группы было выполнено генотипирование пяти однонуклеотидных полиморфизмов (SNP) гена *CDKN2B-AS1* — rs1063192, rs7865618, rs2157719, rs944800 и rs4977756. При использовании алгоритма «Solid Spine» (заданный порог $D' > 0,8$) были выявлены различия в структуре блоков сцепления по исследуемым пяти SNP гена *CDKN2B-AS1* между больными ПОУГ (блоки сцепления отсутствовали) и контролем (установлен блок сцепления, состоящий из трех SNP — rs1063192, rs7865618 и rs2157719). У женщин гаплотип GGG rs1063192–rs7865618–rs2157719 гена *CDKN2B-AS1* ассоциирован с ПОУГ — он является протективным фактором развития заболевания (ОШ = 0,66; $p = 0,006$, $p_{perm} = 0,037$).

Ключевые слова: первичная открытоугольная глаукома, CDKN2B-AS1, полиморфизм, ассоциации, женщины

✉ **Для корреспонденции:** Михаил Иванович Чурносов
ул. Победы, д. 85, г. Белгород, 308015; churnosov@bsu.edu.ru

Glaucoma is a disorder characterized by chronic, progressive optic neuropathy associated with changes in optic nerve head and retinal nerve fiber morphology, which are not attributed to other eye disorders or congenital malformations [1]. Primary open angle glaucoma (POAG) is one the most common forms of glaucoma [2]. The data on the stable sustained incidence rate growth, chronic disease with progressive vision impairment, resulting ultimately in the loss of working ability and disability, demonstrate the sociomedical significance of glaucoma [1]. It should be noted that in the vast majority of cases POAG is diagnosed in patients aged 60–69, commonly having systemic comorbidities. The disorder is almost 1.5 times more often diagnosed in women [1–3].

Genetic factors play a significant role in POAG [4]. Molecular genetic data received to date suggest the involvement of a number of candidate gene polymorphisms in POAG [4–6]. Several genome-wide studies (GWAS) of POAG revealed associations of *CDKN2B-AS1* polymorphic loci with the disorder [7–12].

CDKN2B-AS1 gene is located within the chromosome 9p21 *CDKN2B– CDKN2A* gene cluster. *CDKN2B-AS1* belongs to the group of genes responsible for regulation of the long non-coding RNA (lncRNA) synthesis [13]. lncRNA encoded by the gene interacts with polycomb repressive complex-1 (PRC1) and -2 (PRC2), which results in significant epigenetic alterations (histone methylation and monoubiquitination, etc.). This, in

turn, results in significant structural changes of chromatin and directly affects the expression of genes [13]. It should be noted that GWAS data on POAG require replicative studies in various populations, such as Russian population, which have not been subject to replicative studies to date.

The study was aimed to assess the association of the *CDKN2B-AS1* gene single nucleotide polymorphism (SNP) with POAG in women of the Central Black Earth Region, Russia.

METHODS

The sample included 290 female patients with POAG and 220 female controls. Inclusion criteria: Russian ethnicity, place of birth and residence — Central Black Earth Region of Russia [14]. Exclusion criteria: non-Russian ethnicity, place of birth and/or residence — outside the Central Black Earth Region of Russia.

The group of patients included individuals diagnosed with POAG, their diagnosis was verified based on the clinical and instrumental examination data. POAG was diagnosed based on the following criteria [6]: elevated intraocular pressure (IOP over 21 when measured by pneumotonometry, and over 25 when measured by Maklakov tonometry), glaucomatous optic nerve excavation, characteristic changes in the peripheral visual field. The control group included individuals having no POAG (IOP below 21 when measured by pneumotonometry, and below 25 when measured by Maklakov tonometry, no glaucomatous optic nerve excavation and characteristic changes in the peripheral visual field), other eye disorder or severe somatic comorbid condition associated with ocular lesion.

The group of POAG patients and the control group were comparable in terms of age, body mass index (BMI) and somatic comorbidity rate ($p > 0.05$) (Table 1). Ophthalmic examination was carried out in the specialized department of the St. Ioasaph Belgorod Regional Clinical Hospital.

Genomic DNA obtained from peripheral venous blood with phenol–chloroform extraction was subject to genetic analysis [15]. *CDKN2B-AS1* gene single nucleotide polymorphism was selected for analysis based on the following criteria [16]: 1) association with POAG according to previous genome-wide studies; 2) significant regulatory potential; 3) minor allele frequency of 5% or greater.

SNPs were selected for analysis using the catalog of human genome-wide association studies (GWAS Catalog) [17] and the HaploReg database [18]. Five *CDKN2B-AS1* gene SNPs were included in the study: rs1063192, rs7865618, rs2157719, rs944800, and rs4977756. All five SNPs were associated with POAG based on the previous GWAS data [7–12], had

a significant regulatory potential (rs7865618, rs2157719, rs944800 are located within the region of histone modifications defined as enhancer marks; rs1063192, rs2157719, rs944800, rs4977756 are located within the DNase I hypersensitive sites; rs1063192, rs2157719, rs944800 are located within the region of various transcription factors regulatory DNA elements), and their minor allele frequency exceeded 5%.

DNA samples were genotyped with the CFX96 Real-Time PCR detection system (Bio-Rad; USA) using the TaqMan probes and the tailor-made kits (TestGene; Russia).

Associations of polymorphic loci with POAG were assessed using logistic regression analysis within the framework of allele (for rs1063192, rs7865618, rs2157719, and rs4977756 polymorphisms alleles G vs. A with a minor allele G were analyzed, and for rs944800 locus it was A vs. G with a minor allele A), dominant (for rs1063192, rs7865618, rs2157719, rs4977756 polymorphisms G/G + A/G vs. A/A were analyzed; for rs944800 A/A + G/A vs. G/G were analyzed), additive (G/G vs. A/G (G/A) vs. A/A) and recessive (for rs1063192, rs7865618, rs2157719, rs4977756 polymorphisms G/G vs. A/G + A/A were analyzed; for rs944800 A/A vs. G/A + G/G were analyzed) genetic models using the plink 1.06 software [19], the data were adjusted for covariate (age). Associations were evaluated using odds ratio (OR) and 95% confidence interval (95% CI). Permutation testing was applied to adjust the results for multiple comparisons. P_{perm} value < 0.05 was considered statistically significant.

Lewontin's standardized disequilibrium coefficient (D') and Pearson correlation coefficient (r^2) were used for assessment of linkage disequilibrium and haplotype block identification between five *CDKN2B-AS1* gene SNPs. Haplotype blocks were analyzed with the Haploview v.4.2 software [20] using the Solid Spine algorithm with $D' > 0.8$. Visualization of linkage disequilibrium between studied *CDKN2B-AS1* SNPs was performed using the Haploview v. 4.2 software. Haplotype frequencies were estimated using the EM algorithm. Associations of haplotypes with POAG were assessed using logistic regression analysis (plink 1.06 software), the data were adjusted for covariate (age) and for multiple comparisons (permutation testing was applied — 1000 permutations). Evaluation of haplotype association with the disorder was performed using odds ratio (OR). P_{perm} value < 0.05 was considered statistically significant [21].

RESULTS

Population genetic analysis showed that distribution of all five *CDKN2B-AS1* SNP genotypes in POAG patients and controls satisfied the Hardy–Weinberg equilibrium ($p_{HWE} > 0.05$) (Table 2).

Table 1. Biomedical and clinical anamnestic characteristics of the studied groups

Parameters	Patients	Controls	p
	(*n* = 290)	(*n* = 220)	
Age, years	62.24 ± 11.45	61.78 ± 11.06	0.45
BMI, kg/m^2	28.72 ± 5.19	28.57 ± 5.49	0.76
Somatic comorbidities, % (*n*)			
Cardiovascular system	80.69 (234)	74.55 (164)	0.12
Endocrine system	20.34 (59)	15.91 (35)	0.24
Gastrointestinal tract	14.14 (41)	12.73 (28)	0.74
Urinary tract	7.58 (22)	7.27 (16)	0.99
Respiratory tract	6.55 (19)	5.45 (12)	0.74
Nervous system	18.28 (53)	17.27 (38)	0.86
Other	3.45 (10)	3.18 (7)	1

No significant associations of studied polymorphic *CDKN2B-AS1* loci with POAG were revealed in women (Table 3).

Analysis of linkage disequilibrium between five studied *CDKN2B-AS1* gene polymorphisms using the Solid Spine algorithm ($D' > 0.8$) revealed no haplotype blocks in women with POAG. However, a haplotype block comprising three polymorphisms, rs1063192, rs7865618, and rs2157719, was identified in controls (see Figure). Furthermore, information reported in Figure indicates the existence of recombination hotspot between loci rs2157719 and rs944800 with quite low degree of genetic linkage between rs944800 and rs4977756, as well as high degree of linkage between locus rs4977756 and three polymorphisms (rs1063192, rs7865618 and rs2157719), in the control group. Furthermore, while in the control group there is a zone with D' value about 0.4 (see above), then among patients the D' value for all studied polymorphisms is about 0.6–0.7.

Association of GGG haplotype of the identified *CDKN2B-AS1* haplotype block rs1063192–rs7865618–rs2157719 with POAG in women was defined. The OR value calculated for this haplotype was 0.66 ($p = 0.006$ and $p_{perm} = 0.037$), which demonstrated the protective effect of the haplotype against the disorder in women (Table 4). Association of AGA haplotype with POAG (OR = 5.12; $p = 0.009$) did not reach statistical significance based on the permutation testing results ($p_{perm} = 0.06$).

DISCUSSION

Comparison of patients with POAG and female controls based on five *CDKN2B-AS1* gene SNPs revealed the differences in linkage disequilibrium between the studied loci (low degree on genetic linkage between distinct loci in the control group with a D' value of about 0.4, and almost "uniform" linkage of all studied loci in the group of patients with a D' value about 0.6–0.7), and the related differences in haplotype block structure (when using the Solid Spine algorithm with $D' > 0.8$, no haplotype blocks were identified in POAG patients, however, in female controls, haplotype block comprising three SNPs, rs1063192, rs7865618 and rs2157719, was identified). Association of GGG haplotype of *CDKN2B-AS1* gene rs1063192–rs7865618–rs2157719 with POAG in women (OR = 0.66) together with no significant independent associations of five studied *CDKN2B-AS1* gene SNPs with the disorder were detected.

It is believed that linkage disequilibrium patterns in modern populations are the result of evolution, which reflects both the demographic history of the population (migration, population subdivision, etc.), and the gene-specific factors, related to mutation and recombination rates, selection, etc. [22]. Despite the fact that the use of LD structure for studying the complex human disorders is limited by the population specificity [22], it is believed that the use of haplotypes for association studies instead of distinct SNPs makes it possible to significantly improve the statistical power of the study, especially where the disease susceptibility loci are not analyzed directly, or in case of high degree multilocus linkage disequilibrium [22, 23]. Genetic distance between the studied loci and the "causative" mutation, as well as allele frequency and the "causative" mutation age, has a direct impact on the haplotype testing efficiency [22].

Regardless of the fact that no obvious "causative" mutations for POAG (for example, nonsense mutations or mutations associated with amino acid substitution) have been detected within the chromosomal region comprising the studied *CDKN2B-AS1* gene SNPs to date, a number of papers report high functional significance of polymorphic loci located within the region (effect on the expression of *CDKN2A*, *CDKN2B*, etc.) [8, 12].

Linkage disequilibrium features detected and related features of haplotype block identification between five studied *CDKN2B-AS1* SNPs in the control group may be just a "particular case" of haplotype structure at the "local scale" of

Table 2. Distribution of *CDKN2B-AS1* gene polymorphic loci in POAG patients and female controls

Polimorfism	Rare allele	Frequent allele	Rare allele frequency	Number of studied chromosomes	Genotype distribution, proportion (%) (homozygous for a rare allele/ heterozygous/homozygous for a frequent allele)	Observed heterozygosity	Expected heterozygosity	Significance level for deviations from Hardy–Weinberg equilibrium (p_{HWE})
POAG patients ($n = 290$)								
rs1063192	G	A	0.423	568	53/134/97 (18.66/47.18/34.16)	0.472	0.488	0.627
rs7865618	G	A	0.417	566	52/132/99 (18.38/46.64/34.98)	0.466	0.486	0.541
rs2157719	G	A	0.385	564	45/127/110 (15.96/45.03/39.01)	0.450	0.473	0.450
rs944800	A	G	0.338	574	32/130/125 (11.15/45.30/43.55)	0.453	0.448	0.896
rs4977756	G	A	0.476	572	61/150/75 (21.33/52.45/26.22)	0.525	0.499	0.409
Control group ($n = 220$)								
rs1063192	G	A	0.46	424	43/109/60 (20.28/51.42/28.30)	0.514	0.497	0.679
rs7865618	G	A	0.463	436	47/108/63 (21.56/49.54/28.90)	0.495	0.497	1.000
rs2157719	G	A	0.429	438	41/106/72 (18.72/48.40/32.88)	0.484	0.490	0.890
rs944800	A	G	0.368	440	28/106/86 (12.73/48.18/39.09)	0.482	0.465	0.665
rs4977756	G	A	0.459	438	46/109/64 (21.01/49.77/29.22)	0.498	0.497	1.000

these five loci. As the number of studied loci increases, the overall picture of linkage disequilibrium between multiple loci of this particular chromosomal region is amenable to significant changes (recombination hotspots between distinct loci may be detected in the group of patients as well, the regions of more tight linkage may be revealed in the control group, etc.); in general, at a scale of much larger number of studied loci (compared to five SNPs analyzed during our study) the linkage disequilibrium structure in POAG patients and controls would be similar. Thus, the study [24] aimed to assess linkage disequilibrium and haplotype blocks (the authors used Solid Spine algorithm with D'≥0.75) between 12 *MTHFR* gene SNPs in patients with coronary atherosclerosis and controls revealed three haplotype blocks in patients and two haplotype blocks in the control group. Moreover, the tighter linkage in the *MTHFR* gene 5' region was shown in patients compared to controls. Regardless of the listed above distinct "details" the authors judged about the similarity of LD patterns in the group of patients with coronary atherosclerosis and the control group based on the overall picture of linkage disequilibrium between 12 *MTHFR* gene SNPs (there were similar recombination hotspots, similar haplotype block were detected within the *MTHFR* gene 3' region).

It should be noted that our data on the types of association (genetic risk factor or protective factor) for individual alleles

comprising the glaucoma haplotype (haplotype GGG of *CDKN2B-AS1* gene rs1063192–rs7865618–rs2157719 is considered a protective factor for the development of POAG in women, OR = 0.66) are consistent with literature data on the issue. According to the genome-wide study [25], the minor allele G rs1063192 is associated with smaller optic nerve vertical cup-to-disc ratio ($\beta = -0.014$ mm^2; $p = 6 \times 10^{-11}$) in the European population (the increased optic nerve vertical cup-to-disc ratio is one of the glaucomatous optic neuropathy symptoms [26]); according to GWAS [9] (performed in Japanese population), minor allele G rs1063192 is also a protective factor for POAG (OR = 0.75; $p = 5 \times 10^{-11}$). Low risk of open-angle glaucoma in individuals (European population) having G rs1063192 in their genotype (both homozygous, OR = 0.76, and heterozygous, OR = 0.85) has been also reported in [27]. Association of allele G rs1063192 with smaller optic nerve vertical cup-to-disc ratio and together with protective effect of the allele against POAG in the European population (OR 0.73) have been reported in [26]. Protective effect of allele G rs1063192 against POAG and other types of glaucoma in the European and Asian populations has been also confirmed by meta-analysis [28]. Thus, our data supporting the protective effect of *CDKN2B-AS1* gene allele G rs1063192 (as a part of GGG haplotype of haplotype block rs1063192–rs7865618–rs2157719) against the disorder in women of the Central

Table 3. Association of *CDKN2B-AS1* gene polymorphism with POAG in women

Loci	Alleles, genotypes	Patients, n (%)	Controls, n (%)	OR (95% CI)	p
rs1063192	Sample size	284	212		
	G vs. A (allele model)	240/328 (42.25/57.75)	195/229 (45.99/54.01)	0.86 (0.67–1.11)	0.24
	G/G vs. A/G vs. A/A (additive model)	53/134/97 (18.66/47.18/34.16)	43/109/60 (20.28/51.42/28.30)	0.82 (0.61–1.10)	0.2
	G/G + A/G vs. A/A (dominant model)	187/97 (65.84/34.16)	152/60 (71.70/28.30)	0.69 (0.44–1.08)	0.1
	G/G vs. A/G + A/A (recessive model)	53/231 (18.66/81.34)	43/169 (20.28/79.72)	0.90 (0.54–1.50)	0.68
rs7865618	Sample size	283	218		
	G vs. A (allele model)	236/330 (41.70/58.30)	202/234 (46.33/53.67)	0.83 (0.64–1.07)	0.14
	G/G vs. A/G vs. A/A (sdditive model)	52/132/99 (18.38/46.64/34.98)	47/108/63 (21.56/49.54/28.90)	0.89 (0.67–1.19)	0.43
	G/G + A/G vs. A/A (dominant model)	184/99 (65.02/34.98)	155/63 (71.10/28.90)	0.74 (0.47–1.15)	0.18
	G/G vs. A/G + A/A (recessive model)	52/231 (18.38/81.62)	47/171 (21.56/78.44)	1.05 (0.63–1.75)	0.85
rs2157719	Sample size	282	219		
	G vs. A (allele model)	217/347 (38.48/61.52)	182/256 (42.92/57.08)	0.83 (0.64–1.07)	0.15
	G/G vs. A/G vs. A/A (additive model)	45/127/110 (15.96/45.03/39.01)	41/106/72 (18.72/48.40/32.88)	0.87 (0.65–1.16)	0.34
	G/G + A/G vs. A/A (dominant model)	172/110 (60.99/39.01)	147/72 (67.12/32.88)	0.74 (0.48–1.16)	0.19
	G/G vs. A/G + A/A (recessive model)	45/237 (15.96/84.04)	41/178 (18.72/81.28)	0.97 (0.56–1.66)	0.91
rs944800	Sample size	287	220		
	A vs. G (allele model)	194/380 (33.80/66.20)	162/278 (36.82/63.18)	0.88 (0.67–1.14)	0.32
	A/A vs. G/A vs. G/G (additive model)	32/130/125 (11.15/45.30/43.55)	28/106/86 (12.73/48.18/39.09)	0.80 (0.59–1.08)	0.15
	A/A + G/A vs. G/G (dominant model)	162/125 (56.45/43.55)	134/86 (60.91/39.09)	0.75 (0.49–1.14)	0.18
	A/A vs. G/A + G/G (recessive model)	32/255 (11.15/88.85)	28/192 (12.73/87.27)	0.74 (0.40–1.37)	0.34
rs4977756	Sample size	286	219		
	G vs. A (allele model)	272/300 (47.55/52.45)	201/237 /(45.89/54.11)	1.07 (0.83–1.37)	0.6
	G/G vs. A/G vs. A/A (additive model)	61/150/75 (21.33/52.45/26.22)	46/109/64 (21.01/49.77/29.22)	1.11 (0.82–1.49)	0.5
	G/G + A/G vs. A/A (dominant model)	211/75 (73.78/26.22)	155/64 (70.78/29.22)	1.22 (0.76–1.93)	0.41
	G/G vs. A/G + A/A (recessive model)	61/225 (21.33/78.67)	46/173 (21.01/78.99)	1.07 (0.64–1.76)	0.81

Note: Results were obtained using the logistic regression model; OR — odds ratio, 95% CI — 95% confidence interval (lower and upper bound of 95% CI); *p* — significance level.

Black Earth Region, Russia (OR = 0.66), are consistent with the data of previous studies.

During the previous studies the following data were obtained for *CDKN2B-AS1* gene allele G rs7865618 being a part of the GGG haplotype of haplotype block rs1063192–rs7865618–rs2157719, which, according to our data, is considered a protective factor of POAG in women of the European Russia (OR = 0.66). According to GWAS [8], allele A rs7865618 increases the risk of POAG in Japanese population (OR = 1.56; $p = 2 \times 10^{-9}$); according to genome-wide studies [29, 30], *CDKN2B-AS1* gene allele G rs7865618 is associated with smaller optic nerve vertical cup-to-disc ratio ($\beta = -0.013$; $p = 3 \times 10^{-20}$ for European population) [29] and smaller area of excavation ($\beta = -0.023$; $p = 1 \times 10^{-21}$ in total for European and Asian populations) [30]. Thus, it is worth noting that our data and the existing literature data on the protective effect of *CDKN2B-AS1* gene allele G rs7865618 against POAG and pathogenetically significant signs of POAG (optic nerve vertical cup-to-disc ratio, area of excavation) fit together.

According to literary sources, *CDKN2B-AS1* gene allele G rs2157719 is associated with low risk of POAG in ethnically diverse populations (in Asian population, in Europeans, and African Americans) [11, 12] and smaller optic nerve vertical cup-to-disc ratio ($\beta = -0,013$; $p = 4 \times 10^{-35}$ in total for European and Asian populations) [30]. These data are consistent with our results: allele G rs2157719 being a part of GGG haplotype of haplotype block rs1063192–rs7865618–rs2157719 is considered a protective factor of POAG in women of the European Russia (OR = 0.66).

Despite the fact that a number of GWAS have shown significant associations of *CDKN2B* gene SNPs with glaucoma and related endophenotypes (optic nerve vertical cup-to-disc ratio, area of excavation) [7–12, 25–30], the results of replicative studies performed in various populations are often uncertain, and, in a number of cases, inconsistent, as meta-analysis [28] has shown (*CDKN2B-AS1* polymorphism rs1063192 was analyzed). A number of studies have confirmed association of *CDKN2B-AS1* gene loci with glaucoma/endophenotypes related to glaucoma (optic nerve vertical cup-to-disc ratio) [26, 28, 31, 32]; other studies have revealed no associations of individual *CDKN2B-AS1* gene SNPs with the disorder (for example, rs1063192 and rs4977756 are not associated with POAG in the Indian population [33], in African Americans [34], and in the Pakistan population [35]). The ambiguity of the results obtained by studying the *CDKN2B-AS1* gene loci association with glaucoma are clearly demonstrated by the paper issued in 2021 [33] on meta-analysis of several *CDKN2B-AS1* gene

SNPs, including rs1063192, rs2157719 and rs4977756, which were used in our study: thus, of 18 association studies included in the meta-analysis (among them six studies of POAG in Caucasians), significant associations of rs1063192 with POAG have been shown only in 10 studies; significant associations of rs2157719 with POAG have been shown in three of five studies subjected to analysis; only four of 12 papers report significant associations of rs4977756 with the disorder. The study [34], which showed significant association with POAG only in one locus of African Americans out of 24 studied loci (the sample included 1150 patients and 999 controls), can be consider another good example of ambiguous data on association of *CDKN2B-AS1* SNPs with glaucoma; none of these 24 SNPs were associated with the disorder in the population of west Africa (the sample included 483 patients and 593 controls). Significant independent associations of five *CDKN2B-AS1* gene SNP's with POAG have not been revealed during our study as well.

Such ambiguity of the results may be due to clinical heterogeneity of the studied samples of patients, as well as to the differences in the ethnic makeup of the studied populations. Other possible explanations for the ambiguity of association study results are as follows: unique external factors (environmental factors, lifestyle, etc.) in the distinct ethno-territorial groups, the prevalence of various complex disorders contributing to glaucoma заболеваний (atherosclerosis, diabetes mellitus, coronary heart disease, etc.) in these groups [1], as well as the range of environmental glaucoma risk factors related to the listed reasons, which is taken or not taken into account by the researchers during their studies.

Regardless of the fact that the distinct "major" effects of the studied *CDKN2B-AS1* gene loci on POAG in women has not been defined, it has been shown that the combination of certain alleles of the three studied *CDKN2B-AS1* gene SNPs (GGG rs1063192–rs7865618–rs2157719) in the haplotype defines susceptibility to POAG in women of the Central Black Earth Region, Russia. The vital role of the *CDKN2B-AS1* gene haplotypes in susceptibility to POAG has been also shown in the Indian population [33]: CATA haplotype rs3217992–rs1063192–rs2157719–rs4977756 increased the risk of the disorder by 1.61 times ($p \leq 0.0001$), however, the Bonferroni adjusted distinct effects of the listed loci were not statistically significant. It can be assumed, in case of several "risk" *CDKN2B-AS1* gene alleles in the genotype their regulatory effects [8, 12] add up and overcome some threshold essential for glaucoma susceptibility formation in the population, which was tested during our study.

Table 4. Association of *CDKN2B-AS1* gene polymorphic loci rs1063192–rs7865618–rs2157719 haplotypes with POAG in women

Haplotype	Haplotype frequency		OR	*p*
	Patients (*n* = 290)	Controls (*n* = 220)		
GGG	0.287	0.377	0.66	0.006
AGG	0.03	0.021	2.22	0.075
GAG	0.026	0.008	2.87	0.127
AAG	0.039	0.023	1.92	0.145
GGA	0.066	0.049	1.43	0.321
AGA	0.031	0.014	5.12	0.009
GAA	0.045	0.033	1.67	0.215
AAA	0.475	0.475	0.9	0.483

Note: Results were obtained using the logistic regression model; OR — odds ratio; *p* — significance level
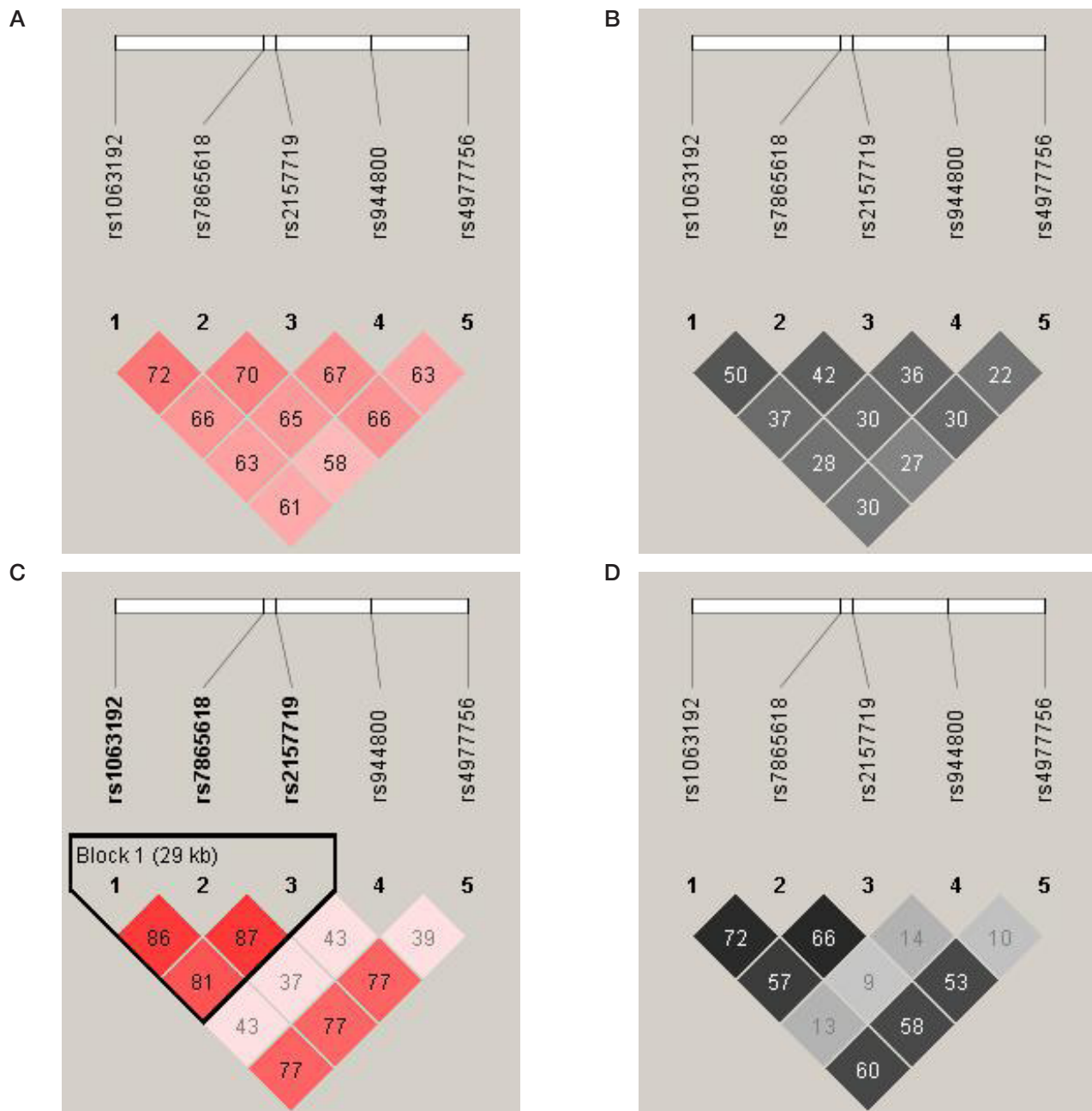
Fig. Linkage disequilibrium patterns between *CDKN2B-AS1* (9p21.3) gene polymorphisms in POAG patients (**A**, **B**) and controls (**C**, **D**) Note: cells in figures on the left contain Lewontin's standardized disequilibrium coefficient *D'*-values (*D'* =1 corresponds to empty cell). Cell color reflects the degree of generic linkage between polymorphisms: *red* — tight linkage (*D′* = 1; LOD > 2); *pink* — significant linkage (*D′* < 1; LOD > 2); *white* — weak linkage (*D′* < 1; LOD < 2). Haplotype blocks are marked by *black* lines. Cells in figures on the right contain Pearson correlation coefficient values (*r²*)

CONCLUSION

The data obtained using the Solid Spine algorithm (*D'* > 0.8) indicate the differences in haplotype blocks for five studied *CDKN2B-AS1* gene SNPs between patients with POAG (no haplotype blocks) and controls (haplotype block was identified consisting of three SNPs: rs1063192, rs7865618, and rs2157719). Association of *CDKN2B-AS1* gene GGG haplotype (rs1063192–rs7865618–rs2157719) with POAG in women of the Central Black Earth Region, Russia, has been defined. This haplotype is considered a protective factor for the development of the disorder (OR = 0.66; p = 0.006, p_{perm} = 0.037).

References

1. Grzybowski A, Och M, Kanclerz P, Leffler C, Moraes CG. Primary open angle glaucoma and vascular risk factors: a review of population based studies from 1990 to 2019. J Clin Med. 2020; 9 (3): 761.
2. Kreft D, Doblhammer G, Guthoff RF, Frech S. Prevalence, incidence and risk factors of primary open-angle glaucoma — a cohort study based on longitudinal data from a German public health in surname. BMC Public Health. 2019; 19: 851.
3. Tham YC, Li X, Wong TY, Quigley HA, Aung T, Cheng CY.

Global prevalence of glaucoma and projections of glaucoma burden through 2040: a systematic review and meta-analysis. Ophthalmology. 2014; 121: 2081–90.

4. Liu Y, Allingham RR. Molecular genetics in glaucoma. Exp Eye Res. 2011; 93: 331–9.

5. Svinareva DI. The contribution of gene-gene interactions of polymorphic loci of matrix metalloproteinases to susceptibility to primary open-angle glaucoma in men. Research Results in Biomedicine. 2020; 6 (1): 63–77. Russian.

6. Tikunova E, Ovtcharova V, Reshetnikov E, Dvornyk V, Polonikov A, Bushueva O, et al. Genes of tumor necrosis factors and their receptors and the primary open angle glaucoma in the population of Central Russia. Int J Ophthalmol. 2017; 10: 1490–4.

7. Gharahkhani P, Burdon KP, Fogarty R, Sharma S, Hewitt AW, Martin S, et al. Common variants near ABCA1, AFAP1 and GMDS confer risk of primary open-angle glaucoma. Nat Genet. 2014; (10): 1120–5.

8. Nakano M, Ikeda Y, Tokuda Y, Fuwa M, Omi N, Ueno M, et al. Common variants in CDKN2B-AS1 associated with optic-nerve vulnerability of glaucoma identified by genome-wide association studies in Japanese. PLoS One. 2012; 7 (3): e33389.

9. Osman W, Low SK, Takahashi A, Kubo M, Nakamura Y. A genome-wide association study in the Japanese population confirms 9p21 and 14q23 as susceptibility loci for primary open angle glaucoma. Hum Mol Genet. 2012; 21(12): 2836–42.

10. Shiga Y, Akiyama M, Nishiguchi KM, Sato K, Shimozawa N, Takahashi A, et al. Genome-wide association study identifies seven novel susceptibility loci for primary open-angle glaucoma. Hum Mol Genet. 2018; 27 (8): 1486–96.

11. Li Z, Allingham RR, Nakano M, Jia L, Chen Y, Ikeda Y, et al. A common variant near TGFBR3 is associated with primary open angle glaucoma. Hum Mol Genet. 2015; 24 (13): 3880–92.

12. Wiggs JL, Yaspan BL, Hauser MA, Kang JH, Allingham RR, Olson LM, et al. Common variants at 9p21 and 8q22 are associated with increased susceptibility to optic nerve degeneration in glaucoma. PLoS Genet. 2012; 8 (4): e1002654.

13. GeneCards: The human gene database. Available from: https://www.genecards.org/.

14. Ponomarenko I, Reshetnikov E, Polonikov A, Sorokina I, Yermachenko A, Dvornyk V, et al. Candidate genes for age at menarche are associated with endometrial hyperplasia. Gene. 2020; 757: 144933.

15. Litovkina O, Nekipelova E, Dvornyk V, Polonikov A, Efremova O, Zhernakova N, et al. Genes involved in the regulation of vascular homeostasis determine renal survival rate in patients with chronic glomerulonephritis. Gene. 2014; 546 (1): 112–6.

16. Golovchenko O, Abramova M, Ponomarenko I, Reshetnikov E, Aristova I, Polonikov A, et al. Functionally significant polymorphisms of ESR1 and PGR and risk of intrauterine growth restriction in population of Central Russia. Eur J Obstet Gynecol Reprod Biol. 2020; 253: 52–7.

17. GWAS Catalog. Available from: http://www.genome.gov/gwasstudies/.

18. HaploReg v4.1. Available from: https://pubs.broadinstitute.org/mammals/haploreg/haploreg.php.

19. PLINK. Available from: http://zzz.bwh.harvard.edu/plink/.

20. Haploview. Available from: http://www.broad.mit.edu/mpg/haploview/.

21. Moskalenko M, Ponomarenko I, Reshetnikov E, Dvornyk V, Churnosov M. Polymorphisms of the matrix metalloproteinase genes are associated with essential hypertension in a Caucasian population of Central Russia. Sci Rep. 2021; 11 (1): 5224.

22. Trifonova EA, Spiridonova MG, Stepanov VA. Genetic diversity and the structure of linkage disequilibrium in the methylenetetrahydrofolate reductase locus. Genetika. 2008; 44 (10): 1410–9. Russian.

23. Schaid DJ. Linkage disequilibrium testing when link age phase is unknown. Genetics. 2004; 166: 505–12.

24. Trifonova EA, Spiridonova MG, Gabidulina TV, Urnov FD, Puzyrev VP, Stepanov VA. Analysis of the MTHFR gene linkage disequilibrium structure and association of polymorphic gene variants with coronary atherosclerosis. Genetika. 2012; 48 (10): 1207–20. Russian.

25. Ramdas WD, van Koolwijk LM, Ikram MK, Jansonius NM, de Jong PT, Bergen AA, et al. A genome-wide association study of optic disc parameters. PLoS Genet. 2010; 6 (6): e1000978.

26. Fan BJ, Wang DY, Pasquale LR, Haines JL, Wiggs JL. Genetic variants associated with optic nerve vertical cup-to-disc ratio are risk factors for primary open angle glaucoma in a US Caucasian population. Invest Ophthalmol Vis Sci. 2011; 52 (3): 1788–92.

27. Ramdas WD, van Koolwijk LM, Lemij HG, Pasutto F, Cree AJ, Thorleifsson G, et al. Common genetic variants associated with open-angle glaucoma. Hum Mol Genet. 2011; 20: 2464–71.

28. Hu Z, He C. CDKN2B gene rs1063192 polymorphism decreases the risk of glaucoma. Oncotarget. 2017; 8 (13): 21167–76.

29. Springelkamp H, Höhn R, Mishra A, Hysi PG, Khor CC, Loomis SJ, et al. Meta-analysis of genome-wide association studies identifies novel loci that influence cupping and the glaucomatous process. Nat Commun. 2014; 5: 4883.

30. Springelkamp H, Mishra A, Hysi PG, Gharahkhani P, Höhn R, Khor CC, et al. Meta-analysis of genome-wide association studies identifies novel loci associated with optic disc morphology. Genet Epidemiol. 2015; 39 (3): 207–16.

31. Chen Y, Hughes G, Chen X, Qian S, Cao W, Wang L, et al. Genetic variants associated with different risks for high tension glaucoma and normal tension glaucoma in a Chinese population. Invest Ophthalmol Vis Sci. 2015; 56 (4): 2595–600.

32. Nunes HF, Ananina G, Costa VP, Zanchin NIT, de Vasconcellos JPC, de Melo MB. Investigation of CAV1/CAV2 rs4236601 and CDKN2B-AS1 rs2157719 in primary open-angle glaucoma patients from Brazil. Ophthalmic Genet. 2018; 39: 194–9.

33. Thakur N, Kupani M, Mannan R, Pruthi A, Mehrotra S. Genetic association between CDKN2B/CDKN2B-AS1 gene polymorphisms with primary glaucoma in a North Indian cohort: an original study and an updated meta-analysis. BMC Med Genomics. 2021; 14 (1): 1.

34. Liu Y, Hauser MA, Akafo SK, Qin X, Miura S, Gibson JR, et al. Investigation of known genetic risk factors for primary open angle glaucoma in two populations of African ancestry. Invest Ophthalmol Vis Sci. 2013; 54 (9): 6248–54.

35. Micheal S, Ayub H, Khan MI, Bakker B, Schoenmaker-Koller FE, Ali M, et al. Association of known common genetic variants with primary open angle, primary angle closure, and pseudoexfoliation glaucoma in Pakistani cohorts. Mol Vis. 2014; 20: 1471–9.

Литература

1. Grzybowski A, Och M, Kanclerz P, Leffler C, Moraes CG. Primary open angle glaucoma and vascular risk factors: a review of population based studies from 1990 to 2019. J Clin Med. 2020; 9 (3): 761.

2. Kreft D, Doblhammer G, Guthoff RF, Frech S. Prevalence. incidence and risk factors of primary open-angle glaucoma — a cohort study based on longitudinal data from a German public health in surname. BMC Public Health. 2019; 19: 851.

3. Tham YC, Li X, Wong TY, Quigley HA, Aung T, Cheng CY. Global prevalence of glaucoma and projections of glaucoma burden through 2040: a systematic review and meta-analysis. Ophthalmology. 2014; 121: 2081–90.

4. Liu Y, Allingham RR. Molecular genetics in glaucoma. Exp Eye Res. 2011; 93: 331–9.

5. Свинарева Д. И. Вклад ген-генных взаимодействий полиморфных локусов матриксных металлопротеиназ в подверженность к первичной открытоугольной глаукоме у мужчин. Научные результаты биомедицинских исследований. 2020; 6 (1): 63–77.

6. Tikunova E, Ovtcharova V, Reshetnikov E, Dvornyk V, Polonikov A, Bushueva O, et al. Genes of tumor necrosis factors and their receptors and the primary open angle glaucoma in the population of Central Russia. Int J Ophthalmol. 2017; 10: 1490–4.

7. Gharahkhani P, Burdon KP, Fogarty R, Sharma S, Hewitt AW, Martin S, et al. Common variants near ABCA1. AFAP1 and GMDS confer risk of primary open-angle glaucoma. Nat Genet. 2014; (10): 1120–5.

8. Nakano M, Ikeda Y, Tokuda Y, Fuwa M, Omi N, Ueno M, et al. Common variants in CDKN2B-AS1 associated with optic-nerve

vulnerability of glaucoma identified by genome-wide association studies in Japanese. PLoS One. 2012; 7 (3): e33389.

9. Osman W, Low SK, Takahashi A, Kubo M, Nakamura Y. A genome-wide association study in the Japanese population confirms 9p21 and 14q23 as susceptibility loci for primary open angle glaucoma. Hum Mol Genet. 2012; 21(12): 2836–42.

10. Shiga Y, Akiyama M, Nishiguchi KM, Sato K, Shimozawa N, Takahashi A, et al. Genome-wide association study identifies seven novel susceptibility loci for primary open-angle glaucoma. Hum Mol Genet. 2018; 27 (8): 1486–96.

11. Li Z, Allingham RR, Nakano M, Jia L, Chen Y, Ikeda Y, et al. A common variant near TGFBR3 is associated with primary open angle glaucoma. Hum Mol Genet. 2015; 24 (13): 3880–92.

12. Wiggs JL, Yaspan BL, Hauser MA, Kang JH, Allingham RR, Olson LM, et al. Common variants at 9p21 and 8q22 are associated with increased susceptibility to optic nerve degeneration in glaucoma. PLoS Genet. 2012; 8 (4): e1002654.

13. GeneCards: The human gene database. Available from: https://www.genecards.org/.

14. Ponomarenko I, Reshetnikov E, Polonikov A, Sorokina I, Yermachenko A, Dvornyk V, et al. Candidate genes for age at menarche are associated with endometrial hyperplasia. Gene. 2020; 757: 144933.

15. Litovkina O, Nekipelova E, Dvornyk V, Polonikov A, Efremova O, Zhernakova N, et al. Genes involved in the regulation of vascular homeostasis determine renal survival rate in patients with chronic glomerulonephritis. Gene. 2014; 546 (1): 112–6.

16. Golovchenko O, Abramova M, Ponomarenko I, Reshetnikov E, Aristova I, Polonikov A, et al. Functionally significant polymorphisms of ESR1 and PGR and risk of intrauterine growth restriction in population of Central Russia. Eur J Obstet Gynecol Reprod Biol. 2020; 253: 52–7.

17. GWAS Catalog. Available from: http://www.genome.gov/gwastudies/.

18. HaploReg v4.1. Available from: https://pubs.broadinstitute.org/mammals/haploreg/haploreg.php.

19. PLINK. Available from: http://zzz.bwh.harvard.edu/plink/.

20. Haploview. Available from: http://www.broad.mit.edu/mpg/haploview/.

21. Moskalenko M, Ponomarenko I, Reshetnikov E, Dvornyk V, Churnosov M. Polymorphisms of the matrix metalloproteinase genes are associated with essential hypertension in a Caucasian population of Central Russia. Sci Rep. 2021; 11 (1): 5224.

22. Трифонова Е. А., Спиридонова М. Г., Степанов В. А. Генетическое разнообразие и неравновесие по сцеплению в локусе метилентетрагидрофолатредуктазы. Генетика. 2008; 44 (10): 1410–19.

23. Schaid DJ. Linkage disequilibrium testing when link age phase is unknown. Genetics. 2004; 166: 505–12.

24. Трифонова Е. А., Спиридонова М. Г., Габидулина Т. В., Урнов Ф. Д., Пузырев В. П., Степанов В. А. Анализ структуры неравновесия по сцеплению и ассоциации полиморфных вариантов гена МТHFR с коронарным атеросклерозом. Генетика. 2012; 48 (10):1207–20.

25. Ramdas WD, van Koolwijk LM, Ikram MK, Jansonius NM, de Jong PT, Bergen AA, et al. A genome-wide association study of optic disc parameters. PLoS Genet. 2010; 6 (6): e1000978.

26. Fan BJ, Wang DY, Pasquale LR, Haines JL, Wiggs JL. Genetic variants associated with optic nerve vertical cup-to-disc ratio are risk factors for primary open angle glaucoma in a US Caucasian population. Invest Ophthalmol Vis Sci. 2011; 52 (3): 1788–92.

27. Ramdas WD, van Koolwijk LM, Lemij HG, Pasutto F, Cree AJ, Thorleifsson G, et al. Common genetic variants associated with open-angle glaucoma. Hum Mol Genet. 2011; 20: 2464–71.

28. Hu Z, He C. CDKN2B gene rs1063192 polymorphism decreases the risk of glaucoma. Oncotarget. 2017; 8 (13): 21167–76.

29. Springelkamp H, Höhn R, Mishra A, Hysi PG, Khor CC, Loomis SJ. et al. Meta-analysis of genome-wide association studies identifies novel loci that influence cupping and the glaucomatous process. Nat Commun. 2014; 5: 4883.

30. Springelkamp H, Mishra A, Hysi PG, Gharahkhani P, Höhn R, Khor CC, et al. Meta-analysis of genome-wide association studies identifies novel loci associated with optic disc morphology. Genet Epidemiol. 2015; 39 (3): 207–16.

31. Chen Y, Hughes G, Chen X, Qian S, Cao W, Wang L, et al. Genetic variants associated with different risks for high tension glaucoma and normal tension glaucoma in a Chinese population. Invest Ophthalmol Vis Sci. 2015; 56 (4): 2595–600.

32. Nunes HF, Ananina G, Costa VP, Zanchin NIT, de Vasconcellos JPC, de Melo MB. Investigation of CAV1/CAV2 rs4236601 and CDKN2B-AS1 rs2157719 in primary open-angle glaucoma patients from Brazil. Ophthalmic Genet. 2018; 39: 194–9.

33. Thakur N, Kupani M, Mannan R, Pruthi A, Mehrotra S. Genetic association between CDKN2B/CDKN2B-AS1 gene polymorphisms with primary glaucoma in a North Indian cohort: an original study and an updated meta-analysis. BMC Med Genomics. 2021; 14 (1): 1.

34. Liu Y, Hauser MA, Akafo SK, Qin X, Miura S, Gibson JR, et al. Investigation of known genetic risk factors for primary open angle glaucoma in two populations of African ancestry. Invest Ophthalmol Vis Sci. 2013; 54 (9): 6248–54.

35. Micheal S, Ayub H, Khan MI, Bakker B, Schoenmaker-Koller FE, Ali M, et al. Association of known common genetic variants with primary open angle, primary angle closure, and pseudoexfoliation glaucoma in Pakistani cohorts. Mol Vis. 2014; 20: 1471–9.

MOLECULAR AND CELLULAR FEATURES OF MANDIBULAR AUTOGRAFTS STUDIED USING RAMAN SPECTROSCOPY

Maksimov GV[1,4] ✉, Sashkina TI[2], Fashutdinov DK[3], Slatinskaya OV[1], Saldusova IV[5], Zaychenko OV[5]

[1] Lomonosov Moscow State University, Moscow, Russia

[2] Pirogov Russian National Research Medical University, Moscow, Russia

[3] A. I. Yevdokimov Moscow State University of Medicine and Dentistry, Moscow, Russia

[4] National University of Science and Technology MISIS, Moscow, Russia

[5] Central State Medical Academy of Department for Presidential Affairs of the Russian Federation, Moscow, Russia

Currently, biophysical studies are of great interest, the results of which are important for development of a method for diagnosis of the cells and tissue condition to be used in clinical practice. The study was aimed to use a non-invasive optical method (Raman spectroscopy) for assessment of changes in the composition and conformation of the molecules of the patient's mandibular cells and tissues. This approach was proposed to increase the informativeness and effectiveness of studying the composition of autografts harvested for augmentation of alveolar processes with bone tissue deficiency (elective bone grafting). In the course of the study the bone tissue samples obtained from three patients aged 51–73 (two men and one woman) were assessed. Raman signals were detected, indicating the presence of phosphate groups and carbonate ions (such as CO_3^{-2}) of the inorganic bone components. Raman bands indicating the presence of collagen, red blood cell hemoglobin, proteins (C–N bonds), lipids (C–H groups of fatty acids and phosphate groups of phospholipids), as well as their OH groups may be considered the markers of periosteum tissue. The general possibility was suggested of studying single cells of autografts using the markers, indicating the presence of collagen, hemoglobin, proteins, lipids (C–H groups of fatty acids of lipids; phosphate groups of phospholipids), and their OH groups. According to the authors, the results obtained can provide a basis for development of the new method for diagnosis of autograft bone using the combination of Raman spectroscopy and light guides.

Keywords: autograft, implant, bone tissue, Raman spectroscopy

ИССЛЕДОВАНИЕ МОЛЕКУЛЯРНО-КЛЕТОЧНЫХ ХАРАКТЕРИСТИК АУТОТРАНСПЛАНТАТОВ НИЖНЕЙ ЧЕЛЮСТИ С ПОМОЩЬЮ МЕТОДА СПЕКТРОСКОПИИ КОМБИНАЦИОННОГО РАССЕЯНИЯ

Г. В. Максимов[1,4] ✉, Т. И. Сашкина[2], Д. К. Фасхутдинов[3], О. В. Слатинская[1], И. В. Салдусова[5], О. В. Зайченко[5]

[1] Московский государственный университет имени М. В. Ломоносова, Москва, Россия

[2] Российский научно-исследовательский медицинский университет имени Н. И. Пирогова, Москва, Россия

[3] Московский государственный медико-стоматологический универститет имени А. И. Евдокимова, Москва, Россия

[4] Национальный исследовательский технологический универститет «МИСиС», Москва, Россия

[5] Центральная государственная медицинская академия Управления делами Президента Российской Федерации, Москва, Россия

В настоящее время большой интерес представляют биофизические исследования, результаты которых важны для формирования методологии диагностики состояния ткани и клеток в клинической практике. Целью данной работы было продиагностировать изменения состава и конформации молекул клеток и ткани нижней челюсти пациента с помощью оптического неинвазивного метода (спектроскопия комбинационного рассеяния (КР). Данный методический подход предложен для повышения информативности и эффективности исследования состава аутотрансплантатов, полученных для аугментации альвеолярных отростков при дефиците костной ткани (планируемая костная пластика). В исследовании использовали образцы костной ткани троих пациентов в возрасте 51–73 лет, двоих мужчин и одной женщины. В костной ткани обнаружены КР-сигналы, свидетельствующие о наличии фосфатных групп и карбонат-ионов (типа CO_3^{-2}) минеральных компонентов кости. Маркерами молекул околокостной ткани могут быть полосы, которые свидетельствуют о наличии коллагена, гемоглобина эритроцитов, белков (C–N-связи), липидов (C–H-групп жирных кислот и фосфатных групп фосфолипидов), а также их OH-групп. Показана принципиальная возможность исследования отдельных клеток аутотрансплантатов с помощью маркеров, свидетельствующих о наличии коллагена, гемоглобина, белков и липидов (C–H-групп жирных кислот липидов; фосфатных групп фосфолипидов), и их OH-групп. По мнению авторов, результаты могут служить основой для формирования новой методологии диагностики костных аутотрансплантатов с помощью совмещения КР-спектроскопии и световодов.

Ключевые слова: аутотрансплантат, имплантат, костная ткань, спектроскопия комбинационного рассеяния.

It is known that dental implants are being successfully used to restore the dental arch continuity in partially and completely edentulous patients [1, 2]. The patients of the dentists often present with significant bone loss in the alveolar process and a part of the jaw, which suggests the procedure to increase the amount of bone tissue prior to implant installation. Bone augmentation is performed using both allo- and autografts, however, it is better to use autografts [3, 4]. Autogenous cortical bone grafts are good for that, harvested from various extraoral body areas: iliac crest, skull cap, tibia, zygomatic bone, as well as the intraoral sites (rami of the mandible, sites within the retromolar region, chin area). Intraoral autogenous bone grafts are used more frequently, since the harvesting procedure is less invasive, surgical approach is more convenient, and the installation procedure is less time-consuming. It is also essential that the distance between donor and recipient sites becomes closer [5, 6].

Osteoregeneration process depends on a number of factors: microarchitectonics, bone density, percentage of cortical and cancellous bone, as well as the levels of pro- and anti-inflammatory cytokines, the markers of bone destruction and regeneration [7–10]. It is well-known that jaws are flat cancellous bones organized into trabeculae. Trabeculae form the shell for red bone marrow, which is responsible for hematopoiesis and blood cell production [11]. Type 1 collagen accounts for 95% of trabecular plate; trabecular plates also contain collagen types 3, 4, 5, 11, and 12 (the other 5%). There are non-collagenous proteins, osteocalcin, osteonectin, osteopontin, bone sialoproteins, phosphoproteins, morphogenetic proteins, and proteoglycans in the intercellular space. Moreover, there are glycoproteins: alkaline phosphatase, osteonectin, thrombospondin, fibronectin, vitronectin, osteopontin, sialoprotein, Wht-glycoproteins. Inorganic components, represented by the hydroxyapatite crystals, account for 30% of bone tissue structure. Bone also contains hydroxyapatite stability regulators: magnesium, strontium and manganese.

Cellular composition of bone tissue consists of osteoprogenitor cells (early progenitors of osteoblasts), osteoblasts, osteocytes, bone lining cells, and osteoclasts. Mature osteoblasts produce type 1 collagen, proteoglycans, and osteocalcin. Immature osteoblasts lay directly adjacent to periosteum. The cytoplasm of those contains small quantities of glycogen granules. Osteoblasts are cells that synthesize bone matrix, cytokines, and growth factors. Alkaline phosphatase and osteocalcin are the osteoblast markers (osteocalcin is the main marker of bone tissue regeneration). Osteocyte formation is the final stage of osteoblast differentiation. Osteocytes do not synthesize bone matrix; osteocytes are involved in osteolysis and metabolic transport. Osteoclasts, being the large multinucleated cells, are responsible for bone resorption. Osteoclasts priduce hydrogen ions together with enzymes (cathepsin and collagenase) involved in the lysis of organic matrix. Alkaline phosphatase is the marker of osteoclasts. The outer surface of spongy osseous tissue is covered by cortical bone, which in turn is covered by periosteum, invaded by blood vessels feeding the bone. The internal layer of periosteum contains osteoblast progenitor cells responsible for bone growth and remodeling [11]. Studying the structure and components of bone tissue is essential for evaluation and forecasting of regeneration, osteogenesis and osseointegration when performing dental implantation [12].

Clearly, it is important to put advanced effective, reliable and non-invasive optical methods, allowing one to allocate the components of bone tissue, oral fluid, and peripheral blood, into dental practice in order to monitor bone tissue structure,

resorption and remodeling. Assessment of bone-to-implant integration and augmentation of the alveolar processes is relevant to surgical dentistry, and is of crucial importance, since it determines the success of treatment.

Prompt diagnosis of osseointegration and bone tissue regeneration impairments is essential. Markers of resorption and regeneration, as well as bone tissue protectors, are well-known. There is a number of methods for detection of those. Biochemical analysis makes it possible to evaluate the treatment and complication prevention results, however, the analysis requires a fairly large amount of the material being sampled. Gas chromatography is a more accurate method, which has the advantage of high reliability of the results. The method's disadvantages are as follows: considerable complexity of investigation, high cost, time-consuming interpretation of the results, and the need for expert assessment.

In recent years, many optical methods have been used in biology and medicine. One of the methods is Raman spectroscopy, the highly sensitive optical method providing express and accurate determination of the composition and conformation of molecules, constituting biological objects: cells, cell fragments, bacteria, viruses, proteins, peptides, lipids [13, 14]. It is worth mentioning that in dentistry there is an emerging body of research using both Raman spectra and giant Raman spectra acquisition [15]. Such approach exhibits high sensitivity; it has been used for identification of the main pathogens of purulent-inflammatory processes in maxillofacial area [16]. What's important is that with the use of giant Raman scattering effect, certain markers of the pathogens have been detected: in *Bacillus subtilius* there were peaks at 657, 726, 1248, 1377, 1466, 1617 cm^{-1}; in *E. coli* these were found at 1140, 1551 cm^{-1}; in *S. aureus* peaks were found at 959, 1006, 1160, 1284, 1530 см$^{-1}$; in *S. haemolyticus* there were peaks at 1327, 1369; in *Ps. aeruginosa* these were found at 675, 1353, 1404, 1605, 1630 cm^{-1}. Thus, giant Raman spectra acquired during treatement make it possible to determine the cause of the inflammation. However, this approach needs firther detailed testing in practice, since the giant Raman scattering effect realization requires the use of nanoparticles (colloidal silver and gold nanoparticles), the toxic effect of which on the cells and tissues of the oral cavity is not yet khown.

Taking into account the informative nature and efficiency of Raman spectroscopy, as well as lack of time-consuming sample preparation, it is important to develop the Raman scattering-based technology for assessment of osseointegration after installation of dental implants in order to define the condition of autograft bone, as well as to search for markers of osteogenesis, resorption and osseointegration involved in the process of reparative regeneration.

The study was aimed to investigate molecular and cellular composition of mandibular autografts using Raman spectroscopy.

METHODS

Augmentation of the mandible prior to implant installation was performed during the study. For this purpose the patients underwent surgical restoration of bone tissue amount using autografts, the condition of which was investigated later. Four samples of cortical and cancellous bone tissue obtained from the left and right retromolar regions of the mandible during the surgical procedure were assessed (see Table). Four autografts were investigated, obtained from three patients aged 51–73: two men and one woman. Inclusion criteria: no somatic pathology; medium-sized mandibular bone defect; no

Table. Studied samples

1 B-v R.E.	Retromolar region	1969	Dental Clinic 2 of MSUMD	Dental Clinic 2 of MSUMD
2 A-a S.G.	Retromolar region	1947	Dental Clinic 2 of MSUMD	Dental Clinic 2 of MSUMD
3 P-a M.L.	Retromolar region	1961	Dental Clinic 2 of MSUMD	Dental Clinic 2 of MSUMD
3 P-a M.L.	Edentulous area (mandibular tooth 6)	1961	Dental Clinic 2 of MSUMD	Dental Clinic 2 of MSUMD

drug intolerance; age 40–60 years. Exclusion criteria: severe somatic illness; drug intolerance; large-sized mandibular bone defect; age under 40 and over 60.

Bone block harvesting from the donor site

After giving the conduction and infiltration anesthesia (sol. Articaini 3.4 mL), the incision was made across the mandibular alveolar process apex in the area of missing teeth, mucoperiosteal flap was peeled off, mandibular alveolar bone was exposed, and the length and width of the bone defect were defined. After giving the conduction and infiltration anesthesia (sol. Articaini 3.4 mL), the 3 cm incisions were made in the left and right retromolar regions, mucoperiosteal flap was peeled off. Using the disc with a protector and the fissure burr, autograft sized 2 × 1 × 0.3 cm or 1.5 × 1 × 0.3 cm was harvested. The autograft bone was split into two thin bone plates using the disc. The wound was closed by the 4–0 Vicryl suture.

The autograft bone samples (size 0,1 mm) were placed into glass capillaries with cross sectional diameter of 1 mm (Agat-Med; Russia) filled with buffer (145 мМ NaCl, 5 мМ KCl, 4 мМ Na_2HPO_4, 1 мМ NaH_2PO_4, 1 мМ $MgSO_4$, 5 мМ glucose (Sigma; USA), pH 7.4). They were stored at a temperature of 4 °C for the period not exceeding 3 hours.

Sample morphology and molecular composition of bone tissue, soft tissues and cells of the mandible were studied using Raman spectroscopy. The following settings of the confocal Raman/fluorescence microscopy NTEGRA-SPECTRA system (NT-MDT; Russia) were used: spectral range of 1000–3000 cm⁻¹; step size of 0.8 cm⁻¹; detection with CCD detector with Peltier-cooling to –50 ° (objective 20× with an aperture of 0.15, grating 600 lines/mm); laser power at sample not exceeding 3 mW, laser excitation wavelength 532 nm, exposure time 10 s, 3 sample exposures. Number of repetitions for the experiment (sample): 12. Spectra processing involved background subtraction and

smoothing of spectra using the Origin2017 software (OriginLab Corporation; USA).

The pilot study was carried out in order to define the possibility of using Raman spectroscopy to assess the condition of the tissues in the maxillofacial region; no statistical analysis was performed.

RESULTS

During the study the sample images and the Raman spectra of the components of autografts (bone tissue, soft tissues and cells), harvested from the retromolar region, were obtained.

Raman spectra of bone tissue of autografts harvested from the retromolar region

During this series of experiments the analysis of autograft bone tissue markers revealed characteristic Raman bands in the spectra of samples, corresponding to collagen, phosphate groups, apatite (PO_4^{3-}), type B carbonate ion (such as CO_3^{-2}), as well as proteins adsorbed to the cell surface (bending N–H vibrations and stretching C–N vibrations), lipids (C–H groups of fatty acids of lipids), and their OH groups.

Thus, in the patient's Raman spectrum of the sample № 2, a number of bands was observed corresponding to phosphate groups PO_4^3 (563, 943, 975 cm⁻¹), collagen (1270 cm⁻¹), type B carbonate ion CO_3^{-2} (1025, 1051 cm⁻¹), proteins and lipids (C–H groups of fatty acids of lipids, 2862, 2890, 2946 cm⁻¹), and their OH groups (3192, 3420, 3559, 3635 cm⁻¹) (Fig. 1). A number of bands were observed corresponding to phosphate groups (426, 583, 938 cm⁻¹), type B carbonate ion CO_3^{-2} (1009, 1023, 1056 cm⁻¹), proteins (bending N–H vibrations and stretching C–N vibrations of protein, 1607 cm⁻¹), lipids (C–H groups of fatty acids of lipids, 2857, 2889, 2948 cm⁻¹), and their OH groups (3204, 3408, 3621 cm⁻¹), together with a
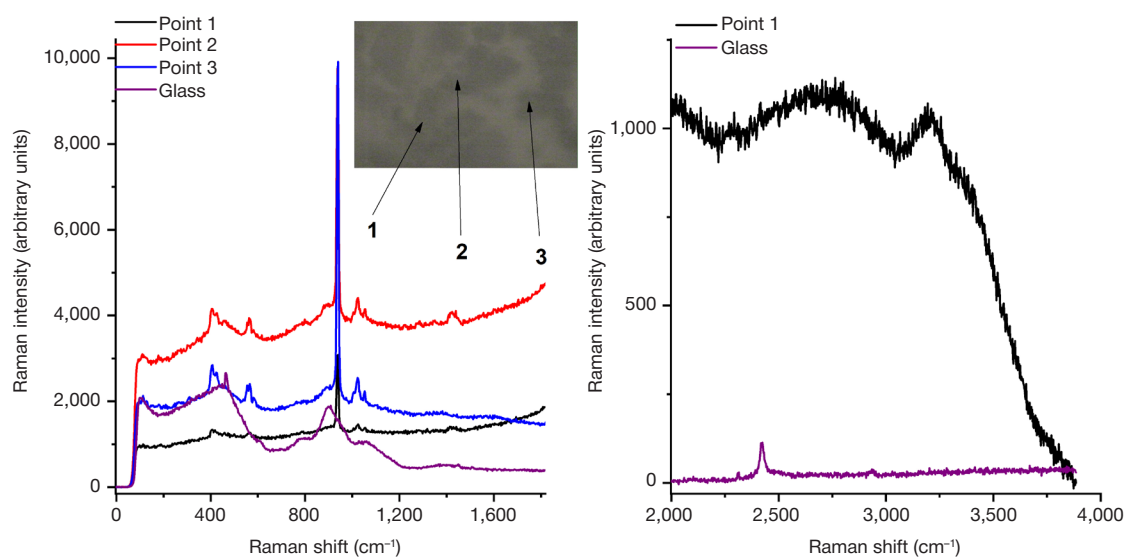
Fig. 1. Raman spectrum of the autograft, sample № 2 (bone tissue and tissue components). The insert in the chart illustrates the image of the sample. The control is the Raman spectrum of the glass, the sample is placed on. X-axis: Raman shift (cm⁻¹); Y-axis: Raman intensity (in arbitrary units)
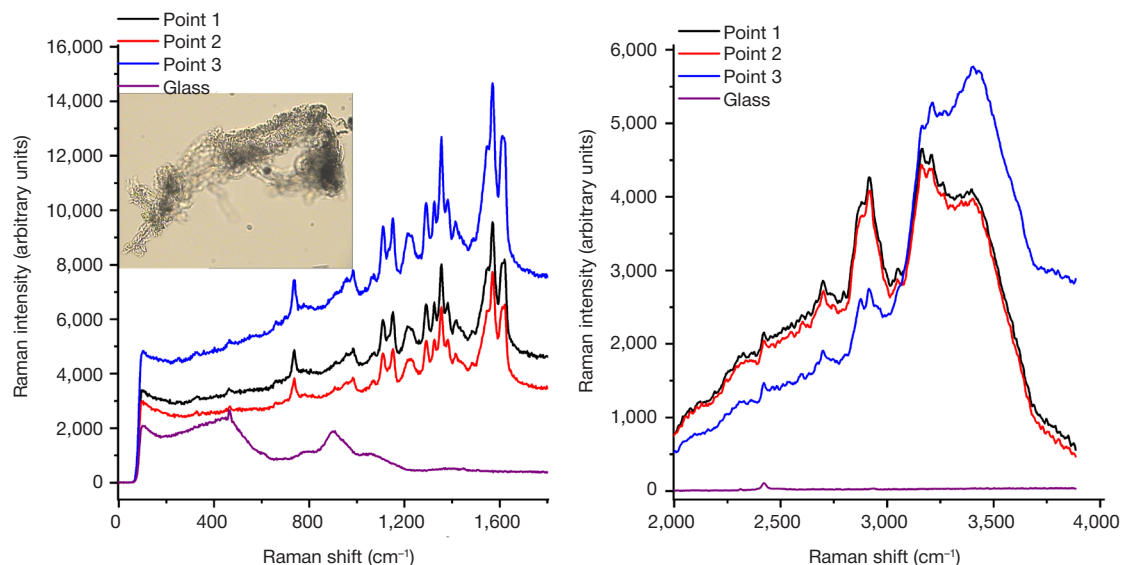
Fig. 2. Raman spectrum of the autograft, sample № 2 (autograft tissues). The insert in the chart illustrates the image of the sample. The control is the Raman spectrum of the glass, the sample is placed on. X-axis: Raman shift (cm⁻¹); Y-axis: Raman intensity (in arbitrary units)

number of bands defining the inorganic composition of bone tissue: phosphate groups PO_4^{-3} (415, 457, 570, 580, 892, 936 cm⁻¹ (phosphate group of apatite)), type B carbonate ion CO_3^{-2} (1007, 1022, 1050 cm⁻¹), as well as OH groups of lipids and proteins, 3209, 3399, 3625 cm⁻¹. The bands were observed defining the inorganic composition of the tissue: phosphate groups PO_4^{3-} (567, 582, 941 cm⁻¹), type B carbonate ion CO_3^{-2} (1004, 1021, 1054 cm⁻¹), and OH groups of adsorbed lipids and proteins (2952, 3214, 3620 cm⁻¹) (see Fig. 1).

Raman spectra of the tissue of autografts harvested from the retromolar region

When developing markers for detection of the autograft components during the operation, it was found that in the Raman spectrum there were a number of bands corresponding to collagen, blood hemoglobin, proteins (amide II groups of proteins), lipids (C–H groups of fatty acids of lipids), and their OH groups. In the patient's Raman spectrum of the sample No. 2 a number of bands were observed, which indicated the presence of collagen (1270 cm⁻¹), hemoglobin (1109, 1151, 1228, 1289, 1353, 1382, 1545, 1570, 1615 cm⁻¹), proteins

(C–N bonds, 3157, 3204 cm⁻¹), lipids (C–H groups of fatty acids, 2697, 2877, 2911, 2964 cm⁻¹; phosphate groups of phospholipids, 924, 961 см⁻¹), and their OH groups (3402, 3588 cm⁻¹) (Fig. 2).

In the patient's Raman spectrum of the sample № 1 a number of characteristic Raman bands were observed, corresponding to vibrations of certain bonds in the protein molecules (for example, 1632 cm⁻¹, amide II of proteins; 2848, 2876, 2918, 2930 cm⁻¹), lipids (C–H groups of fatty acids of lipids), and their OH groups.

Raman spectra of the cells of autografts harvested from the retromolar region

In order to reveal the markers of distinct cells of the autografts, a number of characteristic bands was detected in the spectrum, corresponding to collagen, red blood cell hemoglobin, proteins (amide and C–N bonds), and cellular lipids (C–H groups of fatty acids and phosphate groups of lipids), as well as their OH groups. In the patient's Raman spectrum of the sample № 1 a number of Raman bands were observed corresponding to proteins and lipids (C–H groups of fatty acids of lipids, 2848,
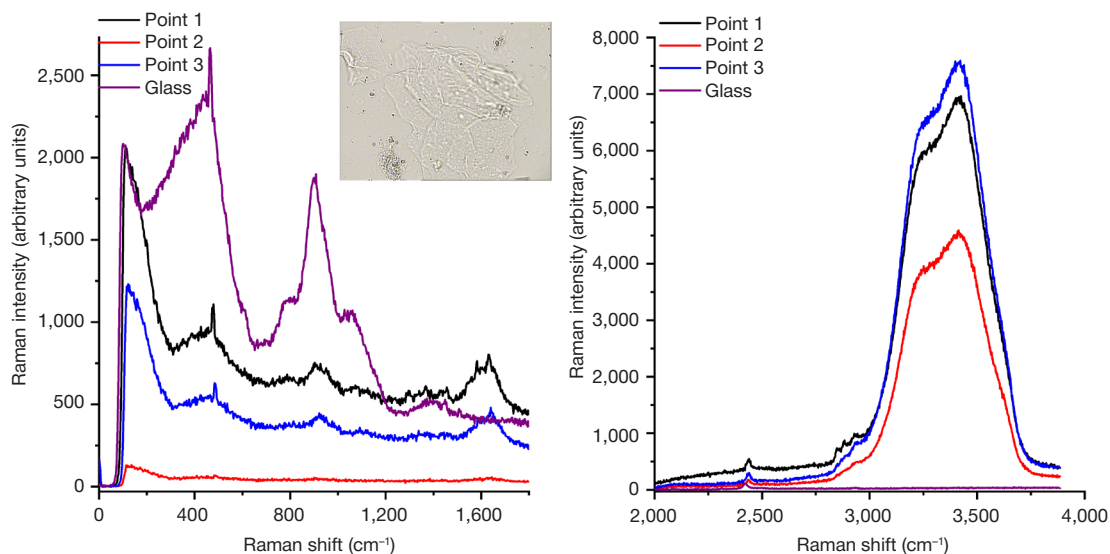
Fig. 3. Raman spectrum of the autograft, sample № 1 (single cell). The insert in the chart illustrates the image of the sample. The control is the Raman spectrum of the glass, the sample is placed on. X-axis: Raman shift (cm⁻¹); Y-axis: Raman intensity (in arbitrary units)
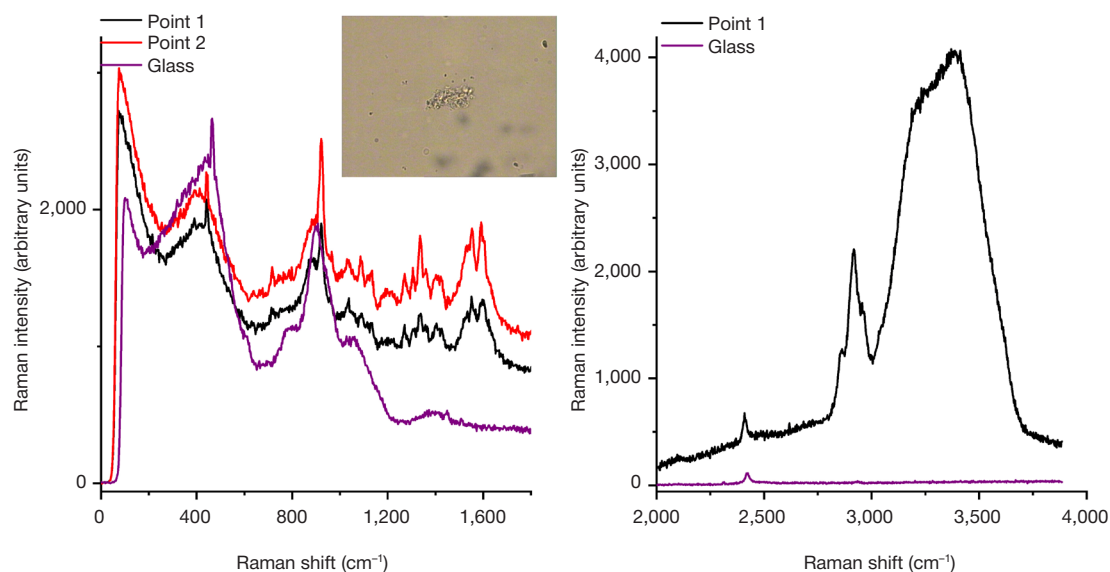
Fig. 4. Raman spectrum of the autograft, sample № 1 (red blood cell). The insert in the chart illustrates the image of the sample. The control is the Raman spectrum of the glass, the sample is placed on. X-axis: Raman shift (cm⁻¹); Y-axis: Raman intensity (in arbitrary units)

2876, 2930 cm⁻¹), and their OH groups (3230, 3420, 3612 cm⁻¹) (Fig. 3–5), collagen (1274 cm⁻¹), red blood cell hemoglobin (1303, 1335, 1363, 1407, 1531, 1550, 1593 cm⁻¹), proteins and lipids (phosphate groups, 924, 961 cm⁻¹), C–H groups of fatty acids of lipids (2848, 2876, 2930 cm⁻¹), and their OH groups (3230, 3420, 3612 cm⁻¹) [18–20]. In the patient's Raman spectrum of the sample № 2 there were a number of characteristic Raman bands, corresponding to proteins (amide, 1621; 2841, 2887, 2950 cm⁻¹) and lipids (phosphate groups, 888, 1432 cm⁻¹), as well as their OH groups (3212, 3402, 3626 cm⁻¹). In the patient's Raman spectrum of the sample No. 2, proteins and lipids were detected (C–H groups of fatty acids of lipids, 2836, 2876, 2946 cm⁻¹), as well as their OH groups (3214, 3397, 3614 cm⁻¹). In the patient's Raman spectrum of the sample № 3 there were a number of characteristic Raman bands corresponding to collagen (1314 cm⁻¹ and 1603 cm⁻¹), proteins (C–N bonds, 2974, 3002, 3932 cm⁻¹), lipids (C–H groups of fatty acids of lipids, 2846, 2902, 2938 cm⁻¹), and their OH groups (3238, 3406, 3607 cm⁻¹) (see Fig. 3–5).

DISCUSSION

In the course of our study we looked for the possibility of Raman signal acquisition of the molecules of tissues and cells during surgical harvesting of tissue for augmentation of alveolar processes with bone tissue deficiency (elective bone grafting) [15–17]. It's obvious that continuous monitoring of the tissue condition during surgery allows the surgeon to promptly change the surgical procedure and to perform further diagnosis [18–20]. During our study we used the optical non-invasive technique for rapid and effective diagnosis of changes in composition and conformation of molecules in the patient's mandibular cells and tissues. We conducted preliminary research and acquired characteristic signals of bone tissue and periosteum tissue. We assume that the use of fiber optic probes and Raman spectroscopy would make it possible to identify problems and defects occurring during the surgical procedure at the molecular level. It has been found that the bands, indicating the presence of phosphate groups (426, 583, 938 cm⁻¹) and type B carbonate ion CO_3^{-2} (1009, 1023, 1056 cm⁻¹), can be
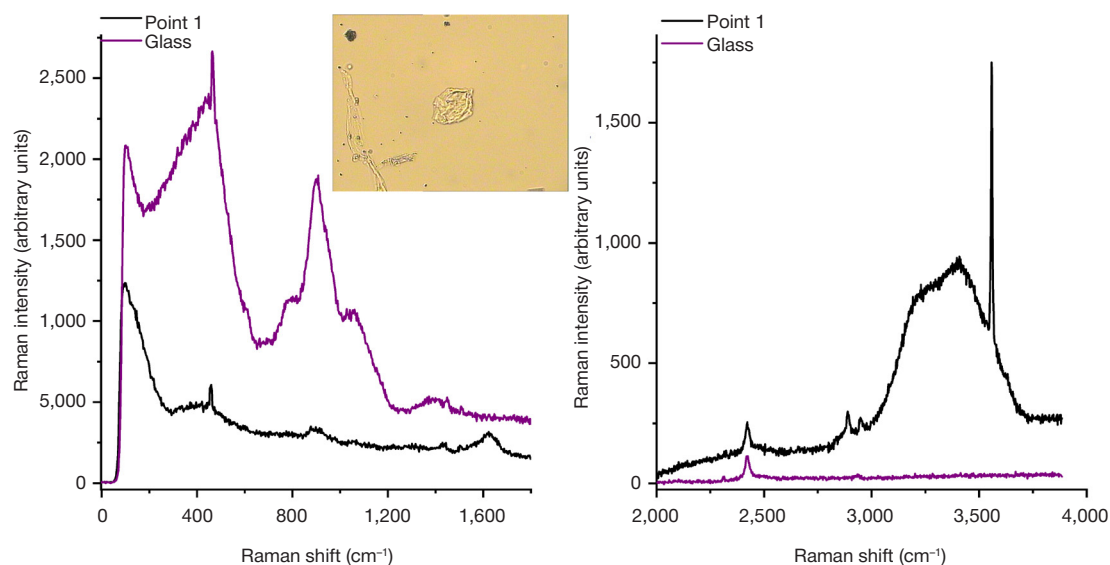
Fig. 5. Raman spectrum of the autograft, sample № 2 (cell). The insert in the chart illustrates the image of the sample. The control is the Raman spectrum of the glass, the sample is placed on. X-axis: Raman shift (cm⁻¹); Y-axis: Raman intensity (in arbitrary units)

considered a characteristic marker for diagnosis of bone tissue condition. This, acquisition of data on these markers makes it possible to evaluate the contribution of these components and the changes of those during the surgical procedure. It is obvious that acquisition of the Raman signal of the cell and tissue population allows to acquire the combined spectrum. In order to identify the specific signal of the periosteum tissue (not bone tissue), the Raman signals have been acquired, indicating the presence of collagen, hemoglobin, various proteins (C–N bonds), lipids (C–H groups of fatty acids and phosphate groups of phospholipids), and their OH groups. Thus, the proposed approach would make it possible to detect changes both in bone tissue and periosteum tissue of the patient's mandible [21, 22].

The important thing about our study is the fact that we have managed to acquire the Raman signals of the distinct cells of autografts, corresponding to distinct molecules of collagen, hemoglobin, proteins and lipids, and their OH groups.

It has been found that Raman scattering may be used for evaluation of the autograft bone condition during transplantation. The data obtained suggest that the spectra of various autograft samples differ. The proposed method of autograft condition evaluation would be used for identification of certain proteins, lipids, and other molecules, which constitute the bone tissue, as well as for quantification of these molecules. During osseointegration, a large number of biologically active molecules are being synthesized, which may indicate enhanced or decreased integration [3, 6].

Thus, Raman signals of specific substances have been acquired in various tissues and cells. Perhaps, the use of advanced equipment and light guides for aquision of signal in the oral cavity during surgery might help to localize the effect on the bone tissue and distinct molecules of the autograft tissue (for example, hemoglobin, collagen, proteins or lipids) or the stem cells of the graft [23].

CONCLUSION

Thus, in the course of the study it has been found that Raman spectroscopy is appropriate for rapid and efficient assessment of molecular composition, as well as qualitative and quantitative assessment of changes in autograft bone used for mandibular bone augmentation. Early detection of factors, impairing osseointegration, and contributing to resorption of bone tissue surrounding the implant, is a key issue of modern dentistry. Therefore, the research directed to address the issue is essential and relevant. The results obtained allow us to suggest the possibility of using Raman spectroscopy for this purpose. The use of Raman spectra acquisition in combination with detection using light guides would allow the dentist to monitor the process of reparative regeneration and osseointegration during dental implantation. Combination of optical diagnosis and rapid digital feature analysis can significantly improve the efficiency of surgical procedure and treatment.

References

1. Tsitsiashvili AM, Panin AM. Ustanovka dental'nyh implantatov v distal'nom otdele verhnej cheljusti posle provedenija kostnoj plastiki metodikoj rotacii kostnogo loskuta. Nauchno-prakticheskij zhurnal «Dental Forum». 2017; (2): 40–45.

2. Kulakov AA, redactor. Dental'naja implantacija. Nacional'noe rukovodstvo. M.: GJeOTAR-Media, 2018; 400 s. Available from: https://www.rosmedlib.ru/book/ISBN9785970445419.html.

3. Neugebauer J, Kistler F, Kistler S, Scheer M, Bayer G, Zoller JE. Autologous bone augmentation. Scientific and practical journal "New in Dentistry". 2019; (241): 6–26.

4. Pankratov AS, Lekishvili MV, Kopeckij IS. Kostnaja plastika v stomatologii i cheljustno-licevoj hirurgii. Osteoplasticheskie materialy. M.: Binom, 2011; 271 s.

5. Hernandez-Alfaro F, Sancho-Puchades M, Guijarro-Mart'ınez R, Total Reconstruction of the Atrophic Maxilla with Intraoral Bone Grafts and Biomaterials: A Prospective Clinical Study with Cone Beam Computed Tomography Validation. Int J Maxillofac Implants 2013; 28 (1): 241–51. Available from: http://dx.doi.org/10.11607/jomi.2405.

6. Khoury F, Hanser T. Mandibular bone block harvesting from the retromolar region: a 10-year prospective clinical study. Int J Oral Maxillofac Implants. 2015; 30 (3): 688–97. DOI: 10.11607/jomi.4117.

7. Jureti AM, Cerovi AR, BeluAiA-Gobi AM, Brekalo PrAo I, Kqiku L, Špalj S, et al. Salivary levels of TNF-A and IL-6 in patients with oral premalignant and malignant lesions. Folia Biol (Praha). 2013; 59: 99–102. Available from: https://fb.cuni.cz/file/5685/fb2013a0012.pdf.

8. Feng X, Shi Y, Xu L, Peng Q, Wang X, Sun W, et al. Modulation of IL-6 induced RANKL expression in arthritic synovium by a transcription factor SOX5. Sci Rep. 2016; 6: 32001. DOI: 10.1038/srep32001.

9. Tereshima A, Takayanagi H. Overview of Osteoimmunology. Calcif Tissue Int. 2018; 102 (5): 503–11. Available from: https://doi.org/10.1007/s00223-018-0417-1.

10. Zorika OA, Abaev ZM, Magomedov RN, Prohodnaya VA, Maksukova ES. Diagnostic value of serum osteomarkets in moderate and severe periodontal disease. Stomatologiya.

11. Smirnov AV, Rumyantsev ASh. Stroenie i funkcii kostnoj tkani v norme i pri patologii. Soobshhenie I. Nefrologija. 2014; 18 (6): 9–25.

12. Bolevich SB, Vojnov VA. Molekuljarnye mehanizmy v patologii cheloveka. Rukovodstvo dlja vrachej. 2012; 206 s.

13. Vlasov AV, Maliar NL, Bazhenov SV, Nikelshparg EI, Brazhe NA, Maksimov GV, et al. Raman Scattering: From Structural Biology to Medical Applications. Crystals, MDPI publishing house (Basel, Switzerland). 2020; 10 (1): 38. Available from: https://doi.org/10.3390/cryst10010038.

14. Rafalsky VV, Zyubin AYu, Moiseeva EM, Samusev IG. Perspektivy primenenija metoda spektroskopii kombinacionnogo rassejanija sveta (ramanovskoj spektroskopii) v kardiologii. Kardiovaskuljarnaja terapija i profilaktika. 2020; 19 (1): 2394. DOI: 10.15829/1728-8800-2020-1-2394.

15. Eremina OE, Semenova AA, Sergeeva EA, Brazhe NA, Maksimov GV, Shehovcova TN, i dr. Spektroskopija gigantskogo kombinacionnogo rassejanija v sovremennom himicheskom analize: dostizhenija i perspektivy ispol'zovanija. Uspehi himii. 2018; 87 (8): 741–70.

16. Alexandrov MT, Margaryan EG. Rationale for the application of surface-enhanced Raman scattering for identification of main pathogens of purulent-inflammatory diseases in maxillofacial area. 2018; 97 (1); 27–32. DOI: 10.17116/stomat201897127-32.

17. Chen X, Wang Z, Duan N, Zhu G, Schwarz EM, Xie C. Osteoblast-osteoclast interactions Connect. Tissue Res. 2017; 59: 99–107. Available from: https://doi.org/10.1080/03008207.2017.1290085.

18. Fukumato S, Martin TJ. Bone as an endocrine organ. Trends Endocrinol Metab. 2009; 20 (5): 230–6. Available from: https://doi.org/10.1038/srep3200.

19. Kylmaoja E, Nakamura M, Tuukkanen J. Osteoclasts and remodeling based bone formation. Curr Stem Cell Res Ther. 2016; I1: 626–33. Available from: https://doi.org/10.2174/1574888X10666151019115724.

20. Sohrabi K, Mushantat A, Esfandiari S, Feine J. How successful

are small — diamond implants? The literature review. Clin Oral Implants Res. 2012; 23 (5): 515–25. Available from: https://doi.org/10.1111/j.1600-0501.2011.02410.x.

21. Yunus N, Masood M, Saub R, Al-Hashedi AA, Taiyeb Ali TB, Thomason JM. Impact of mandibular implant prostheses on the oral health-related quality of life in partially and completely edentulous patients. Clin Oral Implants Res. 2016; 27 (7): 904–9.

Available from: https://doi.org/10.1111/clr.12657.

22. Wessel JJ. Surface-enhanced optical microscopy. JOSA B. 1985; 2 (9): 1538–41. Available from: https://doi.org/10.1364/JOSAB.2.001538.

23. Zhang J, Chen J. Bone Tissue Regeneration — Application of Mesenchymal Stem Cells and Cellular and Molecular Mechanisms. 2017; 12 (5): 357–64. DOI: 10.2174/1574888x11666160921121555.

Литература

1. Цициашвили А. М., Панин А. М. Установка дентальных имплантатов в дистальном отделе верхней челюсти после проведения костной пластики методикой ротации костного лоскута. Научно-практический журнал «Dental Forum». 2017; (2): 40–45.

2. Кулаков А. А., редактор. Дентальная имплантация. Национальное руководство. М.: ГЭОТАР-Медиа, 2018; 400 с. Доступно по ссылке: https://www.rosmedlib.ru/book/ISBN9785970445419.html.

3. Neugebauer J, Kistler F, Kistler S, Scheer M, Bayer G, Zoller JE. Autologous bone augmentation. Scientific and practical journal "New in Dentistry". 2019; (241): 6–26.

4. Панкратов А. С., Лекишвили М. В., Копецкий И. С. Костная пластика в стоматологии и челюстно-лицевой хирургии. Остеопластические материалы. М.: Бином, 2011; 271 с.

5. Hernandez-Alfaro F, Sancho-Puchades M, Guijarro-Mart'ınez R, Total Reconstruction of the Atrophic Maxilla with Intraoral Bone Grafts and Biomaterials: A Prospective Clinical Study with Cone Beam Computed Tomography Validation. Int J Maxillofac Implants 2013; 28 (1): 241–51. Available from: http://dx.doi.org/10.11607/jomi.2405.

6. Khoury F, Hanser T. Mandibular bone block harvesting from the retromolar region: a 10-year prospective clinical study. Int J Oral Maxillofac Implants. 2015; 30 (3): 688–97. DOI: 10.11607/jomi.4117.

7. Jureti AM, Cerovi AR, BeluAiA-Gobi AM, Brekalo PrAo I, Kqiku L, Špalj S, et al. Salivary levels of TNF-A and IL-6 in patients with oral premalignant and malignant lesions. Folia Biol (Praha). 2013; 59: 99–102. Available from: https://fb.cuni.cz/file/5685/fb2013a0012.pdf.

8. Feng X, Shi Y, Xu L, Peng Q, Wang X, Sun W, et al. Modulation of IL-6 induced RANKL expression in arthritic synovium by a transcription factor SOX5. Sci Rep. 2016; 6: 32001. DOI: 10.1038/srep32001.

9. Tereshima A, Takayanagi H. Overview of Osteoimmunology. Calcif Tissue Int. 2018; 102 (5): 503–11. Available from: https://doi.org/10.1007/s00223-018-0417-1.

10. Зорика О. А., Абаев З. М., Магомедов Р. Н., Проходная В. А., Максюкова Е. С. Диагностическая информативность определения остеомаркеров в сыворотке крови при хроническом парализованном пародонтите средней и тяжелой степени. Стоматология. 2019; 98 (1): 17–20.

11. Смирнов А. В., Румянцев А. Ш. Строение и функции костной ткани в норме и при патологии. Сообщение I. Нефрология. 2014; 18 (6): 9–25.

12. Болевич С. Б., Войнов В. А. Молекулярные механизмы в

патологии человека. Руководство для врачей. 2012; 206 с.

13. Vlasov AV, Maliar NL, Bazhenov SV, Nikelshparg EI, Brazhe NA, Maksimov GV, et al. Raman Scattering: From Structural Biology to Medical Applications. Crystals, MDPI publishing house (Basel, Switzerland). 2020; 10 (1): 38. Available from: https://doi.org/10.3390/cryst10010038.

14. Рафальский В. В., Зюбин А. Ю., Моисеева Е. М., Самусев И. Г. Перспективы применения метода спектроскопии комбинационного рассеяния света (рамановской спектроскопии) в кардиологии. Кардиоваскулярная терапия и профилактика. 2020; 19 (1): 2394.

15. Еремина О. Е., Семенова А. А., Сергеева Е. А., Браже Н. А., Максимов Г. В., Шеховцова Т. Н., и др. Спектроскопия гигантского комбинационного рассеяния в современном химическом анализе: достижения и перспективы использования. Успехи химии. 2018; 87 (8): 741–70.

16. Alexandrov M. T., Margaryan E. G. Rationale for the application of surface-enhanced Raman scattering for identification of main pathogens of purulent-inflammatory diseases in maxillofacial area. 2018; 97 (1): 27–32. DOI: 10.17116/stomat201897127-32.

17. Chen X, Wang Z, Duan N, Zhu G, Schwarz EM, Xie C. Osteoblast-osteoclast interactions Connect. Tissue Res. 2017; 59: 99–107. Available from: https://doi.org/10.1080/03008207.2017.1290085.

18. Fukumato S, Martin TJ. Bone as an endocrine organ. Trends Endocrinol Metab. 2009; 20 (5): 230–6. Available from: https://doi.org/10.1038/srep3200.

19. Kylmaoja E, Nakamura M, Tuukkanen J. Osteoclasts and remodeling based bone formation. Curr Stem Cell Res Ther. 2016; I1: 626–33. Available from: https://doi.org/10.2174/1574888X10666151019115724.

20. Sohrabi K, Mushantat A, Esfandiari S, Feine J. How successful are small — diamond implants? The literature review. Clin Oral Implants Res. 2012; 23 (5): 515–25. Available from: https://doi.org/10.1111/j.1600-0501.2011.02410.x.

21. Yunus N, Masood M, Saub R, Al-Hashedi AA, Taiyeb Ali TB, Thomason JM. Impact of mandibular implant prostheses on the oral health-related quality of life in partially and completely edentulous patients. Clin Oral Implants Res. 2016; 27 (7): 904–9. Available from: https://doi.org/10.1111/clr.12657.

22. Wessel JJ. Surface-enhanced optical microscopy. JOSA B. 1985; 2 (9): 1538–41. Available from: https://doi.org/10.1364/JOSAB.2.001538.

23. Zhang J, Chen J. Bone Tissue Regeneration — Application of Mesenchymal Stem Cells and Cellular and Molecular Mechanisms. 2017; 12 (5): 357–64. DOI: 10.2174/1574888x11666160921121555.

THE POTENTIAL OF USING THE BIOLUMINESCENT SYSTEM OF *CHAETOPTERUS VARIOPEDATUS* TO STUDY FERROPTOSIS IN LIVING ORGANISMS

Shcheglov AS ✉, Tsarkova AS

Shemyakin–Ovchinnikov Institute of Bioorganic Chemistry, Moscow, Russia

Pirogov Russian National Research Medical University, Moscow, Russia

Ferroptosis is a form of programmed cell death associated with iron-dependent lipid peroxidation. Novel ferroptosis inducers and suppressors could be instrumental in developing drugs against neurodegenerative disorders and cancer. Prior to embarking on a search for ferroptosis inducers/suppressors, this form of cell death must be studied in living cells and laboratory animals. In addition to two cofactors, luciferase (or photoprotein) of the parchment tubeworm *Chaetopterus variopedatus* requires the presence of iron ions and hydrogen peroxide or organic hydroperoxides to exert its activity. Therefore, the bioluminescence system of the parchment tubeworm can be used to study ferroptosis in living organisms.

✉ **Correspondence should be addressed:** Alexander S. Shcheglov
Miklouho-Maclay, 16/10, Moscow, 117997; jukart@mail.ru

ПЕРСПЕКТИВЫ ИСПОЛЬЗОВАНИЯ БИОЛЮМИНЕСЦЕНТНОЙ СИСТЕМЫ *CHAETOPTERUS VARIOPEDATUS* ДЛЯ МОНИТОРИНГА ФЕРРОПТОЗА В ЖИВЫХ ОРГАНИЗМАХ

А. С. Щеглов ✉, А. С. Царькова

Институт биоорганической химии имени М. М. Шемякина и Ю. А. Овчинникова, Москва, Россия

Российский национальный исследовательский медицинский университет имени Н. И. Пирогова, Москва, Россия

Ферроптоз — особый тип программируемой гибели клеток, связанный с интенсивным окислением липидов под действием свободных ионов двухвалентного железа. Новые индукторы и супрессоры ферроптоза могут стать основой для создания препаратов для лечения нейродегенеративных и онкологических заболеваний. Для поиска таких индукторов (супрессоров) ферроптоза необходимо детектировать этот процесс в живых клетках или у лабораторных животных. Люцифераза (фотопротеин) морского дракона *Chaetopterus variopedatus* для своей активности требует помимо двух кофакторов наличия ионов железа и пероксида водорода (либо органических гидропероксидов). Соответственно биолюминесцентная система морского дракона может быть использована для мониторинга ферроптоза в живых организмах.

✉ **Для корреспонденции:** Александр Сергеевич Щеглов
ул. Миклухо-Маклая, д. 16/10, г. Москва, 117997; jukart@mail.ru

Ferroptosis is a new form of programmed cell death

Programmed cell death is cell death coordinated by specific intracellular mechanisms. It has been described in higher animals, invertebrates, plants, bacteria, and fungi. Programmed cell death plays an immense role in normal organismal development and functioning [1]. It is essential for embryonic development and morphogenesis, tissue remodeling, immune response, elimination of malignant and infected cells. Excessive or insufficient programmed cell death leads to neurodegenerative, autoimmune, oncological and other diseases. The importance of studying programmed cell death was emphasized by two Nobel prizes in physiology and medicine in 2002 and 2016. The first form of programmed cell death to be discovered was apoptosis [2]. Today, at least 10 different nonapoptotic pathways of programmed cell death are known, including autophagy-dependent cell death, necroptosis, ferroptosis, pyroptosis, parthanatos, entosis, NETosis, and some others [1]. Despite extensive research efforts, our knowledge about these processes is still limited.

Ferroptosis is a form of programmed cell death that might hold promise for practical applications. In 2004, it was discovered that a hitherto novel heterocyclic compound erastin caused cell death via a previously unknown nonapoptotic pathway [3]. Erastin directly interacts with mitochondrial voltage-dependent anion channels (VDAC) and its action is inhibited by antioxidants, such as α-tocopherol, butylated hydroxytoluene and β-carotene [4]. It is reported that erastin-induced cell death can be prevented by ferrous iron chelators [5]. In 2012, Dickson et al. proposed the term *ferroptosis* to refer to a new form of cell death associated with intense iron-dependent lipid peroxidation. Genetically, biochemically and morphologically, ferroptosis is distinct from apoptosis, necrosis and autophagia-dependent cell death [1, 6]. Unlike apoptosis, ferroptosis is not

$$Fe^{2+} + ROOH \longrightarrow Fe^{3+} + RO^{\cdot} + OH^{-}$$
$$Fe^{3+} + ROOH \longrightarrow Fe^{2+} + ROO^{\cdot} + H^{+}$$

$$\left. \right\} \begin{array}{c} \textit{luciferase/} \\ \textit{photoprotein} \\ \textit{Chaetopterus} \end{array} \longrightarrow \text{Light 455 nm}$$
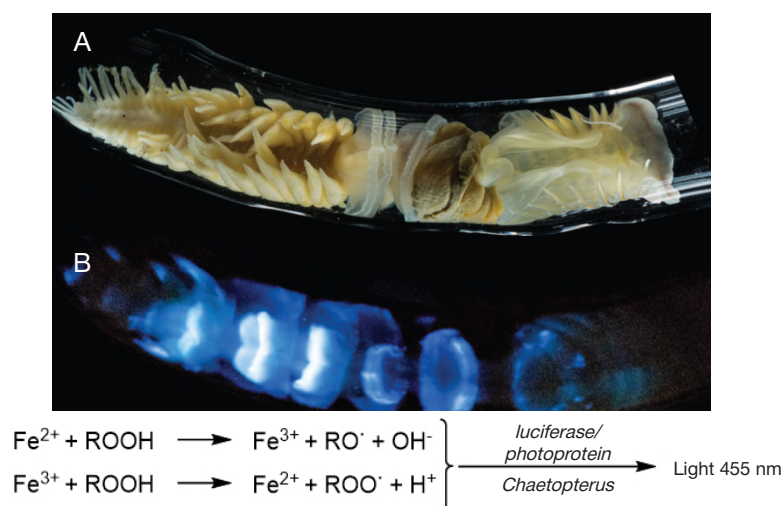
Fig. Bioluminescence of *Chaetopterus variopedatus*; top: a parchment tubeworm outside of its tube in the light (**A**) and in the dark (**B**) (photos provided by Alvaro E. Migotto and Anderson G. Oliveira); bottom: a possible mechanism of bioluminescence (after Mirza JD et al., 2020)

accompanied by cell nucleus transformation and chromatin condensation and is characterized by mitochondrial shrinkage, increased mitochondrial membrane density and vanishing of mitochondrial cristae [5, 6]. The loss of glutathione peroxidase 4 (GPX4) activity leads to iron-dependent lipid peroxidation and the accumulation of lipid hydroperoxides in the cell, resulting in ferroptotic cell death [5, 7]. Ferrous ions accumulation and lipid hydroperoxide generation, which cause cell death, are seen in some neurodegenerative disorders, including Alzheimer's disease, Parkinson's disease, Huntington's disease, Friedreich's ataxia, and other pathologies, such as amyotrophic lateral sclerosis, periventricular leukomalacia, ischemic stroke, traumatic brain injury and acute kidney injury. Development and progression of these disorders are thought to be associated with the activation of the ferroptotic cascade [8]. At the same time, ferroptosis appears to be a promising therapeutic strategy for the treatment of apoptosis-resistant malignant tumors, since cancer cells contain increased amounts of ferrous iron. For example, sorafenib, a drug effective against renal cancer, has been shown to induce ferroptosis [9]. Thus, research into the mechanisms underlying ferroptosis and the search for new ferroptosis inducers/suppressors may facilitate the development of novel drugs against neurodegenerative diseases and cancer. However, prior to a large-scale screening of candidate ferroptosis inducers and suppressors, an effective monitoring system is needed to track this process in living cells and laboratory animals.

The promise of the *Chaetopterus variopedatus* bioluminescent system

Modern biotechnology and diagnostics actively exploit bioluminescence-based methods characterized by high sensitivity and low background signal. Bioluminescence systems are employed for analyte detection, immunological testing, gene expression analysis, drug screening, bioimaging of living organisms, visualization of intracellular structures and processes, cancer studies and infectious diseases research, and environmental monitoring [10]. Bioluminescence systems are common in nature, but few of them have been well characterized and adapted for practical use. The deciphering of yet understudied bioluminescence systems is instrumental in creating new analytical techniques [11]. One such system is the underinvestigated and unusual bioluminescence system of the parchment tubeworm *Chaetopterus variopedatus* (see Figure). These benthic filter-feeding organisms inhabit the tube-shaped "homes". When pulled out of the tubes, the worms emit bright blue light and secrete luminescent mucus. The biological role and molecular underpinnings of this mechanism are still not fully clear [12]. According to earlier reports, the activity of *Chaetopterus variopedatus* photoprotein is dependent on the presence of two cofactors, ferrous iron and hydrogen peroxide or organic hydroperoxides [13]. Later reports demonstrated that the iron-dependent bioluminescent system of the parchment tubeworm functions like the classic "luciferin-luciferase" system [14].

As ferroptosis is characterized by simultaneous accumulation of ferrous iron and generation of reactive oxygen species, the ferroptotic cells expressing *Chaetopterus variopedatus* luciferase would develop a luminescent signal.

Conclusion

Programmed cell death plays an immense role in normal organismal development and maintenance. Dysregulation of programmed cell death leads to neurodegenerative and autoimmune disorders, cancer, etc. Ferroptosis is a nonapoptotic form of programmed cell death associated with intense iron-dependent lipid peroxidation. Research into the mechanisms underlying ferroptosis and the search for new ferroptosis inducers and suppressors has practical implications. The bioluminescent system of the parchment tubeworm is a promising tool for studying ferroptosis in living laboratory organisms.

References

1. Tang D, Kang R, Berghe TV, Vandenabeele P, Kroemer G. The molecular machinery of regulated cell death Cell Research 2019, 29: 347–64, DOI: 10.1038/s41422-019-0164-5.

2. Kerr JF, Wyllie AH, Currie AR. Apoptosis: a basic biological phenomenon with wide-ranging implications in tissue kinetics. Br J Cancer. 1972; 26 (4): 239–57. DOI: 10.1038/bjc.1972.33.

3. Dolma S, Lessnick SL, Hahn WC, Stockwell BR. Identification of genotype-selective antitumor agents using synthetic lethal chemical screening in engineered human tumor cells. Cancer Cell. 2003; 3: 285–96. DOI: 10.1016/S1535-6108(03)00050-3.
4. Yagoda N, von Rechenberg M, Zaganjor E, Bauer AJ., Yang WS, Fridman DJ, et al. RAS-RAF-MEK-dependent oxidative cell death involving voltage-dependent anion channels. Nature. 2007; 447: 864–8. DOI: 10.1038/nature05859.
5. Yang WS, Stockwell BR. Synthetic lethal screening identifies compounds activating iron-dependent, nonapoptotic cell death in oncogenic-RAS-harboring cancer cells. Chem Biol. 2008; 15: 234–45. DOI: 10.1016/j.chembiol.2008.02.010.
6. Dixon SJ, Lemberg KM, Lamprecht MR, Skouta R, Zaitsev EM, Gleason CE, et al. Ferroptosis: an iron-dependent form of nonapoptotic cell death. Cell. 2012; 149: 1060–72. DOI: 10.1016/j.cell.2012.03.042.
7. Angeli JPF, Schneider M, Proneth B, Tyurina YY, Tyurin VA, Hammond VJ, et al. Inactivation of the ferroptosis regulator Gpx4 triggers acute renal failure in mice. Nat Cell Biol. 2014; 16: 1180–91. DOI: 10.1038/ncb3064.
8. Li J, Cao F, Yin H-l, Huang Z-j, Lin Z-t, Mao N, et al. Ferroptosis: past, present and future. Cell Death Dis. 2020; 11 (2): 88. DOI: 10.1038/s41419-020-2298-2.

9. Yan H-F, Zou T, Tuo Q-Z, Xu S, Li H, Belaidi AA, et al. Ferroptosis: mechanisms and links with diseases. Signal Transduct Target Ther. 2021; 6 (1): 49. DOI:10.1038/s41392-020-00428-9.
10. Syed AJ, Anderson JC. Applications of bioluminescence in biotechnology and beyond. Chem Soc Rev. 2021 Mar 18. DOI: 10.1039/d0cs01492c.
11. Oba Y, Stevani CV, Oliveira AG, Tsarkova AS, Chepurnykh TV, Yampolsky IV. Selected least studied but not forgotten bioluminescent systems. Photochem Photobiol. 2017; 93 (2): 405–15. DOI: 10.1111/php.12704.
12. Mirza JD, Migotto ÁE, Yampolsky IV, de Moraes GV, Tsarkova AS, Oliveira AG. Chaetopterus variopedatus bioluminescence: A review of light emission within a species complex. Photochem Photobiol. 2020; 96 (4): 768–78. DOI: 10.1111/php.13221.
13. Shimomura O, Johnson FH. Chaetopterus photoprotein: crystallization and cofactor requirements for bioluminescence. Science. 1968; 159 (3820): 1239–40. DOI: 10.1126/science.159.3820.1239.
14. Purtov KV, Petushkov VN, Rodionova NS, Pakhomova VG, Myasnyanko IN, Myshkina NM, et al. Luciferin-Luciferase system of marine polychaete Chaetopterus variopedatus. Dokl Biochem Biophys. 2019; 486 (1): 209–12. DOI: 10.1134/S1607672919030104.

Литература

1. Tang D, Kang R, Berghe TV, Vandenabeele P, Kroemer G. The molecular machinery of regulated cell death Cell Research 2019, 29: 347–64, DOI: 10.1038/s41422-019-0164-5.
2. Kerr JF, Wyllie AH, Currie AR. Apoptosis: a basic biological phenomenon with wide-ranging implications in tissue kinetics. Br J Cancer. 1972; 26 (4): 239–57. DOI: 10.1038/bjc.1972.33.
3. Dolma S, Lessnick SL, Hahn WC, Stockwell BR. Identification of genotype-selective antitumor agents using synthetic lethal chemical screening in engineered human tumor cells. Cancer Cell. 2003; 3: 285–96. DOI: 10.1016/S1535-6108(03)00050-3.
4. Yagoda N, von Rechenberg M, Zaganjor E, Bauer AJ., Yang WS, Fridman DJ, et al. RAS-RAF-MEK-dependent oxidative cell death involving voltage-dependent anion channels. Nature. 2007; 447: 864–8. DOI: 10.1038/nature05859.
5. Yang WS, Stockwell BR. Synthetic lethal screening identifies compounds activating iron-dependent, nonapoptotic cell death in oncogenic-RAS-harboring cancer cells. Chem Biol. 2008; 15: 234–45. DOI: 10.1016/j.chembiol.2008.02.010.
6. Dixon SJ, Lemberg KM, Lamprecht MR, Skouta R, Zaitsev EM, Gleason CE, et al. Ferroptosis: an iron-dependent form of nonapoptotic cell death. Cell. 2012; 149: 1060–72. DOI: 10.1016/j.cell.2012.03.042.
7. Angeli JPF, Schneider M, Proneth B, Tyurina YY, Tyurin VA, Hammond VJ, et al. Inactivation of the ferroptosis regulator Gpx4 triggers acute renal failure in mice. Nat Cell Biol. 2014; 16: 1180–91. DOI: 10.1038/ncb3064.

8. Li J, Cao F, Yin H-l, Huang Z-j, Lin Z-t, Mao N, et al. Ferroptosis: past, present and future. Cell Death Dis. 2020; 11 (2): 88. DOI: 10.1038/s41419-020-2298-2.
9. Yan H-F, Zou T, Tuo Q-Z, Xu S, Li H, Belaidi AA, et al. Ferroptosis: mechanisms and links with diseases. Signal Transduct Target Ther. 2021; 6 (1): 49. DOI:10.1038/s41392-020-00428-9.
10. Syed AJ, Anderson JC. Applications of bioluminescence in biotechnology and beyond. Chem Soc Rev. 2021 Mar 18. DOI: 10.1039/d0cs01492c.
11. Oba Y, Stevani CV, Oliveira AG, Tsarkova AS, Chepurnykh TV, Yampolsky IV. Selected least studied but not forgotten bioluminescent systems. Photochem Photobiol. 2017; 93 (2): 405–15. DOI: 10.1111/php.12704.
12. Mirza JD, Migotto ÁE, Yampolsky IV, de Moraes GV, Tsarkova AS, Oliveira AG. Chaetopterus variopedatus bioluminescence: A review of light emission within a species complex. Photochem Photobiol. 2020; 96 (4): 768–78. DOI: 10.1111/php.13221.
13. Shimomura O, Johnson FH. Chaetopterus photoprotein: crystallization and cofactor requirements for bioluminescence. Science. 1968; 159 (3820): 1239–40. DOI: 10.1126/science.159.3820.1239.
14. Purtov KV, Petushkov VN, Rodionova NS, Pakhomova VG, Myasnyanko IN, Myshkina NM, et al. Luciferin-Luciferase system of marine polychaete Chaetopterus variopedatus. Dokl Biochem Biophys. 2019; 486 (1): 209–12. DOI: 10.1134/S1607672919030104.

SCHIZOPHRENIA SPECTRUM DISORDERS IN CHILDREN AND ADOLESCENTS: PREVALENCE AND DIAGNOSTICS

Pankova OF, Kazin NM, Ivanova SM ✉

Pirogov Russian National Research Medical University, Moscow, Russia

The significance of studying the prevalence, age- and sex-related differences and diagnostic aspects of schizophrenia spectrum disorders (F2 Schizophrenia, schizotypal and delusional disorders) in pediatric and adolescent patients of mental health facilities is linked to the upcoming release of the International Classification of Diseases, Revision 11 (ICD-11). Its whole chapters have been updated, including disorders in the schizophrenia group. Diagnostic challenges posed by this debilitating group of mental disorders are associated with the diversity of clinical presentations, the incompleteness of psychopathological phenomena syndromes, and vague atypical symptoms. Changes in the prevalence of these disorders identified by the analysis of medical records at a mental health facility for children (a decline in the number of patients with F20, schizophrenia, and a surge in the number of patients with F21, schizotypal disorder) and significant disagreement about and disagreement about the diagnostic criteria for schizophrenia spectrum disorders in children and adolescents, evaluation of their dynamics, outcomes, and the social functioning of the patient necessitate further prospective follow-up studies aimed at overcoming the identified difficulties in the diagnosis, treatment and rehabilitation of such patients.

Keywords: ICD-10, children and adolescents, schizophrenia spectrum disorders, clinical forms, diagnosis, prognosis

СОВРЕМЕННЫЕ ПРОБЛЕМЫ В ИЗУЧЕНИИ РАСПРОСТРАНЕННОСТИ И ДИАГНОСТИКЕ РАССТРОЙСТВ ШИЗОФРЕНИЧЕСКОГО СПЕКТРА У ДЕТЕЙ И ПОДРОСТКОВ

О. Ф. Панкова, Н. М. Казин, С. М. Иванова ✉

Российский национальный исследовательский медицинский университет имени Н. И. Пирогова, Москва, Россия

Актуальность изучения показателей распространенности, половозрастных особенностей и диагностики расстройств шизофренического спектра (раздел F2 Шизофрения, шизотипические и бредовые расстройства) у детей и подростков — пациентов детских психиатрических клиник объясняется предстоящим вступлением в действие Международной классификации болезней (МКБ-11), в которой существенные изменения внесены в целый ряд разделов, включая расстройства из группы шизофрении. Трудности диагностики данной группы инвалидизирующих расстройств связаны с полиморфизмом клинической картины, синдромальной незавершенностью психопатологических феноменов, наличием «стертых» атипичных форм. Выявленные при анализе стационарных карт пациентов одной из детских психиатрических больниц изменения в структуре заболеваемости (уменьшение числа пациентов с диагнозом шизофрении (F20) и значительное увеличение числа пациентов с диагнозом шизотипического расстройства (F21)), а также серьезные противоречия в вопросах диагностики, оценке динамики расстройств, исходов, уровня социального функционирования больных позволяют подчеркнуть необходимость дальнейшего изучения с использованием клинико-катамнестических методов для преодоления выявленных трудностей и противоречий в диагностике, лечении и реабилитации данных пациентов.

Ключевые слова: МКБ-10, дети и подростки, расстройства шизофренического спектра, распространенность, клинические формы, диагностика, прогноз

According to statistics, the detection rate of mental disorders, including psychotic spectrum disorders, in the Russian population is declining [1]. At the same time, a Russian study conducted in 2000–2018 has revealed a rise in psychotic disorders among children and a high prevalence of mental illness among teenagers and children, compared to adults, amid a decline in the child and adolescent population [2].

Schizophrenia spectrum disorders in children and adolescents

The significance of studying schizophrenia spectrum disorders, which comprise a group of debilitating conditions, stems from the high frequency of their manifestation, diversity of clinical presentation, the incompleteness of psychopathological phenomena syndromes, and the occurrence of atypical forms with vague symptoms [3–5]. Such clinical diversity results in the insufficient understanding of the essence and the prognostic role of these conditions, complicating the differentiation between their clinical forms. Diagnostic approaches to schizophrenia vary between countries; being diagnosed with schizophrenia and receiving treatment for this disease has a profound impact on one's mental health and future. In Europe and America, it is advisable to avoid the diagnosis of schizophrenia in children younger than 8–14 years. By contrast, schizophrenia and schizophrenia spectrum disorders are acceptable labels in Russia. The Russian version of ICD-10 has a separate entry for "childhood schizophrenia" under the F20.8 (other schizophrenia) category. The diagnostic aspects of schizophrenia spectrum disorders are demanding special attention in light of the upcoming ICD-11, as the clinical diagnostic paradigm will be shifting from the categorical to

the dimensional principle [6, 7]. Timely diagnosis is no less important than an accurate definition. Multiple foreign and some Russian publications provide evidence that early treatment at the prodromal stage can significantly reduce the risk of the first psychotic episode, improve the long-term outcome, maintain social drive and the high level of the patient's functioning [8–10]. These data underscore the importance of further research into the prevalence, diagnostic challenges and treatment of schizophrenia spectrum disorders.

Recent epidemiological data on schizophrenia spectrum disorders among children and adolescents are very scarce. There are a few publications on the prevalence of the major mental disorders, including schizophrenia spectrum disorders, among children and adolescents in the past 15 years [11, 12].

The analysis of medical records of patients undergoing medical examination and treatment at G. E. Sukhareva Research and Practical Center for Mental Health of Children and Adolescents in 1999–2019 allowed us to identify the main diagnostic challenges and problems of studying the prevalence of schizophrenia and schizophrenia spectrum disorders (F2) in children and adolescents since the adoption of ICD-10 in Russia. Throughout the specified period, the prevalence of F2 disorders remained stable (± standard deviation, SD) at 10.12 ± 1.61. There was an insignificant increase in prevalence (both in relative and absolute values) during the past two years included in the analysis, which coincided with a rise in hospitalizations and probably reflected a growing trend in the prevalence of mental illness in children and adolescents.

Prevalence of schizophrenia spectrum disorders

Fig. 1 shows cumulative data for the entire analyzed period and data for the first and last years of our study. The following schizophrenia spectrum disorders prevailed among children and adolescents: schizophrenia (F20), schizotypal disorder (F21), acute and transient psychotic disorders (F23), and schizoaffective disorder (F25). Together, these conditions accounted for 99.6% of all mental illnesses in the studied cohort and formed the core of the spectrum.

Of all the patients with F2, 48.8% had schizophrenia, about one-third (32.3%) had schizotypal disorder, 11.7% had schizoaffective disorder, and 6.8% had transient psychotic disorder. Importantly, when ICD-10 was first introduced in 1999, schizophrenic patients made up 75.3% of all F2 patients. By 2019, the proportion of schizophrenic patients had decreased 3-fold, accounting for 25.8% of patients in the F2 group. By contrast, the number of patients diagnosed with schizotypal disorder had increased dramatically (6-fold

percentagewise and 19-fold in absolute values). The number of patients with schizoaffective disorder had increased almost 2.5-fold percentagewise and 7.8-fold in absolute values. The prevalence of transient psychotic disorders was the most stable.

The majority of the patients were 11–14 years old, except for the patients with schizoaffective disorder, who were 15–17 years old. Male patients dominated the group of patients with schizophrenia, schizotypal and schizoaffective disorders. Sex differences were minimal in the group of patients with transient psychosis: 53.1% were males and 46.9% were females.

Prevalence dynamics of schizophrenia and schizophrenia spectrum disorders over analyzed period

Fig. 2 shows that F20 and F21 curves behave differently. There is a gradual decline in schizophrenia prevalence, slowing a little in 2013, and a rise in the number of patients with schizotypal disorder in 2007, followed by stabilization until 2016 and a surge in 2017–2019. The level of confidence for the frequency of the diagnoses was assumed to be 0.95.

Trends in prevalence and diagnostic problems associated with schizophrenia spectrum disorders in children and adolescents

The analysis revealed a few trends in the prevalence of schizophrenia spectrum disorders (F2 according to ICD-10) and some problems associated with their diagnosis in children and adolescents. The most salient problem persisting over the last 3 years covered by the analysis was a diagnostic imbalance: a decline in the number of patients with schizophrenia (F20) and a surge in the number of patients with schizotypal disorder (F21). Of all the young inpatients of the Center, 32.2% had F21. In this subgroup, 71.2% were diagnosed with F21.8 schizotypal personality disorder, 6.3% were diagnosed with F21.3 pseudoneurotic schizophrenia, and 15.2% were diagnosed with F21.4 pseudopsychopathic schizophrenia.

Among older patients [13], 11.6% were diagnosed with F21, 47.7% were diagnosed with pseudoneurotic schizophrenia (F21.3) and 35.8% were diagnosed with pseudopsychopathic schizophrenia (F21.4). In 49.6% of cases, the provisional diagnosis of F21–F29 was established before schizophrenia was verified.

In our opinion, the term "schizotypal personality disorder" (F21.8) is incorrect because personality disorder cannot be diagnosed in children and adolescents; but it is legitimate to say that their schizoid traits are progressing. The criteria for
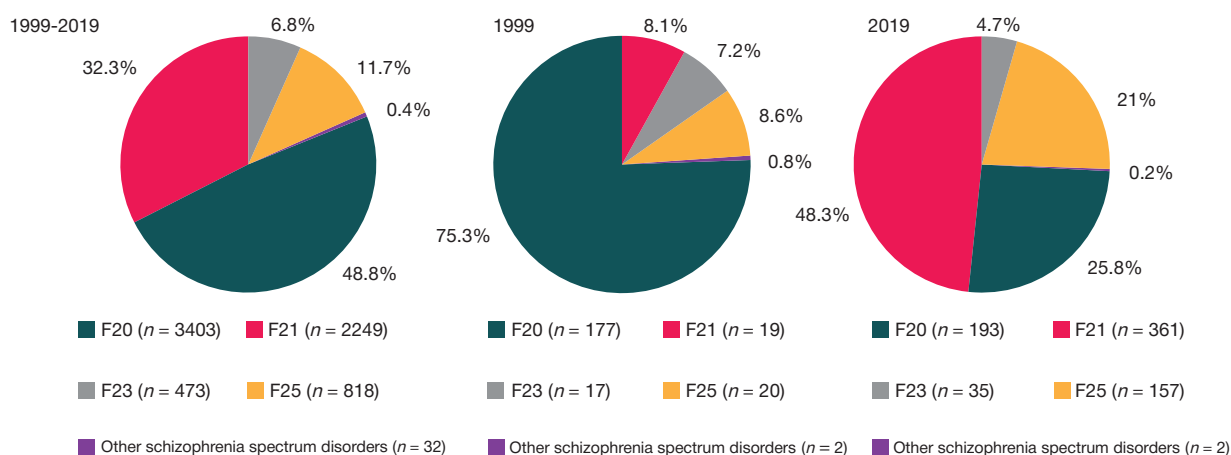

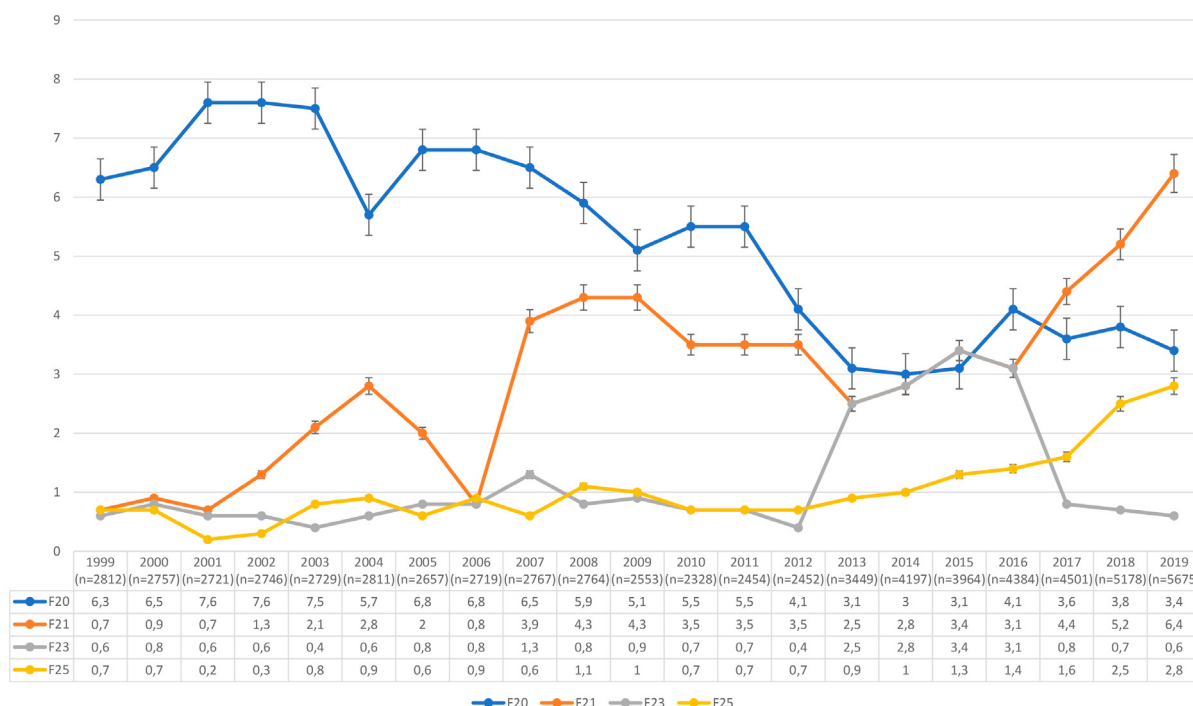**Fig. 1.** Prevalence of schizophrenia spectrum disorders

Fig. 2. Prevalence dynamics of schizophrenia and major schizophrenia spectrum disorders relative to the total number of hospitalized patients

	1999 (n=2812)	2000 (n=2757)	2001 (n=2721)	2002 (n=2746)	2003 (n=2729)	2004 (n=2811)	2005 (n=2657)	2006 (n=2719)	2007 (n=2767)	2008 (n=2764)	2009 (n=2553)	2010 (n=2328)	2011 (n=2454)	2012 (n=2452)	2013 (n=3449)	2014 (n=4197)	2015 (n=3964)	2016 (n=4384)	2017 (n=4501)	2018 (n=5178)	2019 (n=5675)
F20	6,3	6,5	7,6	7,6	7,5	5,7	6,8	6,8	6,5	5,9	5,1	5,5	5,5	4,1	3,1	3	3,1	4,1	3,6	3,8	3,4
F21	0,7	0,9	0,7	1,3	2,1	2,8	2	0,8	3,9	4,3	4,3	3,5	3,5	3,5	2,5	2,8	3,4	3,1	4,4	5,2	6,4
F23	0,6	0,8	0,6	0,6	0,4	0,6	0,8	0,8	1,3	0,8	0,9	0,7	0,7	0,4	2,5	2,8	3,4	3,1	0,8	0,7	0,6
F25	0,7	0,7	0,2	0,3	0,8	0,9	0,6	0,9	0,6	1,1	1	0,7	0,7	0,7	0,9	1	1,3	1,4	1,6	2,5	2,8

the diagnosis of schizotypal personality disorder in children and adolescents do not include character traits; instead, they are based on the symptoms specified in the preamble of the Russian Thesaurus of Psychiatry, which is used to classify mental disorders. The preliminary analysis of medical records revealed that the reported clinical presentations did not meet the criteria for schizotypal disorder in many cases; however, in all age groups the number of patients diagnosed with schizotypal personality disorder (F21.8) increased at discharge.

In our opinion, this diagnostic transformation can be explained by social factors and stigma, which significantly affect clinical decision-making and force the clinician to come up with a diagnosis that would allow the patient to integrate into society. The stigma of schizophrenia has been widely discussed in Russian and foreign publications [14, 15]. Patients and their parents fear being stigmatized. This fear is not irrational because a grave psychiatric diagnosis can reduce career opportunities and chances to marry. Due to fear, patients delay a visit to public or private psychiatrists, psychologists, neurologists, etc. This prevents them from receiving timely health care, which, among other things, includes social and pedagogical interventions, psychotherapy and other types of rehabilitation.

Conclusion

The main candidate explanations of the identified diagnostics problems are a) changes in the clinical presentation of the disease, such as the growing prevalence of non-psychotic forms of schizophrenia spectrum disorders, including attenuated and quasi-psychosis (this is partly supported by the relatively stable number of patients with transient psychosis (F23) and schizoaffective disorder (F25)); b) vague yet diverse symptoms at the prodromal stage before the onset of psychotic symptoms in children and teenagers, a dissociation between the severity of the condition and social functioning, insufficient clarity of diagnostic criteria; c) the stigma of schizophrenia and the tendency to mitigate it be establishing a more socially acceptable diagnosis. The identified difficulties and disagreement about the diagnostic criteria for schizophrenia spectrum disorders in children and adolescents, evaluation of their dynamics, outcomes, and the social functioning of the patient necessitate further prospective follow-up studies.

References

1. Kekelidze ZI, Kazakovcev BA, redaktory. Jepidemiologicheskie pokazateli i pokazateli dejatel'nosti psihiatricheskih sluzhb v Rossijskoj Federacii (2005–2013 gg.). M., 2015; 572 s. Russian.
2. Makushkin EV, Demcheva NK. Dinamika i sravnitel'nyj analiz detskoj i podrostkovoj zabolevaemosti psihicheskimi rasstrojstvami v Rossijskoj Federacii v 2000–2018 godah. Rossijskij psihiatricheskij zhurnal. 2019, 4: 4–15. Russian.
3. Mazaeva NA. Podrostkovyj vozrast i shizofrenija. Psihiatrija. 2008; 2: 16–28. Russian.
4. Makarov IV. Psihiatrija detskogo vozrasta. Rukovodstvo dlja vrachej. Sankt-Peterburg: Nauka i tehnika, 2019; 992 s. Russian.

5. Parnas J. The core Gestalt of schizophrenia. World Psychiatry. 2012; 11 (2): 67.
6. Gaebel W, Jessen F, Kanba S. Neurocognitive disorders in ICD-11: the debate and its outcome. World Psychiatry. 2018; 17 (2): 229–30.
7. Kotov R, Krueger RF, Watson D. A paradigm shift in psychiatric classification: the Hierarchical Taxonomy Of Psychopathology (HiTOP). World Psychiatry. 2018; 17 (1): 24–25.
8. Omelchenko MA, Golubev SA, Nikiforova IYu, Kaleda VG. Risk manifestacii jendogennyh psihozov u bol'nyh s nepsihoticheskimi psihicheskimi rasstrojstvami junosheskogo vozrasta. Zhurnal nevrologii i psihiatrii im. S.S. Korsakova. 2014; 114 (6): 14–20. Russian.
9. Fusar-Poli P, Salazar de Pablo G, Correll CU, Meyer-Lindenberg A,

et al. Prevention of Psychosis: Advances in Detection, Prognosis, and Intervention. JAMA Psychiatry. 2020; 77 (7): 755–65.

10. Stafford MR, Jackson H, Mayo-Wilson E, et al. Early interventions to prevent psychosis: systematic review and meta-analysis. BMJ. 2013; 346: f762. DOI: 10.1136/bmj.f185.

11. Pankova OF, Usacheva EL, Abramov AV, Danilova MY, Dorina IV, Smirnov II, Svintsova AV. Organizational issues relating to the inpatient psychiatric care of children and adolescents in the context of current trends. International Journal of Culture and Mental Health. 2018; 11 (1): 75–86,

12. Pankova OF, Radionov DS, Ivanova SM, Dorina IV. Shizofrenija i rasstrojstva shizofrenicheskogo spektra v klinike sovremennoj detskoj psihiatrii (analiz gospitalizacij v krupnejshuju

psihiatricheskuju kliniku Moskvy). Voprosy psihicheskogo zdorov'ja detej i podrostkov. 2019; 19 (4): 47–56. Russian.

13. Kostyuk GP, Shmukler AB, Golubev SA. Jepidemiologicheskie aspekty diagnostiki shizofrenii v Moskve. Social'naja i klinicheskaja psihiatrija. 2017; 27 (3): 5–9. Russian.

14. Yastrebov VS, Mihaylova II, Gonzhal OA, Trushhelev SA. Faktory stigmatizacii lic s psihicheskimi rasstroi–stvami: metodicheskie rekomendacii. M.: Izd-vo ZAO Justicinform, 200; 22 s. Russian.

15. Sibitz I, Amering M, Unger A, Seyringer ME, Bachmann A, Schrank B, et al. The impact of the social network, stigma and empowerment on the quality of life in patients with schizophrenia. Eur Psychiatry. 2011; 26: 28–33. DOI: https://doi. org/10.1016/j. eurpsy.2010.08.010.

Литература

1. Кекелидзе З. И., Казаковцев Б. А., редакторы. Эпидемиологические показатели и показатели деятельности психиатрических служб в Российской Федерации (2005–2013 гг.). М., 2015; 572 с.

2. Макушкин Е. В., Демчева Н. К. Динамика и сравнительный анализ детской и подростковой заболеваемости психическими расстройствами в Российской Федерации в 2000–2018 годах. Российский психиатрический журнал. 2019, 4: 4–15.

3. Мазаева Н. А. Подростковый возраст и шизофрения. Психиатрия. 2008; 2: 16–28.

4. Макаров И. В. Психиатрия детского возраста. Руководство для врачей. Санкт-Петербург: Наука и техника, 2019; 992 с.

5. Parnas J. The core Gestalt of schizophrenia. World Psychiatry. 2012; 11 (2): 67.

6. Gaebel W, Jessen F, Kanba S. Neurocognitive disorders in ICD-11: the debate and its outcome. World Psychiatry. 2018; 17 (2): 229–30.

7. Kotov R, Krueger RF, Watson D. A paradigm shift in psychiatric classification: the Hierarchical Taxonomy Of Psychopathology (HiTOP). World Psychiatry. 2018; 17 (1): 24–25.

8. Омельченко М. А., Голубев С. А., Никифорова И. Ю., Каледа В. Г. Риск манифестации эндогенных психозов у больных с непсихотическими психическими расстройствами юношеского возраста. Журнал неврологии и психиатрии им. С.С. Корсакова. 2014; 114 (6): 14–20.

9. Fusar-Poli P, Salazar de Pablo G, Correll CU, Meyer-Lindenberg A, et al. Prevention of Psychosis: Advances in Detection, Prognosis,

and Intervention. JAMA Psychiatry. 2020; 77 (7): 755–65.

10. Stafford MR, Jackson H, Mayo-Wilson E, et al. Early interventions to prevent psychosis: systematic review and meta-analysis. BMJ. 2013; 346: f762. DOI: 10.1136/bmj.f185.

11. Pankova OF, Usacheva EL, Abramov AV, Danilova MY, Dorina IV, Smirnov II, Svintsova AV. Organizational issues relating to the inpatient psychiatric care of children and adolescents in the context of current trends. International Journal of Culture and Mental Health. 2018; 11 (1): 75–86,

12. Панкова О. Ф., Радионов Д. С., Иванова С. М., Дорина И. В. Шизофрения и расстройства шизофренического спектра в клинике современной детской психиатрии (анализ госпитализаций в крупнейшую психиатрическую клинику Москвы). Вопросы психического здоровья детей и подростков. 2019; 19 (4): 47–56.

13. Костюк Г. П., Шмуклер А. Б, Голубев С. А.Эпидемиологические аспекты диагностики шизофрении в Москве. Социальная и клиническая психиатрия. 2017; 27 (3): 5–9.

14. Ястребов В. С., Михайлова И. И., Гонжал О. А., Трущелёв С. А. Факторы стигматизации лиц с психическими расстройствами: методические рекомендации. М.: Изд-во ЗАО Юстицинформ, 200; 22 с.

15. Sibitz I, Amering M, Unger A, Seyringer ME, Bachmann A, Schrank B, et al. The impact of the social network, stigma and empowerment on the quality of life in patients with schizophrenia. Eur Psychiatry. 2011; 26: 28–33. DOI: https://doi. org/10.1016/j. eurpsy.2010.08.010.